Outcrop Analogue Studies of Rocks from the Northwest German Basin for Geothermal Exploration and Exploitation: Fault Zone Structure, Heterogeneous Rock Properties, and Application to Reservoir Conditions

Dissertation

zur Erlangung des mathematisch-naturwissenschaftlichen Doktorgrades
"Doctor rerum naturalium"
der Georg-August-Universität Göttingen

im Promotionsprogramm Geowissenschaften / Geographie
der Georg-August University School of Science (GAUSS)

vorgelegt von

Dorothea Reyer

aus Witzenhausen

Göttingen 2013

Betreuungsausschuss:

Prof. Dr. Sonja Philipp
Abteilung Strukturgeologie und Geodynamik
Geowissenschaftliches Zentrum der Georg-August-Universität Göttingen

Dr. Rüdiger Thomas
Forschungsschwerpunkt Geothermische Energie
Leibniz-Institut für Angewandte Geophysik, Hannover

Mitglieder der Prüfungskommission:

Prof. Dr. Sonja Philipp
Abteilung Strukturgeologie und Geodynamik
Geowissenschaftliches Zentrum der Georg-August-Universität Göttingen

Prof. Dr. Martin Sauter
Abteilung Angewandte Geologie
Geowissenschaftliches Zentrum der Georg-August-Universität Göttingen

Dr. Rüdiger Thomas
Forschungsschwerpunkt Geothermische Energie
Leibniz-Institut für Angewandte Geophysik, Hannover

weitere Mitglieder der Prüfungskommission:

Prof. Dr. Jonas Kley
Abteilung Strukturgeologie und Geodynamik
Geowissenschaftliches Zentrum der Georg-August-Universität Göttingen

Prof. Dr. Sharon Webb
Abteilung Experimentelle und Angewandte Mineralogie
Geowissenschaftliches Zentrum der Georg-August-Universität Göttingen

Dr. Bianca Wagner
Abteilung Angewandte Geologie
Geowissenschaftliches Zentrum der Georg-August-Universität Göttingen

Tag der mündlichen Prüfung: 24. Oktober 2013

Abstract

Rock heterogeneities in terms of layering and fault zones are common phenomena in sedimentary basins such as the Northwest German Basin (NWGB). At geothermal projects, these heterogeneous rock properties affect many issues associated with exploration, drilling, and reservoir stimulation. This thesis investigates how high resolution data from outcrop analogues can be used to improve predictions of both normal fault structure and rock mechanical conditions at greater depths.

To better understand normal fault structure and associated fracture systems in sedimentary rocks of the NWGB, 58 outcrop-scale normal fault zones were analysed in detail. The focus was on fracture orientations, densities, apertures and lengths, separately for fault damage zones and host rocks, as well as structural indices. Pronounced differences between carbonate and clastic rocks were found, and mainly in carbonate rocks clear damage zones with increased fracture densities occur. While the maximum aperture is similar for both rock types, the percentage of fractures with large apertures is much higher in the damage zones. In carbonate rocks, damage zone fractures may differ significantly in orientation from that in the host rocks. In clastic rocks, fractures show a similar orientation in both fault damage zones and host rocks. Structural indices indicate that normal fault zones in carbonate rocks are more damage-zone dominated and have more profound effects on enhancing permeability in fluid reservoirs than those in clastic rocks. Based on measured Young's moduli and fracture density distributions, effective stiffnesses E_e within normal faults are calculated and yield a significantly smaller stiffness decrease for clastic-rock damage zones compared with carbonate rocks.

To improve knowledge about properties of typical NWGB rocks, physical (P-wave velocities, porosity, and bulk and grain density) and geomechanical parameters (Uniaxial compressive strength (UCS), Young's modulus, destruction work and indirect tensile strength; each perpendicular and parallel to layering) were determined for 35 outcrop samples taken from quarries and 14 equivalent core samples. A subgroup of these samples, consisting of one volcanic rock sample, three sandstone and three carbonate samples, was used for triaxial tests. Because core material is rare, this thesis aims at predicting in situ rock properties from outcrop analogue samples. Properties of samples from depths are compared with equivalent outcrop samples – that is, same stratigraphic age and comparable sedimentary facies. Equivalence is confirmed using thin section analyses. Empirical relations of UCS with all physical and geomechanical parameters were determined with regression analyses, lithologically separated for outcrop and core samples. Most relations have high coefficients of determination; properties of core samples lie within 90% prediction bands of empirical relations for outcrop samples. Similarly, linearized Mohr-Coulomb failure criteria, expressed in both principal stresses as well in shear and normal stresses were determined from triaxial test sequences. A comparison with core samples shows that it is possible to apply principal stress failure criteria for clastic and volcanic rocks, but less so for carbonates. Expressed in shear and normal stresses, however, applicability is good for all rock types. Transferability of empirical relations to rocks at depths is expected. The most important aspects regarding applicability of obtained criteria are porosity and textural comparability of outcrop equivalents with core samples.

Using FRACOD, fracture propagation in heterogeneous rocks at stimulation treatments was analysed for numerical models involving layered and fractured scenarios characteristic for NWGB. Results of both fault-related fracture systems and geomechanical properties are used as input parameters. Contrasts in Young's modulus and Poisson's ratio between alternating layers were found to have less effect on the fracture trajectory than contrasts in fracture toughness. Scenarios involving a set of parallel pre-existing fractures reveal a complex interaction with an induced hydrofracture.

Presented results of this thesis can be of manifold use: they will help to explore fault-related geothermal reservoirs with high natural permeabilities; laboratory measurements provide approaches as to how to predict mechanical properties at greater depths from outcrop samples, as well as input data for future numerical modelling of geothermal problems; and numerical modelling of hydrofracture propagation in heterogeneous rocks gives insight on relevant parameters affecting fracture path which helps adapting the stimulation strategy to reservoir conditions.

Zusammenfassung

Schichtung und Störungszonen sind typische Phänomene in Sedimentbecken wie dem Nordwestdeutschen Becken. Diese Gesteinsheterogenitäten können großen Einfluss auf viele verschiedene Fragestellungen im Zusammenhang mit der Exploration, dem Bohren und der hydraulischen Stimulation des geothermischen Reservoirs haben. Diese Doktorarbeit liefert Aussagen und Ansätze, wie hoch aufgelöste Daten, die in Aufschlüssen erhoben wurden, für eine verbesserte Vorhersage des Störungszonenaufbaus und der gesteinsmechanischen Eigenschaften in größeren Tiefen verwendet werden können.

Um den Aufbau von Störungszonen und assoziierten Bruchsystemen in Sedimentgesteinen besser zu verstehen, wurden 58 Abschiebungen im Aufschlussmaßstab detailliert analysiert. Der Schwerpunkt lag dabei auf der Analyse von Bruchorientierung, -dichte, -öffnungsweite und -länge – jeweils getrennt betrachtet für Bruchzone und Nebengestein – sowie auf den strukturellen Indizes. Es konnten deutliche Unterschiede zwischen karbonatischen und klastischen Gesteinen festgestellt werden: in karbonatischen Gesteinen treten häufig ausgeprägte Bruchzonen mit erhöhten Bruchdichten auf. Während die maximale Öffnungsweite für beide Einheiten ähnlich ist, ist der Anteil an Brüchen mit großen Öffnungsweiten in der Bruchzone deutlich größer als im Nebengestein. In Karbonatgesteinen kann die Bruchorientierung in der Bruchzone stark von der im Nebengestein abweichen. In klastischen Gesteinen dagegen sind in beiden Einheiten ähnliche Bruchorientierungen zu finden. Die Auswertung der strukturellen Indizes zeigt, dass Abschiebungen in Karbonatgesteinen eher bruchzonen-dominiert sind als solche in klastischen Gesteinen und folglich größeren positiven Einfluss auf die Reservoirpermeabilität haben. Auf Basis der bestimmten Bruchdichtenverteilungen und Elastizitätsmoduli wurden effektive Steifigkeiten E_e innerhalb der Abschiebungen berechnet. Dabei zeigen Bruchzonen in klastischen Gesteinen eine deutlich geringere Abnahme der Steifigkeiten als solche in Karbonatgesteinen.

Um die Kenntnisse über Eigenschaften typischer Gesteine im Nordwestdeutschen Becken zu erweitern, wurden physikalische (V_p-Geschwindigkeit, Porosität, Rohdichte und Korndichte) und gesteinsmechanische Parameter (Einaxiale Druckfestigkeit [UCS], Elastizitätsmodul, Zerstörungsarbeit und Zugfestigkeit; jeweils parallel und senkrecht zur sedimentären Schichtung) an 35 Gesteinsproben aus Aufschlüssen und 14 Bohrkernproben bestimmt. Für einen Teil dieser Proben (eine Vulkanit- sowie jeweils drei Sandstein- und Kalksteinproben) wurden Triaxialmessungen durchgeführt. Da Bohrkernmaterial selten ist, war es Ziel dieser Arbeit, die in-situ-Gesteinseigenschaften anhand von Aufschlussproben vorherzusagen. Die Eigenschaften von Proben aus größeren Tiefen werden dann mit denen äquivalenter Proben verglichen, d.h. Bohrkern und äquivalente Aufschlussprobe haben das gleiche stratigraphische Alter und eine vergleichbare sedimentäre Fazies. Die Äquivalenz der Proben wurde anhand von Dünnschliffen sichergestellt. Empirische Beziehungen bzw. Korrelationen zwischen UCS und allen physikalischen und geomechanischen Parametern wurden mit Regressionsanalysen bestimmt, jeweils lithologisch getrennt für alle Proben (inkl. Bohrkerne) und nur für Aufschlussproben. Die meisten Korrelationen haben ein hohes Bestimmtheitsmaß; die Ergebnisse der Bohrkerne liegen meist innerhalb der 90% Prognosebänder der Korrelationen, die für Aufschlussproben berechnet wurden. Auf ähnliche Weise wurden anhand von mehreren Triaxialmessungen pro Probe linearisierte Mohr-Coulomb Versagenskriterien bestimmt, die sowohl in Hauptnormalspannungen als auch in Normal- und Scherspannungen angegeben werden. Ein Vergleich zeigt, dass es zwar für Klastika und Vulkanite aus Aufschlüssen möglich ist, Versagenskriterien, die in Hauptnormalspannungen ausgedrückt werden, auf Bohrkernproben anzuwenden, aber nicht für Karbonate. Sind die Versagenskriterien allerdings in Normal- und Scherspannungen angegeben, ist die Anwendbarkeit für alle Gesteinsarten gut. Eine Übertragbarkeit der empirischen Beziehungen auf die Tiefe wird abgeleitet. Die wichtigsten Parameter, um die Anwendbarkeit der Aufschlussdaten zu gewährleisten, sind eine vergleichbare Textur und eine ähnliche Porosität von Äquivalenzproben aus Steinbrüchen und Bohrkernproben.

Die Bruchausbreitung infolge einer hydraulischen Stimulation von heterogenen Gesteinen wurde mit dem Programm FRACOD analysiert. Es wurden numerische Modelle erstellt, die für das NWGB

charakteristisch sind und die sowohl geschichtete Abfolgen als auch bereits existierende Brüche berücksichtigen. Die Ergebnisse der Untersuchung von Bruchsystemen in Störungszonen und die gemessenen gesteinsmechanischen Eigenschaften werden als Eingangsparameter verwendet. Die Modellierung zeigt, dass ein großer mechanischer Kontrast zwischen einzelnen Schichten bezüglich Elastizitätsmodul und Poissonkoeffizient geringeren Einfluss auf die Ausbreitungsrichtung des Bruches hat, als stark unterschiedliche Bruchzähigkeiten. Werden bereits existierende Brüche in das Modell eingebaut, zeigt sich eine starke Wechselwirkung mit dem induzierten Hydrobruch.

Die Ergebnisse dieser Doktorarbeit sind von vielfältigem Nutzen. Erstens helfen die Daten bei der Exploration von geothermischen Reservoiren in Störungszonen mit hohen natürlichen Permeabilitäten. Zweitens liefern die Ergebnisse der Labormessungen Aussagen und Ansätze, wie man die mechanischen Gesteinseigenschaften in größeren Tiefen anhand von Aufschlussproben vorhersagen und sie als Eingangsparameter für zukünftige numerische Modellierungen zu geothermischen Fragestellungen heranziehen kann. Außerdem liefert die numerische Modellierung der Bruchausbreitung infolge einer hydraulischen Stimulation in heterogenen Gesteinen Einblicke in die relevanten Parameter, die Einfluss auf die Ausbreitungsrichtung des induzierten Bruches haben. Dieses Wissen wird dabei helfen, die hydraulische Stimulation an die jeweiligen Reservoir-bedingungen anzupassen.

Preface

This thesis entitled "Outcrop Analogue Studies of Rocks from the Northwest German Basin for Geothermal Exploration and Exploitation: Fault Zone Structure, Heterogeneous Rock Properties, and Application to Reservoir Conditions" was written simultaneously to the project "Heterogeneous rock properties, drilling efficiency and fracture propagation" which is part of the collaborative research program *gebo* (Geothermal Energy and High Performance-Drilling) funded by *Niedersächsisches Ministerium für Wissenschaft und Kultur* and *Baker Hughes*. It is the result of work that was done initially as research assistant (May 2009 to October 2010), followed by almost three years as doctor student at the Geoscience Centre of the Georg-August-University of Göttingen, Department of Structural Geology and Geodynamics.

The thesis is submitted to obtain the degree "Doctor rerum naturalium" (Dr. rer. nat.). It is compiled as cumulative dissertation, including following four research articles:

Chapter 4:   **Reyer D**, Bauer JF, Philipp SL (2012) Fracture systems in normal fault zones crosscutting sedimentary rocks, Northwest German Basin. Journal of Structural Geology 45:38-51 (Special Issue on Fault Zones). doi:10.1016/j.jsg.2012.06.002

Chapter 5:   **Reyer D**, Philipp SL. Empirical relations of rock properties of outcrop and core samples from the Northwest German Basin for geothermal drilling. Geothermal Energy Science 2:21-37. doi:10.5194/gtes-2-21-2014

Chapter 6:   **Reyer D**, Philipp SL. Failure and friction criteria based on samples from outcrop analogues for core property prediction. International Journal of Rock Mechanics and Mining Sciences (revised)

Chapter 7:   Meneses Rioseco E, **Reyer D**, Schellschmidt R (2013) Understanding and predicting coupled hydromechanical fracture propagation. Proceedings of European Geothermal Congress 2013, Pisa, PS2-08, 1-12

As part of the research work, several results were previously presented at conferences in talks and posters (listed chronologically):

- **Reyer D**, Bauer JF, Philipp SL (2009) Infrastruktur und Permeabilität von Störungszonen im Unteren Muschelkalk auf der westlichen Grabenschulter des Leinetalgrabens. *Talk and extended abstract*, Geothermiekongress 2009 Bochum Proceedings, TF8
- **Reyer D**, Bauer JF, Philipp SL (2010) Structural geological field methods in outcrop analogues for potential fault-related geothermal reservoirs. *Talk and extended abstract*, Geotectonic Research 96/01, Special Issue, TSK 13 Conference Transcript, p. 48
- **Reyer D**, Philipp SL (2010) Architecture of small-scale fault zones in the context of the Leinetal-graben Fault System. *Poster and abstract*, Geophysical Research Abstracts 12, EGU2010-7995
- **Reyer D**, Bauer JF, Philipp SL (2010) Architektur und Permeabilität von Störungszonen in Sedimentgesteinen des Norddeutschen Beckens. *Talk and extended abstract*, Geothermie-kongress 2010 Karlsruhe Proceedings, F1.3
- Philipp SL, **Reyer D**, Bauer JF (2010) Abschätzung effektiver Elastizitätsmoduli von Sediment-gesteinen in Störungszonen des Norddeutschen Beckens. *Talk and abstract*, GeoDarmstadt 2010
- Philipp SL, **Reyer D** (2010) Mechanical rock properties, fracture propagation and permeability development in deep geothermal reservoirs. *Talk and abstract*, Geophysical Research Abstracts 12, EGU2010-11145

- Hördt A, Beilecke T, Ghergut I, Holzbecher E, Löhken I, Löhken J, Musmann P, Philipp SL, **Reyer D**, Sauter M, Schaumann G, Thomas R (2011) Models of geothermal reservoirs as a basis for interdisciplinary cooperation. *Poster and abstract*, AGU2011
- **Reyer D**, Lünsdorf NK, Sieck P, Philipp SL (2011) Heterogenitäten bohrungsrelevanter Gesteins-eigenschaften im Norddeutschen Becken: Geländestudien und Laboranalysen. *Talk and extended abstract*, Geothermiekongress 2011 Bochum Proceedings, F12
- **Reyer D**, Bauer JF, Philipp SL (2011) Influence of fault zones on fracture systems in sedimentary geothermal reservoir rocks in the North German Basin. *Poster and abstract*, Geophysical Research Abstracts 13, EGU2011-6230
- **Reyer D**, Bauer JF, Philipp SL (2011) Fault zone architecture and fracture systems in sedimentary rocks of the North German Basin. *Poster and abstract*, Geophysical Research Abstracts 13, EGU2011-6403
- **Reyer D**, Lünsdorf NK, Sieck P, Philipp SL (2011) Heterogeneities of rock properties relevant to drilling in the North German Basin: Field studies and laboratory analyses. *Talk and abstract*, Celle Drilling 2011
- **Reyer D**, Philipp SL (2011) Influence of fault zones on fracture systems in sedimentary geothermal reservoir rocks in the North German Basin. *Talk, poster and extended abstract*, European Geothermal PhD-Day 2011, Reykjavik
- Philipp SL, Lim PY, Parchwitz S, **Reyer D** (2011) Numerical models of extension fracture propagation in mechanically layered rocks. *Poster and abstract*, Geophysical Research Abstracts 13, EGU2011-2481
- Philipp SL, **Reyer D**, Afşar F, Meier S, Bauer JF, Parchwitz S (2011) Extension fractures and fault zone structure in layered carbonate rocks. *Poster and abstract*, Geophysical Research Abstracts 13, EGU2011-2475
- Philipp SL, **Reyer D**, Bauer JF (2011) Estimation of effective Young's moduli of sedimentary rocks in fault zones. *Poster and abstract*, Geophysical Research Abstracts 13, EGU2011-2486
- **Reyer D**, Philipp SL (2012) Heterogeneities of mechanical properties in potential geothermal reservoir rocks of the North German Basin. *Talk and abstract*, Geophysical Research Abstracts 14, EGU2012-346
- **Reyer D**, Philipp SL (2012) Heterogeneities of mechanical properties in potential geothermal reservoir rocks of the North German Basin. *Talk, poster and extended abstract*, European Geothermal PhD-Day 2012, Pisa
- **Reyer D**, Philipp SL (2012) Bruchausbreitung und Stimulation von Sedimentgesteinen im Nordwestdeutschen Becken. *Talk and abstract*, GeoHannover 2012
- **Reyer D**, Philipp SL (2012) Erstellung realitätsnaher numerischer Modelle zur Stimulation von potenziellen geothermischen Reservoiren im Nordwestdeutschen Becken. *Talk and extended abstract,* Geothermiekongress 2012 Karlsruhe Proceedings, F8.1
- Vogt E, **Reyer D**, Schulze KC, Bartetzko A, Wonik T (2012) Modeling of geomechanical parameters required for safe drilling of geothermal wells in the North German Basin. *Talk and abstract*, Celle Drilling 2012
- **Reyer D**, Philipp SL (2013) Empirical relations of geomechanical and physical parameters with UCS: Input data for geomechanical models. *Talk, poster and extended abstract*, European Geothermal PhD-Day 2013, Szeged
- **Reyer D**, Afşar F, Philipp SL (2013) Quantification of rock heterogeneities by structural geological field studies combined with laboratory analyses. *Poster and abstract*, Geophysical Research Abstracts 15, EGU2013-7226
- **Reyer D** (2013) Aufschlussanalogstudien über Gesteine des Nordwestdeutschen Beckens für die geothermische Erkundung und Erschließung: Heterogene Gesteinseigenschaften und Anwendbarkeit auf geothermische Reservoirbedingungen. *Talk, poster and abstract*, Geothermiekongress 2013 Essen Proceedings, SB-1

- **Reyer D**, Philipp SL (2013) Applicability of failure criteria and empirical relations of mechanical rock properties from outcrop analogue samples for wellbore stability analyses. *Talk and extended abstract*, In: Philipp SL, Acocella V (ed.) Rock Fractures in Geological Processes, Symposium, Proceedings, 45-48
- **Reyer D**, Philipp SL (2013) Applicability of failure criteria and empirical relations of mechanical rock properties from outcrop analogue samples for wellbore stability analyses. *Poster and abstract*, AGU 2013 Conference Proceedings, MR13A-2222
- Philipp SL, **Reyer D,** Bauer JF, Meier S, Afşar F (2014) Internal structure of fault zones in geothermal reservoirs: Examples from palaeogeothermal fields and potential host rocks. *Abstract*, EGU2014-1203
- Philipp SL, **Reyer D**, Meier S, Bauer JF, Afşar F, Reinecker J (2014) Fault zones and associated fracture systems in palaegeothermal fields and geothermal reservoirs. *Talk and abstract*, GeoFrankfurt 2014, Frankfurt am Main
- **Reyer D**, Philipp SL (2014) Pre-drilling calculation of geomechanical parameters for safe geothermal wells based on outcrop analogue samples. *Poster and a*bstract, EGU2014-1514
- **Reyer D,** Philipp SL (2014) Outcrop analogue studies of rocks from the North German Basin for geothermal exploration and exploitation: Heterogeneous rock properties and application to reservoir conditions. *Talk, poster and extended abstract,* European Geothermal PhD-Day 2014, Darmstadt
- **Reyer D,** Vogt E, Weichmann MJ, Philipp SL (2014) Empirical relations of geomechanical parameters for while-drilling calculation of uniaxial compressive strengths. *Talk and extended abstract*, Celle Drilling 2014, Celle
- **Reyer D,** Vogt E, Weichmann MJ, Philipp SL (2014) While-drilling estimation of uniaxial compressive strengths of geothermal reservoir rocks in the North German Basin. *Talk and abstract*, GeoFrankfurt 2014, Frankfurt am Main

Danksagung

Table of Contents

Table of Symbols and Abbreviations

b	Fracture aperture [mm]
C_0	Unconfined compressive strength [MPa] (triaxial test)
$d_{mean/max}$	Mean/maximum grain size [mm]
D	Specimen's diameter [mm]
D_x, D_y	Displacement discontinuity components in x- and y- direction
E_s	Static Young's modulus [GPa]
E_i	Young's modulus of the intact rock mass [GPa]
E_e	Effective Young's modulus [GPa]
EF1	Wellbore ´Eulenflucht 1´
EGS	Enhanced geothermal systems
Gt1	Wellbore ´Groß Buchholz Gt1´
H	Specimen's height [mm]
HDR	Hot dry rock
i	Hydraulic gradient [-]
k_n	Discontinuity stiffness [MPa]
L/D	Lengh-diameter ratio of specimens
L, ΔL	Original profile length, change in profile length[m]
NGB	North German Basin
NWGB	Northwest German Basin
p_c	Confining pressure [MPa]
Q	Flow rate [m^3/s]
QFL	Quartz, Feldspar, Lithoclasts
R^2	Coefficient of determination [-]
r_i	Value of the residual
$\bar{s}$	Average discontinuity spacing [m]
T_0	Indirect tensile strength [MPa]
TVD	Total vertical depth [m]
UCS	Uniaxial compressive strength [MPa]
V_p	P-wave velocity [m/s]
W	Destruction work [kJ/m^3]
y, y_i	Observed and predicted value of residual analysis
β	Dip angle of fault plane between fault normal and σ_1 [°]
$\Delta\sigma_{max}$	maximum stress difference [MPa]
$\Delta\sigma_{res}$	residual stress difference [MPa]
Δt	Travel time of P-wave [µs/ft]
µ	Failure line slope [-]
μ_i	Coefficient of internal friction [-]
μ_{fric}	Coefficient of friction [-]
ρ_d	Dry bulk density [g/cm^3]
ρ_0	Grain density [g/cm^3]
σ_1	Maximum principal stress [MPa]
σ_2	Intermediate principal stress [MPa]
σ_3	Minimum principal stress [MPa]
σ_n	Normal stress [MPa]
$\sigma_{n,res}$	Residual normal stress [MPa]
τ	Shear stress [MPa]
τ_0	Friction cohesion [MPa]
τ_f	Cohesive strength [MPa]
τ_{res}	Residual shear stress [MPa]
ф	Total porosity [%]

1   General Introduction

1.1 Exploration and exploitation of geothermal energy

In the ever expanding sector of renewable energy in Germany the development of geothermal energy production plays a special role. The term "geothermics" comprises the utilisation of ground heat to generate thermal energy and/or electric power. Main advantage of geothermal energy over other renewable energies (wind and solar power) is its permanent availability and low operating expenses. The performance of a geothermal site depends particularly, but not only, on fluid temperature and flow rate (DiPippo 2005; Huenges 2010). In Germany, there are three regions with considerable geothermal potential: Upper Rhine Graben, Molasse Basin and North German Basin (Figure 1.1a; Paschen et al. 2003). Whereas in the Molasse Basin porous high flow rate aquifers are utilised, the Upper Rhine Graben region benefits from high temperatures in shallow depths (e.g., Paschen et al. 2003). In these regions, there are already several geothermal projects implemented and established. The somewhat larger North German Basin (NGB) is currently under a thorough geothermal investigation. In the NGB the geothermal gradient – the average increase of temperature with depth – usually is from 25 and 40 K/km with an intermediate value of 35 K/km as revealed by the wellbore temperatures of geothermal wells in the NGB (Figure 1.1b). Due to its geothermal gradient the NGB can be classified as low-enthalpy region (Dickson and Fanelli 2003). Geothermal projects in low-enthalpy regions face the problem that prospective geothermal reservoirs with temperatures above 100 °C, which are needed for electric power generation (DiPippo 2005), are found in depths of 3000 m and deeper. The geothermal utilisation of the NGB, therefore, will depend on exploration of comparatively deep reservoirs.
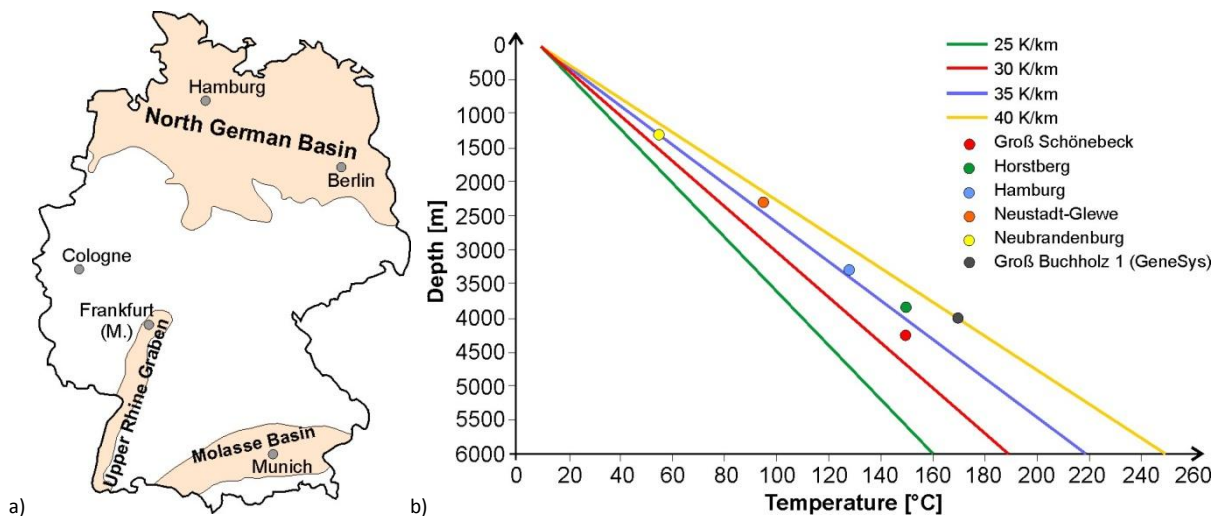
Figure 1.1: a) Location of the three regions in Germany with considerable geothermal potential: North German Basin, Molasse Basin, Upper Rhine Graben (mod. from www.geotis.de); b) Measured bottomhole temperatures of geothermal wells in the North German Basin and geothermal gradients (mod. from Bozau and van Berk 2012; Hesshaus et al. 2013).

As previously stated, the success of a geothermal project depends on both high temperatures and high flow rates (DiPippo 2005). To achieve high flow rates, high reservoir permeabilities are needed. High permeabilities can result either from a high effective matrix-porosity (that is the entity of hydraulically connected pores) or from secondary flow through fractures within the reservoir rocks. In geothermally relevant depths, however, the natural permeability is often small. In general, porosities of sedimentary rocks decrease with increasing overburden load due to compaction and cementation (Schön 1996). Fractures, which form secondary porosities, have smaller apertures compared with surface fractures (Lee and Farmer 1993). Nevertheless, the influence of existing fractures on reservoir permeability is important because already a few fractures, even with small apertures, dominate the fluid transport within porous media (Nelson 1985). Therefore, the task is to

find reservoirs with either a high natural hydraulic permeability, or those which can be stimulated hydraulically to generate new flow paths.

In the NGB, there are different geothermal reservoir types with considerable potential. So far projects have concentrated on conventional hydrothermal reservoirs in porous sedimentary rocks (e.g., Neustadt-Glewe; cf. Figure 1.1b). These projects use thermal waters of deep aquifers. Major problems of hydrothermal projects in the NGB are both low fluid temperature – high-permeability aquifers are found mainly in shallow depths – and, in deeper and hotter reservoirs, small flow rates (Menzel et al. 2000; Huenges 2010; Tischner et al. 2010; Hübner et al. 2012). Investigations for future projects therefore focus on petrothermal reservoirs and utilisation of fault zones. In petrothermal projects, tight sedimentary or crystalline geothermal reservoirs are engineered to facilitate heat extraction. A European petrothermal project, located in Soultz-sous-Forêts (France), is testing the feasibility of so-called HDR (Hot Dry Rock) heat exploitation concepts (e.g., Baumgärtner et al. 2004). According to Paschen et al. (2003) fault zones may have a high geothermal potential because of an assumed high fracture density and consequently, an increased natural hydraulic permeability which, however, requires further investigations. Potential fault-related geothermal reservoirs occur in both sedimentary and volcanic rocks. Fault zones in the upper crust generally consist of two zones with differing hydromechanic behaviour: 1) highly brecciated fault core and 2) mechanically stressed damage zone demonstrated by brittle deformation (Figure 1.2).
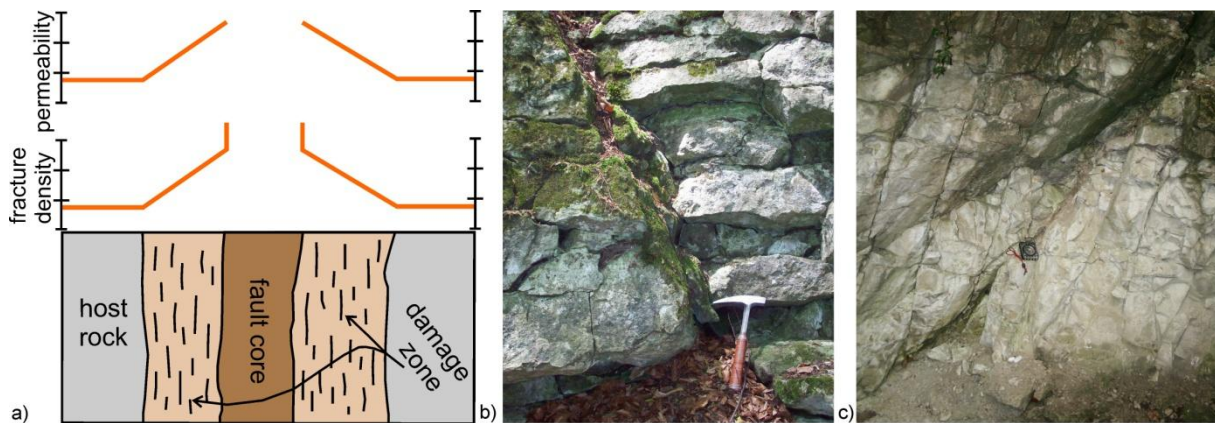
Figure 1.2: a) Internal structure of fault zones; sketch of a typical fault zone and of fracture density and permeability (mod. from Caine et al. 1996; Gudmundsson et al. 2001); b, c) Field pictures of normal faults crosscutting carbonate rocks in outcrops MH (b) and BR (c; for abbreviations please see figure caption 4.2) with different displacements of b) 10 cm and c) 50 cm, respectively. See hammer and geologic compass for scale.

The hydraulic characteristics of fault zones, however, can vary considerably. Fault zone structure, i.e. widths of fault core and damage zone, and fault-related permeability strongly depend on fault zone type (normal, reverse or strike-slip faults), lithology, displacement (Figures 1.2b, c), and orientation within the recent stress field (Aydin 1978; Lindsay et al. 1993; Caine et al. 1996; Faulkner et al. 2010, 2011; Gudmundsson 2011). It is assumed that fractures in fault zones which are oriented parallel to the maximum horizontal stress have higher apertures and respectively conductivities than those with perpendicular orientation (Philipp et al. 2005; Singhal and Gupta 2010). In the NGB, most common fault zone types are normal fault zones which originated due to extension processes (Walter 2007). Strategies for geothermal utilisation of fault zones will therefore focus on this fault zone type. In any case, the target point of the wellbore in the potential fault-related geothermal reservoir has to be chosen with care to strike the damage zone and minimise risks of encountering excessively low hydraulic permeabilities.

Apart from finding a suitable geothermal reservoir at depths, there are further challenges during the implementation of geothermal projects in the NGB. Sedimentary basins such as the NGB are commonly composed of various rock types with different geomechanical properties. These heterogeneous rock properties may result in mechanical layering which is a common phenomenon in sedimentary basins. Drilling projects in mechanically layered successions are often dealing with

wellbore instabilities (e.g., Zeynali 2012). Problems with wellbore stability are a drilling challenge that may considerably increase drilling time and total costs (e.g., Li et al. 2012). To prevent wellbore instabilities it is recommended to have substantiated estimations of the geomechanical properties of reservoir rocks and overlying strata before starting the drilling operation (Zhang 2005). This aids in determining optimal mud weight and wellbore design in order to prevent borehole breakouts, washouts, and tensile fracturing which may lead to wellbore collapse (Figure 1.3; Abdideh and Fathabadi 2013).
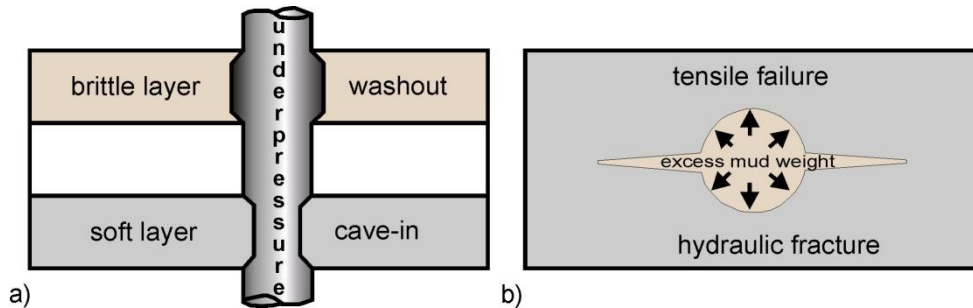
Figure 1.3: Wellbore instabilities in consequence of wrongly chosen mud weight; a) underpressure in the borehole as a result of low mud weight may lead to washout in brittle layers and cavin-in in soft layers, b) with excess mud weight hydraulic fractures are induced by pressures exceeding the tensile strength of the rocks (mod. from Zhang 2005).

When the encountered natural permeability is too low one has to take measures of permeability enhancement. Essentially, enhanced geothermal systems (EGS) involve hydraulic fracturing of the reservoir rocks to increase permeability and reach acceptable fluid extraction rates (Huenges 2010). By means of hydraulic fracturing, natural pre-existing fractures can be both connected and expanded hydraulically; or the hydraulic stimulation simply creates new highly conductive fractures penetrating the geothermal reservoir. However, the complex hydromechanical behaviour of fluid-induced fractures, including their geometry and interaction with pre-existing fractures, has not yet been completely understood and requires further investigations.

1.2 Motivation

The exploration and exploitation of deep geothermal reservoirs requires major investments. A large proportion of the total cost can be attributed to the drilling operation. Simultaneously, the profit margin of geothermal projects, compared with hydrocarbon projects, is rather small. Therefore, it is desirable to avoid any problems at the different stages of geothermal project development which increase costs (Reinicke et al. 2010; http://www.gebo-nds.de).

Handling previously mentioned issues of project development and advancing highly efficient and effective production of geothermal energy with low geological and technical risks relies on profound information about the subsurface, including the geologic situation, lithology, physical and geomechanical rock properties, fracture systems, presence of fault zones, etc. For this purpose, required information is to be acquired before starting the drilling operation. In most cases, however, geothermal project plans rely solely on rough estimations of permeability and geomechanical conditions because survey data are lacking. Information about the subsurface is limited to geophysical exploration methods and existing wellbores. In prospective depths of more than 3000 m the resolution of established geophysical methods, such as seismic and geoelectric operations, is too low to analyse mechanical layering, fault zone structure and associated fracture systems in detail. Wellbores, in contrast, provide high resolution information, but for one small location only and we do not get information on lateral heterogeneities. Determination of rock properties at depths are commonly carried out on drill cores. Borehole sampling, however, is very expensive and in most cases limited to reservoir rocks. That is why core samples are often rare or, in the case of rocks overlying the reservoir, even unavailable.

The main motivation of this study therefore was to investigate the option of obtaining the required information from outcrop analogues. In outcrops we have the unique opportunity to analyse both

structural elements and geomechanical properties of overburden, and reservoir rocks in detail. It is possible to perform extensive studies on fault zones and associated fracture systems. That means, one can obtain detailed information on typical fault zone structures within rock units, which may serve either as potential geothermal reservoir or which have to be drilled through to reach the prospective reservoir. Furthermore, samples from outcrop analogues are cheap and easy to provide. They provide the opportunity to get representative material of the rock units to perform statistically significant rock mechanical tests to gain knowledge about the rock mechanical conditions at greater depths.

1.3 Aims

This study shall contribute to current exploration and exploitation concepts of sedimentary, volcanic and fault-related geothermal reservoirs in the western part of the NGB – the Northwest German Basin (NWGB) – in Lower Saxony regarding utilisation of normal fault zones, and prediction of geomechanical conditions for drilling and stimulation modelling. This thesis aims at providing data and information on normal fault structure and geomechanical rock properties, based on outcrop analogue studies, with emphasis on the influence of rock heterogeneities. This data is needed to either solve or better handle the above stated challenges of geothermal projects, such as prediction of fault-related reservoir permeability, wellbore stability, and fracture propagation while stimulation. These topics shall be investigated by performing structural geological field studies in outcrop analogues of lithostratigraphic units (sedimentary and volcanic rocks) from Permian to Cretaceous. Field studies are supplemented by laboratory analyses of petrophysical (mainly rock mechanical) properties and petrographic analyses of thin sections as well as numerical modelling.

Particular emphasis shall be placed on following topics:

1. Understanding of normal fault structure and associated fracture systems in typical sedimentary rocks of the NWGB

Detailed structural geological field studies on normal fault zone structure and associated fracture systems in sedimentary rocks are performed in outcrop analogues. The aim is to point out differences of normal fault structure regarding fracture density distributions and structural indices subject to lithology. Further, information on the orientation, apertures, and propagation of both fault-related and background fractures shall be gathered to feature differences between fracture systems in host rock and damage zones. This data is needed to determine today's distribution of elastic properties in normal fault zones which are important input data for future hydromechanical modelling of fault-related geothermal reservoirs.

2. Improving knowledge about geomechanical and physical properties of typical rocks of the NWGB

It is often difficult, time consuming, or even impossible to find appropriate information to determine the required rock properties at varying depths before starting the drilling operation. This study aims at determining geomechanical and physical parameters with importance in different stages of geothermal exploitation of many typical rocks of the NWGB such as UCS, failure and friction criteria, tensile strength, Young's modulus, destruction work, P-wave velocity, density, and porosity. Rock strengths shall be obtained with both uniaxial and triaxial testing to include a simulation of reservoir stress conditions. With this data, a database of rock properties valid for the NWGB is to be compiled. It can be used as input data for numerical modelling of geo- and hydromechanical behaviour of rocks.

As an alternative, it is possible to use empirical relations of similar rocks to estimate the specific parameters of interest indirectly. For example, UCS is widely used in wellbore stability analyses and designing subsurface structures (Zhang 2005). There are existing empirical relations to calculate UCS from well logs of adjacent wellbores to generate geomechanical models before starting to drill. Following such an empirical approach, data shall be used to develop empirical relations between UCS and other parameters which either can be measured with well logs or which are of importance at the

drilling process regarding wellbore stability. Existing empirical relations to predict UCS shall be improved and adapted to the conditions in the NWGB.

3. Analysing if rock properties at reservoir conditions are predictable from a database composed of outcrop samples

The aim is to check properties of core samples, which are assumed to represent rock properties at depths, against properties of equivalent samples from outcrop analogues which are easy and cheap to provide. How results which were determined from analogue samples can be applied to reservoir conditions shall be analysed. With this approach the most important aspects of rock facies (i.e., composition, porosity, texture, etc.) when selecting equivalent outcrop samples are to be evaluated.

Multiple tests on several specimens per outcrop sample shall assure high quality results of all geomechanical and physical rock properties as well as failure criteria from triaxial tests. Results of single core sample measurements are to be compared with outcrop sample data by applying statistical methods. Regression analyses shall be used to analyse the statistical significance of empirical relations and failure criteria. Confidence and prediction bands as well as residual plots are used to check the applicability and significance of calculated regression equations of outcrop samples on the prediction of geomechanical properties of core samples.

4. Analysing the effect of heterogeneous rock properties and pre-existing fractures on hydrofracture propagation

Field observations, experiments, and theoretical considerations have shaped a rough picture of the propagation behaviour of fractures which are formed at hydraulic stimulation. However, the complex hydromechanical behaviour of such fluid-induced fractures, including their geometry and interaction with pre-existing fractures, has not yet been completely understood.

With numerical modelling, factors controlling hydrofracture path and geometry in different geological settings shall be analysed. Special emphasis is placed on the hydromechanical behaviour of fluid-induced fractures under NWGB-specific mechanical and hydraulic loading conditions, and on the interaction with pre-existing fractures. For this purpose, information on fracture systems in volcanic rocks and damage zones (see above) as well as geomechanical properties are used as input data for numerical modelling.

1.4 Thesis structure

The thesis consists of eleven chapters. Chapter 1 comprises introductory sections regarding exploration and exploitation of geothermal energy, motivation, as well as aims and structure of the thesis.

Chapter 2 includes a short depiction of the geologic setting of the field study area and the selected outcrop analogues. Outcrops used for normal fault analyses and for rock mechanical testing are summarized in Tables.

Chapter 3 reviews shortly the used methods regarding field studies, laboratory analyses, statistical evaluation, and hydromechanical modelling.

Chapters 4 to 7 comprise four manuscripts. Chapters are self-contained and can stand alone. The first paper is on normal fault zone structure and associated fracture systems (Chapter 4) and is published in a special issue on fault zones of the "Journal of Structural Geology". The second paper is on empirical relations of geomechanical rock properties and is published in "Geothermal Energy Science" (Chapter 5). Chapter 7 comprises an article presented at the European Geothermal Congress 2013. The manuscript on failure and friction criteria of outcrop and core samples (Chapter 6) is currently under review in the "International Journal of Rock Mechanics and Mining Sciences".

Chapter 4 concentrates on field studies of fracture systems associated with numerous normal fault zones crosscutting sedimentary rocks. The paper presents data on fracture orientations, densities,

apertures and lengths, as well as fault zone structure separately for fault damage zones and host rocks. Differences between carbonate and clastic rocks are analysed. Based on laboratory measurements of Young's moduli and field measurements of fracture densities, calculations of effective stiffnesses E_e, that is the Young's moduli of the in situ rock masses, are performed to analyse today's distribution of elastic properties in normal fault zones. The results are of great importance for modelling the hydromechanical behaviour of normal fault zones in subsurface fluid reservoirs.

The contribution of the co-authors was on the one hand collaborating to field works and interpreting the results. On the other hand the contribution includes discussions about the topic and the structure of the manuscript at an early stage, supplemented by critical reviews of the manuscript.

Chapter 5 comprises investigations of various rock properties with importance in different stages of geothermal exploitation and drilling of typical rocks from the NWGB. Geomechanical (uniaxial compressive strength (UCS), static Young's modulus, destruction work and indirect tensile strength both perpendicular and parallel to layering) and physical parameters (P-wave velocities, porosity, and bulk and grain density) are determined for 35 rock samples from quarries and 14 core samples of sandstones and carbonate rocks. Regression analyses (linear- and non-linear) for UCS with all other parameters were performed to generate empirical relations. The comparability of core and outcrop samples is evaluated with statistical methods such as confidence and prediction bands. The presented equations may help predict UCS values for sedimentary rocks at depth, and thus develop suitable geomechanical models for the adaptation of the drilling strategy on rock mechanical conditions in the NWGB.

The contribution of the co-author includes discussions about the topic as well as critical reviews of the manuscript before submission.

Chapter 6 presents investigations of failure and friction criteria for typical NWGB rocks. Reservoir stress conditions were simulated by conventional triaxial test sequences with varying confining pressures. The aim is to analyse applicability of Mohr-Coulomb failure and friction criteria based on outcrop samples on samples from wells and deep quarry levels. Database consists of one volcanic, three sandstone, and two carbonate samples with equivalent outcrop samples from the NWGB. Equivalence of core and outcrop samples is evaluated using thin section analyses with focus on porosity, cementation, grain size, and mineralogical composition. For outcrop samples, linear regression analyses were performed to calculate Mohr-Coulomb failure and friction criteria from triaxial measurements sequences supplemented by the determination of 90% confidence and prediction bands. Criteria were then applied to the core samples. That is, outcrop failure criteria are used to calculate and predict, respectively, resulting shear stresses. The residuals between calculated and measured shear stresses are presented.

The contribution of the co-author was discussing about the topic before starting the triaxial test series and the structure of the manuscript at an early stage, supplemented by a critical review of the finished manuscript.

Chapter 7 comprises results of numerical modelling of stimulation treatments in typical scenarios of the NGB which may be of geothermal interest. With FRACOD, coupled hydromechanical modelling of fluid-induced fracture propagation was performed. Particular focus was given to layered successions typical for the NGB. The model geometries are adapted to the encountered sedimentary layering of Middle Bunter in the wellbore Groß Buchholz Gt1. Core samples, used for rock mechanical studies in Chapters 5 and 6, were partially taken from the same wellbore. Geomechanical and physical parameters, presented in Chapters 5 and 6 are used as input data for hydromechanical models. For investigations of the trajectory of fluid-induced fractures in this heterogeneous succession, the parameters Young's modulus, Poisson's ratio, and fracture toughness are varied over the total range of observed values for the Middle Bunter from core and outcrop samples. Furthermore, fracture propagation in a set of parallel fractures, similar to fracture systems common in damage zones and

volcanic rocks, is modelled to analyse the interaction between pre-existing fractures and induced hydrofracture regarding fracture path and apertures.

This article was written by Ernesto Meneses Rioseco (Leibniz Institute for Applied Geophysics). I contributed to the model built-up regarding geometry development and providing input parameters as well as to the geoscientific interpretation of the modelling results.

Chapter 8 contains continuative results from laboratory measurements. Aspects of sandstone texture and composition are investigated regarding possible correlations with UCS. In addition, for each sample, presented in Chapter 5, the shape and scale effect on UCS values is shortly investigated by regression analysis of the two unconfined compressive strengths (2:1 and 1:1 length-diameter ratio). The change of Young's modulus with increasing confining pressure was assessed for all samples with triaxial tests (cf., Chapter 6). Finally, the effect of varying fault angles on failure criteria expressed in both principal stresses and normal/shear stresses is investigated.

Chapter 9 contains a comprehensive discussion of the results presented in Chapter 4 to 8. Special emphasis is placed on effects of rock heterogeneities on normal fault structure, mechanical rock properties, and fracture propagation simulated with hydromechanical models.

Chapter 10 contains summarizing conclusions drawn from the results that were presented in the four manuscripts and the continuative results of laboratory analyses (Chapters 4-8).

Chapter 11 explores perspectives deduced from achieved results regarding future geothermal exploration and exploitation in the NWGB.

2   Geologic setting and field work

The NGB initiated in the Late Carboniferous to Permian due to rifting processes subsequent to the Variscan Orogenesis (e.g., Ziegler 1990). The sedimentary succession is characterised by changing sedimentation environments from marine to continental conditions. Therefore the NGB is comprised of mainly carbonate and clastic rocks with some intercalated evaporates leading to very heterogeneous rock mechanical conditions which shall be investigated in this thesis. More details about the geologic setting are described in Chapter 4, Section 2.

Field study area is located at the southern and western margins of the NWGB, mostly within Lower Saxony (Figure 2.1). Sedimentary and volcanic rocks that occur at geothermal relevant depths in the centre and north of the NWGB crop out at the basin margins and can be studied and sampled in quarries. The field studies concentrate on two main topics:

1. Analyses of normal fault zone structure and associated fracture systems

2. Systematic sampling for analyses of heterogeneous geomechanical properties
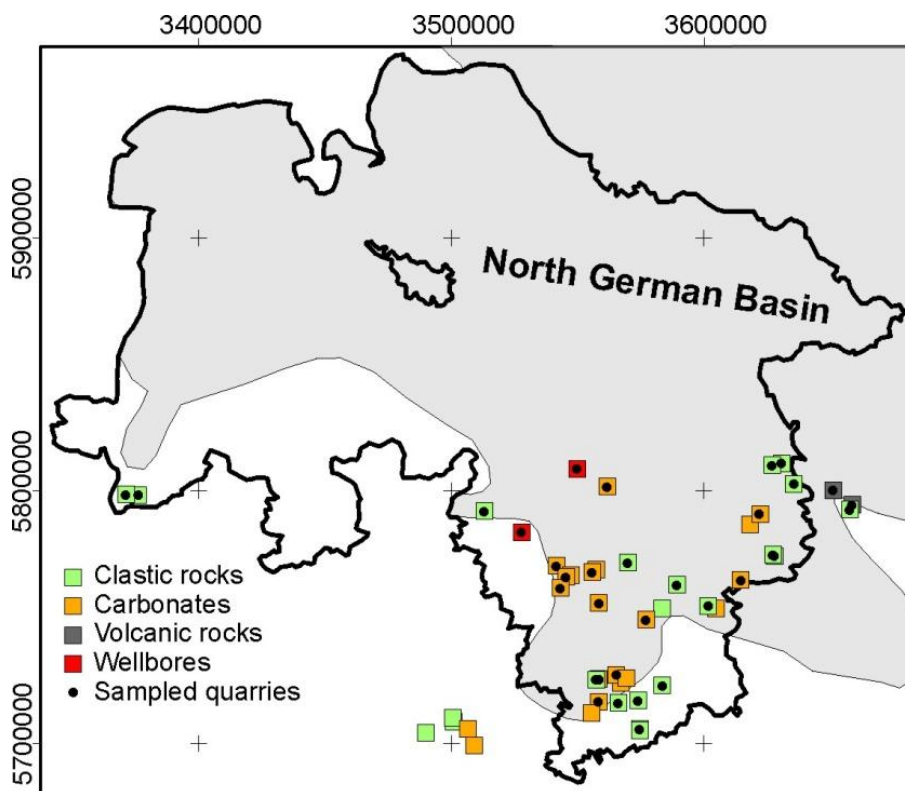
Figure 2.1: Location and lithology of all studied outcrops and wellbores at the southwestern margins of the North German Basin in Lower Saxony, Germany. Sampled quarries are marked (see key).

Structural geological field analyses and sampling were carried out in 40 outcrops, including quarries, road cuts, etc., exposing stratigraphic units of Upper Carboniferous to Upper Cretaceous. In 22 of these outcrops fracture system parameters associated with normal fault zones crosscutting sedimentary rocks were analysed (Table 2.1). Thirty-five normal faults are hosted in carbonate rocks, seventeen in clastic rocks and six in the so-called "Rogenstein", an oolitic limestone (cf. Chapter 4).

Table 2.1: List of all outcrops in which normal fault zone studies were carried out (cf. Figure 2.1); quarries, which are printed in bold italic, were additionally sampled for geomechanical testing; sample-ID in parenthesis (cf. Table 2.2).

Outcrop	Lithology	System	Local Name	Location (R, H)
Höver (KrCa)	Chalk marl		Kreidemergel	3561295, 5801360
Eberholzen	Limestone		Turon-Kalk	3557065, 5768455
Brüggen (BrCe)	Limestone	**Cretaceous**	Cenoman-Kalk	3555425, 5767345
Obernkirchen (OK)	Sandstone		Wealden-Sst.	3512950, 5791580
Varrigsen (GVa)	Limestone		Gigas Schichten	3558025, 5755240
Marienhagen	Limestone	**Jurassic**	Korallenoolith	3547340, 5766700
Salzhemmendorf (ShJk)	Limestone		Korallenoolith	3541455, 5769995
Velpke (koVe)	Sandstone		Rhät-Sst.	3630335, 5810610
Evessen	Limestone		Trochitenkalk (mo1)	3617845, 5786375
Hessenbühl	Limestone		Trochitenkalk (mo1)	3505140, 5705550
Hardgesen (H)	Limestone		Schaumkalk	3558030, 5725220
Emmenhausen (EM)	Limestone		mo1+Wellenkalk	3557935, 5716250
Elvese (EL1-3)	Limestone	**Triassic**	Gelbkalk+Wellenkalk	3567815, 5726650
Ossenfeld	Limestone		Wellenkalk	3555225, 5711735
Papenberg	Limestone		Wellenkalk	3566650, 5723480
Petersberg	Limestone		Wellenkalk	3508880, 5698940
Steinberg	Sandstone		Solling-Folge	3500675, 5708355
Erbbegräbnis	Sandstone		Detfurth-Folge	3500200, 5709950
Heeseberg (suHe)	Rogenstein		Rogenstein	3627660, 5773810
Bilshausen (BiSu)	Sandstone		Bernburg-Folge	3583215, 5722735
Seesen	Sandstone	**Permian**	Rotliegend-Sst.	3582945, 5753280
Marsberg	Siltstone	**Carboniferous**	Oberkarbon	3489506, 5703830

Sst.: Sandstone; F.: Formation

In 29 outcrops oriented samples were taken to measure the physical and geomechanical properties of the rocks. Additionally, failure and friction criteria are determined for eighteen of these samples. For studies on applicability of outcrop sample results on reservoir conditions fourteen samples from two wellbores were taken (Figure 2.1, Table 2.2; cf. Chapters 5-6).

Table 2.2: All samples from outcrops and wellbores (cf., Fig. 2.1) with sample-ID, local name, lithology, stratigraphical units, and core sample depths.

Sample-ID	Lithology	System	Local Name	
KrCa	Chalk marl		Kreidemergel	
GoSa	Sandstone		Sudmerberg-Formation	
HoT	Marl		Rotpläner	
BrCe	Limestone	**Cretaceous**	Cenoman-Kalk	
OLH	Sandstone		Hils-Sst.	
GiUK	Sandstone		Gildehaus-Sst.	
FrUK	Sandstone		Bentheimer-Sst.	
OK	Sandstone		Wealden-Sst.	
ThüJ	Limestone		Serpulit	
GVa	Limestone		Gigas Schichten	
OKDa	Limestone	**Jurassic**	Oberer Kimmeridge	
ShJk	Limestone		Korallenoolith	
HSDi, HSDi2	Limestones		Heersumer Schichten	
AlWo	Sandstone		Aalen-Sst.	
koQ	Sandstone		Rhät-Sst.	
koVe	Sandstone		Rhät-Sst.	
kuWe	Siltstone		Lettenkohlen-Sst.	
EM	Limestone		Trochitenkalk (mo1)	
H	Limestone		Schaumkalk	
EL1, EL2, EL3	Limestones	**Triassic**	Wellenkalk	
soWa	Shale-Gypsum		Röt 1	
smHN	Sandstone		Hardegsen-Folge	
smD	Sandstone		Detfurth-Folge	
smVG, smVG2	Sandstones		Volpriehausen-Folge	
suHe	Limestone		Rogenstein	
BiSu	Sandstone		Bernburg-Folge	
BeRo, BeRoK	Sandstones		Rotliegend-Sst.	
DöRo	Andesite	**Permian**	Rotliegend-Vulkanit	
FL2, FL6	Rhyolites		Rotliegend-Vulkanit	
	Wellbore 1: Eulenflucht 1 (EF1)			
	Wellbore 2: Groß Buchholz (Gt1)			**TVD [m]**
Gt1WS1	Sandstone		Wealden-Sst.	1221
Gt1WS2	Sandstone	**Cretaceous**	Wealden-Sst.	1211
EF1WS	Sandstone		Wealden-Sst.	35
EF1GS	Limestone		Gigas Schichten	210
EF1OK	Limestone		Oberer Kimmeridge	243
EF1UKK	Limestone	**Jurassic**	Korallenoolith	282
EF1KO	Limestone		Korallenoolith	286
EF1HS	Limestone		Heersumer Schichten	325
Gt1DU1	Sandstone		Detfurth-Folge	~3535.8
Gt1DU2	Sandstone		Detfurth-Folge	~3534.3
Gt1DU3	Sandstone	**Triassic**	Detfurth-Folge	~3534.7
Gt1DW	Siltstone		Detfurth-Folge	~3537.2
Gt1VS1	Sandstone		Volpriehausen-Folge	~3655.5
Gt1VS2	Sandstone		Volpriehausen-Folge	~3657.8

Sst.: Sandstone; TVD: Total vertical depth

3   Methodology

The methods used for this thesis include extensive structural geological field studies, carried out in outcrop analogues, and laboratory analyses. Laboratory analyses comprise thin section analyses (rock composition and texture) and measurements of physical (density, porosity, P-wave velocity) and rock mechanical properties (failure and friction criteria, tensile and uniaxial compressive strength, Young's modulus, destruction work).

In the following Sections, the methods used to determine afore mentioned parameters are shortly reviewed.

3.1 Field studies

For all normal fault zones scanline surveys were performed to measure the fracture density distributions transverse to the major slip surface (Figure 3.1a). From the variation of fracture frequencies in the outcrop we determined the damage-zone widths of the normal faults as that part of the fault zone with abrupt significant increase in fracture frequency compared with the host rock.

Each scan line was placed at the structural position of maximum exposed displacement. Structural elements associated with normal faults, including extension fractures, shear fractures, deformation bands and fault cores, were recorded and characterised in detail. For every fracture its orientation (strike direction and dip angle), aperture and length are measured. Relative to the bed thickness fracture termination is analysed, distinguishing 'stratabound' and 'non-stratabound' fractures (Figure 3.1b). Profile lengths were adapted to the total fault zone width to obtain fracture data for both damage zones and undisturbed host rocks. For more details, please see Chapter 4.

In freshly exposed parts of quarries, representative oriented samples were taken for rock testing. In most cases, samples were directly quarried out of single layers by quarriers. Special attention was paid to sample only unfaulted and undamaged parts of the quarries.

a)   b)

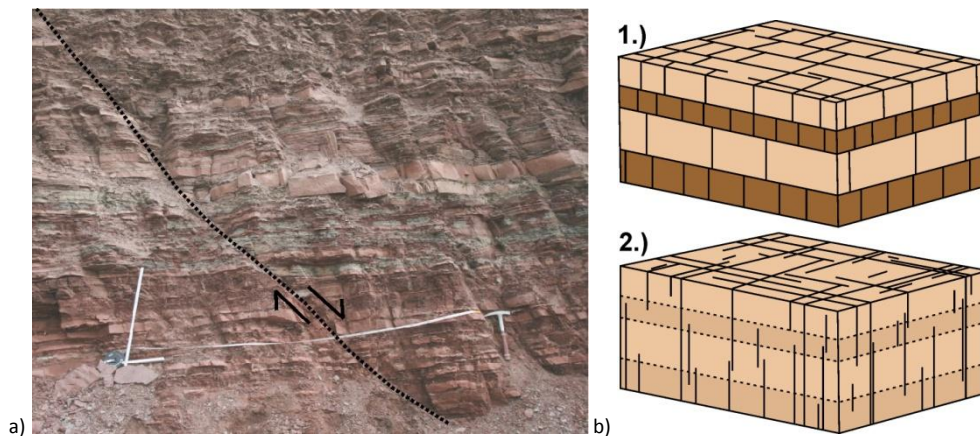**Figure 3.1: a) Scan line placed at maximum exposed displacement of normal fault zone. See hammer on the lower right side for scale. b) Heterogeneities of rock mechanical properties in sedimentary rocks and their effects on fracture propagation: 1.) Strong mechanical layering and mostly stratabound fractures; 2.) Slight mechanical layering and mostly non-stratabound fractures (Odling et al., 1999).**

3.2 Laboratory analyses

3.2.1 Thin section analyses and point-counting

Composition and texture of all triaxial test samples were determined by analysis of one thin section per sample with a transmitted light microscope (Zeiss Axioplan 2). A lithological description can be found in the paper on failure and friction criteria (Chapter 6, Sections 4.2, 4.3).

Additionally, the mineralogical composition of all sandstone samples was measured quantitatively. From each thin section a total of 500 grains was analysed while counting with a half-automated point counter (Petrolog lite). Point spacing was 0.2-0.4 mm on each line, depending on the grain size. Equally spaced lines all over the thin section were used. In Chapter 6 (Section 4.1), results are presented in QFL-plots (McBride 1963) considering only quartz, feldspar and lithoclasts. A more comprehensive presentation is found in Chapter 8.1.

3.2.2 Specimen preparation

Oriented rock samples were taken in outcrops. Using water-cooled diamond hollow drills cylindrical specimens are prepared both parallel and perpendicular to the sedimentary layering. For uniaxial compression tests diameters of 40 mm (length-diameter-ratio (L/D) of 2:1) and 50 mm (L/D 1:1) are required. Diameters of 40 mm are used for Brazilian tests, and of 30 mm for triaxial tests, respectively. These specimens were cut water-cooled on a diamond saw to the appropriate lengths (see next sections). For uniaxial compression and triaxial tests, the specimens' flat surfaces were ground plane-parallel on a water-cooled grinder.

P-wave velocities were determined (Tektronix TDS 5034B; 1 MHz rectangular pulse) for all samples to eliminate defective specimens. P-wave velocities are presented in Chapter 5.

3.2.3 Density and porosity measurements

At the Leibniz Institute for Applied Geophysics (LIAG; Petrophysics and Borehole Geophysics), density measurements were performed. With a GeoPyc 1360 (Micromeritics) the bulk density ρ_d [g/cm^3] was determined on dry cylindrical specimens (diameter 30 mm; lengths 40 mm), setting measured volume and mass in relation. For the same samples, we measured the grain density ρ_0 [g/cm^3] with Ultrapyknometer 1000 (Quantachrome) at room temperature using 99.9% helium, previously measured bulk densities ρ_d and masses of the samples. The porosity, Φ, given in [%], is calculated as ratio of bulk and grain density. Results of density and porosity measurements are presented in Chapter 5.

3.2.4 Uniaxial compression tests

The uniaxial compression test (ISRM 2007; Figure 3.2) was performed for dry specimens with two different L/D: between 2.0 and 2.5 for determination of both, normal UCS and static elastic modulus (Young's modulus), and between 1.0 and 1.1 for maximum UCS. Both parameters were measured parallel and perpendicular to the sedimentary layering.
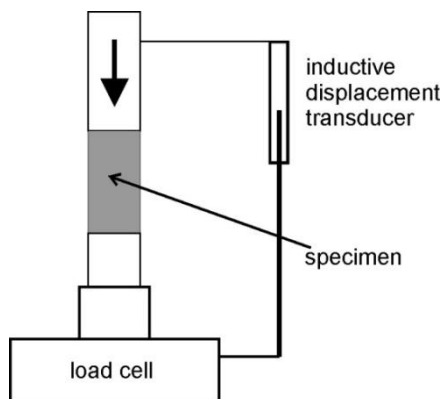

Figure 3.2: Schematic set-up of uniaxial testing apparatus.

After a pre-load of about 70% of UCS (only for 2:1 specimens), the specimens were loaded to failure at a constant rate of stress application of approximately 0.5 MPa/s. During the loading process, axial

stress and strain were recorded. The static Young's modulus, E_s, is determined from the stress-strain curve of pre-loaded 2:1 specimen. For rock samples showing brittle failure, the destruction work, W (Thuro 1997), was determined as the area below the stress strain curve, given in kJ/m^3.

For each sample, a minimum of five, better six specimens were measured both parallel and perpendicular to sedimentary layering to consider variations of strength in consequence of rock heterogeneities. Due to limited material core sample strength values were determined from only two to three specimens per sample.

Results of 2:1 UCS measurements are presented in Chapter 5. A comparison of results from different L/D ratios is given in Chapter 8.2.

3.2.5 Brazilian test

In the Brazilian test (ISRM 2007; diametral compressive strength test), diametral compressive load F is applied to a disc-shaped rock specimen (diameter D: 40 mm; height H: 15-20 mm) until tensile failure occurs (Figure 3.3). The specimens were loaded until failure at a constant rate of load application of approximately 30 N/s. With the F_{max} values, determined by Brazilian tests, the indirect tensile strength T_0 [MPa] was calculated. For each sample, a minimum of six, better nine specimens were measured in both directions: parallel and perpendicular to sedimentary layering. Due to limited material core sample tensile strength values were determined from only four to five specimens per sample. Results of Brazilian tests are presented in Chapter 5.
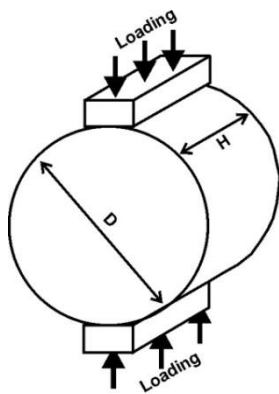
Figure 3.3: Schematic set-up of Brazilian test apparatus with definition of specimen's height H and diameter D.

3.2.6 Triaxial tests

At the Ruhr-University of Bochum, Department of Geophysics, conventional triaxial tests were performed on six core samples with equivalent samples from outcrop analogues as well as 12 additional selected samples from quarries. For each outcrop sample a total of five cylindrical specimens were measured. Due to limited core material it was only possible to measure one to two specimens per core sample. Specimens have diameters of 30 mm and lengths of 60 to 65 mm.

For triaxial tests, a pressure vessel using oil as the confining medium is utilized (Figure 3.4). To prevent oil penetrating the specimen, pistons and specimen are jacketed by a rubber tube. The rock samples, loaded with a constant confining pressure, are strained in axial direction with a constant velocity of 5.4 mm/h until failure occurs. Confining pressure is determined by a pressure gage (± 0.01 MPa). Changes in confining pressures in the vessel while loading are counteracted by movement of the volumometer piston keeping confining pressure constant within ± 0.02 MPa. Displacement transducers measure the volumometer position (± 0.3 mm) as well as the axial displacement (± 0.04 mm). The axial load is determined with an external load cell (± 0.5 kN).
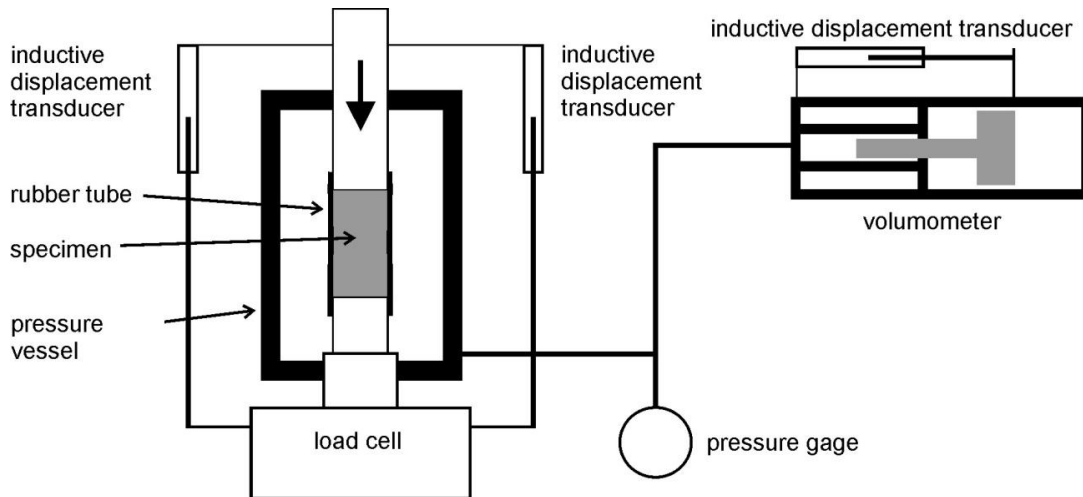
Confining pressures are chosen with respect to the maximum depths in which the different rock units occur. For example, maximum depth of Wealden sandstone (Lower Cretaceous) in Lower Saxony is 2500-3000 m (NIBIS Kartenserver 2012). In the NGB this depth corresponds to a minimum principal stress of 60 MPa (Röckel and Lempp 2003). The set of triaxial measurements of Wealden sandstone sample (OK; cf. Table 2.2) is consequently performed with confining pressures of 10, 20, 30, 50 and 60 MPa (cf. Chapter 6). For stratigraphic units which occur at greater depths, appropriate higher confining pressures are chosen.

Confining pressure, specimen's volume changes, axial displacement and axial load are recorded continuously. Recorded data were examined with the software MATLAB according to the standardized method of the Ruhr-University of Bochum (personally communicated by Dr. Duda). This procedure secures the data quality of the achieved parameters peak stress, residual stress, Poisson's ratio, and Young's modulus for all samples.

Linear fracture and friction criteria are derived from linear regressions of maximum ($\Delta\sigma_{max}$) and residual stress differences ($\Delta\sigma_{res}$) and confining pressure p_c. The Mohr-Coulomb failure criterion, expressed in principal stresses, is

$$\Delta\sigma_{max} = C_0 + \mu \, p_c \qquad\qquad \text{Eq. 1}$$

with unconfined compressive strength C_0 and the slope of the failure line μ (Jaeger et al. 2007). Mohr-Coulomb failure criterion, expressed in normal and shear stresses, is

$$\tau = \tau_f + \mu_i \, \sigma_n \qquad\qquad \text{Eq. 2}$$

with: $\quad \tau = \Delta\sigma_{max}/2 \, \sin(2\beta) \qquad\qquad \text{Eq. 3}$

$$\sigma_n = p_c + \Delta\sigma_{max}/2(1+\cos(2\beta)) \qquad\qquad \text{Eq. 4}$$

τ_f is the cohesive strength and μ_i is the coefficient of internal friction. Shear (τ) and normal stresses (σ_n) are calculated taking into account the dip angle β - angle between fault normal and maximum principal stress σ_1 - of observed induced shear fractures (Figure 3.5).
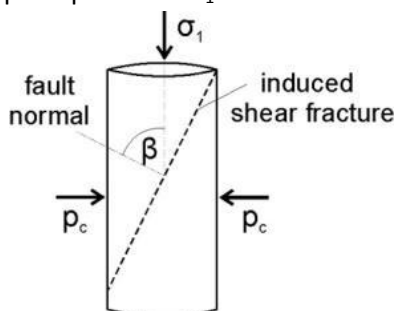
Figure 3.5: Definition of dip angle β of the induced shear fracture in the test specimen subject to maximum principal stress σ_1 and confining pressure p_c at conventional triaxial tests (mod. from Fjaer et al. 2008).

Friction criterion is calculated with friction cohesion (τ_0) and coefficient of friction (μ_{fric}) from residual shear (τ_{res}) and normal stresses ($\sigma_{n,res}$):

$$\tau_{res} = \tau_0 + \mu_{fric}\, \sigma_{n,res} \qquad\qquad \text{Eq. 5}$$

with:
$$\tau_{res} = \Delta\sigma_{res}/2\,\sin(2\beta) \qquad\qquad \text{Eq. 6}$$

$$\sigma_{n,res} = p_c + \Delta\sigma_{res}/2\,(1+\cos(2\beta)) \qquad\qquad \text{Eq. 7}$$

Results are compiled and extensively discussed in Chapter 6.

3.3 Statistical Analyses

This study includes lots of measurements to generate appropriate and trust-worthy results of rock properties. Both univariate and bivariate statistical analyses were used to interpret and investigate these data appropriately. Statistical analyses were performed with Origin 8.5G.

Univariate analyses comprise calculations of mean values and standard deviations for all geomechanical and physical parameters which are measured on several specimens per sample. Results are presented in Chapter 5, Sections 4.1 and 4.2. Bivariate analyses comprise linear and nonlinear regression analyses to estimate possible relationships between different parameters. The goal of regression analysis is to learn more about the relationship between an independent (predictor) variable and a dependent (criterion) variable (e.g., Wooldridge 2009).

In Chapter 5, regression analyses are used to analyse relationships of UCS (L/D of 2:1) with the parameters porosity Φ, bulk density ρ_d, compressional wave velocity V_p, static Young's modulus E_s, destruction work W, and indirect tensile strength T_0. Different regression analyses were performed for each pair of parameters. In the first step all samples together are taken into account. The second step comprises a separate analysis for sandstone and carbonate samples. In each case, regressions were made both for outcrop samples only and for all samples including core samples to examine if results from core samples plot in the same range of values as outcrop samples. For more details, please see Chapter 5.

In Chapter 6, linear regression analyses are used to determine Mohr-Coulomb failure and friction criteria from triaxial test data of outcrop samples. The statistical significance of all these regression equations and empirical relations, respectively, is evaluated by calculating coefficients of determination, residuals as well as 90% confidence and prediction bands:

Coefficients of determination

The coefficient of determination R^2 gives the dimension of the variance of the dependent variable which is predictable from an independent variable. It is a measure of how certain one can be in making predictions from the calculated regression equation. R^2 therefore evaluates the model fit of the respective regression equation (Brink 2010).

Confidence and prediction bands

A confidence band covers the area in which the true curve of the empirical relation plots with a prescribed probability, in this case 90%. It consequently represents the uncertainty of the true position of the curve. The width of the confidence band displays the quality of the best-fit curve (Wooldridge 2009).

A prediction band, in contrast, encloses the area which contains with a prescribed probability single results of future measurements of samples from the same data set (Wooldridge 2009). It can therefore be used for analysing the quality of predicted values of future measurements using the best-fit empirical relation.

Residual plots are used to assess the quality of the regression. The residual is defined as (Brink 2010):

$$r_i = y - y_i \qquad\qquad \text{Eq. 8}$$

where y is the observed value and y_i the predicted value. Residual plots of failure and friction criteria can be found in Chapter 6. The failure and friction criteria determined for equivalent outcrop samples were applied to respective core samples. That is, outcrop failure criteria are used to calculate and predict resulting shear stresses. This method bases on the assumption that core sample failure and friction values belong to the same population as the original data set of outcrop samples. That is, the determined outcrop failure and friction criteria are applied on core sample data, to analyse, if there is a statistical possibility that properties of core samples are predictable from outcrop data. For core samples, residuals between calculated and measured shear stresses and maximum differential stresses, respectively, were determined with Eq. 8. Results are presented in percent deviation to ensure comparability between the different samples.

3.4 Hydromechanical modelling with FRACOD

Fracture propagation code (FRACOD) is a 2D modelling code that was developed for the simulation of fracture initiation and growth in elastic and isotropic rocks and rock failure analysis (Shen et al. 2013). The code is based on the boundary element method (BEM). The BEM is an integral method which solves the problem in terms of surface values (Brebbia and Dominguez 1992). The advantage over other methods (e.g., finite element method: FEM) is that the problem requires discretizing solely of boundaries, not of the whole volume. That is, in FRACOD 2D-models fracture surfaces are represented by line elements. Complex geometries can be reproduced correctly and, in comparison with FEM, the modelling time is reduced. Especially, for surface problems, such as fracture propagation modelling, BEM gives exact values because values are integrated over the boundary and not extrapolated over an element (FEM).
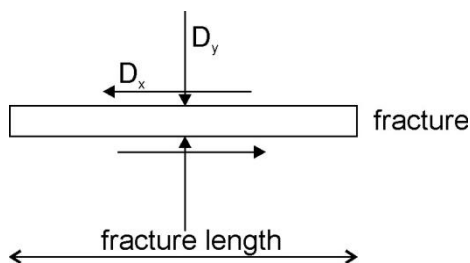
Figure 3.6: Constant displacement discontinuity components D_x and D_y (Shen 2013).

FRACOD utilises the Displacement Discontinuity Method (DDM), one of the three commonly used BEM (Shen et al. 2013). DDM respects the fact that a fracture has two surfaces (boundaries), one effectively coinciding with the other. It bases on the analytical solution to the problem of a constant discontinuity in displacement over a finite line segment in the 2D-plane of an elastic solid (Figure 3.6; Shen 2013). The displacement discontinuity D is determined from differences in displacement between the two sides of the segment, respectively the boundary element, in x and y direction, given by the components D_x and D_y.

FRACOD analyses fracture initiation and propagation in tension (mode I), shear (mode II) and mixed mode of solid intact or fractured rocks (Figure 3.7a). For this purpose, FRACOD incorporates a proposed fracture criterion for fracture propagation by Shen and Stephansson (1993), the G-criterion. In the G-criterion the strain energy release rate at the fracture tip is divided into mode I and mode II deformation. The failure load and its direction are calculated using the sum of normalized values of mode I and mode II deformation. Its mode I component is defined by the tensile strength of rocks; in mode II fracture toughnesses are used. For tensile fracture initiation, the tensile strength is used, for shear fracture initiation, the Mohr-Coulomb failure criterion (cf. Chapter 3.2.6). With measured rock property data, customer-specific adaptations can be made with respect to the modelled rock units. Besides model geometry, boundary conditions, and far-field stresses, following

input data can be included: pre-existing fractures, elastic properties of the rock mass (Young's modulus, Poisson's ratio), fracture toughness, fracture stiffness, fracture friction and cohesion (Shen et al. 2013).
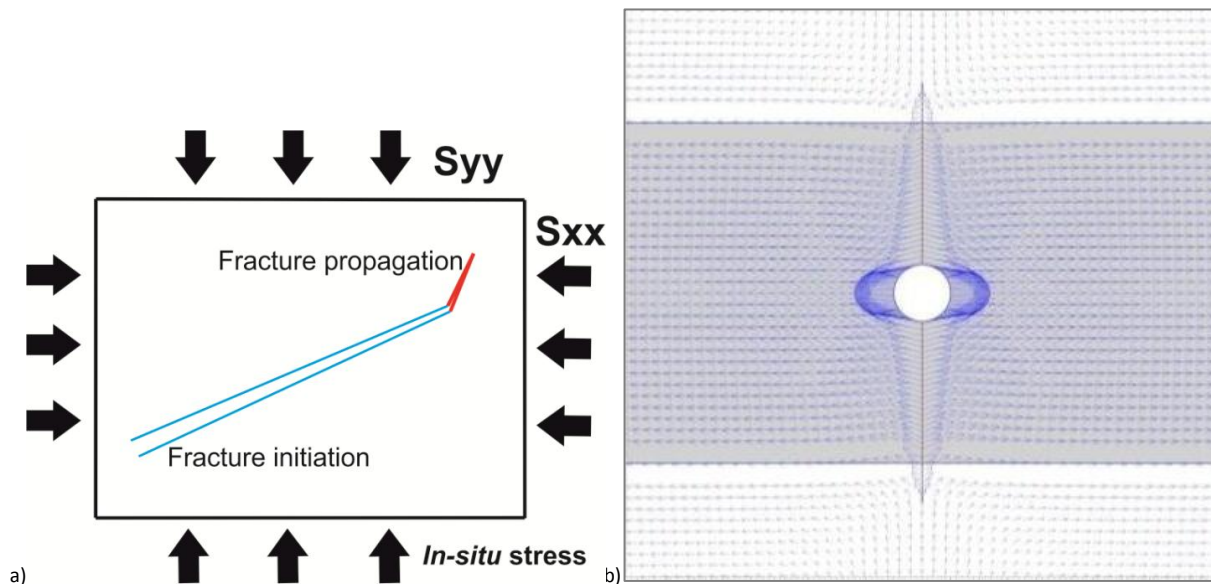
Figure 3.7: a) Schematic sketch of fracture initiation and further propagation within far-field or in-situ stresses as considered in FRACOD; b) Schematic representation of the fluid flow mechanism considered in FRACOD. Note the predominant fracture fluid flow and minor drainage into the rock mass. Different background colours (white and gray) refer to different material properties. Red solid line depicts the hydrofracture. White circle displays the injection hole. Blue arrows exhibit the displacement field (cf. Chapter 7).

Fully coupled hydromechanical modelling of fluid-induced fracture propagation in various model geometries is performed. One scenario displays the fracture propagation in the heterogeneous sedimentary alternation of the Middle Bunter in wellbore Groß Buchholz Gt1. Presented rock properties of samples Gt1DU1-3 and Gt1DW (Detfurth-Folge) were used, which were taken from Gt1 cores. The fracture toughnesses are deduced from measured Young's modulus values according to Yuan and Xi (2011). Another scenario includes pre-existing parallel fractures according to typical fractures in damage zones (cf. Chapter 4) and volcanic rocks. This scenario was calculated for various rock types with determined rock properties. In each case, standard deviations give the used variation of property values. Hydromechanical modelling results are presented in Chapter 7.

4 Fracture systems in normal fault zones crosscutting sedimentary rocks, Northwest German Basin

Dorothea Reyer, Johanna F. Bauer, Sonja L. Philipp

University of Göttingen, Geoscience Centre, Goldschmidtstraße 3, 37077 Göttingen, Germany

Abstract

Field studies of fracture systems associated with 58 normal fault zones crosscutting sedimentary rocks were performed in the Northwest German Basin. Fracture orientations, densities, apertures and lengths, as well as fault zone structural indices, were analysed separately for fault damage zones and host rocks. The results show a pronounced difference between carbonate and clastic rocks: mainly in carbonate rocks we found presence of clear damage zones, characterised by higher fracture densities than in the host rocks. While the maximum aperture is similar for both units, the percentage of fractures with large apertures is much higher in the damage zones than in the host rocks.

Based on laboratory measurements of Young's moduli and field measurements of fracture densities, we calculate effective stiffnesses E_e, that is the Young's moduli of the in situ rock masses, within the normal fault zones. Compared with carbonate rocks, E_e computed for clastic-rock damage zones decreases significantly less due to lower fracture densities. We conclude that normal fault zones in carbonate rocks have more profound effects on enhancing permeability in fluid reservoirs than those in clastic rocks. The results are of great importance for modelling the hydromechanical behaviour of normal fault zones in subsurface fluid reservoirs.

1. Introduction

Normal fault zones are of great interest in terms of crustal fluid flow because they may be zones of increased permeability (e.g., Caine et al., 1996; Caine and Forster, 1999; Faybishenko et al., 2000; Sibson, 2000; Gudmundsson, 2001, 2011; Agosta et al., 2007; Meneghini et al., 2007; Faulkner et al., 2010) and therefore might have a high geothermal potential (Arnorsson, 1995a,b; Paschen et al., 2003; Philipp, 2007; Brogi, 2008). In the Northwest German Basin (NWGB) normal fault zones are of interest as possible geothermal reservoirs (Kehrer et al., 2007; Musmann et al., 2011; Schaumann et al., 2011; http://www.gebo-nds.de). To obtain high flow rates, as well as to minimise the risk in terms of borehole stability while drilling in the NWGB, it is important to assess in detail the fracture distribution within normal fault zones crosscutting sedimentary rocks. With the aim of gaining new insights on fracture orientation, density, aperture and length of NWGB-normal fault zones, we perform structural analysis of selected outcrop analogues. The studied outcrops expose rocks of comparable stratigraphy, lithology and facies to those found at depth.

The simplest description of a normal fault zone structure - and of fault zones in general - considers two major mechanical units, namely a fault core and a damage zone (cf. Caine et al., 1996; Faulkner et al., 2010). The fault core is a narrow zone, formed through repeated slip on the principal fault plane (Faulkner et

al., 2010). Commonly it is brecciated, has a very low stiffness and rather deforms in a plastic manner (Lindsay et al., 1993; Gudmundsson, 2011), whereas cemented fault rocks may have high stiffnesses (Agosta et al., 2007). The damage zone surrounds the fault core and is a wider zone mechanically affected by slip. It is characterised by a high fracture density with still discernible former host rock fabric (e.g., Caine et al., 1996). This two-mechanical-units structure may be difficult to apply to all rock lithologies because different deformation mechanisms may be of importance in different rocks. For example, in porous rocks deformation bands may form (e.g., Aydin, 1978; Antonellini et al., 1994; Johansen et al., 2005), whereas in carbonate rocks there may be stylolites due to dissolution processes (Tondi et al., 2006). In this study, however, the simple damage-zone/fault-core model for normal fault description is convenient since the focus is on the fluid transport potential of normal fault zones, mainly through open fractures.

Depending on the relative displacement across the fracture plane, open fractures are either extension fractures or shear fractures. For extension fractures, the relative displacement is perpendicular to the fracture plane, whereas for shear fractures the relative displacement is parallel to it (Hudson and Harrison, 1997; Jaeger et al., 2007; Twiss and Moores, 2007; Gudmundsson, 2011). However, in the field it is often difficult to distinguish clearly between the different

fracture types. In the following text, we therefore use the general term 'fracture' if the distinction was impossible. Damage zone fractures have various sizes ranging from micrometre-scale to centimetre- to metre-scale. Fractures are typically either parallel or perpendicular to the main fault plane (Stewart and Hancock, 1991; Caine et al., 1996; Agosta and Kirschner, 2003; Agosta and Aydin, 2006; Gudmundsson, 2011). In the fault damage zone, the fracture density (as the number of fractures per unit length) commonly increases towards the fault core (e.g., Simmenes and Gudmundsson, 2002; Agosta and Kirschner, 2003; De Joussineau and Aydin, 2007; Gudmundsson et al., 2010; Gudmundsson, 2011).

To obtain high flow rates in a fluid reservoir, one very important fracture parameter is the fracture aperture. Based on the 'cubic law' (Eq. (1); De Marsily, 1986), a simplified model for flow rate Q [m3/s] calculation where fracture roughness is not taken into account, the cube of the aperture value b [m] is considered:

$$Q = Cb^3i \qquad (1)$$

where C is a constant including the fracture width [m], the fluid density [kg/m3], the dynamic viscosity [Pa s] and the acceleration due to gravity [m/s2], i [-] is the hydraulic gradient. The aperture cumulative frequency commonly follows a power law (Guerriero et al., 2011). That is, most fractures have very small apertures and wider fracture apertures are rare. From Eq. (1), however, it follows that the apertures and lengths of microfractures are too small to have great effects on the resulting fluid flow through normal fault zones. This is the reason why we only analyse fractures with an aperture visible with the naked eye and a length of several centimetres.
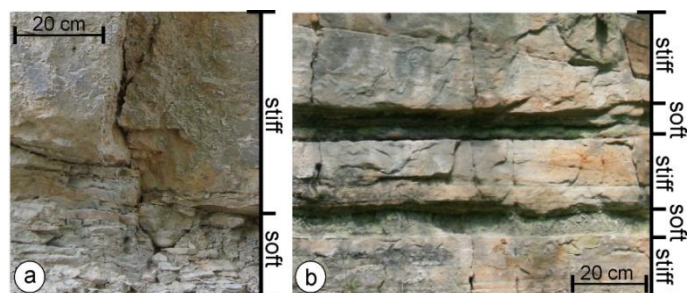

Fig. 4.1. Mechanical layering in sedimentary alternations due to different lithologies. a) Alternation of stiff massy limestones (top) and soft laminated marls (bottom) affecting fracture propagation (Lower Muschelkalk); b) Alternation of stiff sandstones and soft shales (back weathered beds) of Middle Bunter. Fractures mostly are restricted to individual sandstone beds.

A well-connected fracture network is also of great importance to get high permeabilities and flow rates. For analyses of connectivity we distinguish between 'stratabound' fractures, that is, fractures that are restricted to individual beds, and 'non-stratabound' fractures which propagate through several beds

generating fluid flow paths (Odling et al., 1999). In layered rocks such as those of the sedimentary succession in the NWGB, fracture propagation is commonly affected by the mechanical layering (Fig. 4.1) due to stiffness contrasts among adjacent sedimentary beds with different lithologies (Helgeson and Aydin, 1991; Hutchinson and Suo, 1992; Brenner, 2003; Gross and Eyal, 2007). Thus mechanical layering needs to be understood to predict fracture patterns in the subsurface. It is well known (e.g., Brown, 1981; Chang et al., 2006; Hoek, 2007) that well cemented sandstones and limestones have considerably higher values of strengths and stiffness than shales and marls. In the field, we use this relationship to distinguish soft (low Young's modulus) and stiff (higher Young's modulus) sedimentary beds based on lithology.

This paper has two main aims. First, we present the results of structural geological field studies carried out in 58 normal fault zones in sedimentary rocks. Results are shown separately for carbonate- and clastic rocks. We consider the normal fault zone orientations in the context of local geological settings, and focus on damage zone widths, hanging wall and footwall widths as well as overall fault zone displacements. Differences between host rocks and damage zones in terms of fracture orientations, propagation, path, length and aperture are described in detail. In addition, we present the results of mechanical-property measurements of the intact rocks (host rocks) from outcrop samples. The second aim is to use the fracture data and mechanical rock properties to assess analytically the Young's moduli distribution in normal fault zones crosscutting the sedimentary rocks of NWGB. The results of this work will provide input parameters for future numerical models of the hydromechanical behaviour of normal fault zones. Due to normal fault's self-similarity (cf. King, 1983; Turcotte, 1989; Torabi and Berg, 2011), it should be possible to apply presented results to hydromechanical models of larger normal fault zones in fluid reservoirs.

2. Geologic setting

The NWGB (Fig. 4.2), located in Northwest Germany and the southern North Sea, is part of the North German Basin (NGB) which belongs to the intracontinental Central European Basin (Walter 2007). The NGB was initiated in the Late Carboniferous to Permian due to rifting processes with associated volcanism subsequent to the Variscan Orogenesis (Betz et al. 1987; Ziegler 1990). Due to thermally induced subsidence, Rotliegend volcanism started, followed by the sedimentation of Rotliegend clastics and the deposition of several kilometres of sediments from the Upper Rotliegend to the Quaternary (e.g., Baldschuhn et al. 1996).
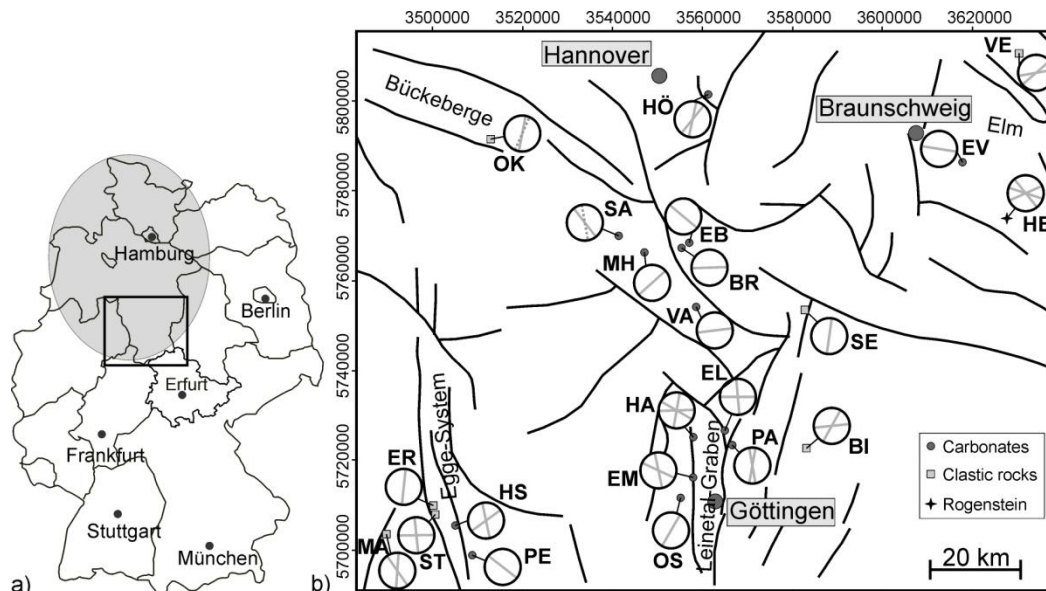
Fig. 4.2. a) Map of Germany and its federal states with the rough location of the NW-German Basin (grey area) and the field study area shown in b); b) Field study area in the southern NWGB; black lines represent important fault systems (simplified after Meiburg 1982; Henningsen and Katzung 2006). Small symbols (see key) represent outcrop localities. In the circles the main normal fault orientations for each outcrop are marked with grey lines (dashed lines represent orientations of fault zones with non-normal components). The abbreviations for the outcrops in the Leinetal-Graben are as follows: EM-Emmenhausen, HA-Hardegsen, EL-Elvese, PA-Papenberg, OS-Ossenfeld (all Middle Triassic), BI-Bilshausen (Lower Triassic). In the Egge-System are MA-Marsberg (Upper Carboniferous), ST-Steinberg, ER-Erbbegräbnis (both Lower Triassic), HS-Hessenbühl, PE-Petersberg (both Middle Triassic). The northern outcrops are OK-Obernkirchen, HÖ-Höver, EB-Eberholzen, BR-Brüggen (all Cretaceous), SA-Salzhemmendorf, MH-Marienhagen, VA-Varrigsen (all Upper Jurassic), VE-Velpke (Upper Triassic), EV-Evessen (Middle Triassic), HE-Heeseberg (Lower Triassic), SE-Seesen (Permian).

The Rotliegend is composed of continental redbeds (Schröder et al. 1995; Glennie 1998) that are discordantly separated from the Zechstein evaporates. Red-coloured clastic rocks, typical for the Lower Triassic (Lower and Middle Bunter), are covered with shales and evaporites (Upper Bunter; Menning and Hendrich 2005). In the Middle Triassic carbonate sediments were deposited (Lower and Upper Muschelkalk) alternating with evaporites (Middle Muschelkalk; Röhl, 1990). The Upper Triassic (Keuper) was characterised by terrestrial sediments (Betz et al. 1987). In the Lower Jurassic (Liassic), because of a worldwide sea level rise marine shales were deposited (Wehner et al. 1989). In the Middle Jurassic (Dogger), more sandstone layers intercalated the marine shales due to decreasing water depths (Menning and Hendrich 2005). In the early Upper Jurassic, the NWGB began to subside and a marine carbonate succession was deposited (Kockel 2002). During the Early Cretaceous, shallow marine carbonates and minor continental sediments (Wealden) formed. Subsequently, a change of the depositional environment towards open marine conditions occurred so that the resulting sedimentary succession consists, up to the end of the Cretaceous, of marls (Mutterlose and Bornemann 2000).

The Permian thermal subsidence was replaced by an east-west extension during the Triassic. In the Jurassic, north-south (N-S) orientated grabens, such as the Leinetal-Graben, formed and, as a consequence, movements of Zechstein salt started (Ziegler 1990). In the Upper Jurassic to Lower Cretaceous the tectonic regime changed to NeS compression causing uplift and reactivation of NW-striking faults and further salt mobilisations. In the Late Cretaceous to Early Cenozoic compressional tectonics due to Alpine Orogenesis (Ziegler 1990) caused fault inversion and, consequently, pronounced erosion of Cretaceous sediments (Petmecky et al., 1999). This phase was replaced by an overall uplift until the end of the Cretaceous (Kockel 2002).

Our study area (Fig. 4.2a, b) is located in the Lower Saxony Basin (LSB), a sub-basin of the NWGB (Betz et al. 1987; Ziegler 1990; Glennie 1998; Scheck-Wenderoth and Lamarche 2005). The study area suffered differential subsidence due to dextral movements along NW-SE-trending faults and, meanwhile, reactivation of Permo-Carboniferous faults (Betz et al. 1987). The Late Cretaceous inversion determined pronounced transpressive slip along preexisting faults (Betz et al. 1987). In particular, faults along the northern and southern margins of the LSB were reactivated (Betz et al. 1987). This led to the preferred development of major fault zones with net normal displacements which may show components of either reverse or strike-slip displacement.

3. Field study area and analysed normal fault zones

The field study area (Fig. 4.2a, b) is located in the southern part of NWGB where two large fault systems crop out: the Leinetal-Graben and the Egge-System. We also studied some less faulted areas in the Weser- and Leine-hills. Structural geological field analyses were carried out in 22 outcrops exposing stratigraphic units of
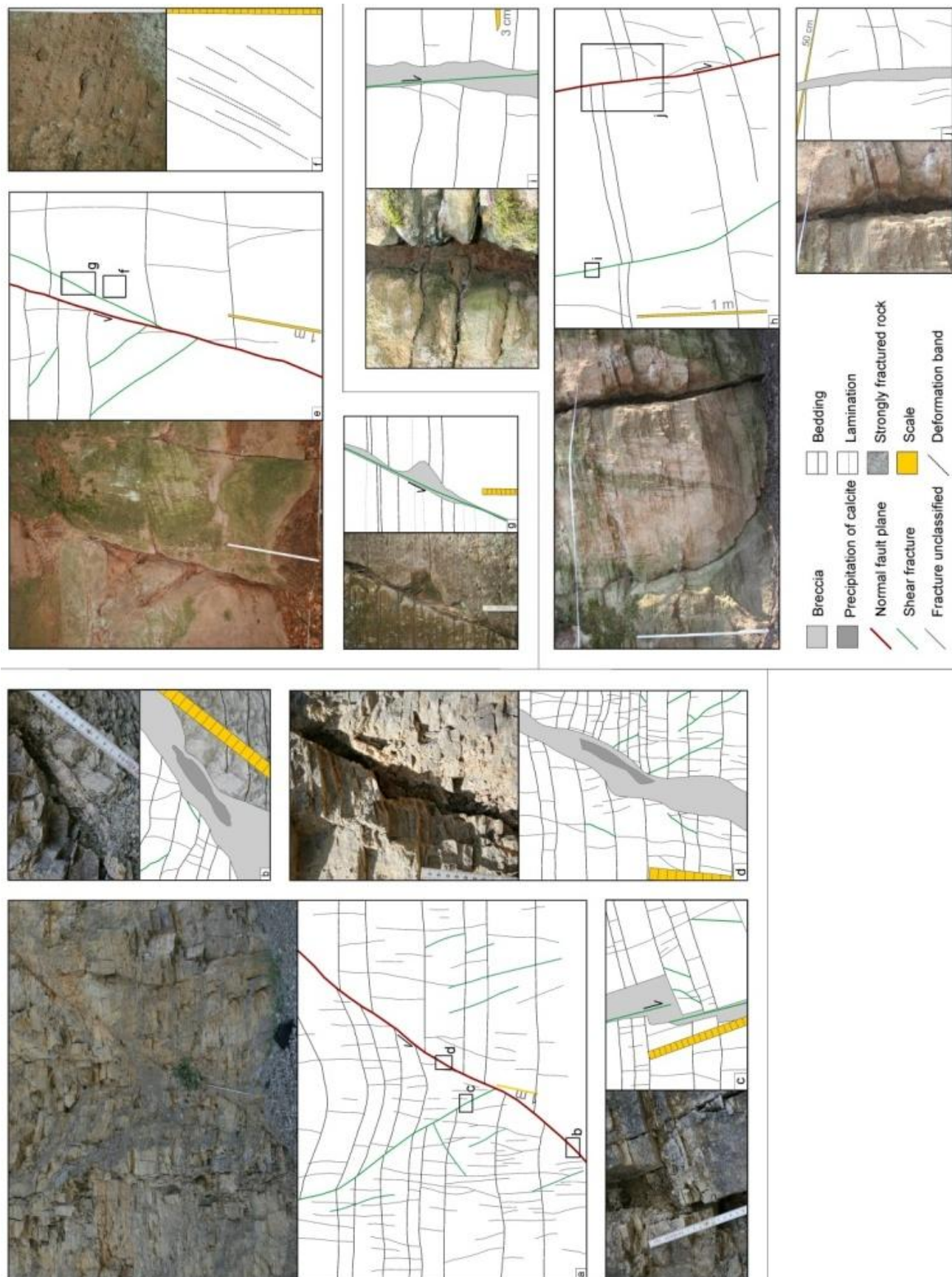
Fig. 4.3. Field photographs of three normal fault zones and structural elements therein (see key; for outcrop locations see Fig. 4.2). a-d) Carbonate rock outcrop EL (Lower Muschelkalk): a) (015/55)-dipping normal fault zone with 1.3 m displacement (View E); b) Brecciated fault core at low-angle position of normal fault with precipitation of calcite and strongly fractured footwall damage zone; c) Shear fractures en-echelon in thin bedded limestone-marl alternation; d) Brecciated fault core at high angle position of normal fault zone with precipitation of calcite and similar fracture densities in footwall and hanging wall; e-g) Sandstone outcrop ST (Middle Triassic): e) (267/74)-dipping normal fault zone with 1.5 m displacement (View S); f) Deformation bands in footwall damage zone, orientation sub-parallel to normal fault plane; g) Shear fracture and bedding-parallel decomposition of hanging-wall rock; h-j) Rogenstein outcrop HE (Lower Bunter): h) (158/78)-dipping normal fault zone with 23 cm displacement (View NE); i) Mixed-mode fracture with large aperture (partly due to weathering) and small displacement (2 mm); j) Brecciated fault core in slightly fractured damage zone.

Upper Carboniferous to Upper Cretaceous ages. We analysed fracture parameters of 58 normal fault zones with displacements of a few centimetres to 50 m. Thirty-five of these normal fault zones are hosted in carbonate rocks, seventeen in sandstones/conglomerates and six in an oolithic limestone with a high porosity (see Figs. 4.2b and 4.3). Latter rocks, called 'Rogenstein', are composed of cemented ooids (Usdowski 1962). In the analysed faulted carbonate rock outcrops there are rocks of Middle Triassic (EM, EL, HA, PA, PE, EV, HS; all abbreviations in Figure caption 4.2), Upper Jurassic (SA, VA, MH) and Upper Cretaceous (BR, EB, HÖ) ages. The clastic rock outcrops are of Upper Carboniferous (MA), Lower Permian (SE), Triassic (BI, ST, ER, VE) and Lower Cretaceous (OK) ages. The 'Rogenstein', defined above, is of Lower Triassic age (HE).

Fig. 4.3 presents field examples of normal fault zones in the three different lithologies. Structural elements, including extension fractures, shear fractures, deformation bands and fault cores, are shown in detail. In all examples most fractures are sub-vertical open extension fractures; fracture densities vary (Figs. 4.3a, c, d, e, h). Along some of the shear fractures (mostly synthetic and antithetic to the main fault planes) small brecciated zones may develop (Figs. 4.3c, g). In the fault cores within carbonate rocks calcite precipitation is common (Figs. 4.3b, d). In clastic rocks and Rogenstein fault cores rather show small brecciated zones, partly opened by weathering (Figs. 4.3e, h, j).

Because of the tectonic inversion (Section 2), two of the studied normal fault zones indicate reactivation (compressional structures or strike-slip displacement;

SA, OK). These fault zones are marked in all the following figures. For small normal fault zones, the maximum displacements were measured by comparing the sedimentary beds perpendicular to fault-strike on both sides of the fault planes (Figs. 4.3a, d, e, h, j). When the displacement exceeds outcrop scale, however, the displacement was determined using lithological data from the quarries.

By adopting a scan line methodology, for all fault zones we measured the fracture density distribution perpendicular to the major slip surface using a measuring tape. Each scan line was placed at the structural position of maximum exposed displacement. Because we dealt with many small-scale fault zones, and did not observe overlapping fault segments within the outcrops (cf. Figs. 4.3a, e, h), this position is expected to be located more or less in the central position of the normal fault zone. When possible, however, we measured both the widths of the fault damage zones and the displacements at several positions to improve the data quality. To obtain fracture data for both damage zones and undisturbed host rocks, we adapted the profile lengths to the width of individual fault damage zones. For every fracture we measured its orientation (strike direction and dip angle), aperture (with a calliper) and length, defined as the linear vertical distance between the two tips in the section (also referred to as 'fracture height'). Finally, we analysed the fracture length relative to the bed thickness, distinguishing 'stratabound' and 'non-stratabound' fractures (cf. Section 1).
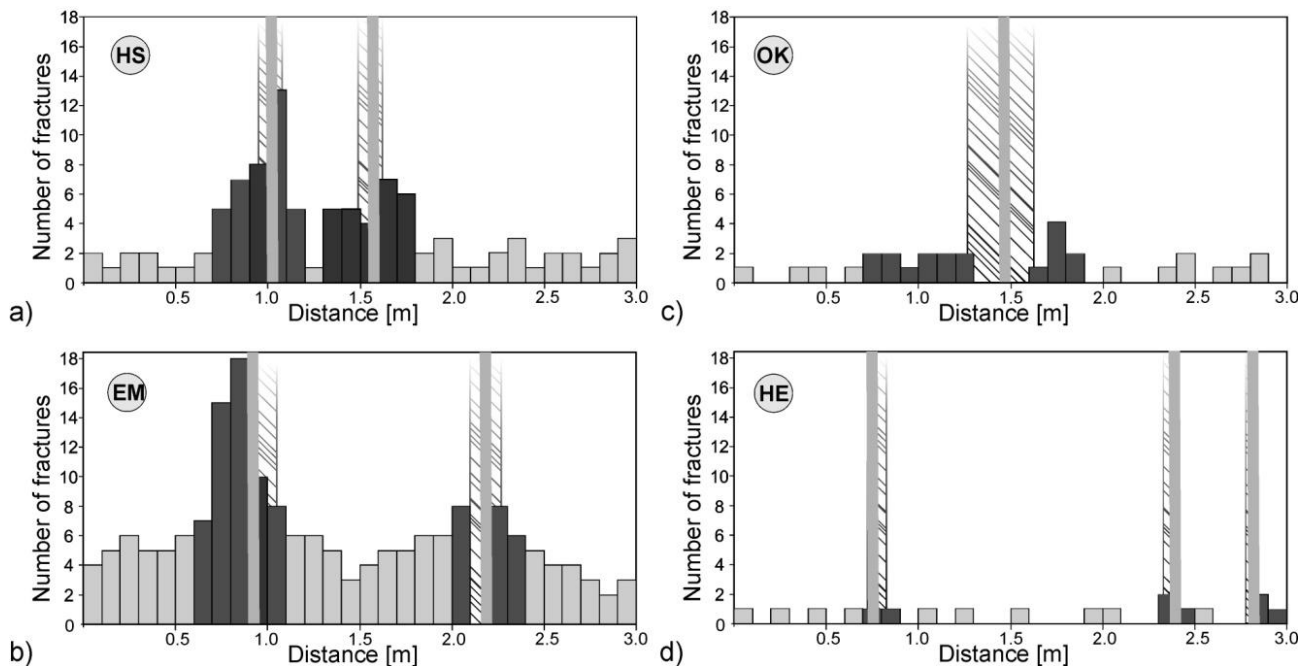
Fig. 4.4. Fracture density distributions perpendicular to normal fault planes for a) HS: Upper Muschelkalk, b) EM: Lower Muschelkalk, c) OK: Lower Cretaceous sandstone, d) HE: Lower Bunter, Rogenstein (outcrop abbreviations in Figure caption 4.2). The grey lines represent the fault plane locations, the dark grey bars show the damage zone widths and the striped rectangles define regions with strong brecciation, so that not every fracture could be detected.
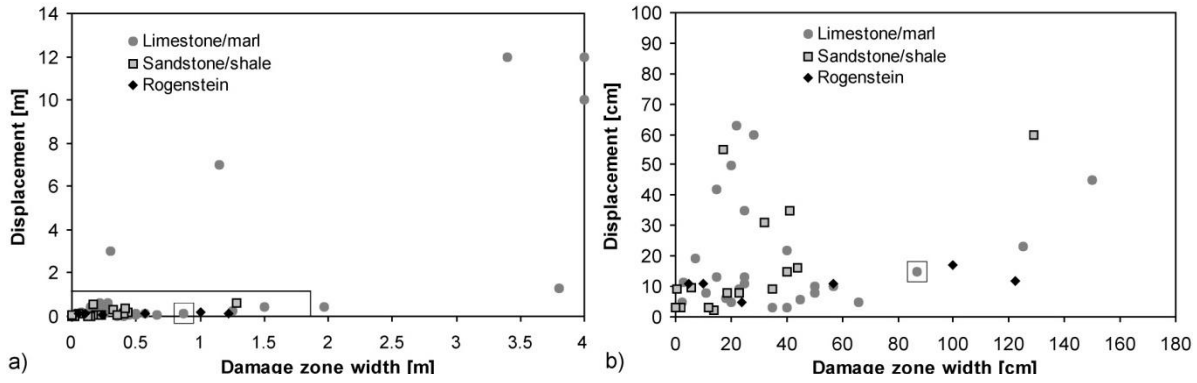
Fig. 4.5. Damage zone width vs. displacement for: a) small-scale to medium-scale normal faults (n=54; without oblique-slip fault OK; inverted fault SA marked by rectangle) and b) only small-scale normal faults (displacements smaller than 70 cm; n=47). The grey box in (a) represents the detail shown in (b).

4. Field results

4.1. Fault zone orientation

The outcrops are mainly located in two fault systems: the Leinetal-Graben and the Egge-System. Seven outcrops are in the vicinity of the N- to NNE-striking Leinetal-Graben faults, five outcrops are associated with the NNW-striking Egge-System faults and 14 outcrops are in the less faulted regions affected by salt-controlled deformation (Fig. 4.2b).

Most of the studied normal fault zones strike parallel to regional structures, others are either conjugate (Anderson 1905) or perpendicular to them. For example, in the EM limestones in (Lower Muschelkalk; Leinetal-Graben; Fig. 4.2b) normal fault zones are either parallel to the NNW-striking western boundary fault or are conjugate to it. In the ST sandstones (Middle Bunter; cf. Fig. 4.3e-g) normal fault zones are either parallel or perpendicular to the major fault (Fig. 4.2b).
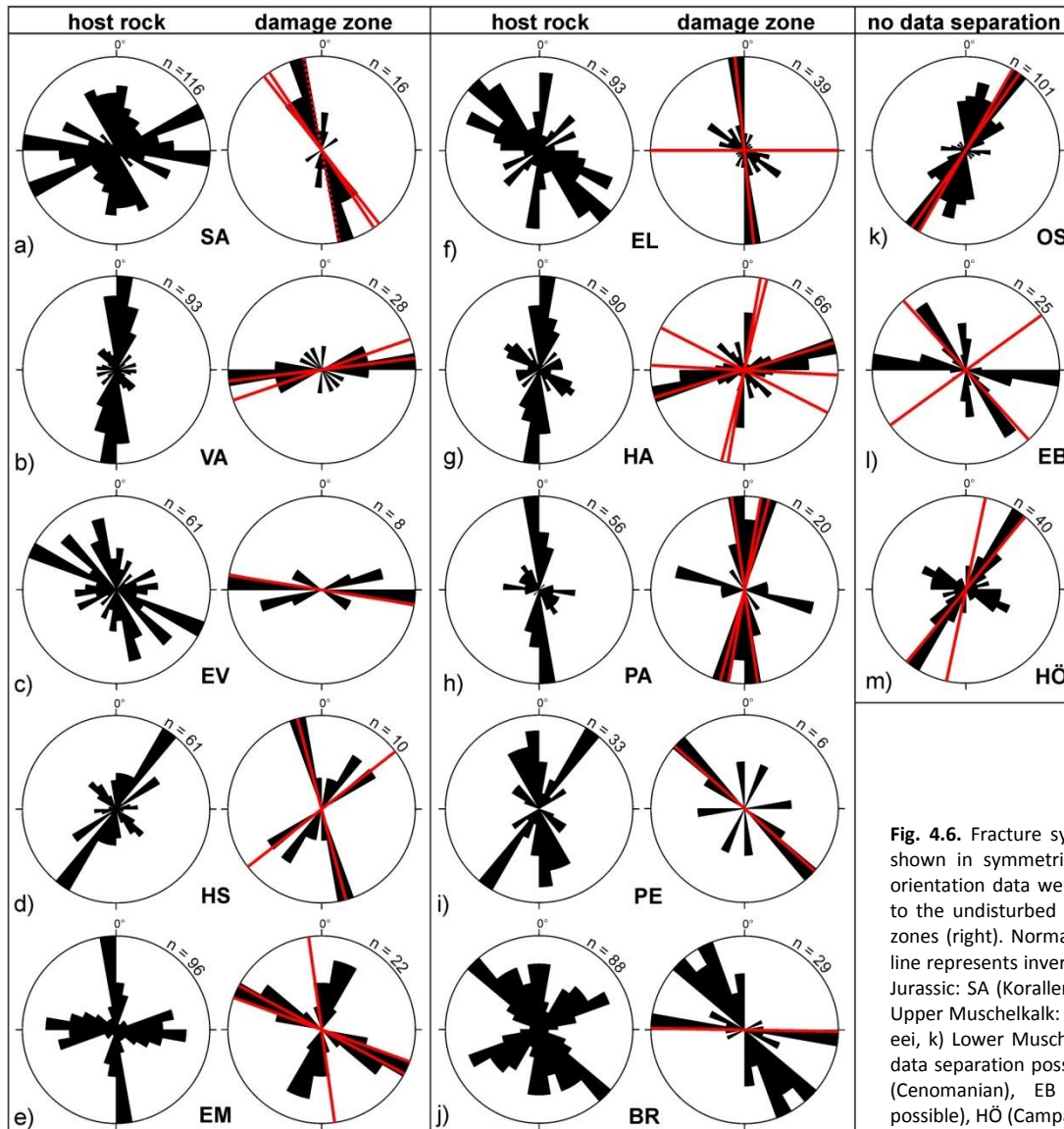
Fig. 4.6. Fracture systems of carbonate rock outcrops shown in symmetrical rose diagrams. If possible the orientation data were separated in fractures belonging to the undisturbed host rocks (left) or to the damage zones (right). Normal fault zone strike marked (dashed line represents inverted normal fault in SA); a, b) Upper Jurassic: SA (Korallenoolith), VA (Gigas-Schichten); c, d) Upper Muschelkalk: EV (weighted to profile length), HS; eei, k) Lower Muschelkalk: EM, EL, HA, PA, PE, OS (no data separation possible); j, l, m) Upper Cretaceous: BR (Cenomanian), EB (Turonian, no data separation possible), HÖ (Campanian, no data separation possible).
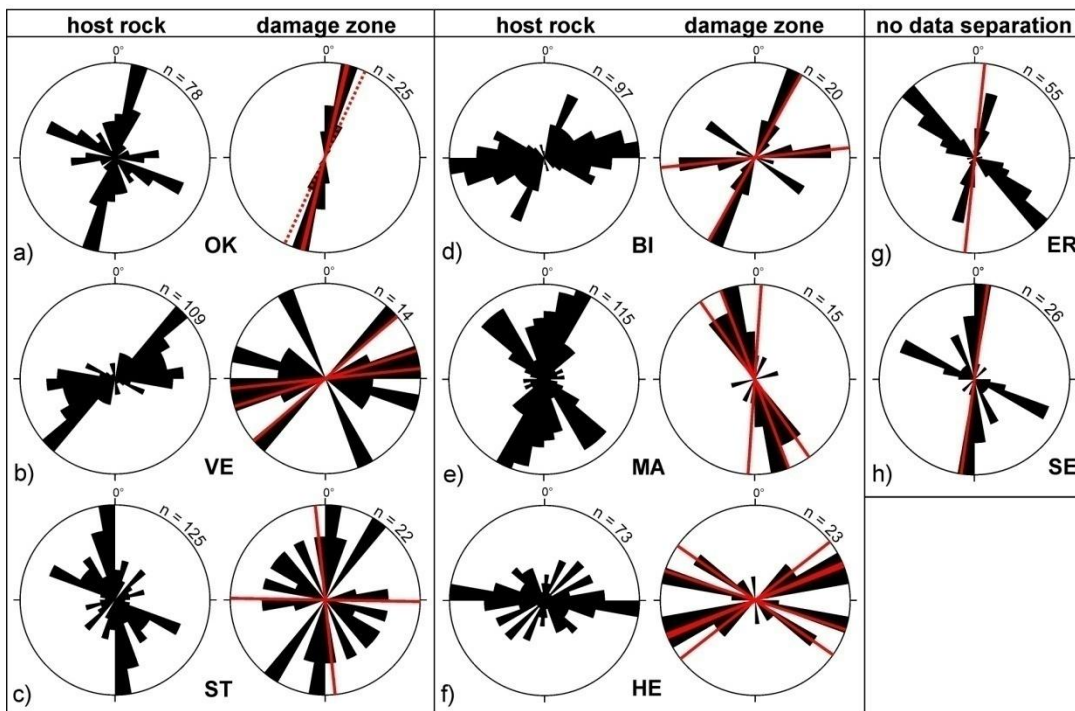
Fig. 4.7. Fracture systems of clastic rock and Rogenstein outcrops shown in symmetrical rose diagrams. If possible the orientation data were separated in fractures belonging to the undisturbed host rock (left) or to the damage zones (right). Normal fault zone strike marked (dashed line represents oblique-slip fault in OK); a) Lower Cretaceous: OK; b) Upper Keuper: VE; c, g) Middle Bunter: ST (Solling Formation), ER (Detfurth Formation, no data separation possible); d) Lower Bunter: BI; e) Upper Carboniferous: MA; g) Lower Bunter: HE (Rogenstein); h) Upper Rotliegend: SE (no data separation possible).

4.2. Fracture density distribution

To obtain a well-founded characterisation of the fracture systems in normal fault zones we determined the fracture density distributions perpendicular to the normal fault planes. That is, we analysed the widths of the damage zones on both sides of the fault planes and how the fracture densities in the damage zones increase compared with the host rocks. In Fig. 4.4, we show representative diagrams for carbonate rocks of Upper (Fig. 4.4a) and Lower Muschelkalk (Fig. 4.4b), Lower Cretaceous sandstone (Fig. 4.4c) and Rogenstein (Fig. 4.4d).

The aforementioned data show a considerable difference between carbonate and clastic rocks. In both clastic rocks (Fig. 4.4c) and porous 'Rogenstein' (Fig. 4.4d), the fracture density does not increase significantly towards the major slip surfaces. In carbonate rocks, in contrast, there is a higher fracture density close to them (Figs. 4.4a, b). In particular, in the Upper Muschelkalk (Fig. 4.4a) the fracture density is, on average, lower than in the thin-bedded limestone-marl alternation of the 'Wellenkalk' (Lower Muschelkalk; Fig. 4.4b).

4.3. Fault damage zone width

A poor positive correlation between damage zone width and fault throw is found in both carbonates and clastic rocks (Fig. 4.5), while data of normal fault zones in Rogenstein show a better correlation. The positive correlation is similar to that documented by Faulkner et al. (2011). In general, the resulting damage zone widths in carbonate rocks are higher than in clastic rocks. Wider clastic rock damage zones, however, may occur in strongly layered rocks, that is, sedimentary alternations with small bed thicknesses comprised of rocks with both different lithologies and varying mechanical properties, such as sandstone/shale or limestone/marl.

4.4. Fracture orientation

For 21 of the 22 outcrops we could collect detailed fracture data. Orientation data are presented, using symmetrical rose diagrams, separately for carbonate and clastic rocks. If possible, we distinguish between fractures present in host rocks and fault damage zones (Figs. 4.5 and 4.6).

The fracture system present in the carbonate host rocks consist of either two or three fracture sets. The main fracture set is commonly parallel to regional structures (e.g., major fault zones; cf. Section 4.1). The second and third fracture sets strike at an angle of about 30° and perpendicular to the main one, respectively (Fig. 4.6). Many normal fault zones strike differently from the regional fracture orientations in the host rocks. That is, for these normal fault zones, the main orientations of the fractures in host rocks and damage zones are deviating (Figs. 4.6b-g, i, j). Damage zone fractures are predominantly sub-parallel to the major slip surfaces; fractures with differing strike directions are rare. If existing, differing fracture orientations are perpendicular or at 30° to the major slip surfaces (Figs. 4.6d, f-h, j). Few fractures in damage zones correspond to the host rock's main regional fracture sets; these fractures can be interpreted as background fractures rather than fault-related fractures (Figs. 4.6a, d).

In clastic sedimentary rocks the fracture systems of the host rocks consist of two main fracture sets. The more

common one is mostly parallel to major regional faults (cf. Fig. 4.2b), the second one is either perpendicular (Fig. 4.7a) or at 30° to it (Figs. 4.7b-g). The fracture densities in the clastic fault damage zones are much lower than in carbonate rocks (cf. Fig. 4.4). In some cases, the clastic fault damage zone is comprised of deformation bands, which are not taken into account here and therefore are not shown in the rose diagrams. Damage zone fractures predominantly strike parallel to the major slip surfaces. In comparison to the damage zone fractures in carbonate rocks, which commonly show deviating strike directions between host rock and fault zone, for clastic rocks it is worth to note that the fracture orientations mostly are similar to the orientations of predominant fracture strike in the host rocks. This is very pronounced for the normal fault zones in Wealden sandstone (Fig. 4.7a), in the Rogenstein of Lower Bunter (Fig. 4.7f) and in the Upper Rotliegend conglomerate (Fig. 4.7h).

All the aforementioned clastic units have in common that they are relatively homogeneous because layering is not very distinct. In sandstones of Rhaetian (Fig. 4.7b) and Middle Bunter (Solling Formation, Fig. 4.7c) age, fracture orientations are generally oblique to the major slip surfaces. In the Lower Bunter (Fig. 4.7d) and the Upper Carboniferous rocks (Fig. 4.7e), fractures are sub-parallel to the fault planes. In the Upper Carboniferous, however, the normal fault strike deviates from the strike direction of the main fracture set in the host rock (Fig. 4.7e). For the strongly layered Detfurth Formation (Middle Bunter, Fig. 7g), it is difficult to distinguish damage zone and host rock. Nevertheless, for this fault zone we determine two fracture sets both striking at an angle of about 30° to the major slip surface.

4.5. Fracture vertical extension

For the analysed normal fault zones the ratios of non-stratabound and stratabound fractures are shown separately for host rocks and damage zones (Fig. 4.8). In general, there is an increase of non-stratabound fractures within fault damage zones. For clastic rocks, the average amount of non-stratabound fractures
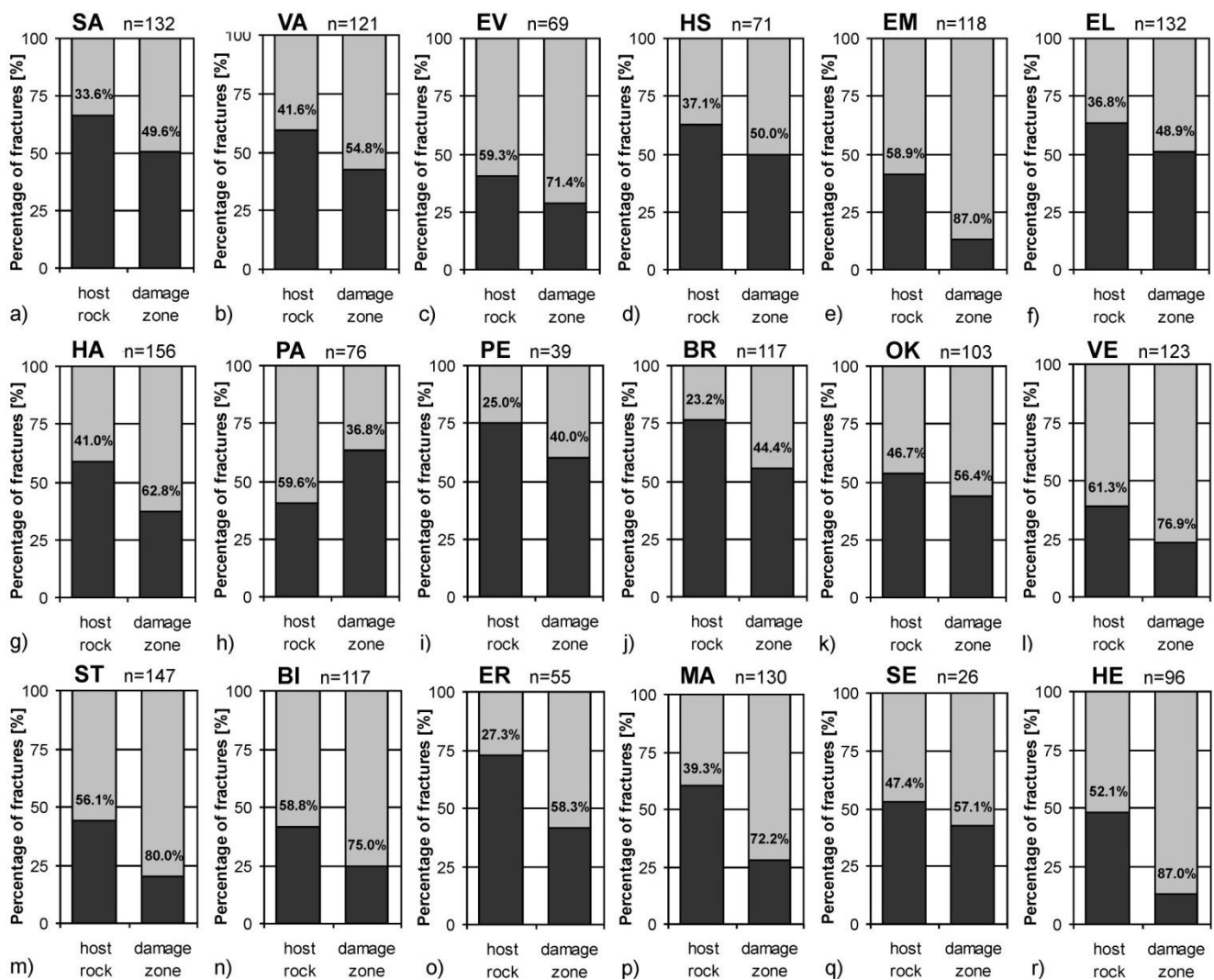
Fig. 8. Fracture propagation in host rocks compared with damage zones. The dark grey bars represent stratabound fractures; the light grey bars stand for non-stratabound fractures. The percentages relate to the amount of non-stratabound fractures. A-j) Carbonate rocks: a, b) Upper Jurassic; c, d) Upper Muschelkalk; e-i) Lower Muschelkalk; j) Upper Creataceous; l-q) Clastic rocks: k) Lower Cretaceous; l) Upper Keuper; m, o) Middle Bunter; n) Lower Bunter; p) Upper Carboniferous; q) Upper Rotliegend; r) Rogenstein: Lower Bunter.

increases from 48% (host rocks) to 68% (fault damage zones), whereas for carbonate rocks the mean value increases from 41.5% (host rock) to 55% (fault damage zone). That is, the general percentage of non-stratabound fractures in carbonate rocks is lower than in clastic rocks. Additionally, the amount of non-stratabound fractures in damage zones compared with the host rocks increases less.

Mechanically layered rocks, defined by abrupt lithological changes affecting fracture propagation (Narr and Suppe 1991; Hoek 2007), are the 'Wellenkalk', a limestone-marl alternation of the Lower Muschelkalk (Figs. 4.8f-i), the Upper Rotliegend (Fig. 4.8q), a conglomerate-shale alternation, and the sandstone-shale alternations of the Upper Carboniferous (Fig. 4.8p) and Detfurth Formation (Middle Bunter; Fig. 4.8o). In these mechanically layered alternations the number of stratabound fractures is generally higher than in more homogeneous units, such as the Upper Muschelkalk (Figs. 4.8c, d), the Upper Jurassic (Fig. 4.8b), the Upper Keuper (Fig. 4.8l) and the Solling Formation (Middle Bunter; Fig. 4.8m). Although the marly carbonate rocks of the Upper Cretaceous (Fig. 4.8j) are also relatively homogeneous, they are predominantly crosscut by stratabound fractures. The marl shows significant decomposition along the lamination which results in large numbers of internal layer-parallel fractures arresting many of the vertical fractures.

4.6. Fracture length and aperture

We plot the fracture apertures and lengths against their strike for carbonate rocks, clastic rocks and Rogenstein (Fig. 4.9). For carbonate rocks, the widest apertures of fault-related fractures are similar to those present only in the host rocks. The percentage of fractures with large apertures, however, is much higher for fractures in damage zones than in the host rocks (Fig. 4.9, left). In many cases, fractures sub-parallel to major slip surfaces show higher values of aperture (Figs. 4.9a, c, d, f, g, h). The distribution of fracture lengths (Fig. 4.9, right) correlates with the apertures, which is consistent with longer fractures being commonly characterised by wider apertures (Figs. 4.9a, c, d, f, g, h). In the host rocks (Fig. 4.9, black squares), fractures sub-parallel to the major slip surfaces show higher values of aperture and length (Figs. 4.9a, d, f, g). More commonly, however, the widest and longest fractures are oriented like the most common major fracture sets (Figs. 4.9a-e, h, i).

In both clastic rocks and Rogenstein, fractures have similar trends of aperture and length. The parameters are positively correlated to each other. In most cases, the percentage of fractures with larger apertures and great lengths is higher in fault damage zones than in the host rock. Further, in damage zones there are much fewer fractures with small apertures and short lengths, although the largest apertures and lengths occur both in host rocks and damage zones (Figs. 4.9k-m, o-q). In the Rogenstein (Fig. 4.9r), the longest fault-related fractures are sub-parallel to the normal fault planes. In the Upper Cretaceous sandstone (OK; Fig. 4.9k), the only clastic rock outcrop with an orthogonal fracture set, fractures have a bimodal distribution; in fact, they are either very long or very short. The longer fractures predominantly belong to the major fracture set and strike sub-parallel to the major slip surface.

4.7. Comparison of hanging wall and footwall fault damage zone widths

Fault damage zone widths are often unequal for hanging walls and footwalls (Withjack et al. 1995; Berg and Skar 2005). For normal fault zones with displacements of more than 10 cm, Fig. 4.10 shows the ratio of hanging wall and footwall widths. Almost every normal fault zone plots below the 1:1 trend. That is, for the studied normal fault zones the hanging walls' deformation affects a larger volume than that of the footwalls. The average width ratio is 0.32, which means that the damage zone in the hanging wall has about three times the thickness of the footwall damage zone.

4.8. Structural indices

From the data we determined the mean structural indices of the normal fault zones, that is, the ratio of damage zone widths and total fault-zone widths (Caine et al. 1996). By their nature structural indices can obtain values from 0 to 1.

Normal fault zones in clastic rocks show smaller total fault-zone widths than those in carbonate rocks (Fig. 4.11a). Further, the structural indices of normal faults zones in clastic rocks are comparatively low because of their thin damage zones. However, there is a wide scatter in carbonate-rock normal fault zone data. Clastic-rock normal fault zones with large structural indices commonly are characterised by the presence of deformation bands. The Rogenstein normal fault zones have intermediate values (Fig. 4.11a).
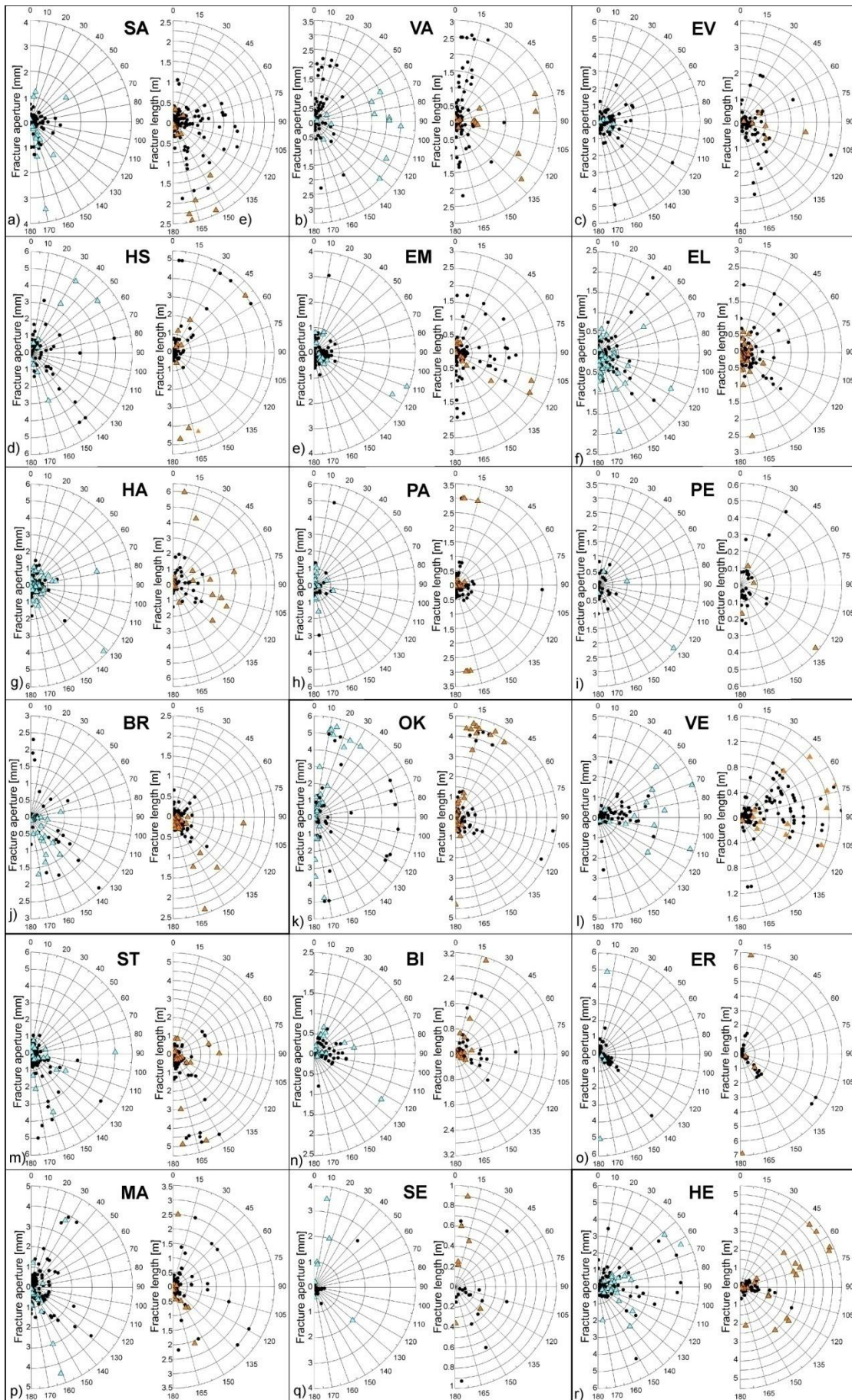
Fig. 4.9. Apertures (left) and fracture lengths (right) versus strike; the scales of fracture length diagrams are always adapted to the outcrop heights; the black circles represent the host-rock and the coloured triangles the damage zone fractures. a-j) Carbonate rocks: a, b) SA, VA: Upper Jurassic, c, d) EV, HS: Upper Muschelkalk, e-i) EM, EL, HA, PA, PE: Lower Muschelkalk, j) BR: Upper Cretaceous; k-q) Clastic rocks: k) OK: Lower Cretaceous, l) VE: Upper Keuper; m, o) Middle Bunter: ST-Solling Form., ER-Detfurth Formation, n) BI: Lower Bunter, p) MA: Upper Carboniferous, q) SE: Upper Rotliegend; r) HE: Rogenstein, Lower Bunter.

In previous sections we showed how mechanical layering affects the fracture attributes. To reveal how such mechanical layering influences the widths of both damage zones and fault cores and, consequently, the structural indices F_m, we plot F_m against the amount of lithologically defined soft beds (low stiffness) such as

shales or marls (Fig. 4.11b; cf. Section 1; Brown 1981; Hoek 2007). In contrast to the 'Wellenkalk' (Lower Muschelkalk; EL, PA, PE), a carbonate-rock unit with varying amounts of marl layers, in Upper Muschelkalk (EV, HS) and "Werksteinbänke" (literally: "building-stone beds") of the Lower Muschelkalk (EM, HA) include fewer marly beds. Upper Cretaceous (BR, EB) and Upper Jurassic rocks (SA, VA) have no distinct mechanical layering; the amount of relatively soft marl layers intercalating the limestone beds is low. In the studied clastic alternations, relatively soft clastic lithologies are shales or siltstones (Brown 1981; Hoek 2007) with differing amounts. Highest amounts occur in Middle Bunter (ER) and Carboniferous (MA), intermediate amounts in Lower Bunter (BI). Results show that, for carbonate rocks with maximum percentage of marl layers of 12%, the structural index correlates negatively with the amount of soft marl layers (Fig. 4.11b). For clastic rocks there is no such correlation.
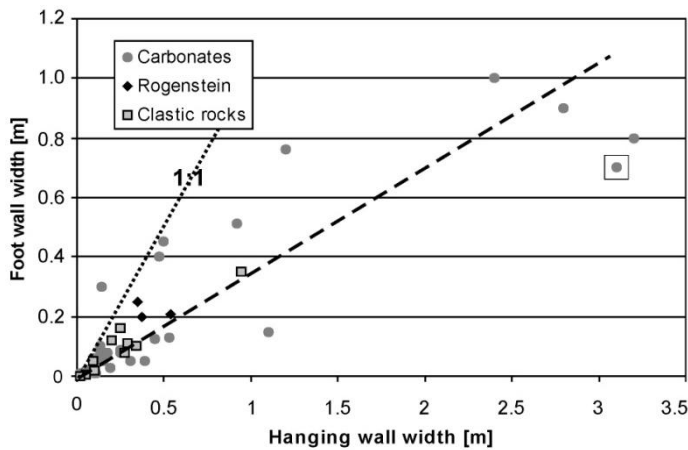
Fig. 4.10. Hanging wall widths vs. footwall widths of normal fault zones with a minimum displacement of 10 cm (n=43). The trends represent the lines of equal (1:1) widths (dotted line) and of average width ratios (dashed line). Inverted fault SA is marked by a rectangle.

5. Stiffness data and analytical modelling

For predictions of fault- and fracture-related permeability in fluid reservoirs, such as geothermal,

hydrocarbon and ground water, numerical models are widely used (e.g., Zhang and Sanderson 1996; Caine and Forster 1999; Manzocchi et al. 1999; Rawling et al. 2001; Brenner 2003; Gudmundsson 2011). To build realistic models of hydromechanical behaviour, for example in simulating hydraulic stimulation of normal fault zones in NWGB rocks, it is important to know the mechanical properties of the rocks at its best.

In the outcrops we took representative rock samples to determine the mechanical properties of the analysed rocks. We perform compression tests (Mutschler 2004) to obtain the rock's Uniaxial Compressive Strength (UCS) and static Young's modulus. In situ static Young's moduli and UCS, however, tend to be lower than those measured of the same rock types in the laboratory (Heuze 1980). There is an inverse correlation of in situ Young's modulus with fracture density (Walsh 1965; Priest 1993) which is important for the stiffness distribution within normal fault zones. This is mainly because fractures reduce the stiffnesses of in situ rock masses whereas rock samples measured in the laboratory are nearly free of fractures. According to Priest (1993), there is a negative correlation of the number of discontinuities (fractures of low or zero tensile strengths in the rock) and its effective Young's modulus (the Young's modulus affected by fracturing). For normal fault zones this means that the Young's moduli perpendicular to the major slip surfaces vary significantly. In the fault damage zone, the fracture density commonly increases towards the fault core, which means that the effective Young's modulus of the rock mass decreases proportionally. To obtain an estimate on how much these Young's moduli differ, we use the analytical model by Priest (1993; Eq. (2)):

$$E_e = \sigma_n \frac{L}{\Delta L} = \left(\frac{1}{E_i} + \frac{1}{\bar{s} k_n} \right) \qquad (2)$$

where E_e is the effective Young's modulus of the rock mass, $\bar{s}$ is the stress normal to the fracture planes, L is the original length of the profile, ΔL is the change in
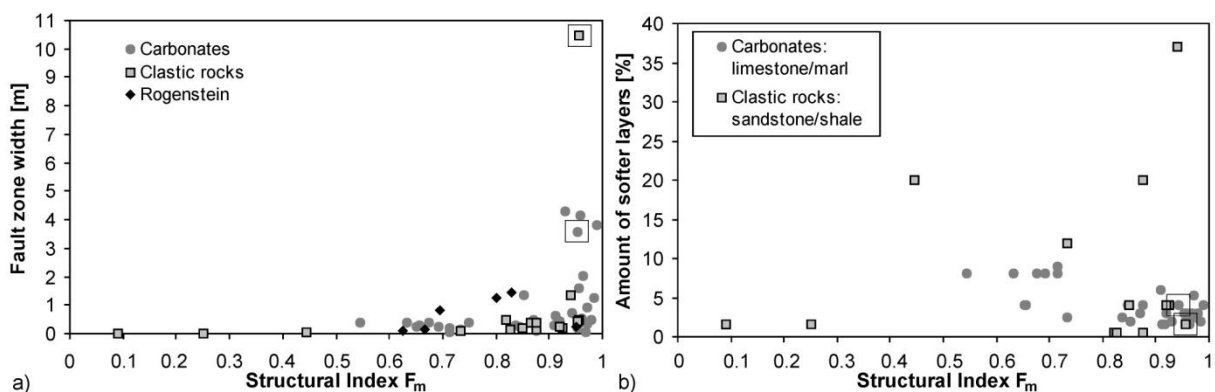
Fig. 4.11. a) Mean structural index Fm (Caine et al., 1996) vs. normal fault zone width (n=58) separately for carbonate rocks (circles), clastic rocks (squares) and the Rogenstein (diamonds); b) Mean structural index Fm vs. amount of relatively soft layers. This plot includes only normal fault zones in stratigraphic units with mechanical layering (n=50). Fault zones with non-normal components are marked by rectangles.

length, E_i is the Young's modulus of the intact rock, s is the average discontinuity spacing (i.e., the inverse of the discontinuity density) and k_n is the stiffness of the discontinuities. For the discontinuity stiffness k_n of macrofractures, 20% of UCS values is a reasonable approximation for near-surface conditions based on experiments and theoretical considerations by Priest (1993). This approximation is used in the calculations below, using measurements of UCS parallel to the layering, i.e., perpendicular to the fractures.

For the four normal fault zones presented as examples in Fig. 4.4, the determined Young's moduli and UCS of the intact rocks samples are:

1. Upper Muschelkalk (HS): E_i 37 GPa, UCS 90 MPa,
2. Lower Muschelkalk (EM): E_i 50 GPa, UCS 150 MPa,
3. Lower Creataceous (OK): E_i 18 GPa, UCS 91 MPa,
4. Lower Bunter (HE): E_i 42 GPa, UCS 106 MPa.

We then use the parameters E_i and UCS, together with the fracture densities (Fig. 4.4), to obtain the effective Young's moduli E_e distributions within the fault zones perpendicular to the normal fault planes (Fig. 4.12).

The results show that, in all cases, there is a clear decrease of E_e in the damage zones compared with the host rocks (Fig. 4.12). The decrease of E_e is more pronounced for carbonate rocks (up to one hundredth of the Young' modulus of the intact rock mass;

Figs. 4.12a, b) due to their high fracture densities. In the host rocks, however, the effective Young's moduli are approximately one tenth of those measured in laboratory. Compared with the carbonate rocks, the stiffness decrease in clastic rocks is less significant (Figs. 4.12c).

6. Discussion

6.1. Effective Young's moduli

Knowing in situ rock mechanical properties is very important in terms of adopting a hydraulic stimulation strategy on the conditions at reservoir depth. In particular, Young's modulus and strengths of the reservoir rocks are important input parameters for numerical models of normal fault zone stimulation and borehole stability within normal fault zones (e.g., Nawrocki and Dusseault 1995; Gudmundsson 2001; Hazzard et al. 2002). It is well known that stiffness (Young's modulus), measured in laboratory, is much higher than that of in situ rock masses because of the smaller amount of discontinuities (Priest 1993; Gudmundsson 2011). Variations of in situ mechanical properties across fault zones can be measured in outcrops using a Schmidt hammer (Steer et al. 2011). Seismic (e.g., Mooney and Ginzburg 1986) and ultrasonic measurements (e.g., Agosta et al. 2007) commonly show reduced P-wave velocities in fault
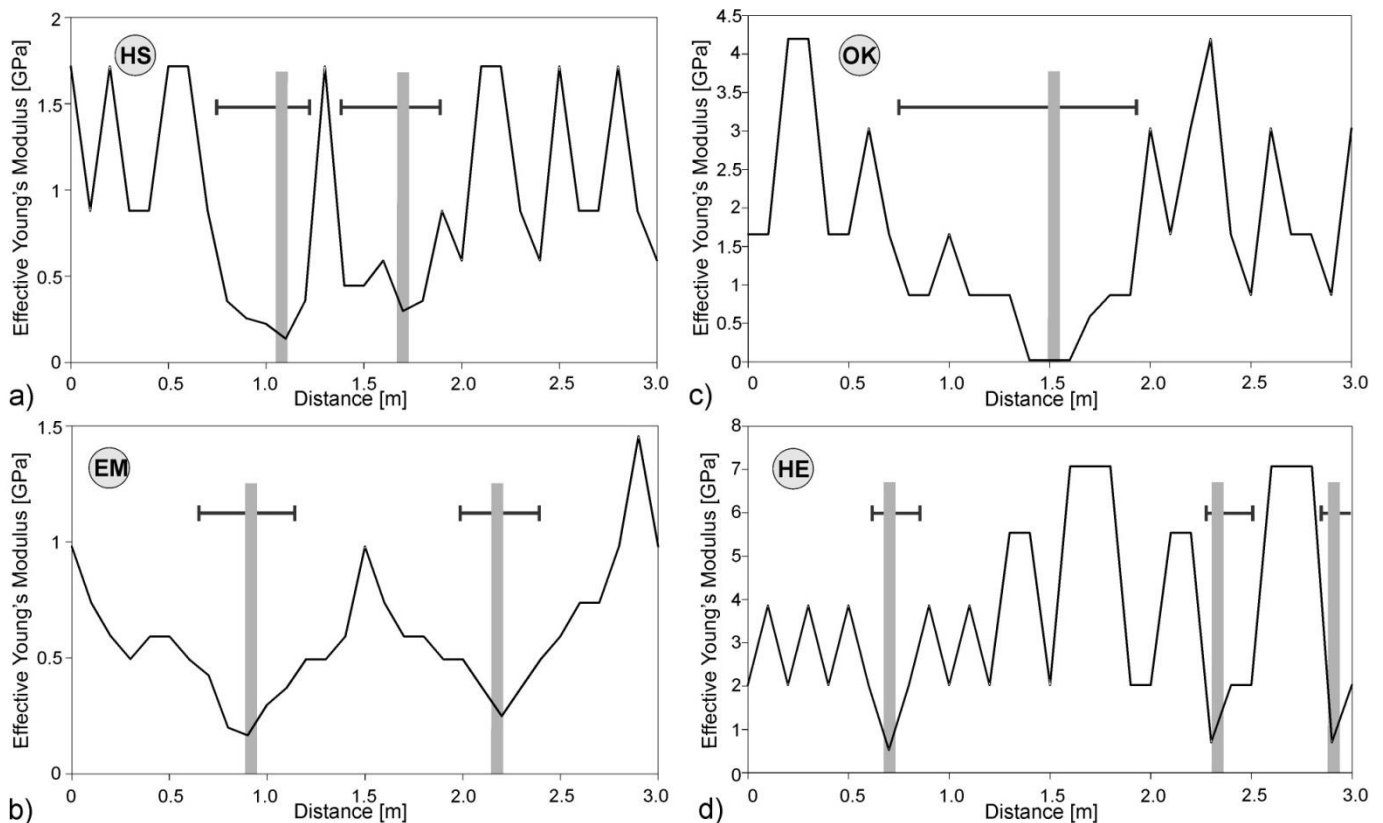
Fig. 4.12. Distribution of effective Young's moduli perpendicular to the normal fault planes (grey lines) and damage zone widths (dark grey bars) for a) HS: Upper Muschelkalk, b) EM: Lower Muschelkalk, c) OK: Lower Cretaceous sandstone, d) HE: Lower Bunter e Rogenstein (Fig. 4.4). The initial Young's moduli E_i and the UCS of the intact rock for the four examples, measured in laboratory, are: a) HS: E_i 37 GPa, UCS 90 MPa; b) EM: E_i 50 GPa, UCS 150 MPa; c) OK: E_i 18 GPa, UCS 91 MPa; d) HE: E_i 42 GPa, UCS 106 MPa.

damage zones, which allow estimations of Young's moduli. A number of parameters may increase (e.g., confining pressure; Nur and Simmons 1969; You 2003) or decrease the in situ Young's modulus (water content, temperature, porosity, etc.; Nur and Simmons 1969; Christensen 1985; Hawkins and McConnell 1992). In particular, the density of open fractures determines the in situ mechanical rock properties (Walsh 1965; Priest 1993; Steer et al. 2011).

With estimations of the effective Young's moduli (E_e) distribution in normal fault zones (Eq. (2)) we show that the decrease of the E_e-values compared with E_i is more distinct for carbonate rocks than for clastic rocks and Rogenstein (Section 5). The measured Young's moduli E_i of the four intact rock samples have a range, which does not correlate with the calculated E_e-values for each of these cases. Additionally, the variation of 20%-UCS-values used is rather small, so that both parameters, E_i and UCS, cannot explain the observed differences in E_e-decrease. The fracture densities (Fig. 4.4), in contrast, correlate negatively with calculated E_e-values.

From that we derive that fracture density is the most important parameter in the calculations of the E_e-distributions within normal fault zones. Weakening of the rock mass due to normal faulting may therefore be more pronounced in carbonate rocks than in clastic rocks.

6.2. Normal fault zone structure

The fault-zone classification by Caine et al. (1996) focuses on the effects on fault zone permeability according to their internal structure, setting into relation the widths of fractured damage zones and fault cores. Being predominantly interested in macrofractures and their positive effects on fault zone permeability, we focus on normal fault zones with distinct fracture-dominated damage zones. The damage zones used for calculation of structural indices are generally characterised by a significant fracture density increase compared with background fracture density.

Data show that there is a wide range of structural indices for clastic rocks from very low to relatively high (Fig. 4.11a). Reasons for this wide F_m-range in clastic rocks may include different grain sizes, clay contents or porosities. Studies of fault zones in porous rocks (Aydin 1978; Antonellini and Aydin 1994; Antonellini et al. 1994; Tondi et al. 2006) imply a relationship between porosity and deformation mechanism. Because the damage zones in porous rocks are dominated by deformation bands, an inverse correlation of porosities and mean structural indices would be expected (Tondi et al. 2012). Although we did not make any microstructural analyses, our macroscopic data show

that in the damage zone of the fine grained and low porosity sandstone (OK) only fractures and no deformation bands occur. In contrast, in sandstones with both larger grain sizes and high porosities (ST and SE) we observed deformation bands.

For carbonate rocks with maximum percentage of marl layers of 12% the structural index correlates negatively with the amount of soft marl layers (cf. Section 4.8, Fig. 4.11b). That means, the thicknesses of the fault cores tend to increase with the increasing amount of marl layers. The more soft layers there are in a sedimentary succession, the lower is the structural index of a cutting normal fault zone. Normal fault zones in clastic rocks are narrower than those in carbonates, which also have higher structural indices and fault zone widths. We conclude that normal fault zones in carbonate rocks may act more like distributed conduits (Caine et al. 1996). This means that within the normal fault zone there is preferred fluid flow parallel to the major slip surfaces, but also perpendicular fluid flow is enabled due to both thin fault cores and many fractures with oblique strike. Normal fault zones in clastic rocks, in contrast, behave more like localised barriers or, alternatively, as combined conduit-barrier systems (Caine et al. 1996). They do not allow fault-perpendicular flow and due to small fracture densities even fault-parallel flow is only slightly enhanced compared with host rock permeability. Therefore, normal fault zones in carbonate rocks seem to affect the resulting reservoir permeability more positively than those in clastic rocks or Rogenstein.

Our analyses of the fault damage zones show that the damage zones are significantly thicker in the hanging walls compared with the footwalls (Fig. 4.10). Only for one fault zone we observed a wider footwall damage zone. The mean values of all other studied normal faults show three times wider damage zones in hanging walls than in footwalls. Similar 3:1-ratios have been observed by Berg and Skar (2005). Other authors, however, documented 2:1-ratios (e.g., Agosta and Aydin 2006). For our small-scale normal fault zones, we conclude that the most important cause of the asymmetric deformation pattern is related to the asymmetric stress field that develops during fault propagation within the hanging wall (cf. White et al. 1986; Aarland and Skjerven 1998; Berg and Skar 2005).

Data show that the Rogenstein carbonates are characterised by fault zone structures similar to those within clastic rocks (Figs. 4.7, 4.9, 4.11a, 4.12). Due to their grainy texture, the porosity of Rogenstein is relatively high and, like in porous coarse grained sandstones, the fault damage zones of small-scale

normal fault zones do not show a higher fracture density in the vicinities of the major slip surfaces.

6.3. Fracture vertical extension

Data show that, concerning fluid flow in carbonate rocks, it is essential if there is a strong mechanical layering: in units with smaller mechanical layer thicknesses the average fracture density is higher and the abrupt increase in the damage zones is more distinct, inducing higher fracture-controlled permeabilities compared with host rocks. The importance of fractures for reservoir permeability, however, does not only depend on fracture density but also on fracture connectivity, which can be analysed at their terminations (Fig. 4.8). Data show that the amount of stratabound fractures (Odling et al. 1999) depends on the existence of layer-parallel heterogeneities in the rock mass (Jaeger et al. 2007). Many fractures become arrested at contacts between layers of different Young's moduli (mechanical layering) due to a change of the local stress field. In rocks with many layer-parallel heterogeneities such as the Upper Cretaceous (BR) and some parts of the Lower Muschelkalk ('Wellenkalk'; EL, PA, PE) there might be a high fracture density but a poor fracture connectivity. The Detfurth Formation (ER; Middle Bunter), as an example of a clastic rock with a pronounced mechanical layering, shows both low fracture density and poor fracture connectivity. Compared with the Lower Muschelkalk, the fracture-controlled permeability through normal fault damage zones in this formation should be significantly lower.

6.4. Regional geological position of studied normal fault zones

Major NWGB-faults have been reactivated during basin history. That is why, for the studied small-scale normal fault zones, we had to check if they also show signs of inversion. During fault inversion, compressional structures (e.g, rollover structures, anticlines, compressional shear fractures, short-cut thrusts, fault rotation, etc.) develop (McClay 1989; Williams et al. 1989; Sibson 1995). These additional structures can affect rock mass permeability; compressional structures may enhance bedding-parallel fluid flow due to low-angle thrust faults/shear fractures or horizontal hydro- and microfractures, but reduce vertical permeability due to aperture reduction because of high horizontal stresses (Sibson 1995). In most studied small-scale normal faults we did not observe any of these structures concluding that these are pure extension features. In contrast, in hanging wall damage zone of one medium-scale normal fault zone (SA), we observed some compressional shear fractures but no other compressional structures. Data of slightly inverted fault

SA show no significant differences to pure normal fault zones. One normal fault zone in OK is rather an oblique-slip fault, i.e., has a strike-slip component. It shows a relatively high fault zone width but all other parameters plot within the scatter of the pure normal fault zones. For the aforementioned reasons, we conclude that for the studied small-scale normal fault zones inversion is not significant.

Another interesting question is if there is any relation of fault-zone parameters (e.g., structural indices) to the orientation of the normal fault zones in the NWGB. Some data, i.e., the Lower- Muschelkalk-outcrops in the Leinetal-Graben, show a clear dependency of fault damage zone widths on fault orientation (HA, EL, PA; Reyer et al. 2009). The fault strike is either parallel or perpendicular to the N-S-striking major boundary faults of the Leinetal-Graben. Those with parallel orientations have wider damage zones and, hence, higher structural indices. In siliclastic fault damage zones there commonly are many minor faults striking predominantly parallel to the major slip surfaces (Odling et al. 2004). Our data show that the same may occur for some carbonate rocks such as the Lower Muschelkalk. In carbonate rocks, however, these minor fault zones do not act as barriers to fluid flow as they probably do in siliclastic rocks (Odling et al. 2005) but rather have fracture-dominated damage zones with high apertures implying an increased fault-parallel permeability, both in homogeneous rock units and mechanically layered rocks.

7. Conclusions

Data on fractures collected within 58 normal fault zones cropping out in 22 exposures of sedimentary rocks of the NWGB show:

1. Most of the fault-related fractures have an orientation similar to the fault strike; a minor fracture set strikes perpendicular to them. The aperture of these fault-related fractures is much higher than aperture of background fractures. The percentage of non-stratabound fractures is higher in fault damage zones than in host rocks.

2. Fracture density distributions in normal fault zones show that, for damage zones in carbonate rocks, there is a distinct increase towards the fault planes. This does not occur in clastic rocks.

3. Calculated effective Young's moduli (stiffnesses) - based on Uniaxial Compressive Strength and Young's modulus measurements (intact host rock samples) and fracture density data - give interesting insights on today's distribution of elastic properties in normal fault zones needed for hydromechanical modelling. Due to higher fracture densities the computed effective

Young's moduli E_e of damage zones in carbonate rocks are much lower than in clastic rocks and Rogenstein.

4. The structural indices indicate that normal fault zones in carbonate rocks are more damage-zone dominated than those in clastic rocks. In carbonate rocks, fractures in the damage zones may differ significantly in orientation from that in the host rocks. In both clastic rocks and Rogenstein carbonates, fractures show a similar orientation in both fault damage zones and host rocks. For carbonate rocks with strong mechanical layering of limestones and marls, there is an inverse correlation of structural indices and the amount of marl layers.

5. The presented data lead to the conclusion that there is a higher positive effect of normal fault zones on permeability increase in carbonate rocks compared with that in clastic rocks. Due to normal fault's self-similarity, it should be possible to apply presented results to hydromechanical models of larger normal fault zones.

Acknowledgements

References

Aarland, R.K., Skjerven, J., 1998. Fault and fracture characteristics of major fault zone in the northern North Sea: analyses of 3D seismic and oriented cores in the Brage Field (Block 31/4). In: Coward, M.P., Daltaban, T.S., Johnson, H. (Eds.), 1998. Structural Geology in Reservoir Characterization, vol. 127, pp. 209-229.

Agosta, F., Kirschner, D.L., 2003. Fluid conduits in carbonate-hosted seismogenic normal faults of central Italy. Journal of Geophysical Research 108 (B4), 2221. http://dx.doi.org/10.1029/2002JB002013.

Agosta, F., Aydin, A., 2006. Architecture and deformation mechanism of a basin-bounding normal fault in Mesozoic platform carbonates, central Italy. Journal of Structural Geology 28, 1445-1467.

Agosta, F., Prasad, M., Aydin, A., 2007. Physical properties of carbonate fault rocks, fucino basin (Central Italy): implications for fault seal in platform carbonates. Geofluids 7, 19-32.

Anderson, E.M., 1905. The dynamics of faulting. Transactions of the Edinburgh Geological Society 8 (3), 387-402.

Antonellini, M., Aydin, A., 1994. Effect of faulting on fluid flow in porous sandstones: petrophysical properties. American Association of Petroleum Geologists Bulletin 78. http://dx.doi.org/10.1306/BDFF90AA-1718-11D7-8645000102C1865D.

Antonellini, M., Aydin, A., Pollard, D.D., 1994. Microstructure of deformation bands in porous sandstones at Arches National Park, Utah. Journal of Structural Geology 16, 941-959.

Arnorsson, S., 1995a. Geothermal systems in Iceland: structure and conceptual models. 1. High-temperature areas. Geothermics 24, 561-602.

Arnorsson, S., 1995b. Geothermal systems in Iceland: structure and conceptual models. 2. Low-temperature areas. Geothermics 24, 603-629.

Aydin, A., 1978. Small faults formed as deformation bands in sandstone. Pure and Applied Geophysics 116, 913-930.

Baldschuhn, R., Frisch, U., Kockel, F., 1996. Geotektonischer Atlas von Nordwest-Deutschland, 1:300.000. BGR, Hannover.

Berg, S.S., Skar, T., 2005. Controls on damage zone asymmetry of a normal fault zone: outcrop analyses of a segment of the Moab fault, SE Utah. Journal of Structural Geology 27, 1803-1822.

Betz, D., Führer, F., Greiner, G., Plein, E., 1987. Evolution of the Lower Saxony Basin. Tectonophysics 137, 127-170.

Brenner, S.L., 2003. Field Studies and Models of Hydrofractures in Heterogeneous Reservoirs. PhD thesis. University of Bergen, Norway.

Brogi, A., 2008. Fault zone architecture and permeability features in siliceous sedimentary rocks: Insights from the Rapolano geothermal area (Northern Apennines, Italy). Journal of Structural Geology 30, 237-256.

Brown, E.T. (Ed.), 1981. Rock Characterization, Testing & Monitoring: ISRM Suggested Methods. Pergamon, Oxford, pp. 171-183.

Caine, J.S., Evans, J.P., Forster, C.B., 1996. Fault zone architecture and permeability structure. Geology 24, 1025-1028.

Caine, J.S., Forster, C.B., 1999. Fault zone architecture and fluid flow: Insights from field data and numerical modeling. Geophysical Monograph 113, 101-127.

Chang, C., Zoback, M.D., Khaksar, A., 2006. Empirical relations between rock strength and physical properties in sedimentary rocks. Journal of Petroleum Science and Engineering 51, 223-237.

Christensen, N.I., 1985. Measurement of dynamic properties of rock at elevated temperatures and pressures. In: Annual Book of Standards for Testing and Materials, Special Technical Publications, vol. 869. ASTM International, pp. 93-107.

De Joussineau, G., Aydin, A., 2007. The evolution of the damage zone with fault growth in sandstone and its multiscale characteristics. Journal of Geophysical Research-Solid Earth 112, B12401. http://dx.doi.org/10.1029/2006JB004711.

De Marsily, G., 1986. Quantitative Hydrogeology. Academic Press, New York.

Faulkner, D.R., Jackson, C.A.L., Lunn, R.J., Schlische, R.W., Shipton, Z.K., Wibberley, C.A.J., Withjack, M.O., 2010. A review of recent developments concerning the structure, mechanics and fluid flow properties of fault zones. Journal of Structural Geology 32, 1557-1575.

Faulkner, D.R., Mitchell, T.M., Jensen, E., Cembrano, J., 2011. Scaling of fault damage zones with displacement and the implications for fault growth processes. Journal of Geophysical Research 116, B05403. http://dx.doi.org/10.1029/2010JB007788.

Faybishenko, B., Witherspoon, P.A., Benson, S.M. (Eds.), 2000. Dynamics of Fluids in Fractured Rocks. American Geophysical Union, Washington DC.

Glennie, K.W. (Ed.), 1998. Petroleum Geology of the North Sea; Basic Concepts and Recent Advances. Blackwell Science Geology and Petroleum Geology, Oxford, UK.

Gross, M.R., Eyal, Y., 2007. Throughgoing fractures in layered carbonate rocks. GSA Bulletin 119, 1387-1404.

Gudmundsson, A., 2001. Fluid overpressure and flow in fault zones: field measurements and models. Tectonophysics 336, 183-197.

Gudmundsson, A., 2011. Rock Fractures in Geological Processes, first ed. Cambridge University Press, New York.

Gudmundsson, A., Simmenes, T.H., Larsen, B., Philipp, S.L., 2010. Effects of internal structure and local stresses on fracture propagation, deflection, and arrest in fault zones. Journal of Structural Geology 32, 1643-1655.

Guerriero, V., Vitale, S., Ciarcia, S., Mazzoli, S., 2011. Improved statistical multi-scale analysis of fractured reservoir analogues. Tectonophysics 504, 14-24.

Hawkins, A.B., McConnell, B.J., 1992. Sensitivity of sandstone strength and deformability to changes in moisture content. Quarterly Journal of Engineering Geology and Hydrogeology 25, 115-130.

Hazzard, J.F., Young, R.P., Oates, S.J., 2002. Numerical modeling of seismicity induced by fluid injection in a fractured reservoir. In: Mining and Tunnel Innovation and Opportunity, Proceedings of the 5th North American Rock Mechanics Symposium, Toronto, Canada, pp. 1023-1030.

Helgeson, D.E., Aydin, A., 1991. Characteristics of joint propagation across layer interfaces in sedimentary rocks. Journal of Structural Geology 13, 897-911.

Henningsen, D., Katzung, G., 2006. Einführung in die Geologie Deutschlands, seventh ed. Spektrum, Berlin.

Heuze, F., 1980. Scale effects in the determination of rock mass strength and deformability. Rock Mechanics and Rock Engineering 12, 167-192.

Hoek, E., 2007. Practical Rock Engineering. Updated ed., North Vancouver, B.C.

Hudson, J.A., Harrison, J.P., 1997. Engineering Rock Mechanics: An Introduction to the Principles. Pergamon, Oxford.

Hutchinson, J.W., Suo, Z., 1992. Mixed mode cracking in layered materials. Advances in Applied Mechanics 29, 63-191.

Jaeger, J.C., Cook, N.G.W., Zimmerman, R.W., 2007. Fundamentals of Rock Mechanics, fourth ed. Blackwell Publishing, Malden, USA.

Johansen, T.E.S., Fossen, H., Kluge, R., 2005. The impact of syn-faulting porosity reduction on damage zone architecture in porous sandstone: an outcrop example from the Moab Fault, Utah. Journal of Structural Geology 27, 1469-1485.

Kehrer, R., Orzol, J, Jung, R, Jatho, R, Junker, R, 2007. The GeneSys project: a contribution of GEOZENTRUM Hannover to the development of enhanced geothermal systems. Zeitschrift der deutschen Gesellschaft für Geowissenschaften 158, 119-132.

King, G., 1983. The accommodation of large strains in the upper lithosphere of the earth and other solids by self-similar fault systems - the geometrical origin of b-Value. Pure and Applied Geophysics 121, 761-815.

Kockel, F., 2002. Rifting processes in NW Germany and the German North Sea sector. Netherlands Journal of Geosciences/Geologie en Mijnbouw 81, 149-158.

Lindsay, N.G., Murphy, F.C., Walsh, J.J., Watterson, J., 1993. Outcrop studies of shale smears on fault surfaces. In: Flint, S., Bryant, I. (Eds.), The Geological Modelling of Hydrocarbon Reservoirs and Outcrop Analogues. International Association of Sedimentologists Special Publication, vol. 15, pp. 113-123.

Manzocchi, T.,Walsh, J.J., Nell, P., Yielding, G., 1999. Fault transmissibility multipliers for flow simulation models. Petroleum Geoscience 5, 53-63.

McClay, K.R., 1989. Analogue models of inversion tectonics. In: Geological Society, London, Special Publications, vol. 44, pp. 41-59.

Meiburg, P., 1982. Saxonische Tektonik und Schollenkinematik am Ostrand des Rheinischen Massivs. Geotekt. Forschung 62, 1-267.

Meneghini, F., Marroni, M., Pandolfi, L., 2007. Fluid flow during accretion in sediment-dominated margins: evidence of a high-permeability fossil fault zone from the Internal Ligurian accretionary units of the Northern Apennines, Italy. Journal of Structural Geology 29, 515-529.

Erläuterungen zur Stratigraphischen Tabelle von Deutschland 2005(ESTD 2005). In: Menning, M., Hendrich, A. (Eds.). Newsletter on Stratigraphy 41. Berlin, Stuttgart.

Mooney, W.D., Ginzburg, A., 1986. Seismic measurements of the internal properties of fault zones. Pure and Applied Geophysics 124, 141-157.

Musmann, P., Thomas, R., Buness, H., 2011. Seismische Erkundung von geologischen Störungszonen am Beispiel des Leinetalgrabens: Erste Ergebnisse. In: 71. Jahrestagung der Deutschen Geophysikalischen Gesellschaft, Conference Proceedings, Köln, GR P05, p. 90.

Mutschler, T, 2004. Neufassung der Empfehlung Nr. 1 des Arbeitskreises "Versuchstechnik Fels" der Deutschen Gesellschaft für Geotechnik e.V.: Einaxiale Druckversuche an zylindrischen Gesteinsprüfkörpern. Bautechnik 81/10, 825-834.

Mutterlose, J., Bornemann, A., 2000. Distribution and facies patterns of Lower Cretaceous sediments in northern Germany: a review. Cretaceous Research 21, 733-759.

Narr, W., Suppe, J., 1991. Joint spacing in sedimentary rocks. Journal of Structural Geology 13, 1037-1048.

Nawrocki, P.A., Dusseault, M.B., 1995. Modelling of damaged zones around openings using radius-dependent Young's modulus. Rock Mechanics and Rock Engineering 28, 227-239.

Nur, A., Simmons, G., 1969. The effect of saturation on velocity in low porosity rocks. Earth and Planetary Science Letters 7, 183-193.

Odling, N.E., Gillespie, P., Bourgine, B., Castaing, C., Chiles, J.P., Christensen, N.P., Fillion, E., Genter, A., Olsen, C., Thrane, L., Trice, R., Aarseth, E., Walsh, J.J., Watterson, J., 1999. Variations in fracture system geometry and their implications for fluid flow in fractured hydrocarbon reservoirs. Petroleum Geoscience 5, 373-384.

Odling, N.E., Harris, S.D., Knipe, R.J., 2004. Permeability scaling properties of fault damage zones in siliclastic rocks. Journal of Structural Geology 26, 1727-1747.

Odling, N.E., Harris, S.D., Vaszi, A.Z., Knipe, R.J., 2005. Properties of fault damage zones in siliclastic rocks: a modelling approach. In: Geological Society, London, Special Publications, vol. 249, pp. 43-59.

Paschen, H., Oertel, D., Grünwald, R., 2003. Möglichkeiten geothermischer Stromerzeugung in Deutschland. TAB Arbeitsbericht 84.

Petmecky, S., Meier, L., Reiser, H., Littke, R., 1999. High thermal maturity in the Lower Saxony Basin: intrusion or deep burial? Tectonophysics 304, 317-344.

Philipp, S.L., 2007. Bedeutung von Störungszonen und Bruchsystemen für die Permeabilität: Vergleich natürlicher Paläoreservoire mit stimulierten geothermischen Reservoiren. In: Geothermiekongress 2007, Bochum, Conference Proceedings, pp. 224-230.

Priest, S.D., 1993. Discontinuity Analysis for Rock Engineering. Chapman and Hall, London.

Rawling, G.C., Goodwin, L.B., Wilson, J.L., 2001. Internal architecture, permeability structure, and hydrologic significance of contrasting fault-zone types. Geology 29, 43-46.

Reyer, D., Bauer, J.F., Philipp, S.L., 2009. Infrastruktur und Permeabilität von Störungszonen im Unteren Muschelkalk auf der westlichen Grabenschulter des Leinetalgrabens. In: Geothermiekongress 2009, Bochum, Conference Proceedings. ISBN 13: 978e3-932570-64-3, TF8.

Röhl, U., 1990. Parallelisierung des norddeutschen Oberen Muschelkalks mit dem süddeutschen Hauptmuschelkalk anhand von Sedimentationszyklen. Geologische Rundschau 79, 13-26.

Schaumann, G., Grinat, M., Günther, T., 2011. Tiefe Erkundung des Leinetal-Störungssystems mit geoelektrischen und elektromagnetischen Messungen. In: 71. Jahrestagung der Deutschen Geophysikalischen Gesellschaft, Conference Proceedings, Köln, GR P06, p. 90.

Scheck-Wenderoth, M., Lamarche, J., 2005. Crustal memory and basin evolution in the Central European Basin System e New insights from a 3D structural model. Tectonophysics 397, 143-165.

Schröder, L., Plein, E., Bachmann, G.H., Gast, R.E., Gebhardt, U., Graf, R., Helmuth, H.-J., Pasternak, M., Porth, H., Süssmuth, S., 1995. Stratigraphische Neugliederung des Rotliegend im Norddeutschen Becken. Geologisches Jahrbuch A148, 3-21.

Sibson, R.H., 1995. Selective fault reactivation during basin inversion: potential for fluid redistribution through fault-valve action. In: Geological Society, London, Special Publications, vol. 88, pp. 3-19.

Sibson, R.H., 2000. Fluid involvement in normal faulting. Journal of Geodynamics 29, 469-499.

Simmenes, T.H., Gudmundsson, A., 2002. Fracture Frequencies, Mechanical Properties, Stress Fields, and Fluid Transport of Large Fault Zones in West Norway. EGS XXVII General Assembly, Nice, abstract 4924.

Steer, P., Bigot, A., Cattin, R., Soliva, R., 2011. In-situ characterization of the effective elasticity of a fault zone, and its relationship to fracture spacing. Journal of Structural Geology 33, 1541-1553.

Stewart, I.S., Hancock, P.L., 1991. Scales of structural heterogeneity within neotectonic normal fault zones in the Aegean region. Journal of Structural Geology 13, 191-204.

Tondi, E., Antonellini, M., Aydin, A., Marchegiani, L., Cello, G., 2006. The role of deformation bands, stylolites and sheared stylolites in fault development in carbonate grainstones of Majella Mountain, Italy. Journal of Structural Geology 28, 376-391.

Tondi, E., Cilona, A., Agosta, F., Aydin, A., Rustichelli, A., Renda, P., Giunta, G., 2012. Growth processes, dimensional parameters and scaling relationships of two conjugate sets of compactive shear bands in porous carbonate grainstones, Favignana Island, Italy. Journal of Structural Geology 37, 53-64.

Torabi, A., Berg, S.S., 2011. Scaling of fault attributes: a review. Marine and Petroleum Geology 28, 1444-1460.

Turcotte, D.L., 1989. Fractals in geology and geophysics. Pure and Applied Geophysics 131, 171-196.

Twiss, R.J., Moores, E.M., 2007. Structural Geology, second ed. W.H. Freeman, New York.

Usdowski, H.E., 1962. Die Entstehung der kalkoolithischen Fazies des norddeutschen Unteren Buntsandsteins. Beiträge zur Mineralogie und Petrographie 8, 141-179.

Walsh, J.B., 1965. The effect of cracks on the uniaxial elastic compression of rocks. Journal of Geophysical Research 70, 399-411.

Walter, R., 2007. Geologie von Mitteleuropa, seventh ed. Schweizerbarth, Stuttgart.

Wehner, H., Gerling, P., Hiltmann, W., Kockel, F., 1989. Erdöl-Charakteristik und Öl-Muttergestein-Korrelation im Niedersächsischen Becken. Nachrichten der Deutschen Geologischen Gesellschaft 41, 77-78.

White, N.J., Jackson, J.A., McKenzie, D.P., 1986. The relationship between the geometry of normal faults and that of the sedimentary layers in their hanging walls. Journal of Structural Geology 8, 897-909.

Williams, G.D., Powell, C.M., Cooper, M.A., 1989. Geometry and kinematics of inversion tectonics. In: Geological Society, London, Special Publications, vol. 44, pp. 3-15.

Withjack, M.O., Islam, Q.T., La Pointe, P.R., 1995. Normal faults and their hanging-wall deformation: an experimental study. American Association of Petroleum Geologists Bulletin 79, 1-18.

You, M., 2003. Effect of confining pressure on the Young's modulus of rock specimen. Chinese Journal of Rock Mechanics and Engineering. 2003-01.

Zhang, X., Sanderson, D.J., 1996. Numerical modelling of the effects of fault slip on fluid flow around extensional faults. Journal of Structural Geology 18, 109-119.

Ziegler, P., 1990. Geological Atlas of Western and Central Europe, second ed. Geological Society Publishing House/Shell International Petroleum Maatschappij B.V.

5 Empirical relations of rock properties of outcrop and core samples from the Northwest German Basin for geothermal drilling

Dorothea Reyer, Sonja L. Philipp

University of Göttingen, Geoscience Centre, Goldschmidtstraße 3, 37077 Göttingen, Germany

Abstract

Information about geomechanical and physical rock properties, particularly uniaxial compressive strength (UCS), are needed for geomechanical model development and updating with logging-while-drilling methods to minimise costs and risks of the drilling process. The following parameters with importance at different stages of geothermal exploitation and drilling are presented for typical sedimentary and volcanic rocks of the Northwest German Basin (NWGB): physical (P-wave velocities, porosity, and bulk and grain density) and geomechanical parameters (UCS, static Young's modulus, destruction work and indirect tensile strength both perpendicular and parallel to bedding) for 35 rock samples from quarries and 14 core samples of sandstones and carbonate rocks.

With regression analyses (linear- and non-linear) empirical relations are developed to predict UCS values from all other parameters. Analyses focus on sedimentary rocks and were repeated separately for clastic rock samples or carbonate rock samples as well as for outcrop samples or core samples. Empirical relations have high statistical significance for Young's modulus, tensile strength and destruction work; for physical properties, there is a wider scatter of data and prediction of UCS is less precise. For most relations, properties of core samples plot within the scatter of outcrop samples and lie within the 90% prediction bands of developed regression functions. The results indicate the applicability of empirical relations that are based on outcrop data on questions related to drilling operations if the database contains a sufficient number of samples with varying rock properties. The presented equations may help to predict UCS values for sedimentary rocks at depth, and thus develop suitable geomechanical models for the adaptation of the drilling strategy on rock mechanical conditions in the NWGB.

1. Introduction

In Germany, the North German Basin (NGB) is one region with considerable geothermal low-enthalpy potential (Paschen et al., 2003). To utilise this potential, deep wellbores have to be drilled to reach prospective geothermal reservoir rocks at depths of 3000-6000 m. Well construction is therefore the main expense factor of geothermal projects in this region. In sedimentary successions such as the NGB, one of the major problems and expenditures may be related to wellbore stability issues (e.g. Dusseault, 2011; Zeynali, 2012). Such wellbore instabilities are recognised as a drilling challenge that may considerably increase drilling costs and safety risks (Proehl, 2002; York et al., 2009; Li et al., 2012). The profit margin of geothermal projects, however, is rather small compared with hydrocarbon projects. Therefore, a substantial reduction of costs for well construction and completion is desirable (cf. www.gebo-nds.de).

Evaluation of in situ rock mechanical behaviour requires different information. Important input data include estimates of mechanical conditions, pore pressures, and stress state. According to Zeynali (2012), two of the most important mechanical factors affecting wellbore stability are the mechanical properties of rock - including anisotropy of strengths and elastic moduli (e.g. Heap et al., 2010) - and in situ stresses existing in different layers of rock. Development of a geomechanical model before starting the drilling operation is a powerful tool to prevent wellbore instabilities and minimise drilling costs of geothermal wells (Khaksar et al., 2009). For drilling through a rock mass, such model captures the initial equilibrium state that describes the stresses, pore pressure, and geomechanical properties. With logging-while-drilling data the initially computed geomechanical model can be continuously adapted to the conditions at depth.

For such geomechanical modelling, the uniaxial compressive strength (UCS) is the most important geomechanical input parameter (Chang et al., 2006; Nabaei and Shahbazi, 2012; Vogt et al., 2012). There already exist several software approaches for building and updating geomechanical models (Settari and Walters, 2001; geomechanics software, e.g. GMI – www.baker-hughes.com). Generally, such geomechanical modelling software uses empirical relationships that were developed for hydrocarbon reservoirs. To date there do not exist such relationships for geothermal reservoirs of the NGB. Here, the geological setting may be completely different leading to other rock mechanical conditions. Therefore, existing

methods for geomechanical modelling have to be reviewed carefully and adapted where needed.

There are several relevant parameters with importance given to different stages of geothermal exploitation and drilling. Physical properties such as density, ρ, and P- and S-wave velocities, v_p and v_s (compressional and shear wave velocities), are parameters that can be measured directly in wellbores; the porosity, Φ, is derivable from such well logs (Edlmann et al. 1998). The dynamic Young's modulus is derived from velocity and density logs (Fricke and Schön, 1999; Zoback, 2007; Rider and Kennedy, 2011). Geomechanical parameters are important for reservoir exploitation and drilling operations. The static Young's modulus, E_s, is interesting in terms of predictions of fracture propagation (Jaeger et al., 2007; Gudmundsson, 2011). The indirect tensile strength, T_0, gives information about the rock's resistance to tensile fractures. These parameters are of interest in terms of dimensioning of hydraulic fracturing operations, wellbore stability and drilling mud selection (e.g. Zoback, 2007). The destruction work, W, is one parameter providing information on the amount of energy needed to destroy the rock while drilling. It is known to correlate with the drilling efficiency which is a term used to describe the effects of a number of geological and machine parameters on the drilling velocity (Thuro, 1997). Therefore, it is desirable to make reasonable assumptions about these parameters for drilling through the rock units. To do so, we need empirical relations between UCS and parameters which are either knowable before drilling or determinable with logging-while-drilling tools. With well logs from existing adjacent boreholes, a geomechanical model can be built using empirical relations between rock-strength values and physical parameters. Empirical relations can then be used for validation of the geomechanical model while- and after-drilling by updating the model continuously with logging data.

Determining geomechanical and physical parameters directly from core material, however, is expensive and time-consuming because a large number of core samples are needed, and core material is rare (e.g. Khaksar et al., 2009). Therefore, in this study we aim to improve predictions of mechanical properties for rocks at depth. First, we present data on geomechanical and physical properties of representative rock types of the NGB. We sampled 35 mainly sedimentary rocks of the western sub-basin of the NGB, the Northwest German Basin (NWGB), from Lower Permian to Upper Cretaceous, exposed in outcrop analogues, i.e. quarries. In addition to these outcrop samples, we analysed 14 core samples from two wellbores with the same stratigraphic units, comparable lithologies and facies as

equivalent samples to analyse mechanical property changes due to uplift and alteration. Secondly, we used the data of sedimentary rocks to perform regression analyses, together with calculation of coefficients of determination (R^2), between UCS and the described parameters, separately for outcrop samples only and including core samples. To analyse the statistical significance of the developed regression functions, 90% confidence and prediction bands are added. The rock properties of core samples are compared with the results of outcrop samples from the developed equations of outcrop samples to examine the relevance of outcrop samples for predicting rock properties at depths. The regression functions may help predict UCS values for sedimentary rocks at depth, and thus develop a suitable geomechanical model for the adaptation of the drilling strategy on rock mechanical conditions.

2. Geologic setting and sample locations

The study area is part of the NWGB, the western part of the NGB, located in northwestern Germany (Walter, 2007). The NGB initiated in the Late Carboniferous–Permian due to rifting processes subsequent to the Variscan orogenesis (Betz et al., 1987; Ziegler, 1990). From marine to continental conditions, the sedimentary succession is characterised by changing sedimentation environments. Therefore, the NWGB is comprised of mainly carbonate and clastic rocks with some intercalated evaporates leading to very heterogeneous rock mechanical conditions.
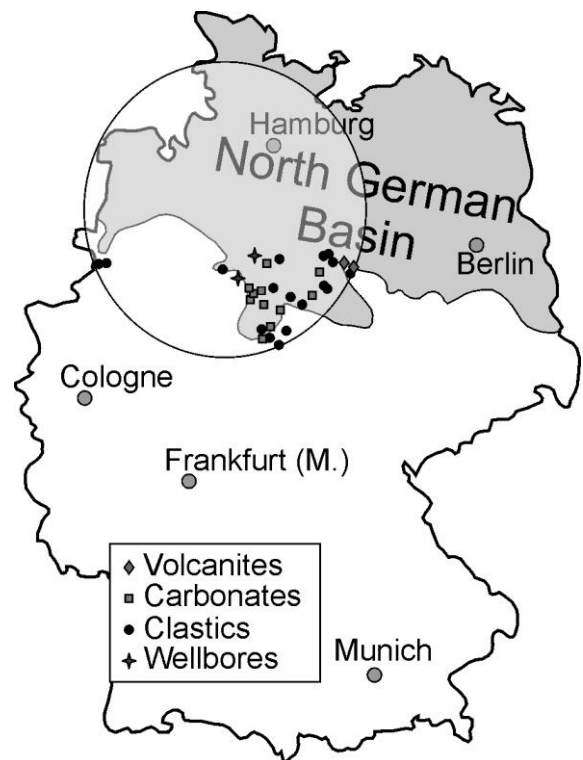

Fig. 5.1. North German Basin (mod. after www.geotis.de) with the locations of sampled wellbores and quarries and the exposed rock types (see key) in the NWGB (rough location marked).

Table 5.1. All samples from outcrops and wellbores with sample ID, local name, lithology, stratigraphical units, and core sample depths.

Sample-ID	Lithology	System	Local Name	
KrCa	Chalk marl		Kreidemergel	
GoSa	Sandstone		Sudmerberg-Fm.	
HoT	Marl		Rotpläner	
BrCe	Limestone	**Cretaceous**	Cenoman-Kalk	
OLH	Sandstone		Hils-Sst.	
GiUK	Sandstone		Gildehaus-Sst.	
FrUK	Sandstone		Bentheimer-Sst.	
OK	Sandstone		Wealden-Sst.	
ThüJ	Limestone		Serpulit	
GVa	Limestone		Gigas Schichten	
OKDa	Limestone	**Jurassic**	Oberer Kimmeridge	
ShJk	Limestone		Korallenoolith	
HSDi,HSDi2	Limestone		Heersumer Sch.	
AlWo	Sandstone		Aalen-Sst.	
koQ	Sandstone		Rhät-Sst.	
koVe	Sandstone		Rhät-Sst.	
kuWe	Siltstone		Lettenkohlen-Sst.	
EM	Limestone		Trochitenkalk	
H	Limestone		Schaumkalk	
EL1-3	Limestone	**Triassic**	Wellenkalk	
soWa	Gypsum		Röt 1	
smHN	Sandstone		Hardegsen-F.	
smD	Sandstone		Detfurth-Folge	
smVG,2	Sandstone		Volpriehausen-F.	
suHe	Limestone		Rogenstein	
BiSu	Sandstone		Bernburg-F.	
Bero,BeroK	Sandstone		Rotliegend-Sst.	
DöRo	Andesite	**Permian**	Rotliegend-Vulkanit	
FL2, FL6	Rhyolites		Rotliegend-Vulkanit	
	Wellbore 1: Eulenflucht 1 (EF1)			
	Wellbore 2: Groß Buchholz (Gt1)			**TVD**
Gt1WS1	Sandstone		Wealden-Sst.	1221 m
Gt1WS2	Sandstone	**Cretaceous**	Wealden-Sst.	1211 m
EF1WS	Sandstone		Wealden-Sst.	35 m
EF1GS	Limestone		Gigas Schichten	210 m
EF1OK	Limestone		Oberer Kimmeridge	243 m
EF1UKK	Limestone	**Jurassic**	Korallenoolith	282 m
EF1KO	Limestone		Korallenoolith	286 m
EF1HS	Limestone		Heersumer Schicht	325 m
Gt1DU1	Sandstone		Detfurth-Folge	~ 3535.8 m
Gt1DU2	Sandstone		Detfurth-Folge	~ 3534.3 m
Gt1DU3	Sandstone	**Triassic**	Detfurth-Folge	~ 3534.7 m
Gt1DW	Siltstone		Detfurth-Folge	~ 3537.2 m
Gt1VS1	Sandstone		Volpriehausen-F.	~ 3655.6 m
Gt1VS2	Sandstone		Volpriehausen-F.	~ 3657.8 m

Sst Sandstone; *F* Folge; *TVD* Total vertical depth; *Fm* Formation

The study area is located at the southern and western margins of the western region of the North German Basin (Fig. 1; cf. Reyer et al., 2012). Sedimentary rocks that occur at geothermally relevant depths in the centre and north of the NWGB crop out at the basin margins and can be sampled in quarries. In such outcrop analogues, listed in Table 5.1, we took samples of two main rock types: carbonate rocks (Triassic, Jurassic, and Cretaceous age) and sandstones (Permian, Triassic, Jurassic, and Cretaceous age; Table 5.1). Three Rotliegend volcanic rock (Permian) samples are included

to obtain rock property data over a wide range of lithologies present in the NWGB (Fig. 1). For four carbonate rock units and three sandstone units, the equivalent core samples were identified and sampled from two wellbores: Groß Buchholz (Gt1) and Eulenflucht 1 (EF1; Table 5.1).

3. Methods

3.1. Density and porosity

The bulk density, ρ_d [g/cm^3], was determined from dry cylindrical specimens with a GeoPyc 1360 (Micromeritics), setting measured volume and mass in relation. For the same specimens, we measured the grain density, ρ_0 [g/cm^3], with an Ultrapyknometer 1000 (Quantachrome) at room temperature using 99.9% helium, previously measured ρ_d and specimen's mass.

The total Φ, given in [%], was calculated from ρ_0 and ρ_d. Samples are separated in low- (0-10%), medium- (10-20%), and high-porosity (> 20%) rocks for further interpretation of rock mechanical properties.

3.2. Rock testing

Uniaxial compression tests were performed stress-controlled at a constant rate of 0.5 MPa/s on specimens with length-diameter ratios of 2-2.5 to determine UCS and E_s (ISRM, 2007). For each outcrop sample, six specimens with diameters of 40 mm were measured, both parallel and perpendicular to sedimentary bedding or, for volcanic rocks, with respect to surface orientation. Core samples were tested only perpendicular to bedding due to limited core material. v_p is measured (Tektronix TDS 5034B; 1 MHz rectangular pulse) to eliminate defective specimens. E_s is determined at the linear-elastic deformation path of the stress-strain curve. For rock samples showing brittle failure, we calculated W (Thuro, 1997), as the area below the stress-strain curve given in kilojoules per cubic metre.

T_0 is measured both parallel and perpendicular to sedimentary bedding on specimens with diameters of 40 mm and lengths of 15-20 mm with Brazilian tests (ISRM, 2007). Both parallel and perpendicular to bedding, a minimum of nine (outcrop samples) and four specimens (core samples), respectively, were tested.

3.3. Statistical analyses

For each sample, both parallel and perpendicular to bedding, mean values and standard deviations of the tested specimens were calculated for geomechanical parameters and v_p. We performed regression analyses (linear and non-linear) of mean values for UCS with Φ, ρ_d, v_p, and E_s and for W and T_0 with UCS, respectively. Different regression analyses were made for each pair

of parameters: (1) all samples to obtain a good overview, (2) sandstone samples only, and (3) carbonate samples only. In each case, regressions were made both for outcrop samples only and for all samples including core samples. For outcrop sample equations 90% confidence and prediction bands are included. Confidence bands represent the 90% certainty of regression curve estimation based on limited sample data (Wooldridge, 2009; Brink, 2010). Prediction bands cover the range in which the values of future measurements of associated samples lie with a probability of 90%. Based on these bands core sample results are compared with outcrop results.

4. Experimental results

4.1. Physical properties

In Tables 5.2 and 5.3, mean values of dry bulk density, grain density, calculated porosities, and P-wave velocities of all rock samples are listed. The approximate lithology is given to better appraise the following data analyses.

For sandstones and carbonates, we have sample data over a wide range of porosities; the lowest porosities occur in core samples. Accordingly, the dry bulk density values show a wide range. Grain densities of carbonates are highest due to a higher mineral density of the carbonates' main component calcite as compared with quartz. The grain densities strongly depend on the amount of heavy minerals: (1) hematite-rich Triassic sandstones have high ρ_0 values (> 2.7 g/cm^3); (2) carbonate samples with increased grain densities contain large amounts of ferrous carbonates. v_p values clearly depend on lithology. Carbonate samples show mean values of v_p from 3277 m/s (porous chalk marl: KrCa) to 6158 m/s (massy matrix limestone: EL2). Mostly, the standard deviations of carbonate samples are high. This is pronounced in carbonates with either a high presence of lithoclasts or due to rock heterogeneities. v_p in sandstones are considerably slower than in carbonate rocks. The lowest values relate to high porosities. In volcanic rock samples, v_p is rather high (about 5300 m/s) with small variation and standard deviations.

4.2. Rock mechanical properties

In Table 5.4, mean values of the geomechanical parameters of all samples are listed. The standard deviations of all measurements for every sample are given. Measured parameter values of the eight clastic core samples are higher than those of the 14 outcrop samples. The differences between outcrop and core samples of carbonate rocks are, in contrast, rather small. Parameter values of the three volcanic rock

samples are considerably higher than of sedimentary outcrop samples.

Table 5.2. Lithology, dry bulk density, grain density, porosity and P-wave velocity for outcrop samples.

Sample ID	Specified lithology	ρ_d [g/cm^3]	ρ_0 [g/cm^3]	Φ [%]	$v_p \pm$ SD [m/s]
KrCa	Porous chalk marl	2.18	2.86	23.9	3277 ± 84
GoSa	Medium-grained sandstone	2.53	2.69	6	3772 ± 70
HoT	Marl	2.59	2.73	5.2	5116 ± 199
BrCe	Bioclast-bearing matrix LS	2.66	2.77	3.8	4674 ± 258
OLH	Medium-grained sandstone	2.09	2.77	24.6	2291 ± 63
GiUK	Medium-grained sandstone	2.11	2.68	21.6	2576 ± 130
FrUK	Fine-grained sandstone	2.36	2.68	12.1	2172 ± 87
OK	Medium-grained sandstone	2.29	2.80	18.3	2942 ± 120
ThüJ	Bioclast-rich matrix LS	2.07	2.83	26.7	4262 ± 215
GVa	Porous sparry LS	2.29	2.96	22.8	3967 ± 106
OKDa	Bioclast-rich matrix LS	2.63	2.83	7.2	5134 ± 100
ShJk	Bioclast-bearing oolite	2.61	2.74	4.6	5171 ± 154
HSDi	Micro-sparry LS	2.53	2.78	9.1	5084 ± 350
HSDi2	Bioclast-rich sparry LS	2.40	2.78	13.7	4787 ± 236
AlWo	Medium-grained sandstone	2.09	2.69	22.5	3000 ± 184
koQ	Medium-grained sandstone	2.27	2.84	20.1	3222 ± 36
koVe	Fine-grained sandstone	2.34	2.77	15.6	2980 ± 38
kuWe	Siltstone	2.59	2.68	3.4	3951 ± 126
EM	Bioclast-rich sparry LS	2.71	2.79	2.9	5607 ± 164
H	Porous sparry LS	2.40	2.77	13.2	4888 ± 73
EL1	Dolomitic LS	2.53	2.98	15.1	4683 ± 133
EL2	Massy matrix LS	2.74	2.75	0.3	6158 ± 8
EL3	Dolomitic LS	2.66	2.94	9.4	4526 ± 23
soWa	Shale-gypsum alternation	2.33	2.39	2.5	3690 ± 120
smHN	Medium-grained sandstone	2.26	2.71	16.6	2574 ± 64
smD	Medium-grained sandstone	2.38	2.76	13.7	2986 ± 22
smVG	Medium-grained sandstone	2.32	2.72	14.4	2948 ± 78
smVG2	Medium-grained sandstone	2.17	2.74	20.6	2074 ± 89
suHe	Sparry oolite	2.71	2.75	1.5	5368 ± 136
BiSu	Medium-grained sandstone	2.15	2.79	22.9	2110 ± 6
BeRoK	Conglomeratic sandstone	2.58	2.67	3.2	3564 ± 78
BeRo	Medium-grained sandstone	2.52	2.69	6.6	3426 ± 29
DöRo	Andesite	2.72	2.72	0.1	5449 ± 23
FL2	Rhyolite	2.63	2.64	0.1	5260 ± 44
FL6	Rhyolite	2.69	2.69	0.1	5342 ± 64

LS limestone; ρ_d dry bulk density; ρ_0 grain density; Φ porosity; v_p P-wave velocity; *SD* standard deviation

Table 5.3. Lithology, dry bulk density, grain density, porosity and P-wave velocity for core samples (abbreviations in Table 5.2).

SampleID	Specified lithology	ρ_d	ρ_0	Φ	$v_p \pm$ SD
Gt1WS1	Coarse-grained sandstone	2.40	2.84	15.5	4854 ± 38
Gt1WS2	Medium-grained sandstone	2.58	2.79	7.6	2950 ± 267
EF1WS	Medium-grained sandstone	2.25	2.79	19.4	2638 ± 28
EF1MM	Shale-Gypsum	2.88	2.95	2.4	5808 ± 110
EF1GS	Sparry LS	2.48	2.78	10.8	5832 ± 65
EF1OK	Bioclast-rich matrix LS	2.72	2.78	2.1	5732 ± 50
EF1UKK	Bioclast-rich sparry LS	2.76	2.77	0.2	5412 ± 53
EF1KO	Sparry oolite	2.72	2.79	2.6	6053 ± 59
EF1HS	Bioclast-rich sparry LS	2.18	2.82	22.8	3831 ± 87
Gt1DU1	Medium-grained sandstone	2.69	2.70	0.4	4981 ± 33
Gt1DU2	Coarse-grained sandstone	2.73	2.75	1.0	3410 ± 78
Gt1DU3	Medium-grained sandstone	2.67	2.77	3.6	4906 ± 96
Gt1DW	Siltstone	2.83	2.87	1.1	5166 ± 123
Gt1VS1	Medium-grained sandstone	2.71	2.72	0.1	4745 ± 62
Gt1VS2	Coarse-grained sandstone	2.69	2.77	2.8	4539 ± 54

Table 5.4. Mean values of the geomechanical parameters UCS, Young's modulus, destruction work, and indirect tensile strength, measured perpendicular and parallel to layering, for all samples including standard deviations.

Outcrop samples	UCS ± SD par. / perp. [MPa]	Es ± SD parallel / perp. [GPa]	W ± SD parallel / perp. [kJ/m³]	T₀ ± SD parallel / perp. [MPa]
KrCa	36 ± 7 / 31 ± 4	12.7 ± 1.2 / 13.5 ± 1.1	106 ± 20 / 133 ± 30	2.0 ± 0.6 / 2.7 ± 0.8
GoSa	35 ± 2 / 75 ± 11	7.9 ± 0.5 / 30.3 ± 11.1	215 ± 26 / 213 ± 41	2.6 ± 0.4 / 5.9 ± 0.3
HoT	81 ± 7 / 112 ± 15	40.6 ± 4.2 / 34.1 ± 6.8	263 ± 60 / 332 ± 67	5.2 ± 1.0 / 8.0 ± 1.7
BrCe	126 ± 5 / 91 ± 29	44.1 ± 4.0 / 26.8 ± 6.1	282 ± 17 / 301 ± 15	6.7 ± 0.9 / 7.6 ± 0.6
OLH	37 ± 7 / 23 ± 10	15.1 ± 5.5 / 10.9 ± 6.5	118 ± 19 / 50 ± 6	3.1 ± 0.3 / 3.1 ± 0.3
GiUK	56 ± 2 / 47 ± 4	19.7 ± 4.6 / 15.7 ± 2.1	175 ± 25 / 198 ± 41	4.1 ± 0.4 / 3.1 ± 0.2
FrUK	45 ± 7 / 55 ± 4	12.0 ± 3.5 / 13.7 ± 4.5	245 ± 21 / 248 ± 38	2.4 ± 0.3 / 2.8 ± 0.4
OK	82 ± 6 / 73 ± 7	19.3 ± 1.5 / 18.0 ± 2.6	394 ± 34 / 404 ± 17	3.8 ± 0.9 / 4.2 ± 0.8
ThüJ	23 ± 5 / 26 ± 5	14.7 ± 1.3 / 13.3 ± 3.9	69 ± 10 / 77 ± 9	2.3 ± 0.4 / 2.7 ± 0.4
GVa	48 ± 1 / 53 ± 11	14.5 ± 2.4 / 14.9 ± 4.7	151 ± 13 / 174 ± 36	3.5 ± 0.6 / 4.8 ± 0.4
OKDa	79 ± 1 / 71 ± 24	35.6 ± 6.8 / 30.2 ± 1.8	207 ± 24 / 137 ± 20	6.3 ± 0.6 / 4.5 ± 0.6
ShJk	97 ± 3 / 109 ± 3	46.4 ± 3.3 / 43.4 ± 8.0	499 ± 67 / 558 ± 91	5.2 ± 1.1 / 6.5 ± 1.0
HSDi	58 ± 12 / 74 ± 13	37.3 ± 6.6 / 27.7 ± 0.9	203 ± 31 / 317 ± 21	5.5 ± 1.5 / 6.9 ± 0.7
HSDi2	- / 48 ± 4	- / 36.5 ± 3.8	- / 215 ± 78	4.3 ± 1.7 / 6.6 ± 1.0
AlWo	21 ± 3 / 48 ± 9	6.1 ± 0.9 / 15.8 ± 2.5	90 ± 11 / 154 ± 17	1.3 ± 0.2 / 4.1 ± 0.6
koQ	64 ± 8 / 85 ± 12	16.1 ± 1.5 / 20.1 ± 1.2	395 ± 36 / 378 ± 60	2.9 ± 0.5 / 3.6 ± 0.7
koVe	86 ± 5 / 112 ± 6	20.6 ± 2.4 / 24.1 ± 2.3	638 ± 53 / 699 ± 91	4.4 ± 0.7 / 4.9 ± 1.0
kuWe	41 ± 4 / 63 ± 19	17.3 ± 1.7 / 20.7 ± 2.0	202 ± 5 / 142 ± 13	5.9 ± 1.0 / 6.0 ± 0.7
EM	82 ± 10 / 75 ± 7	47.0 ± 4.2 / 36.9 ± 4.1	299 ± 64 / 339 ± 54	7.0 ± 1.8 / 6.1 ± 1.2
H	46 ± 4 / 38 ± 1	16.5 ± 2.6 / 24.5 ± 6.5	154 ± 43 / 89 ± 18	4.2 ± 0.8 / 4.0 ± 1.1
EL1	96 ± 12 / 159 ± 20	30.8 ± 2.5 / 31.3 ± 1.2	410 ± 68 / 542 ± 76	5.5 ± 1.2 / 10.2 ± 2.6
EL2	162 ± 19 / 179 ± 19	81.6 ± 6.5 / 49.2 ± 1.4	546 ± 43 / 479 ± 37	7.5 ± 1.3 / 9.0 ± 2.2
EL3	- / 104 ± 11	- / 28.6 ± 2.3	- / 424 ± 53	6.2 ± 1.5 / 10.3 ± 1.9
soWa	32 ± 5 / -	20.6 ± 5.6 / -	66 ± 10 / -	2.2 ± 0.4 / 4.2 ± 1.1
smHN	32 ± 4 / 43 ± 11	13.4 ± 2.2 / 12.5 ± 4.9	141 ± 8 / 181 ± 26	1.8 ± 0.5 / 2.6 ± 0.7
smD	137 ± 8 / 133 ± 7	27.5 ± 2.4 / 27.9 ± 2.5	521 ± 86 / 561 ± 57	5.5 ± 0.9 / 7.7 ± 0.9
smVG	61 ± 1 / 64 ± 4	13.4 ± 2.4 / 12.4 ± 0.7	282 ± 2 / 366 ± 22	2.4 ± 0.7 / 2.8 ± 0.4
smVG2	29 ± 3 / 31 ± 4	6.1 ± 0.7 / 6.8 ± 1.2	111 ± 28 / 245 ± 21	2.3 ± 0.3 / 2.6 ± 0.3
suHe	65 ± 6 / 99 ± 10	71.5 ± 6.8 / 41.8 ± 4.6	426 ± 45 / 476 ± 100	6.0 ± 1.4 / 7.7 ± 2.3
BiSu	44 ± 2 / 46 ± 1	8.9 ± 2.3 / 10.3 ± 1.8	186 ± 24 / 228 ± 14	2.0 ± 0.3 / 2.2 ± 0.3
BeRo	66 ± 7 / 81 ± 2	17.0 ± 4.0 / 19.5 ± 2.5	281 ± 42 / 333 ± 73	3.1 ± 1.0 / 4.0 ± 0.7
DöRo	236 ± 19 / 223 ± 25	41.8 ± 5.8 / 41.1 ± 4.3	873 ± 75 / 1052 ± 116	13.9 ± 2.0 / 18.8 ± 2.9
FL2	124 ± 18 / 186 ± 18	44.1 ± 4.6 / 39.0 ± 5.2	738 ± 85 / 744 ± 68	9.8 ± 2.3 / 10.6 ± 1.8
FL6	173 ± 21 / 243 ± 24	46.0 ± 4.8 / 46.2 ± 4.6	1004 ± 96 / 986 ± 29	12.9 ± 2.5 / 15.7 ± 2.0

Core samples	UCS ± STD perp. [MPa]	Es ± STD perp.[GPa]	W ± STD perp. [kJ/m3]	T₀ ± STD parallel / perp. [MPa]
Gt1WS1	152 ± 15	43.6 ± 4.4	677 ± 34	3.6 ± 1.0 / 7.2 ± 0.2
Gt1WS2	65 ± 7	19.8 ± 2.0	636 ± 32	1.3 ± 0.1 / 2.8 ± 1.0
EF1WS	88 ± 15	28.2 ± 5.4	333 ± 5	3.9 ± 0.5 / 4.1 ± 0.5
EF1MM	16 ± 4	51.5 ± 5.3	28 ± 1	2.7 ± 1.4 / 5.0 ± 1.3
EF1GS	172 ± 18	41.3 ± 4.2	549 ± 27	8.2 ± 1.4 / 8.7 ± 2.6
EF1OK	149 ± 15	35.2 ± 4.0	334 ± 17	6.0 ± 1.7 / 7.7 ± 2.0
EF1UKK	132 ± 19	49.7 ± 1.4	320 ± 16	6.2 ± 2.1 / 7.4 ± 1.8
EF1KO	160 ± 19	55.8 ± 1.8	584 ± 65	7.0 ± 1.6 / 7.4 ± 1.9
EF1HS	122 ± 11	30.2 ± 3.1	235 ± 12	7.3 ± 1.5 / 6.3 ± 1.7
Gt1DU1	147 ± 23	33.0 ± 0.3	635 ± 19	4.5 ± 1.6 / 12.1 ± 3.4
Gt1DU2	107 ± 4	25.4 ± 3.2	541 ± 27	5.7 ± 0.4 / 6.5 ± 1.5
Gt1DU3	164 ± 20	37.0 ± 5.9	907 ± 45	9.3 ± 2.7 / 10.2 ± 0.7
Gt1DW	141 ± 12	35.9 ± 3.5	304 ± 49	6.1 ± 2.1 / 11.2 ± 3.0
Gt1VS1	128 ± 28	37.2 ± 9.6	342 ± 32	3.6 ± 1.5 / 7.9 ± 1.6
Gt1VS2	187 ± 15	35.1 ± 2.8	707 ± 35	7.0 ± 1.7 / 8.3 ± 1.2

UCS uniaxial compressive strength; *Es* static Young's modulus; *W* destruction work; *T₀* indirect tensile strength; *SD* Standard deviation

5. Empirical relations of rock properties with UCS

The rock property data, presented above, may be used directly to calibrate an existing geomechanical model by attaching UCS values to log profiles and deducing equivalent values of tensile strength and destruction work using empirical relations. In situ rocks and core samples, however, may have completely different rock properties. Thus, we compare properties of core samples and outcrop samples to analyse if properties of in situ rocks can be predicted based on data from outcrop samples from the same geologic setting. In Table 5, the results of regression analyses for the different parameters, presented in following sections, are summarised.

5.1. Empirical relations for UCS prediction

5.1.1 Density and porosity

Porosity and bulk density are two parameters that can be determined with geophysical logs. Many previous studies showed that there are strong correlations between UCS and both parameters (e.g. Lama and Vutukuri, 1978; Jizba, 1991; Wong et al., 1997; Palchik, 1999).

In Fig. 2, both porosity and bulk density are plotted against UCS measured perpendicular and parallel to bedding. It is obvious that there is a wide scatter of data resulting in rather poor statistical significance of the empirical relations (Table 5.5). However, the prediction of in situ properties based on outcrop sample results is one of the main questions of this study. It is conspicuous that in
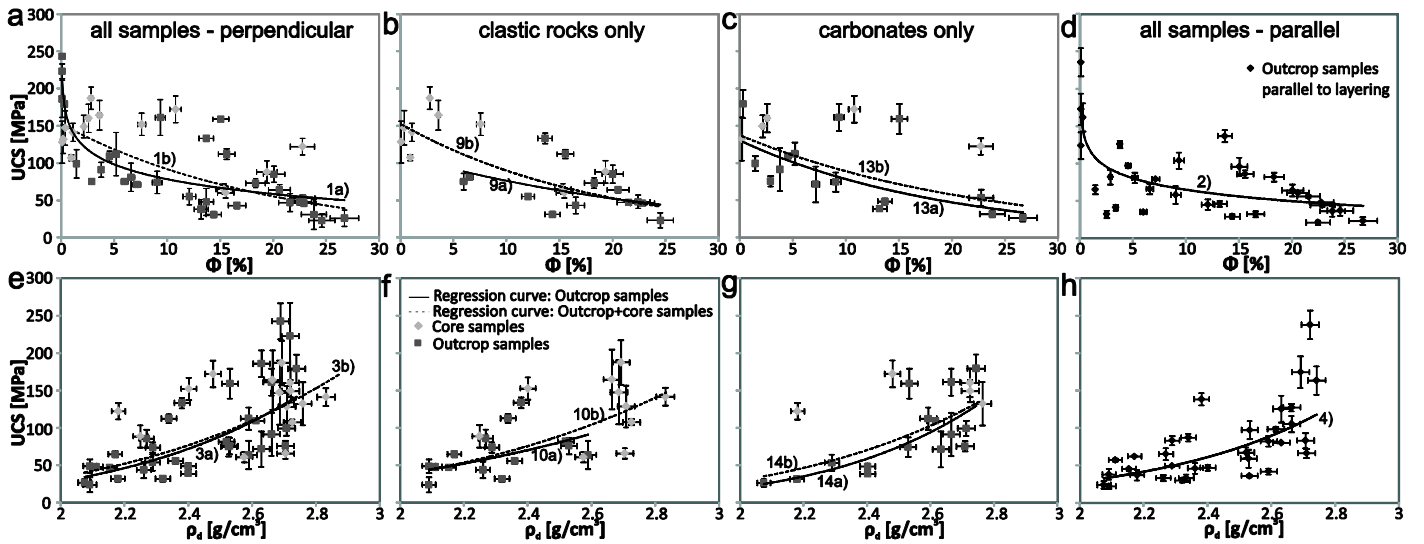
Fig. 5.2. UCS measured perpendicular to layering versus a-c) Φ and e-g) ρ_d, respectively, separately for all samples (a, e; n=49), only clastic rock samples (b, f; n=24) and only carbonate samples (c, g; n=20) for outcrop and core samples; regression curves shown for both quarry and core samples and quarry samples only. UCS measured parallel to layering versus d) Φ and h) ρ_d (n=33); for regression equations see Table 5.5. For UCS, error bars stand for standard deviations of all measurements of every sample (Table 5.4). For density and porosity, error bars represent measuring accurancies of 1% and 5%, respectively.

all cases, and especially for carbonates, outcrop and core samples show a similar range of both Φ and ρ values. Though clastic core samples plot far above the regression curve of UCS-Φ of outcrop samples this is mainly based on the lack of outcrop samples with low porosities (Fig. 5.2b). For UCS-ρ, however, core samples plot along an extension of the regression curve for outcrop data (Fig. 5.2f). Data therefore show that, if core samples are included, the best fit regression curve is similar to the one with outcrop data only.

5.1.2. P-wave velocity

Many studies show that UCS correlates positively with v_p and travel time, respectively (Freyburg, 1972; McNally, 1987; Kahraman, 2001;

Sharma and Singh, 2008). v_p is one parameter determined easily with borehole acoustic logs (e.g.,Fricke and Schön, 1999; Rider and Kennedy, 2011) and it may be relevant for the geomechanical model validation and logging-while-drilling.
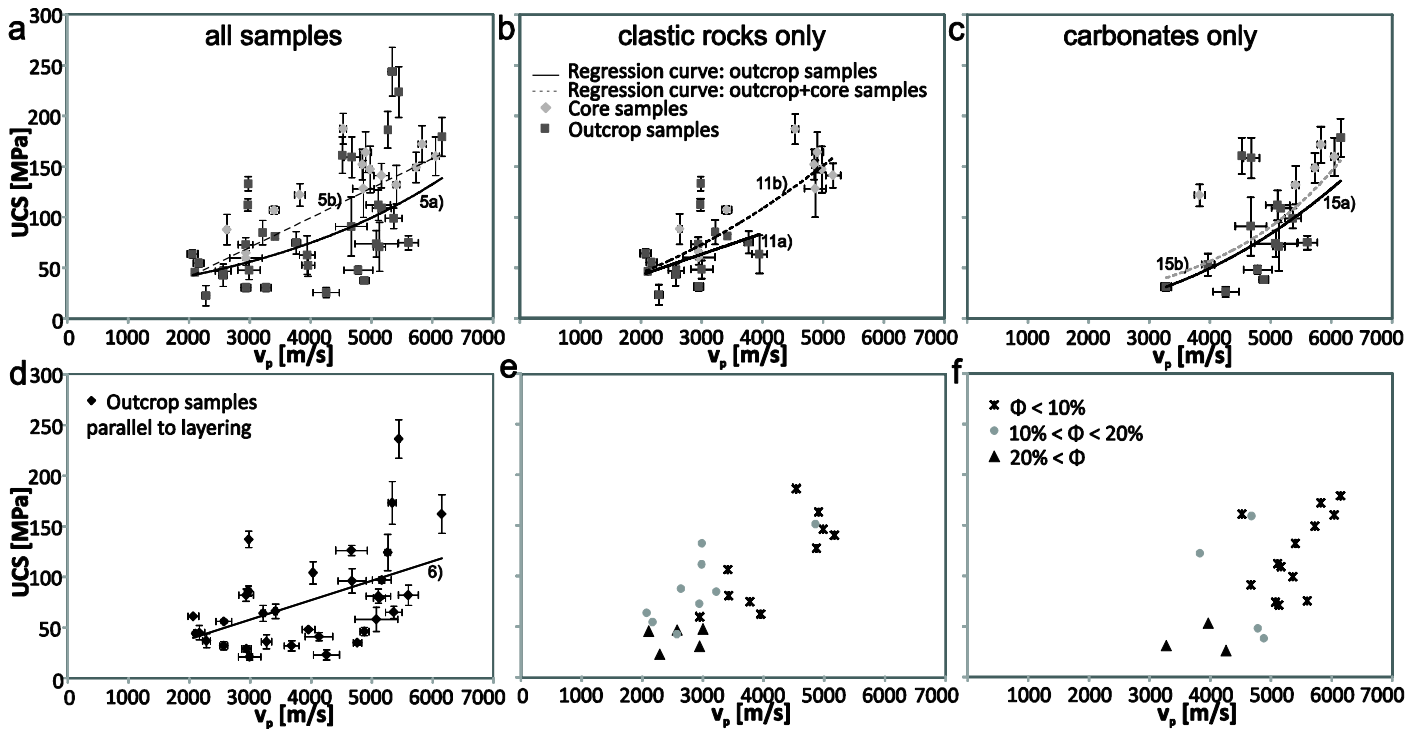

Fig. 5.3. v_p versus UCS for specimens taken perpendicular to layering for outcrop and core samples separately for a) all samples (n=49), b) only clastic rock samples (n=24) and c) only carbonate samples (n=20); d) v_p versus UCS for all specimens taken parallel to layering (n=33); regression curves shown for both quarry and core samples and quarry samples only; for regression equations see Table 5.5. Error bars stand for standard deviations of all measurements of every sample (Tables 5.2-5.4). e, f) v_p versus UCS for low, medium and high-porosity samples of clastic rocks (e) and carbonates (f).

UCS-v_p data show a wide scatter for all samples both perpendicular and parallel to bedding (Figs. 5.3a, d). The coefficients of determination are rather poor for both outcrop samples only and core samples included (Table 5.5). However, there are only small differences between best fit curves for outcrop samples only and core samples included. Especially for carbonates the regression curve differs only slightly when core samples are included (Fig. 5.3c).

There is some deviation for clastic rocks due to lacking low-porosity outcrop samples (Fig. 5.3b). The coefficient of determination is yet considerably higher if core samples are included (Eq. 11b).
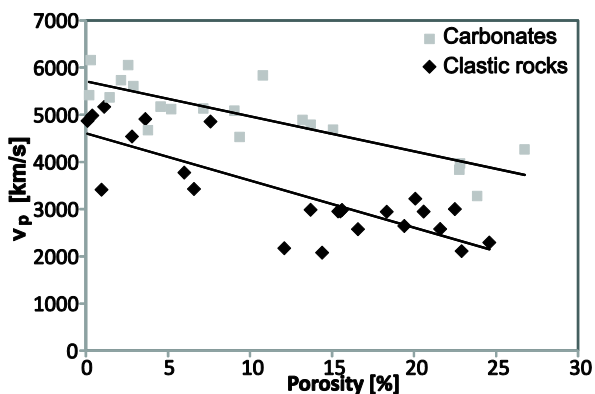

Fig. 5.4. Porosity versus v_p for carbonates and clastic rocks (see key) with linear regression lines.

There are conspicuous interdependencies between UCS, v_p and porosity for both clastic rocks and carbonates.

High porosity clastic and carbonate rocks have lowest UCS and v_p values, and low porosity samples have highest values (Figs. 5.3e, f). If porosities are plotted versus P-wave velocities (Fig. 5.4) there is a clear linear relationship for carbonates at higher v_p values. The mineralogical composition of clastic rock samples is more heterogeneous compared with carbonate samples reflected in a wider scatter of v_p values at lower UCS values. v_p values strongly depend on mineral composition due to the minerals' different elastic wave velocities (e.g., Gebrande et al. 1982). Sandstones' main component quartz has a considerably lower v_p than calcite, the main component of carbonates. v_p of dolomite is lower, too. Consequently, two samples with dolomitic composition (EL1, EL3) plot above the regression curve of carbonates (Fig. 5.3c).

5.1.3. Young's modulus

Former studies showed that, in most cases, there is a strong correlation between E_s and UCS (Sachpazis, 1990; Aggistalis et al., 1996; Palchik, 1999; Dinçer et al., 2004). Our data, shown in Fig. 5, are in good agreement with these studies, especially for the lithologically separated plots (Figs. 5.5b, c). Coefficients of determination are in most cases high. To better analyse the statistical significance of the developed regression functions for outcrop samples, 90% confidence and prediction bands are added.
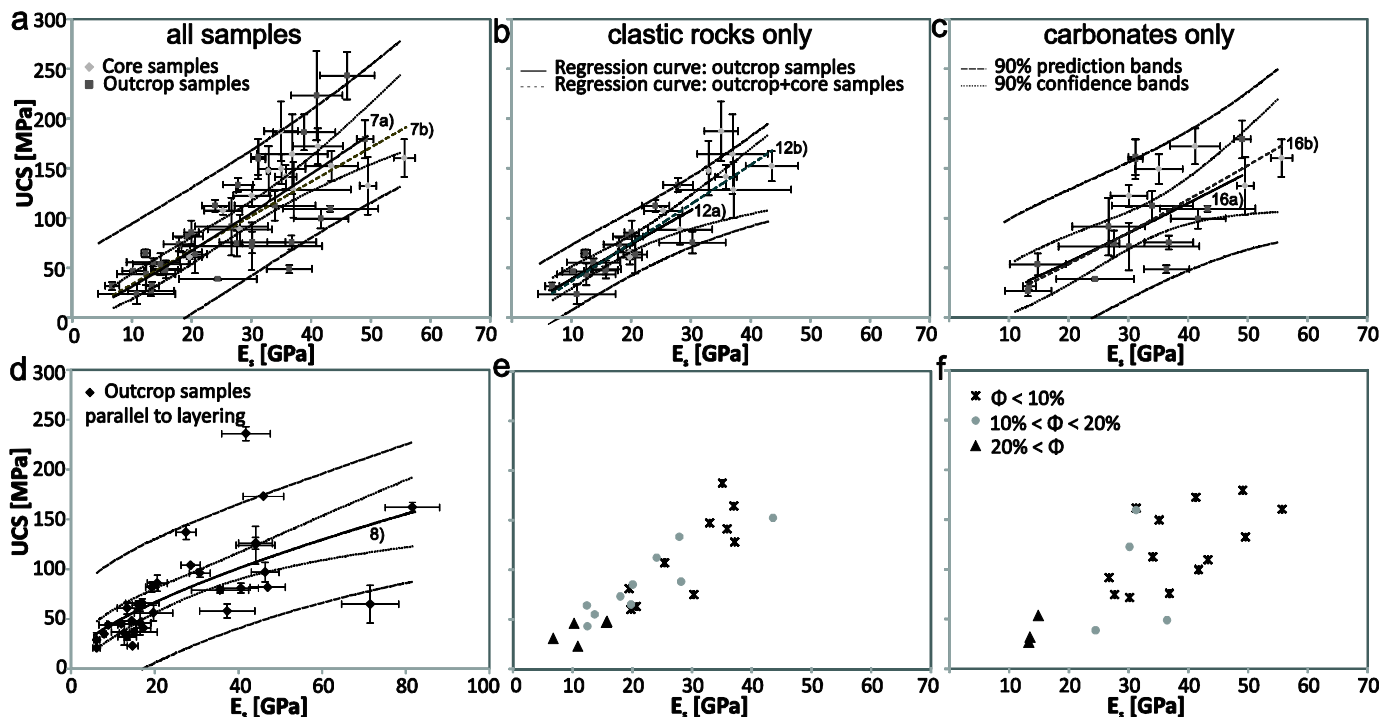

Fig. 5.5. E_s versus UCS for specimens taken perpendicular to layering for outcrop and core samples separately for a) all samples (n=49), b) only clastic rock samples (n=24) and c) only carbonate samples (n=19); d) E_s versus UCS for all specimens taken parallel to layering (n=33). Regression curves shown for both quarry and core samples and quarry samples only; 90% prediction and confidence bands are included; for regression equations see Table 5.5. Error bars stand for standard deviations of all measurements of every sample (Table 5.4). e, f) E_s versus UCS for low, medium and high-porosity samples of clastic rocks (e) and carbonates (f).

Table 5.5. Summarised results of statistical analyses for the correlation of UCS with different parameters of both outcrop and core samples and outcrop samples only with coefficients of determination R^2.

	Outcrop samples only			Outcrop samples and drill cores		
	Eq.	Empirical relation	R^2	Eq.	Empirical relation	R^2
All samples	1a	$UCS = -28.6\ln(\Phi)+144.2$	0.675	1b	$UCS=151.95e^{-0.051\Phi}$	0.526
	2 *	$UCS = -22.2\ln(\Phi)+115.9$	0.558			
	3a	$UCS=0.775\rho^{5.16}$	0.571	3b	$UCS=1.285\rho^{4.66}$	0.520
	4 *	$UCS=0.568e^{1.943\rho}$	0.498			
	5a	$UCS=23.763e^{0.0003Vp}$	0.314	5b	$UCS=0.029v_p - 19.09$	0.405
	6 *	$UCS=0.019v_p$	0.269			
	7a	$UCS=2.474E_s^{1.102}$	0.590	7b	$UCS=3.335E_s^{1.008}$	0.686
	8 *	$UCS=7.538E_s^{0.698}$	0.639			
Sandstones	9a	$UCS=110.73e^{-0.037\Phi}$	0.206	9b	$UCS=152.6e^{-0.053\Phi}$	0.608
	10a	$UCS=3.453\rho^{3.427}$	0.266	10b	$UCS=2.245\rho^{4.0132}$	0.493
	11a	$UCS=0.025v_p^{0.980}$	0.185	11b	$UCS=4E\text{-}06v_p^2+0.009v_p+11.5$	0.651
	12a	$UCS=4.319E_s^{0.944}$	0.682	12b	$UCS=3.364E_s^{1.035}$	0.822
Carbonates	13a	$UCS=129.95e^{-0.051\Phi}$	0.517	13b	$UCS=137.08e^{-0.043\Phi}$	0.390
	14a	$UCS=0.319\rho^{5.953}$	0.708	14b	$UCS=1.116\rho^{4.741}$	0.476
	15a	$UCS=2E\text{-}07v_p^{2.351}$	0.351	15b	$UCS=8.535e^{0.0005Vp}$	0.360
	16a	$UCS=1.928E_s^{1.098}$	0.576	16b	$UCS=1.783E_s^{1.138}$	0.616
All samples	17a	$W=3.953UCS$	0.824	17b	$W=5.954UCS^{0.9023}$	0.678
	18 *	$W=3.026UCS1.07$	0.816			
	19a	$T_0=0.0002UCS^2+0.023UCS+2.30$	0.861	19b	$T_0=0.0002UCS^2+0.02UCS+2.35$	0.787
	20 *	$T_0=3E\text{-}05UCS^2+0.047UCS+1.01$	0.797			
Sandstones	21a	$W=2.867UCS^{1.102}$	0.729	21b	$W=7.164UCS^{0.889}$	0.611
	22a	$T_0=0.0002UCS^2+0.0065UCS+2.46$	0.581	22b	$T_0=1.9125e^{0.01UCS}$	0.758
Carbonates	23a	$W=3.714UCS^{0.98}$	0.804	23b	$W=4.851UCS^{0.906}$	0.769
	24a	$T_0=3.79\ln(UCS)-9.997$	0.862	24b	$T_0=0.407UCS^{0.609}$	0.817

*, parallel to layering

If all lithologies are plotted together, there is a certain scatter of data both perpendicular and parallel to bedding reflected in wide 90% prediction bands (Figs. 5.5a, d). Parallel to bedding the E_s values tend to be slightly higher than if perpendicular. For small UCS and E_s values the relationship between the parameters is excellent, and with higher values the scatter increases considerably. The core samples comply with the data of outcrop samples. When core results are included, the quality of regression analysis fit is even improved and is demonstrated by a higher coefficient of determination (Fig. 5.5a; Table 5.5).

If sandstone samples are plotted separately the coefficient of determination is high and confidence and prediction bands, respectively, are narrow (Table 5.5; Fig. 5.5b). It has to be considered that the sampled carbonates are both matrix and sparry limestones with varying amount of bioclasts (cf. Tables 5.2, 5.3). These more-heterogeneous compositions of carbonate samples are reflected in statistically less satisfactory results (Table 5.5; $R^2 = 0.576$) with wider prediction and confidence bands (Fig. 5.5c). The increase of the regression curve is lower than for sandstone samples; that is, a carbonate sample is expected to have a higher E_s value than a sandstone sample of similar UCS. For both, sandstones and carbonates, equivalent core samples match the scatter of outcrop data well and lie within the 90% prediction bands. There are only minor changes of regression curves if core samples are included (Figs. 5.5b, c).

There is a known relationship between porosity and Young's modulus of rocks (e.g., Rajabzadeh et al., 2012). Therefore, we redraw the UCS-E_s data of sandstones and carbonates with different marks for low, medium and high-porosity rocks (Figs. 5.5e, f). Sandstones and carbonates with high porosities have lowest UCS and E_s values; the differences between medium and low-porosity rocks are less pronounced. Both porosity classes include medium UCS and E_s values as well as high values.

5.2. Deriving rock properties from UCS

5.2.1. Destruction work

The destruction work is an important parameter for dimensioning and planning of drilling projects and correlates with drilling efficiency (Thuro, 1997). Rocks which strongly deform while loading have high W values because for specimen failure, more energy is needed. W, calculated as the area below the stress-strain curve of the uniaxial compression test, is plotted against UCS of the different samples (Fig. 5.6).

Regression analyses show that power-law functions fit best in most cases, and coefficients of determination are rather high in all cases. To analyse the statistical significance, 90% confidence and prediction bands are added.

For outcrop samples parallel and perpendicular to bedding, the fit is excellent with narrow bands (Figs. 5.6a, d; Table 5.5). There are, however, clear lithological differences of the W values. For carbonates, core samples show a considerable deviation from the

regression function of outcrop data more to lower W values for similar UCS (Fig. 5.6c). For sandstones, core samples show a wider scatter, in some cases even beyond the 90% prediction bands of outcrop samples (Fig. 5.6b). The slope for clastic rock samples is considerably steeper than that of carbonate rocks (Fig. 5.6c). That is, more energy is needed to destruct a sandstone sample than a carbonate sample of the same UCS value. From that we infer that sandstone samples receive more deformation at the same applied stress than carbonate samples.

In the same way as we did for UCS-E_s values (Figs. 5.5e, f), UCS-W data of sandstones and carbonates with low, medium and high-porosity rocks are plotted separately (Figs. 5.6e, f). Also in this case, sandstones and carbonates with high porosities have the lowest UCS and W values; the differences between medium and low-porosity rocks are less clear. For carbonate samples, however, we recognise that low-porosity samples tend to have higher UCS and W values than high-porosity samples (Fig. 5.6f).
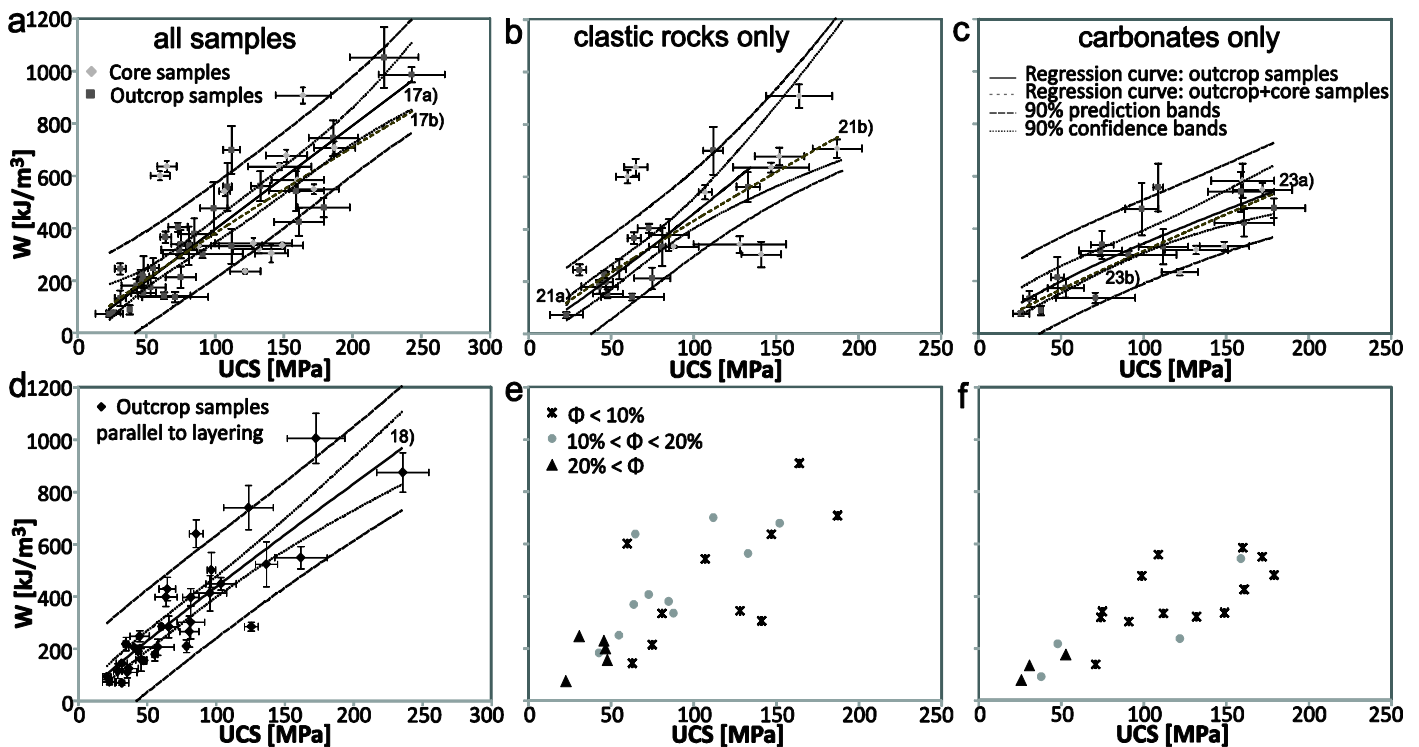

Fig. 5.6. UCS versus W for specimens taken perpendicular to layering for outcrop and core samples separately for a) all samples (n=49), b) only clastic rock samples (n=24) and c) only carbonate samples (n=18); d) UCS versus W for all specimens taken parallel to layering (n=33). Regression curves shown for both quarry and core samples and quarry samples only; 90% prediction and confidence bands are included; for regression equations see Table 5.5. Error bars stand for standard deviations of all measurements of every sample (Table 5.4). e-f) UCS versus W for low, medium and high-porosity samples of clastic rocks (e) and carbonates (f).

5.2.2. Indirect tensile strength

For rocks, there is a known correlation between compressive and tensile strength with a factor of approximately 10 between these two parameters (e.g. Hobbs, 1964; Lockner, 1995). Our results are in good accordance; coefficients of determination are high in all

cases with very narrow confidence and prediction bands. Overall, the values of core samples are similar to the values of outcrop samples and plot within the 90% prediction bands. Both regression functions, developed for clastic rocks, are very similar, and core results fit well within the scatter that is quite similar to outcrop results

(Fig. 5.7b; Eqs. 22a, b). For carbonates, the equivalent core samples also plot within the 90% prediction bands (Fig. 5.7c).

However, there are clear lithological differences in the indirect tensile strength values of the outcrop samples (Figs. 5.7b, c). For low UCS, T_0 values of clastic rock samples are lower than those of carbonates; for high UCS, however, the increase of T_0 values is less for carbonates, leading to higher values of clastic rock samples.

We plot UCS-T_0 data of sandstones and carbonates with low, medium and high-porosity rocks (Figs. 5.7e, f; see key). This empirical relation also shows that high-porosity samples of clastic rocks and carbonates have the lowest UCS and T_0 values; the differences between medium and low-porosity rocks are less clear. In contrast to the UCS-W relation (Fig. 5.6) where carbonates tend to have higher values, we recognise that in this case low-porosity sandstone samples tend to have higher UCS and T_0 values.
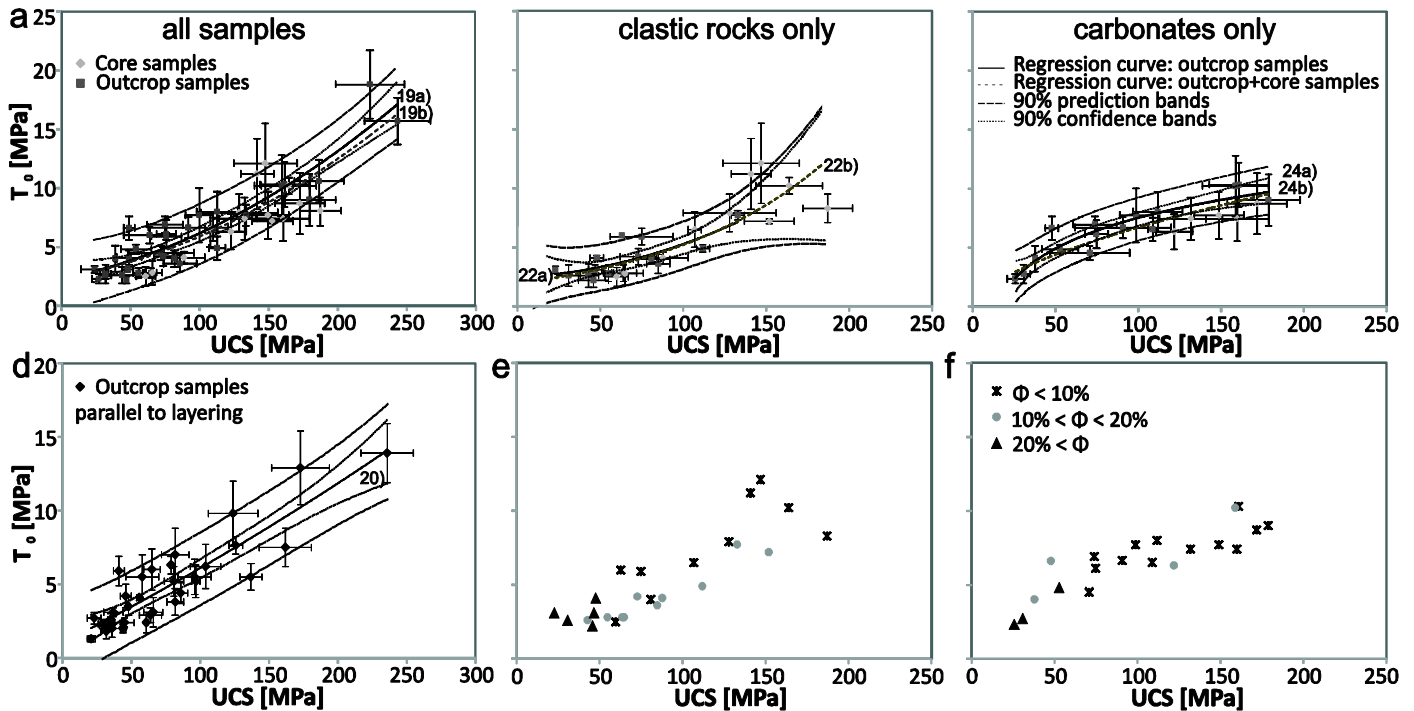

Fig. 5.7. UCS versus T_0 for specimens taken perpendicular to layering for outcrop and core samples separately for a) all samples (n=49), b) only clastic rock samples (n=24) and c) only carbonate samples (n=18); d) UCS versus T_0 for all specimens taken parallel to layering (n=33). Regression curves shown for both quarry and core samples and quarry samples only; 90% prediction and confidence bands are included; for regression equations see Table 5.5. Error bars stand for standard deviations of all measurements of every sample (Table 5.4). e-f) UCS versus T_0 for low, medium and high-porosity samples of clastic rocks (e) and carbonates (f).

6. Discussion

6.1. Applicability of empirical relations to predict in situ rock properties

A comparison of empirical relations, determined from outcrop samples only, with properties of core samples gives information on parameter changes due to load removal and beginning of alteration. We found that the developed empirical relations with or without core samples are quite similar for all analysed parameters (cf. Sect. 5, Table 5.5). Simply, core samples have similar or only slightly higher values than outcrop samples. That is, the ratios of UCS with the considered parameters do not change considerably. Based on these findings it is assumed that these parameter-UCS ratios remain unaffected by unloading. Only the destruction work shows some divergence between outcrop and core samples. For carbonates with high UCS, destruction-

work values of core samples tend to be lower than those of outcrop samples with comparable UCS resulting in a steeper regression function for outcrop samples only (Fig. 5.6c). That is, for the destruction of core samples less energy is needed than for outcrop samples. This may be caused by higher porosities of outcrop samples where more energy can be absorbed by pore-space destruction before brittle failure occurs. The destruction work, measured in the laboratory, correlates with the in situ drillability of rocks (Thuro, 1997). Therefore, the destruction work, measured in laboratory, is strongly related to field-work efforts.

The UCS-E_s relationship indicates that clastic and carbonate rocks including their core equivalents show different behaviour. A carbonate rock is expected to have a higher E_s compared with a clastic rock of the same UCS (Fig. 5.5). The intensity of deformation

depends on the rock strength, the stresses applied and the time over which the stresses are acting and accumulating. It is known that carbonate rocks react differently to stresses than clastic rocks (e.g., Lockner, 1995; Jaeger et al., 2007). On long-term stress applications clastic rocks may receive more brittle deformation than carbonate rocks due to pressure-solution and slip-folding processes which are typical phenomena in carbonates (Fossen, 2010). These are deformation processes which act on a longer timescale. At drilling operations, however, there is only a short-term stress application on the rock mass similarly to laboratory experiments. That is, the UCS-E relationship is developed for a similar timescale as the goal of this study, namely drilling applications, and not for long-term deformation processes.

All data in this study were determined in laboratory measurements of dry rock specimens. Applying the results to in situ conditions is non-trivial for some parameters because rocks at depth are loaded by overburden and confining pressures and are commonly saturated with fluids. Saturation and pressures have strong effects on some of the described parameters.

The P-wave velocity is one parameter which can be determined easily by using a borehole acoustic log. It has to be taken into account that v_p measurements in boreholes comprise a larger volume which may include fractures and are obtained with different frequencies than laboratory measurements. Therefore, in most cases, saturated samples, measured in laboratory, give higher v_p values than in situ rocks determined from well logs (e.g. Popp and Kern, 1994; Zamora et al., 1994). Laboratory measurements of dry specimens will give lower velocities than those of fully saturated samples (Nur and Simmons, 1969). Kahraman (2007) showed that for sedimentary rocks there is a strong linear correlation between P-wave velocities of dry v_p^d and saturated rocks v_p^w. Most rocks show significant trends of UCS reduction with increasing degree of saturation (Shakoor and Barefield, 2009; Karakul and Ulusay, 2013). For Miocene limestones, there is a reduction of UCS and T_0 values with increasing saturation (Vásárhelyi, 2005). Similarly, Baud et al. (2000) showed that there is a weakening effect of water on sandstone. Triaxial tests have shown that compressive strength and Young's modulus of rocks positively correlate with confining pressure (Nur and Simmons, 1969; You, 2003; Zoback, 2007).

All laboratory measurements have been carried out on high-quality samples where discontinuities such as fractures are absent. In situ rocks, in contrast, typically include fractures. That is, UCS and E_s values measured with laboratory tests tend to be higher than those measured in situ (Priest, 1993; Huang et al., 1995). The presented data of Young's modulus were determined with uniaxial compressive tests, which give static Young's modulus values referring to fracture propagation (cf., Section 1; Jaeger et al., 2007). In boreholes, from acoustic logs, dynamic Young's moduli are obtained (Zoback, 2007; Rider and Kennedy, 2011). The comparison of dynamic and static Young's moduli is complicated. Discontinuities such as fractures have different effects on static measurements of Young's modulus and P-wave propagation. Martínez-Martínez et al. (2012), for example, showed that, for carbonate rocks, there is only a poor linear relationship which can be corrected by using v_p and Poisson's ratio.

This shows that transfer to in situ conditions has to be considered carefully for each parameter individually.

For validation purposes, it is advisable to apply the developed equations on logging data of wellbores in the NWGB for UCS calculation. It would then be possible to compare the calculated UCS values with the actual UCS values measured with cores of the same wellbore (cf., Vogt et al., 2012). The estimation of rock strength is not only possible with empirical relations as presented in this study but also with micromechanical methods (e.g, Sammis and Ashby, 1986; Zhu et al., 2011), which are powerful tools to understand failure processes in rock. To build a geomechanical model before starting the drilling operation, such micromechanical methods may be a good supplemental option when using data from adjacent wellbores.

6.2. Comparison with previous studies

Many empirical relations between UCS and other parameters were developed. In Table 5.6, selected equations are presented. None of these relations, however, refer to the NWGB. These functions fit best for the geological situation the analysed samples belong to and are only valid for the defined range of parameter values (cf. Fig. 5.8). In most cases, the functions relate to a specific lithology.

The presented regression analyses show that coefficients of determination of the regression curves for carbonates have, in most cases, smaller values compared with sandstone samples. Carbonate samples from the NWGB include sparry and matrix limestones, bioclast-rich limestones, oolites, marls, and dense and porous limestones (cf. Tables 5.2, 5.3). This means that the lithology of sampled carbonates is much more variable than that of sandstones. This may be one reason for the wider range of mechanical and physical data and the poorer relations of UCS-E_s (Eqs. 12b, 16b), UCS-v_p (Eqs. 11b, 15b), and UCS-Φ (Eqs. 9b, 13b). In former studies on limestones (e.g. McNally, 1987;

Sachpazis, 1990; Bradford et al., 1998; Chang et al., 2006) the lithology, for which the empirical relation was developed, is specified. Accordingly, the presented relationships are more trustworthy if they refer to a specific lithology (cf. Eqs. 9-16, 21-24). If only general assumptions of UCS values are needed (e.g. from well logs of heterogeneous stratifications) or the lithology of the respective wellbore section cannot be defined precisely, it appears to be better to apply the empirical relations generated for all samples (Eqs. 1-8, 17-20).

To compare the regression functions, developed in this study, with the relations of previous studies we use a graphic representation considering the range of parameter values for which the relations were developed (Table 5.6; Fig. 5.8). Differences between the functions are depicted. For clastic rocks, there are significant variations for small porosities (Fig. 5.8a.1). Vernik et al. (1993; Eq. 25) predict much higher UCS for low-porosity sandstones ($\Phi<15\%$) and lower UCS for high-porosity sandstones ($\Phi>25\%$) than Eqs. 9a and 9b. They, however, determined UCS values from triaxial testing, which gives higher UCS values than uniaxial compressive strength measurements (cf. Zoback, 2007). The effects of small discontinuities on rock strength are smaller when confining pressure is applied.

For carbonate rock samples, however, the calculated regression functions (Eqs. 13a, b) fit perfectly well with previous studies (Fig. 5.8a.2). Only for high-porosity carbonate rocks ($\Phi>15\%$) are the smallest variations from Eq. (30) in the range of 10 MPa for UCS.

The errors of the empirical relations between UCS-v_p and UCS-Δt, respectively, are high for all studies (cf. Table 5.5). The determined regression functions of previous studies are, however, quite similar to Eq. (11b) for clastic rocks (Fig. 5.8b). The UCS-v_p relation of Freyburg (1972; Eq. 34) is in good accordance with our results. The data relate to sandstones from the Middle Bunter and Lower Bunter (Thuringia, Germany) as well. The comparability of the equations is therefore also based on similar sedimentary conditions of the analysed rocks.

Eqs. 15a, b lead to much higher UCS values for high v_p than the relationship published by Kahraman (2001; Eq. 35), who considered not only carbonate samples. There are also bigger differences between our results and other equations (Eqs. 31, 32) which both include different kinds of rock. The regression function obtained by Sharma and Singh (2008), for example, is based on only three sandstone samples together with many other samples of different rock types (volcanic, sedimentary, and metamorphic) and therefore differs too much from the samples analysed in this study so that they cannot be compared. McNally (1987) published empirical relations of UCS-Δt for different stratigraphic units in Australia. The functions relating to clastic units (Eqs. 29, 30) are comparable with Eq. (11b), but only for low Δt values ($\Delta t < 75$ µs/ft; Fig. 5.8b).

Table 5.6. Correlations between UCS and the parameters porosity, P-wave velocity, travel time and Young's modulus reported by other authors.

Eq.	Parameter	UCS2:1 [MPa]	Rock type	Reference
25	Φ	$254(1-0.027\Phi)$ [Φ in %]	Clastic rocks	Vernik et al. 1993
26		$277e^{-0.1\Phi}$ [Φ in %]	Sandstones ($0.2<\Phi<33\%$)	Chang et al. 2006
27		$143.8e^{-0.0695\Phi}$ [Φ in %]	High UCS limestones ($5<\Phi<20\%$)	Chang et al. 2006
28		$135.9e^{-48\Phi}$ [Φ in %]	High UCS limestones ($0<\Phi<20\%$)	Chang et al. 2006
29	$v_p / \Delta t$	$1277e^{-0.036\Delta t}$ [Δt in µs/ft]	Sandstones	McNally 1987
30		$1174e^{-0.0358\Delta t}$ [Δt in µs/ft]	Clastic rocks	McNally 1987
31		$56.71v_p-192.93$ [v_p in km/s]	Limestones, clastic rocks ($3.9<v_p<5.2$ km/s)	Çobanoğlu and Çelik 2008
32		$0.0642v_p-117.99$ [v_p in m/s]	Different kinds of rock ($1800<v_p<3000$ m/s)	Sharma and Singh 2008
33		$9.95v_p^{1.21}$ [v_p in km/s]	Different kinds of rock ($1<v_p<6.3$ km/s)	Kahraman 2001
34		$0.035v_p-31.5$ [v_p in m/s]	Sandstones	Freyburg 1972
35	E_s/E	$2.667E_s-4.479$ [E_s in GPa]	Carbonate rocks	Sachpazis 1990
36		$2.28+4.1089E_s$ [E_s in GPa]	Sandstones	Bradford et al. 1998
37		$46.2e^{0.000027E}$ [E in MPa]	Sandstones	Chang et al. 2006
38		$0.4067E^{0.51}$ [E in MPa]	Limestones ($10<UCS<300$ MPa)	Chang et al. 2006

UCS uniaxial compressive strength; Φ porosity; E_s static Young's modulus; Δt travel time; v_p P-wave velocity
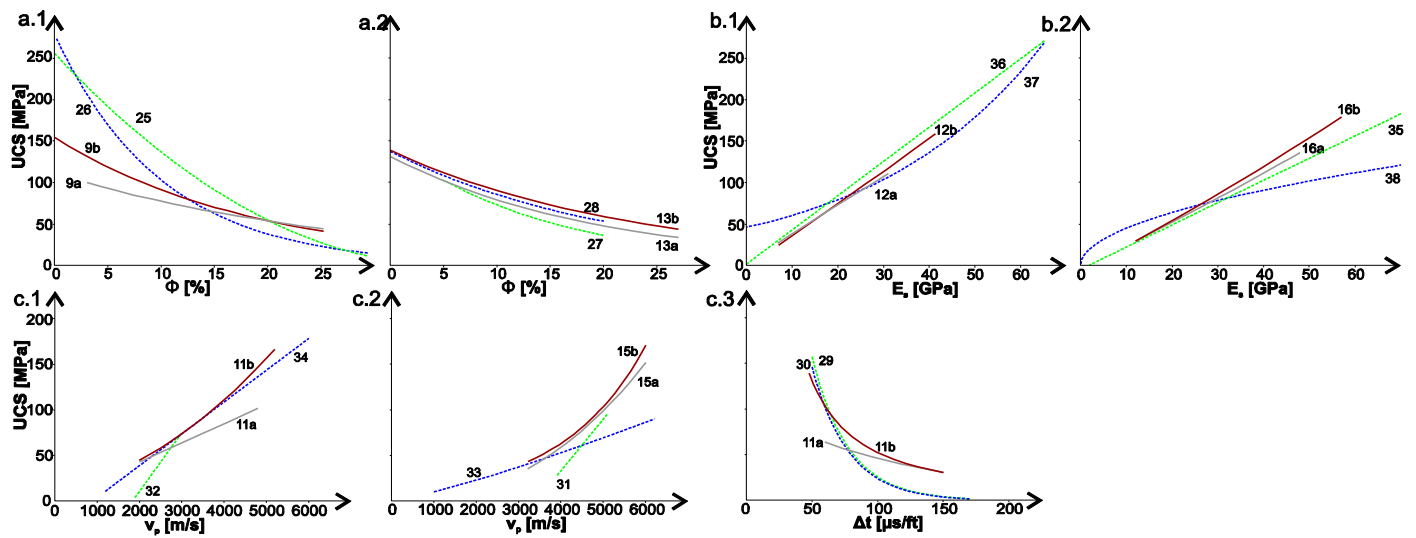
Fig. 5.8. Correlations between UCS and the parameters a) porosity, b) E_s and c) v_p separately for clastic rocks and carbonates; correlations from this study and those published by other authors (equation numbers shown) consider the range of parameter values for which the functions are valid.

In comparison with the two relationships presented above, UCS-Φ and UCS-v_p, it is noteworthy that calculated regression functions for UCS-E_s of both carbonate rock samples and sandstones are in good accordance with previous studies (Table 5.6; Fig. 5.8c). Only the limestone function by Chang et al. (2006; Eq. 38) predicts higher UCS for small E_s values and lower UCS for high E_s values than Eq. (8c). The study of Chang et al. (2006), however, is not based on measurements of the static Young's modulus but of the dynamic Young's modulus. As discussed above, the comparability of dynamic and static Young's moduli is complicated because discontinuities have different effects on the measurements of static Young's modulus and acoustic wave propagation.

Overall, the obtained empirical relations are similar to equations developed in previous studies but, in some cases, show considerable differences. These variations mostly relate either to differences in lithologies the study is based on (Eqs. 31, 32), or to different ways of parameter determination (Eqs. 25, 38). The presented data set and empirical relations, however, give new and comprehensive information about mechanical and physical properties of sedimentary and volcanic rocks valid for the NWGB. Nevertheless, they are not only interesting for regional drilling projects or geomechanical modelling. They also supplement and enlarge the existing published results on rock properties, and the new relations may be applied to other sedimentary basins similar to the NWGB.

7. Conclusions

Geomechanical and physical parameters with importance in different stages of geothermal exploitation are measured for 35 outcrop samples from quarries and 14 core samples of the Northwest German Basin. Rock properties of these core samples are compared with results of outcrop samples by using regression analyses. The following conclusions can be made:

1. Simple regression analyses for UCS with the parameters porosity, bulk density, and P-wave velocity indicate that the statistical significance for these parameters is low. The developed equations yield distinct under- and over-predictions of UCS values. Data show, however, that properties of core samples fit perfectly well within the scatter of outcrop samples. That is, the developed regression functions work well for at least estimating core sample properties with comparatively small deviation. For drilling applications these equations are highly substantial because they allow a continuous update of the original geomechanical model with logging-while-drilling methods for the calculation of optimum mud weights to avoid wellbore instabilities.

2. The developed empirical relations for Young's modulus, destruction work and indirect tensile strength with UCS show high statistical significance. Core samples plot within 90% prediction bands. Regression analyses indicate that prediction of destruction work and tensile strength from UCS by outcrop data is possible. The applicability of these equations to rocks from greater depths is therefore assumed. The ratio between UCS and parameter values is the same for both outcrop and core samples. That is, data indicate that parameters of core sample are predictable from equations developed from an outcrop sample data set.

3. The presented data and regression equations may help to predict UCS values for sedimentary rocks at depth, and thus develop suitable geomechanical models for the adaptation of the drilling strategy on rock mechanical conditions in the Northwest German Basin and similar sedimentary basins.

Acknowledgements

References

Aggistalis, G., Alivizatos, A., Stamoulis, D., and Stournaras, G.: Correlating uniaxial compressive strength with Schmidt hardness, point load index, Young's modulus, and mineralogy of gabbros and basalts (Northern Greece), Bull. Int. Assoc. Eng. Geol., 54, 3-11, 1996.Baud, P., Zhu, W., and Wong, T.-f.: Failure mode and weakening effect of water on sandstone, J. Geophys. Res. B: Solid Earth, 105 (B7), 16371-16389, 2000.

Betz, D., Führer, F., Greiner, G., and Plein, E.: Evolution of the Lower Saxony Basin, Tectonophys., 137, 127-170, 1987.

Bradford, I. D. R., Fuller, J., Thompson, J., and Walsgrove, T. R.: Benefits of assessing the solids production risk in a North Sea reservoir using elastoplastic modelling, SPE/ISRM Eurock '98, Trondheim, 261-269, 1998.

Brink, D.: Essentials of Statistics. 2nd ed. David Brink & Ventus Publishing, bookboon.com, ISBN: 978-87-7681-408-3; 2010.

Chang, C., Zoback, M. D., and Khaksar, A.: Empirical relations between rock strength and physical properties in sedimentary rocks, J. Pet. Sci. Eng., 51, 223-237, 2006.

Çobanoğlu, I., and Çelik, S. B.: Estimation of uniaxial compressive strength from point load strength, Schmidt hardness and P-wave velocity, Bull. Eng. Geol. Environ., 67, 491-498, 2008.

Dinçer, I., Acar, A., Çobanoğlu, I., and Uras, Y.: Correlation between Schmidt hardness, uniaxial compressive strength and Young's modulus for andesites, basalts and tuffs, Bull. Eng. Geol. Environ., 63, 141-148, 2004.

Dusseault, M. B.: Geomechanical challenges in petroleum reservoir exploitation, KSCE J. Civ. Eng., 15(4), 669-678, 2011.

Edlmann, K., Somerville, J. M., Smart, B. G. D., Hamilton, S. A., and Crawford, B. R.: Predicting rock mechanical properties from wireline porosities, SPE/ISRM Eurock 47344, 1998.

Fossen, H.: Structural Geology. Cambridge University Press, New York, 2010.

Freyburg, E.: Der Untere und Mittlere Buntsandstein SW-Thüringen in seinen gesteinstechnischen Eigenschaften, Ber. Dtsch. Ges. Geol. Wiss. A Berlin, 17(6), 911-919, 1972.

Fricke, S., and Schön, J.: Praktische Bohrlochgeophysik. Enke, Stuttgart, 1999.

Gebrande, H., Kern, H., and Rummel, F.: Elasticity and inelasticity. In: Hellwege, K.-H. (ed.), Landolt–Bornstein Numerical Data and Functional Relationship in Science and Technology, New Series; GroupV. Geophys. Space Res., 1, Physical Properties of Rocks, Subvolume b. Springer, Berlin, 1-233, 1982.

Gudmundsson, A.: Rock Fractures in Geological Processes. Cambridge University Press, New York, 2011.Heap, M. J., Faulkner, D. R., Meredith, P.G., and Vinciguerra, S.: Elastic moduli evolution and accompanying stress changes with increasing crack damage: implications for stress changes around fault zones and volcanoes during deformation. Geophys. J. Int., 183, 225-236, 2010.

Hobbs, D. W.: The tensile strength of rocks, Int. J. Rock Mech. Min. Sci. Geomech. Abstr., 1/3, 385-396, 1964.

Huang, T. H., Chang, C. S., and Yang, Z. Y.: Elastic moduli for fractured rock mass, Rock Mech. Rock Eng., 28, 135-144, 1995.

ISRM: The Complete ISRM Suggested Methods for Rock Characterization, Testing and Monitoring: 1974-2006. Suggested Methods Prepared by the Commission on Testing Methods, International Society for Rock Mechanics, R. Ulusay & J. A. Hudson (eds.), Compilation Arranged by the ISRM Turkish National Group, Ankara, Turkey, 2007.

Jaeger, J. C., Cook, N. G. W., and Zimmerman, R. W.: Fundamentals of Rock Mechanics. Blackwell, Malden USA, 2007.

Jizba, D. L.: Mechanical and Acoustical Properties of Sandstones. Dissertation, Stanford University, 1991.

Kahraman, S.: Evaluation of simple methods for assessing the uniaxial compressive strength of rock, Int. J. Rock Mech. Min. Sci., 38, 981-994, 2001.

Kahraman, S.: The correlations between the saturated and dry P-wave velocity of rocks, Ultrason., 46, 341-348, 2007.

Karakul, H., and Ulusay, R.: Empirical correlations for predicting strength properties of rocks from P-wave velocity under different degrees of saturation, Rock Mech. Rock Eng., 46, 981-999, 2013.

Khaksar, A., Taylor, P. G., Kayes, T., Salazar, A., Rahman, K.: Rock strength frlom Core and logs: Where we stand and ways to go, SPE EUROPEC/EAGE, 121972, 2009.

Lama, R. D., and Vutukuri, V. S.: Handbook on Mechanical Properties of Rocks – Testing Techniques and Results, Vol. II. Trans Tech Publications, Clausthal, 1978.

Li, S., George, J., and Purdy, C.: Pore-pressure and wellbore-stability prediction to increase drilling efficiency, J. Pet. Technol., 64, 99-101, 2012.

Lockner, D. A.: Rock Failure, Rock physics and phase relations, American Geophysical Union, Washington D.C., 127-147, 1995.

Martínez-Martínez, J., Benavente, D., and García-del-Cura, M. A.: Comparison of the static and dynamic elastic modulus in carbonate rocks, Bull. Eng. Geol. Environ., 71, 263-268, 2012.

McNally, G. H.: Estimation of coal measures rock strength using sonic and neutron logs, Geoexplor., 24, 381-395, 1987.

Nabaei, M., and Shahbazi, K.: A new approach for predrilling the unconfined rock compressive strength prediction, Pet. Sci. Technol., 30/4, 350-359, 2012.

Nur, A., and Simmons, G.: The effect of saturation on velocity in low porosity rocks, Earth Planet. Sci. Lett., 7, 183-193, 1969.

Palchik, V.: Influence of porosity and elastic modulus on uniaxial compressive strength in soft brittle porous sandstones, Rock Mech. Rock Eng., 32, 303-309, 1999.

Paschen, H., Oertel, D., and Grünwald, R.: Möglichkeiten geothermischer Stromerzeugung in Deutschland. TAB Arbeitsbericht 84, 2003.

Popp, T., and Kern, H.: The influence of dry and water saturated cracks on seismic velocities of crustal rocks – A comparison of experimental data with theoretical model, Surv. Geophys., 15, 443-465, 1994.

Priest, S. D.: Discontinuity Analysis for Rock Engineering. Chapman and Hall, London, 1993.

Proehl, T. S.: Geomechanical uncertainties and exploratory drilling costs, SPE/ISRM Rock Mechanics Conference, Irving, USA, 2002.

Rajabzadeh, M. A., Moosavinasab, Z. and Rakhshandehroo, G.: Effects of rock classes and porosity on the relation between uniaxial compressive strength and some rock properties for carbonate rocks, Rock Mech. Rock Eng., 45, 113-122, 2012.

Reyer, D., Bauer, J. F., and Philipp, S. L.: Fracture systems in normal fault zones crosscutting sedimentary rocks, Northwest German Basin, J. Struct. Geol., 45, 38-51, 2012.

Rider, M., and Kennedy, M.: The Geological Interpretation of Well Logs. Rider-French Consulting Ltd., 2011.

Sachpazis, C. I.: Correlating Schmidt hammer rebound number with compressive strength and Young's modulus of carbonate rocks, Bull. Int. Assoc. Eng. Geol., 42, 75-83, 1990.

Sammis, C. G. and Ashby, M. F.: The failure of brittle porous solids under compressive stress states, Acta. Metall., 34, 511-526, 1986, doi: 10.1016/0001- 20656160(86)90087-8.

Settari, A., and Walters, D. A.: Advances in coupled geomechanical and reservoir modeling with applications to reservoir compaction, SPE 74142, SPEJ (September 2001), 335-342, 2001.

Shakoor, A., and Barefield, E. H.: Relationship between unconfined compressive strength and degree of saturation for selected sandstones, Environ. Eng. Geosci., 15, 29-40, 2009.

Sharma, P. K., and Singh, T. N.: A correlation between P-wave velocity, impact strength index, slake durability index and uniaxial compressive strength, Bull. Eng. Geol. Environ., 67, 17-22, 2008.

Thuro, K.: Drillability prediction: geological influences in hard rock drill and blast tunnelling, Geol. Rundsch., 86, 426-438, 1997.

Vásárhelyi, B.: Statistical analysis of the influence of water content on the strength of the miocene limestone, Rock Mech. Rock Eng., 38, 69-76, 2005.

Vernik, L., Bruno, M., and Bovberg, C.: Empirical relations between compressive strength and porosity of siliciclastic rocks, Int. J. Rock Mech. Min. Sci. Geomech. Abstr., 30, 677-680, 1993.

Vogt, E., Reyer, D., Schulze, K. C., Bartetzko, A., and Wonik, T.: Modeling of geomechanical parameters required for safe drilling of geothermal wells in the North German Basin, Celle Drilling, Celle, Germany, 2012.

Walter, R.: Geologie von Mitteleuropa. Schweizerbarth, Stuttgart, 2007.

Wong, T.-f., David, C., and Zhu, W.: The transition from brittle faulting to cataclastic flow in porous sandstones: mechanical deformation, J. Geophys. Res., 102, 3009-3025, 1997.

Wooldridge, J.M.: Introductory Econometrics: A Modern Approach. 4th ed. Mason: South-Western, Cengage Learning; 2009.

York, P., Pritchard, D., Dodson, J. K., Rosenberg, S., Gala, S., and Utama, B.: Eliminating non-productive time associated with drilling trouble zones, Offshore Technology Conference 2009, Houston, USA, 2009.

You, M.: Effect of confining pressure on the Young's modulus of rock specimen, Chin. J. Rock Mech. Eng., 22(1), 53-60, 2003.

Zamora, M., Sartoris, G., and Chelini, W.: Laboratory measurements of ultrasonic wave velocities in rocks from the Campi Flegrei volcanic system and their relation to other field data, J. Geophys. Res., 99, 13,553-13,561, 1994.

Zeynali, M. E.: Mechanical and physico-chemical aspects of wellbore stability during drilling operations, J. Pet. Sci. Eng., 82-83, 120-124, 2012.

Zhu, W., Baud, P., Vinciguerra, S., and Wong, T.-f.: Micromechanics of brittle faulting and cataclastic flow in Alban Hills tuff, J. Geophys. Res. B: Solid Earth, 116 (6), art. no. B06209, doi: 10.1029/ 2010JB008046, 2011.

Ziegler, P.: Geological Atlas of Western and Central Europe. Geological Society Publishing House/Shell International Petroleum Maatschappij B.V., 1990.

Zoback, M. D.: Reservoir Geomechanics. Cambridge University Press, New York, 2007.

6   Failure and friction criteria based on samples from outcrop analogues for core property prediction

Dorothea Reyer, Sonja L. Philipp

University of Göttingen, Geoscience Centre, Goldschmidtstraße 3, 37077 Göttingen, Germany

Abstract

Knowledge of rock failure and friction criteria helps to avoid wellbore stability issues. Because drill core material is rare, in most cases it is not viable to perform complete triaxial test series with core samples to determine their failure criteria. In this study it is analysed if Mohr-Coulomb failure and friction criteria for drill cores may be predictable utilising equivalent samples from outcrop analogues. Our database consists of three sandstone and two carbonate core samples from two wellbores and one volcanic rock sample from a deep quarry level, and equivalent outcrop samples from the Northwest German Basin. Equivalence of core and outcrop samples is evaluated using thin section analyses with focus on texture, cementation, grain size, porosity, and mineralogical composition. For the stratigraphic units not represented in drill cores, ten outcrop samples were also included.

Conventional triaxial tests were performed. Criteria for outcrop samples were obtained separately and the resulting 90% confidence and prediction bands compared with core sample results. If there is good equivalence regarding texture and porosity, it is concluded that obtained failure criteria are applicable for core property prediction. Grain size and mineralogical composition are of minor importance for the addressed question. Friction data are in good accordance with Byerlee friction; no considerable differences of friction between core and outcrop samples were detected.

Applicability of outcrop sample failure and friction criteria for wellbore stability analyses is concluded when equivalence of chosen outcrop samples, regarding textural similarity, especially grain interlocking and cementation of sandstone samples, and porosity is ensured.

1. Introduction

At drilling projects in sedimentary basins composed of various rock types with different rock mechanical properties, wellbore instabilities are common (e.g. [1]). Wellbore instabilities are recognised as a drilling challenge that may considerably increase drilling costs and safety risks [2-4]. To prevent stability problems while drilling and thereby minimise the total cost, it is recommended to develop suitable geomechanical models beforehand. Geomechanical models comprise assumptions on stresses, pore pressures and predicted rock mechanical properties of the whole wellbore profile. Based on these assumptions, such geomechanical models help to calculate the optimal mud weight to prevent both borehole breakouts and tensile fracturing leading to wellbore failure and mud loss [5-7]. Depending on rock strengths, wellbore orientation and in situ stresses (magnitudes and directions), large stress concentrations may be induced between formation and near-wellbore area when a hole-wall is established by drilling [8]. If such stress concentrations reach the failure criteria of a specific rock, the rock fails, i.e., breaks. This condition will be referred to as wellbore failure. Friction criteria, however, give information on reactivation of pre-existing weakened zones such as fractures and fault zones [9].

This study aims at predicting failure and friction criteria of potential geothermal reservoir rocks and overburden rocks. As example the North German Basin (NGB) is used, which has a considerable low-enthalpy geothermal potential [10]. Its subsurface is well explored with numerous hydrocarbon wells [11] and there is a broad knowledge about the sedimentary alternation and facies distribution.

For such predictions, we perform conventional triaxial tests and complementary thin section analyses. At best, criteria are derived from core samples. Unfortunately, drill cores from geologic settings comparable to the explored geothermal reservoir are rare so that the direct link with mechanical properties is not possible. In particular, from the younger rock units above, that have to be drilled through to reach the reservoir, core samples are in most cases even unavailable. In these rock units, however, many cases of wellbore instabilities occur [1,5,12]. Equivalent samples from outcrop analogues of these units, in contrast, are easy and cheap to provide. We therefore investigate if it is possible to

apply fracture and friction criteria, determined on equivalent samples taken from quarries, to conditions at larger depths. For this purpose we sampled drill cores from different stratigraphic units from two wellbores in the western NGB: Groß Buchholz 1 (Gt1; e.g. [13]) and Eulenflucht 1 (EF1; e.g. [14]). We then looked for equivalent samples from outcrop analogues for all core samples. Here, "equivalent" means that the outcrop sample is of the same stratigraphic age and of comparable sedimentary facies and composition as the associated core sample. Such equivalent outcrop samples were taken in quarry parts as freshly exposed as possible to minimise changes of mechanical properties as a consequence of exposure. Core samples were not available for all stratigraphic units that have to be drilled through to reach potential geothermal reservoirs. Therefore, we included outcrop samples from additional stratigraphic units to obtain a comprehensive rock mechanical data base for the NGB. These additional samples are four limestones and five sandstones from different stratigraphic ages as well as one volcanic rock (Lower Permian - Rotliegend).

2. Geologic setting and rock samples

The Northwest German Basin (NWGB), the western part of the NGB [15], initiated in the Late Carboniferous to Permian era due to rifting processes subsequent to the Variscan Orogenesis [16,17]. Thermally induced subsidence with isochronic volcanism was initiated and the sedimentation of Rotliegend clastics began. Subsequently, from the Zechstein (Late Permian) to the Quaternary, heterogeneous sediments were deposited (e.g. [18]). The sedimentary succession is characterised by changing sedimentation environments from marine to continental conditions. The NGB is comprised of mainly carbonate and clastic rocks with some intercalated evaporates leading to heterogeneous rock mechanical conditions.
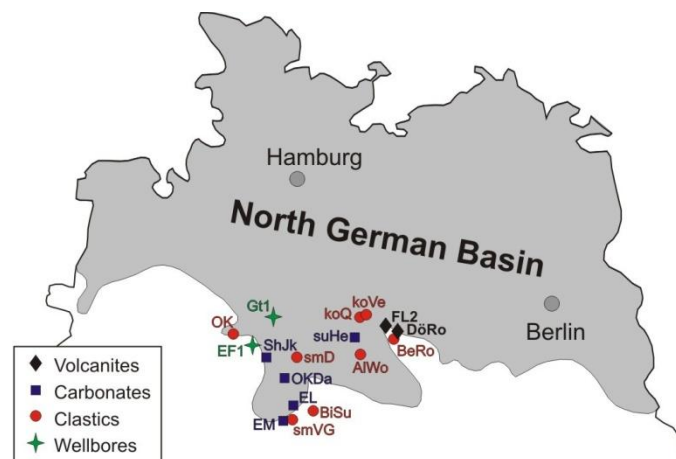

Fig. 6.1. Location of outcrops and wellbores at the southern margins of the Northwest German Basin.

The study area is located at the southern margin of the NWGB (Fig. 6.1; cf. [19]). We took sedimentary core samples from two wellbores (Table 6.1) with Upper Jurassic to Lower Cretaceous and Middle Triassic ages: two carbonate rock units and three sandstone units. Sedimentary rocks, which occur at larger depths in the centre and north of the NWGB, crop out at the basin margin in the South and may be sampled. In such outcrop analogues we took samples, equivalent to the core samples, regarding stratigraphic ages, facies, and textural aspects. From a quarry of Permian volcanic rocks, two different base levels were sampled: one from the second level, just a few meters below surface (*FL2*), and the other from the sixth level at about 85 m depth (*FL6*; Table 6.1). The sample from the deeper level is considered to be representative for larger depth. To enlarge the database of fracture and friction criteria of NWGB rocks, an additional five sandstone, four carbonate and one volcanic rock samples were taken in quarries.

Table 6.1. Sample IDs, lithologies, stratigraphic ages of all samples; for core samples, total vertical depths are included; samples in bold are equivalent to samples from wellbores and deeper quarry levels.

Sample ID	Lithology	System	Local Name	
OK	Sandstone	**Cretaceous**	Wealden-Sst.	
OKDa	Limestone		Oberer Kimmeridge	
ShJk	Limestone	**Jurassic**	Korallenoolith	
AlWo	Sandstone		Aalen-Sst.	
koQ	Sandstone		Rhät-Sst.	
koVe	Sandstone		Rhät-Sst.	
EM	Limestone		Trochitenkalk	
H	Limestone		Schaumkalk	
EL1-2	Limestone	**Triassic**	Wellenkalk	
smD	Sandstone		Detfurth-Folge	
smVG	Sandstone		Volpriehausen-F.	
suHe	Limestone		Rogenstein	
BiSu	Sandstone		Bernburg-F.	
Bero	Sandstone		Rotliegend-Sst.	
DöRo	Andesite	**Permian**	Rotliegend-Vulkanit	
FL2	Rhyolites		Rotliegend-Vulkanit	
Wellbore 1: Eulenflucht 1 (EF1)				
Wellbore 2: Groß Buchholz (Gt1)				**TVD [m]**
Gt1WS1	Sandstone		Wealden-Sst.	1221
EF1WS	Sandstone	**Cretaceous**	Wealden-Sst.	35
EF1OK	Limestone		Oberer Kimmeridge	243
EF1UKK	Limestone	**Jurassic**	Korallenoolith	282
EF1KO	Limestone		Korallenoolith	286
Gt1DU1	Sandstone		Detfurth-Folge	~3535.8
Gt1DU2	Sandstone		Detfurth-Folge	~3534.3
Gt1DU3	Sandstone	**Triassic**	Detfurth-Folge	~3534.7
Gt1VS1	Sandstone		Volpriehausen-F.	~3655.6
Gt1VS2	Sandstone		Volpriehausen-F.	~3657.8
FL6	Rhyolite	**Permian**	Rotliegend-Vulkanit	85

Sst Sandstone; *F* Folge; *TVD* Total vertical depth

3. Methods and procedures

3.1. Sample preparation and characterisation

Triaxial tests were performed on cylindrical specimens which were diamond-drilled to a diameter of 30 mm and sawed and ground square within 0.02 mm parallelism to a length of 60 to 65 mm. Drilling, sawing and grinding were done using water as cooling fluid. The comparably small specimen size is because of limited core material. Specimen size of outcrop samples is adapted to core specimens to ensure comparability of results.

For sample characterisation basic physical properties were measured. The bulk density, ρ_d [g/cm^3], was determined with a GeoPyc 1360 (Micromeritics) on dry specimens. For the same samples, the grain density is measured with Ultrapyknometer 1000 (Quantachrome) at room temperature using 99.9% helium, previously measured bulk densities and masses of the samples. The porosity, Φ [%], is calculated as ratio of bulk and grain density. P-wave velocities were determined with Tektronix TDS 5034B (1 MHz rectangular pulse).

3.2. Experimental procedures

Petrographic analyses of all samples were performed by thin section analyses with a transmitted light microscope (Zeiss Axioplan 2). The mineral composition of sandstone samples was determined by counting with a half-automated point counter (Petrolog lite). One thin section per sample with a total of 500 grains on equally spaced lines was analysed. Depending on grain size, point spacing was 0.2-0.4 mm on each line.

For triaxial tests, a pressure vessel with oil as confining medium was used. To prevent oil penetrating the specimen, pistons and specimen are jacketed by a rubber tube. The rock samples, loaded with a constant confining pressure, are strained in axial direction with a constant velocity of 5.4 mm/h until failure occurs. Confining pressure, specimen's volume changes, axial displacement and axial load are recorded continuously.

Triaxial testing is performed at room temperature. Five specimens per outcrop sample are measured to generate sufficient data to obtain Mohr-Coulomb failure and friction criteria. The number of specimens per core sample was one to two depending on how much core material was available. Triaxial test results of core samples are used to compare failure values of samples from greater depths with failure and friction criteria derived from equivalent outcrop samples.

Linear fracture and friction criteria are derived from linear regressions of shear (τ) and normal stresses (σ_n).

Mohr-Coulomb failure criterion is

$$\tau = \tau_f + \mu_f \, \sigma_n \qquad \qquad Eq.\ 1$$

with: $\quad \tau = \Delta\sigma_{max} / \, 2 \sin(2\beta) \qquad Eq.\ 2$

$\qquad \quad \sigma_n = p_c + \Delta\sigma_{max} / \, 2(1+\cos(2\beta)) \qquad Eq.\ 3$

τ_f is the cohesion and μ is the coefficient of internal friction (tangens of friction angle). Shear and normal stresses are calculated taking into account the dip angle β of observed induced shear fractures where β is the angle between the normal of the failure plane and maximum principal stress σ_1 [20].

Friction criterion is calculated with friction cohesion (τ_0) and coefficient of friction (μ_{fric}) from residual shear (τ_{res}) and normal stresses ($\sigma_{n,res}$):

$$\tau_{res} = \tau_0 + \mu_{fric} \, \sigma_{n,res} \qquad \qquad Eq.\ 4$$

with: $\quad \tau_{res} = \Delta\sigma_{res} / \, 2 \sin(2\beta) \qquad Eq.\ 5$

$\qquad \quad \sigma_{n,res} = p_c + \Delta\sigma_{res} / \, 2(1+\cos(2\beta)) \qquad Eq.\ 6$

For each outcrop sample linear regression analyses of triaxial test results at different confining pressures are performed. If possible, 90% confidence and prediction bands are included. Confidence bands represent the 90% certainty of regression curve estimation based on limited sample data. Prediction bands cover the range in which the values of future measurements of associated samples lie with a probability of 90% [21,22]. Based on these bands core sample results are compared with results of outcrop samples to analyse the predictability of core properties.

4. Thin section analyses

4.1. Mineralogical composition of sandstone samples

The three sandstone types, analysed in detail with samples from quarries and drill cores, are the Wealden sandstone (Lower Cretaceous), Detfurth sandstone and Volpriehausen sandstone (both Middle Bunter, Triassic).

The Wealden sandstone is represented by outcrop sample *OK* and two core samples from two different wellbores and different depths: *Gt1WS* and *EF1WS* (see Table 6.1). Detfurth sandstone is extensively sampled from cores. Outcrop sample *smVG* (Volpriehausen sandstone) and both core samples have similar grain sizes and rounding, but *Gt1VS2* shows a mineralogical composition differing from *smVG* (Fig. 6.2).
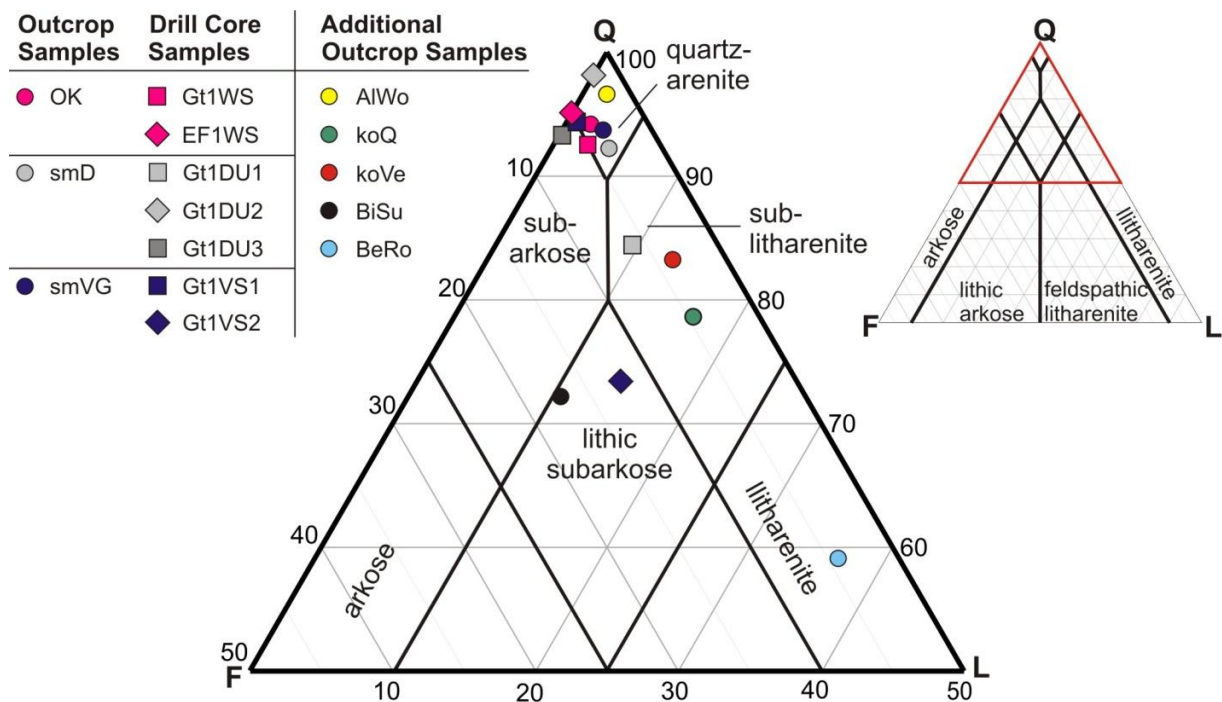
Fig. 6.2. Classification of sandstone samples (see key) according to McBride [23] determined with point-counting with 500 counts.

Mineralogical compositions of sandstone samples are presented in QFL plot (Fig. 6.2) taking into account only quartz, feldspar and lithoclasts (cf. [23]). The quartz contents of all sandstone samples are rather high Wealden sandstones, Detfurth sandstones as well as *Gt1VS2* plot within the quartzarenite field with very low amounts of lithic fragments. Quartz contents of *Gt1DU1*, *smVG* and *Gt1VS1*, respectively, are somewhat lower. The QFL composition of each core sample is similar to its equivalent outcrop sample. That is, the mineralogical comparability of the samples is given except for sample *Gt1DU1*.

The outcrop sandstone samples without core equivalence show increasing quartz contents with decreasing stratigraphic age and cover a wide range of quartz contents.

4.2. Comparison of samples from greater depths with equivalent outcrop samples

For this study it is important to estimate similarities and differences of samples from depths with equivalent outcrop samples. With this knowledge we are able to understand and interpret possible differences in failure and friction criteria between core and outcrop samples. Here, "equivalent" means that the outcrop sample is of the same stratigraphic age, of comparable sedimentary facies, texture, and composition as the associated core sample. The porosity, although its influence on mechanical rock properties is known [24,25], is of minor importance for decision of equivalence but is aspired to be similar. The textural and compositional comparability of core and outcrop samples is controlled by petrographic analyses of thin sections.

In Figure 6.3, thin section images with transmitted light are presented for outcrop sandstone samples. The medium grained Wealden sandstone samples *OK* (outcrop), *EF1WS* and *Gt1WS* (both core samples) are all characterised by high porosities of 16% to 19% and intermediate grain rounding. *OK* and *EF1WS* are well sorted and the quartz cementation is intermediate; *Gt1WS,* in contrast, has a stronger quartz cementation and contains higher amounts of clay minerals aggregating in clay layers (Fig. 6.3). For the samples *OK* and *EF1WS* we therefore confirm a comparability of texture. *Gt1WS* deviates slightly because of the appearance of clay layers and stronger cementation, although other parameters (porosity, grain size, rounding) are similar to sample *OK*.

Core samples from the Detfurth Formation are mainly medium-grained, well sorted hematite-rich sandstones from fluvial deposition environments. Single grains are subrounded and indicate interlocking in consequence of strong compaction leading to low porosities of < 4% (Fig. 6.3). Quartz cementation is pronounced. Only core sample *Gt1DU1* (Detfurth-sandstone) shows an internal lamination based on grain size changes and intercalated clay laminae which may lead to a different mechanical behaviour of this core sample compared with the other samples from Detfurth Formation. Additionally, the amount of lithoclasts in *Gt1DU1* is somewhat higher than in all other Detfurth samples (cf. Section 4.1). The equivalent outcrop sample *smD* has similar characteristic interlocking of single grains. It, however, features a higher porosity of 13.7%.
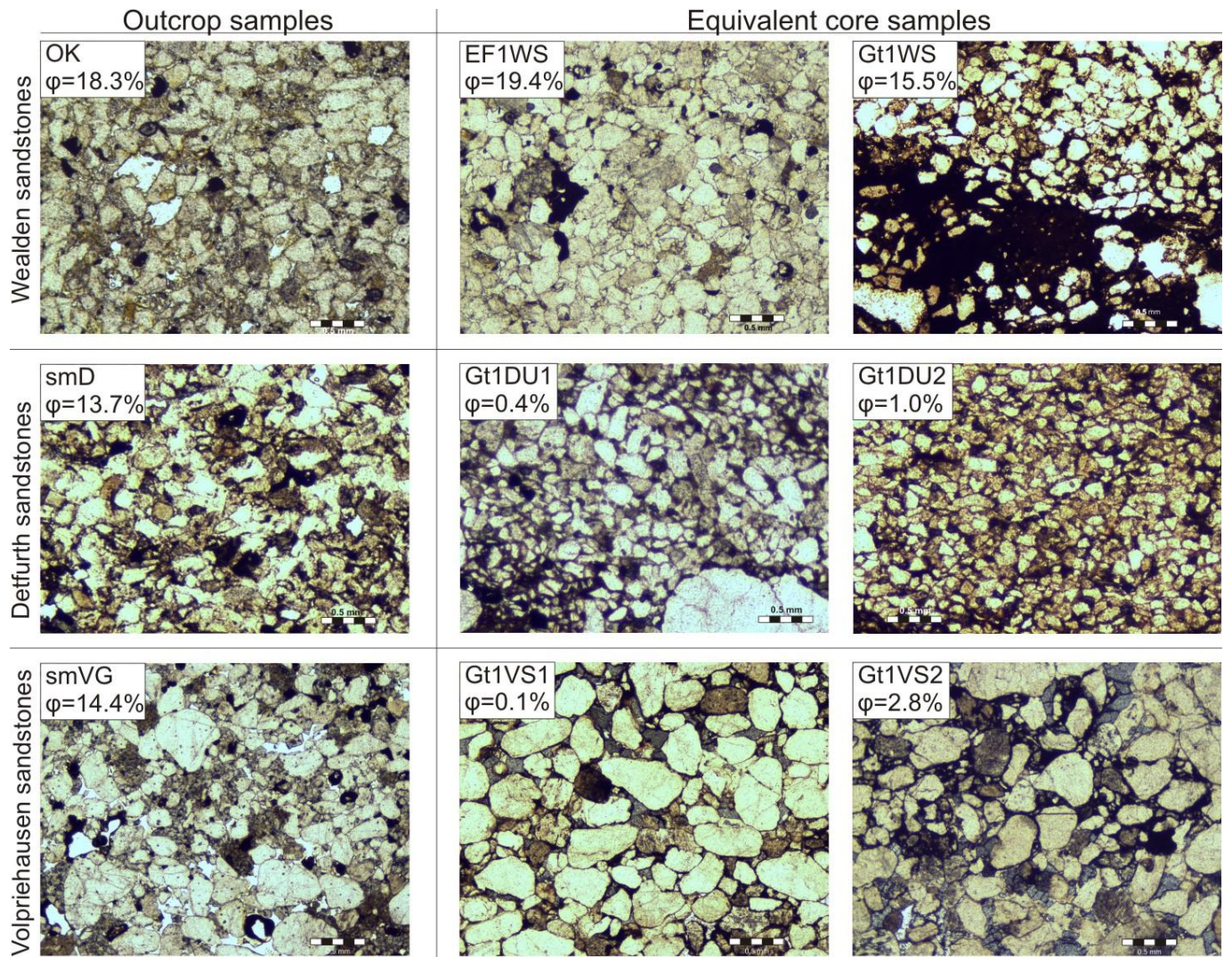
Fig. 6.3. Thin section images with transmitted light of sandstone samples from outcrops with core samples. Scale of 0.5 mm and porosities φ are displayed. For abbreviations see Table 6.1.
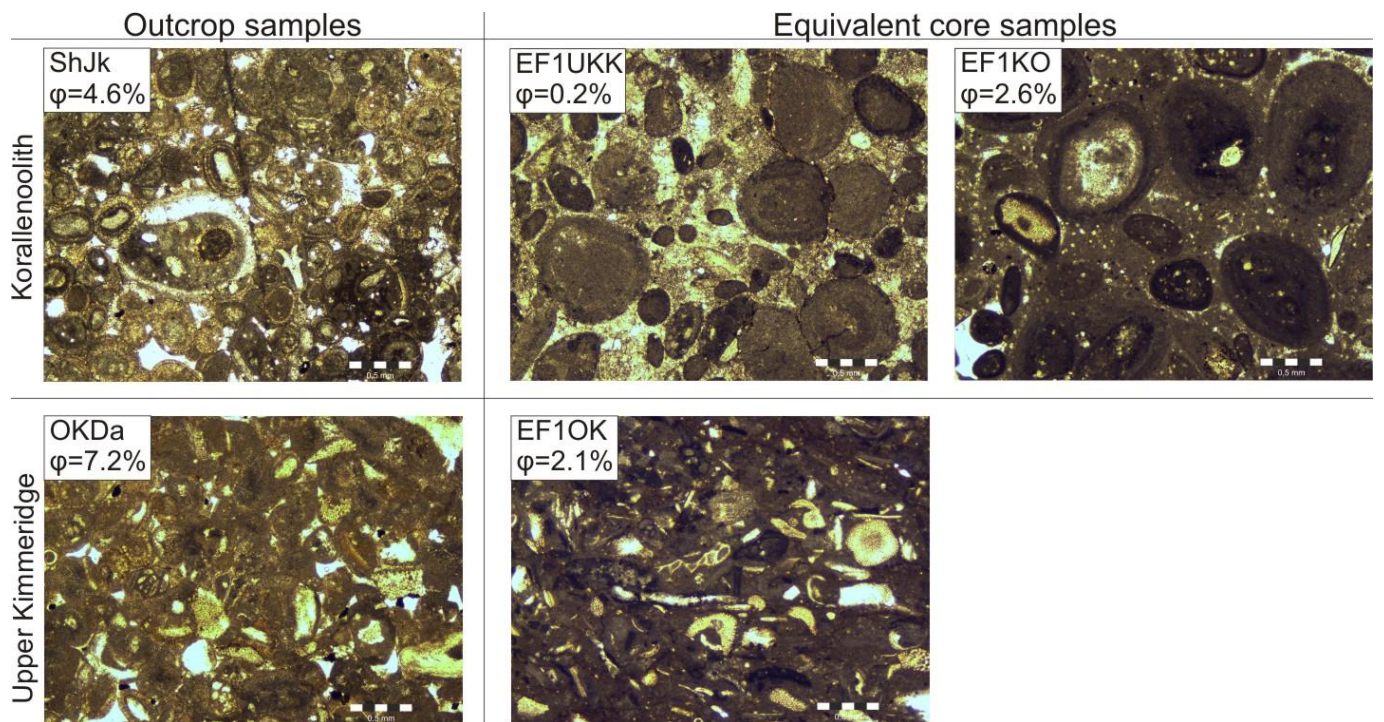

Fig. 6.4. Thin section images with transmitted light of limestone samples from outcrops with core samples. Scale of 0.5 mm and porosities φ are displayed. For abbreviations see Table 6.1.

All Volpriehausen samples are hematite-rich medium- to coarse-grained sandstones with considerable amounts of mica minerals. They are characterised by well-rounded and well-sorted quartz grains. There are slightly larger mean grain sizes in samples *smVG* and *Gt1VS1* compared with *Gt1VS2*. Core samples have extremely low porosities (< 3%) due to strong quartz cementation; outcrop samples, however, are less strongly cemented and have high porosities of 14.4%. Apart from these porosity differences, the texture of Volpriehausen sandstones is quite similar.

In Figure 6.4, limestone core samples with their equivalent outcrop samples are shown in thin section images. Samples *ShJk*, *EF1UKK* and *EF1KO* are massy limestones from Oxfordium (Upper Jurassic). They mainly consist of ooids with some bioclasts (mainly corals) and peloids in sparry calcite cement. The regional name is "Korallenoolith". *EF1KO* has microsparry calcite cement and is more fine-grained than in the other two samples. The components do not retrace any internal lamination in any case. All three samples have low porosities between 0.2 and 4.6%.

The Upper Malm is a heterogeneous stratigraphic unit consisting of different types of carbonate rocks. The sampled carbonate rocks are matrix limestones with differing amounts of bioclasts. *EF1OK* and *OKDa* ("Oberer Kimmeridge") include higher amounts of bioclasts with widths of some micrometers (Fig. 6.4). The amount of matrix is considerably lower in *EF1OK* than in *OKD*a, and *OKDa* has an intermediate porosity (7.2%); the porosity of *EF1OK* is only 2.1%. That is why there is only a moderate equivalence of *EF1OK* and *OKDa* regarding texture although the samples are from the same stratigraphic unit.

The volcanic samples *FL2* and *FL6* are both from the same outcrop. *FL2* was sampled at the extraction level 2. *FL6*, in contrast, originates from the lowest level more than 85 meters below extraction level 2 (cf. Table 6.1). Mineralogically both samples are rhyolites with coarse-grained idiomorphic or hypidiomorphic crystals (mainly plagioclase and alkali feldspar) in a light grey fine-grained matrix (Fig. 6.5). Porosities are in both cases very low (0.1%). In sample *FL2* there are some aspects of beginning of weathering such as mineral transformation along fracture planes.
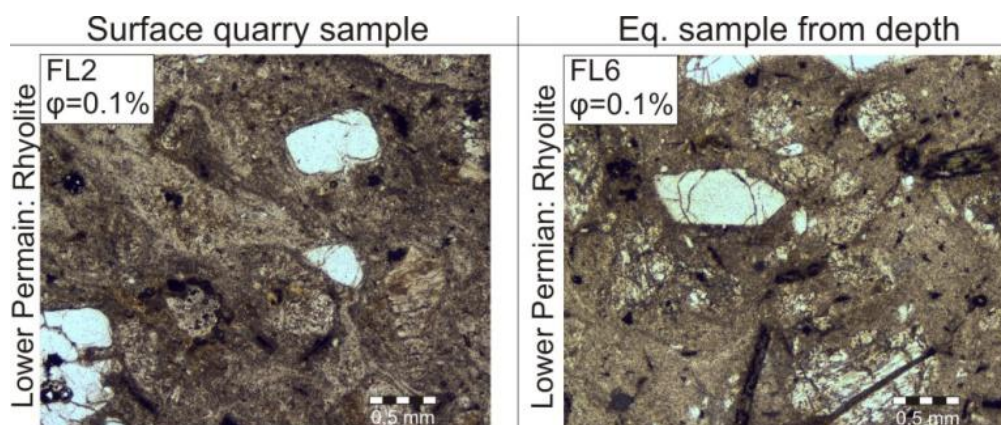

Fig. 6.5. Thin section images with transmitted light of Andesite samples from different extraction levels of the same quarry. Scale of 0.5 mm and porosity φ are displayed. For abbreviations see Table 6.1.

4.3. Additional outcrop samples

In addition to the thin section analyses of core samples with equivalent outcrop samples analogues (Section 4.2), we present thin section images of four carbonates, five sandstones and one volcanic rock from quarries (Fig. 6.6).

EM is a bioclast-rich sparry limestone with low porosity of 2.9% of Middle Triassic age, more explicitly Upper Muschelkalk 1 (regional name: Trochitenkalk). *EL1* (Lower Muschelkalk) is a microsparitic dolomitic limestone without any fossils and high porosity of 15.1%. According to Dunham's classification [26] it can be classified as mudstone. The second sample from

Lower Muschelkalk, *EL2* (Wellenkalk), is a massy matrix limestone with very low porosity (0.3%). It shows an indistinct lamination and sporadically thin layers with bioclasts. Sample *suHe* (Lower Bunter: Lower Bunter) consists of ooids in a sparry calcite matrix and can be classified as oolite. Porosity of this so called Rogenstein is 1.5%.

AlWo (Middle Jurassic, Aalen sandstone) is medium-grained with well-rounded grains and very good sorting. It has a very high porosity (22.5%) and is poorly cemented with quartz. *koVe* (Upper Triassic, Rhaetian) is a fine-grained sandstone with very good sorting and poor rounding as a consequence of strong interlocking of quartz grains. In contrast, *koQ*, which is also of

Rhaetian age, is medium-grained and the grains show good sorting and intermediate rounding. Both Rhaetian sandstones are well cemented with quartz; both have intermediate porosities of 15.6% (*koVe*) and 20.1% (*koQ*), respectively. *BiSu* (Lower Bunter), a medium-grained sandstone, shows an internal lamination in consequence of many intercalated clay bands and clasts. Its grains are well-rounded but poorly sorted, the porosity is high (22.9%). *BeRo* (Rotliegend) is a well-cemented coarse-grained sandstone with low porosity (6.6%). Grains are well-rounded but poorly sorted. In comparison with other sandstone samples, the amount of lithoclasts in sample *BeRo* is rather high.

Sample *DöRo* is a volcanic rock of Lower Permian (Rotliegend) age with coarse-grained hypidiomorphic plagioclase crystals in a fine-grained matrix. Mineralogically it is termed Andesite.
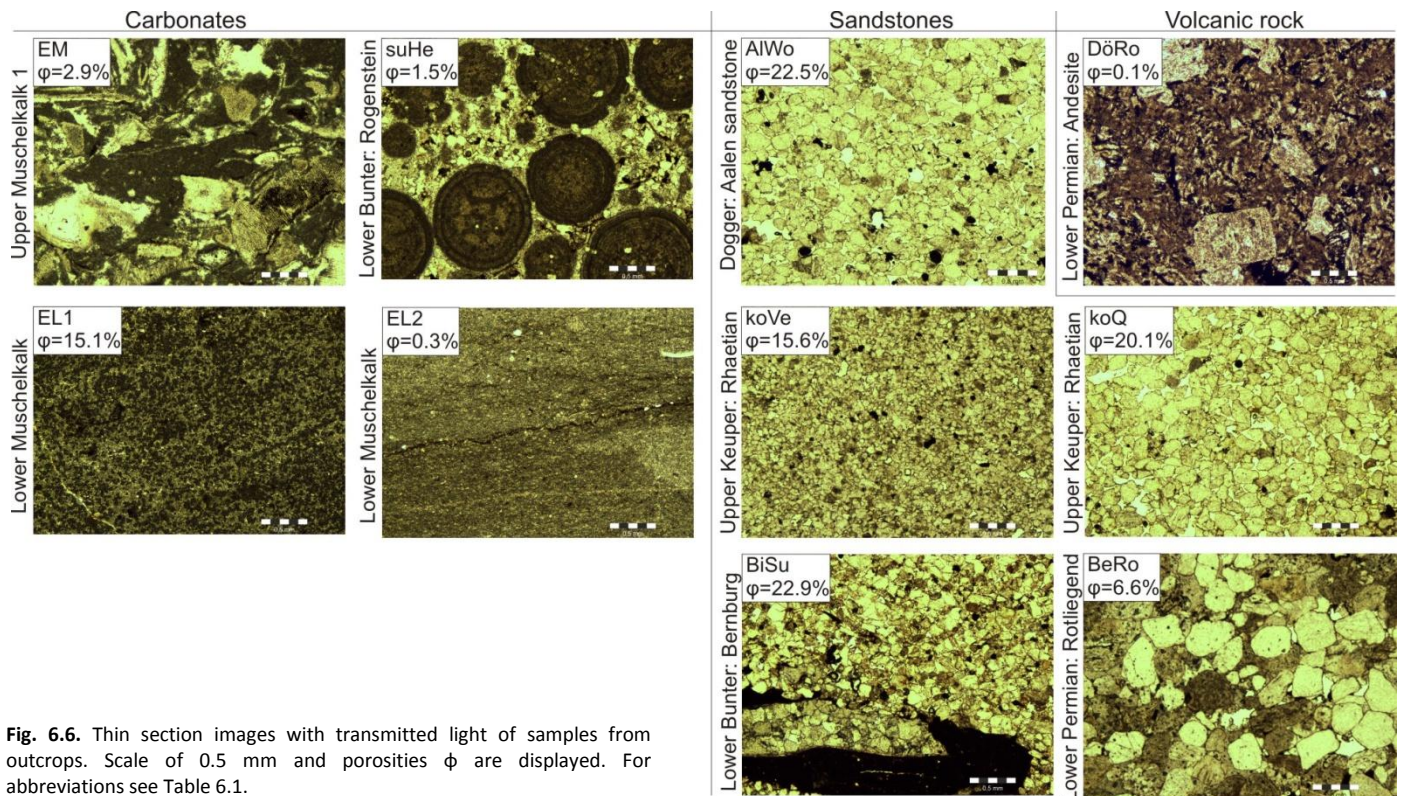

Fig. 6.6. Thin section images with transmitted light of samples from outcrops. Scale of 0.5 mm and porosities φ are displayed. For abbreviations see Table 6.1.

5. Triaxial test data

In Figure 6.7, as an example, stress-strain curves of triaxial test series of outcrop samples *ShJk* (oolite – Upper Jurassic) and *smD* (sandstone – Middle Bunter, Detfurth) including their core sample equivalents are presented.

The carbonate samples all have more or less the same slope at the linear-elastic part of the stress-strain curves (i.e. Young's modulus). The peak stress of *EF1UKK* (20MPa) is comparable with *ShJk*, measured at the same confining pressure, whereas sample *EF1KO* has a higher peak strength probably due to its finer grained matrix (cf., Fig. 6.4). Sandstone sample *smD* is characterised by generally more variable peak stresses and associated strains compared with *ShJk*. Deformation of core samples during loading is less than that of *smD* which is reflected in steeper stress-strain curves and consequently, higher Young's moduli, which, however, have no effects on failure criteria calculation. It is conspicuous that the strengths of core samples are similar to, or slightly higher than strengths of outcrop samples measured at the same confining pressures (Fig. 6.7, *smD*).
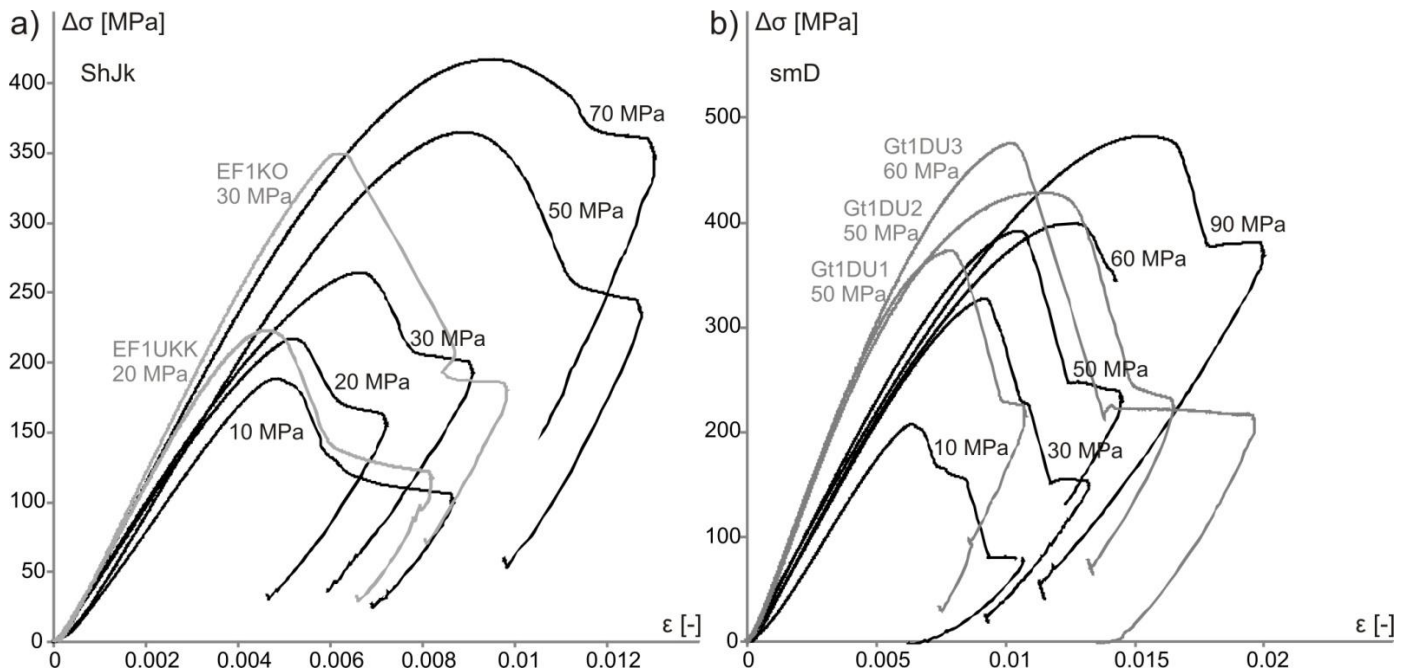
Fig. 6.7. Exemplified stress-strain curves of triaxial test series of outcrop samples *ShJk* (oolite) and *smD* (sandstone). Curves of equivalent core samples (grey; cf., Table 6.1) are included for comparison; respective confining pressures are given.

6. Failure and friction criteria

Linearized Mohr-Coulomb failure and friction criteria were calculated from triaxial test sequences for all outcrop samples (Tables 6.2, 6.3). Additionally, linear regression analyses are performed adding 90% confidence and prediction bands of determined failure and friction criteria. The criteria determined for outcrop samples were then applied to equivalent core samples to calculate shear stresses (τ) and residual shear stress (τ_{res}) values for core samples (Figs. 6.8, 6.9). These calculated values of τ and τ_{res} are then compared with the directly measured values. The residuals between calculated and measured shear stresses are presented in %-residual plots to ensure comparability of results. That is, failure and friction criteria of outcrop samples are used to calculate and predict, respectively, resulting shear stresses.

In Figure 6.8, shear stresses are plotted as functions of normal stresses separately for all outcrop-core sample couples. With linear regression analyses, failure criteria of equivalent outcrop samples are calculated, 90% confidence bands are added. For sandstone samples *smD*, *smVG* and *OK*, failure criteria are less precise than those of carbonate and volcanic rock samples which is reflected in wider confidence bands. Core sample values tend to plot slightly above the Mohr-Coulomb failure line. That is, core samples can stand slightly higher axial stresses before failure. However, core samples plot within confidence bands and calculated residuals plot far below the 25% deviation line in most cases.

Exception is sample *Gt1WS* (equivalent: *OK*). *Gt1WS* was already described in Section 4.1 as the only clastic rock sample with suboptimal comparability to the equivalent outcrop sample. Carbonate core samples *EF1UKK* and *EF1KO* are in good accordance with failure criteria of equivalent outcrop sample *ShJk*. *EF1UKK* plots directly on the failure line. The positive deviation of the microsparry *EF1KO* of ~18% is still a good approximation for property prediction. Volcanic rock sample *FL6* from depth plots perfectly well within confidence bands of *FL2*. Therefore, an applicability of outcrop Mohr-Coulomb failure criteria on core samples is postulated.

Table 6.2. Linearized Mohr-Coulomb failure criteria expressed in normal and shear stresses of outcrop samples.

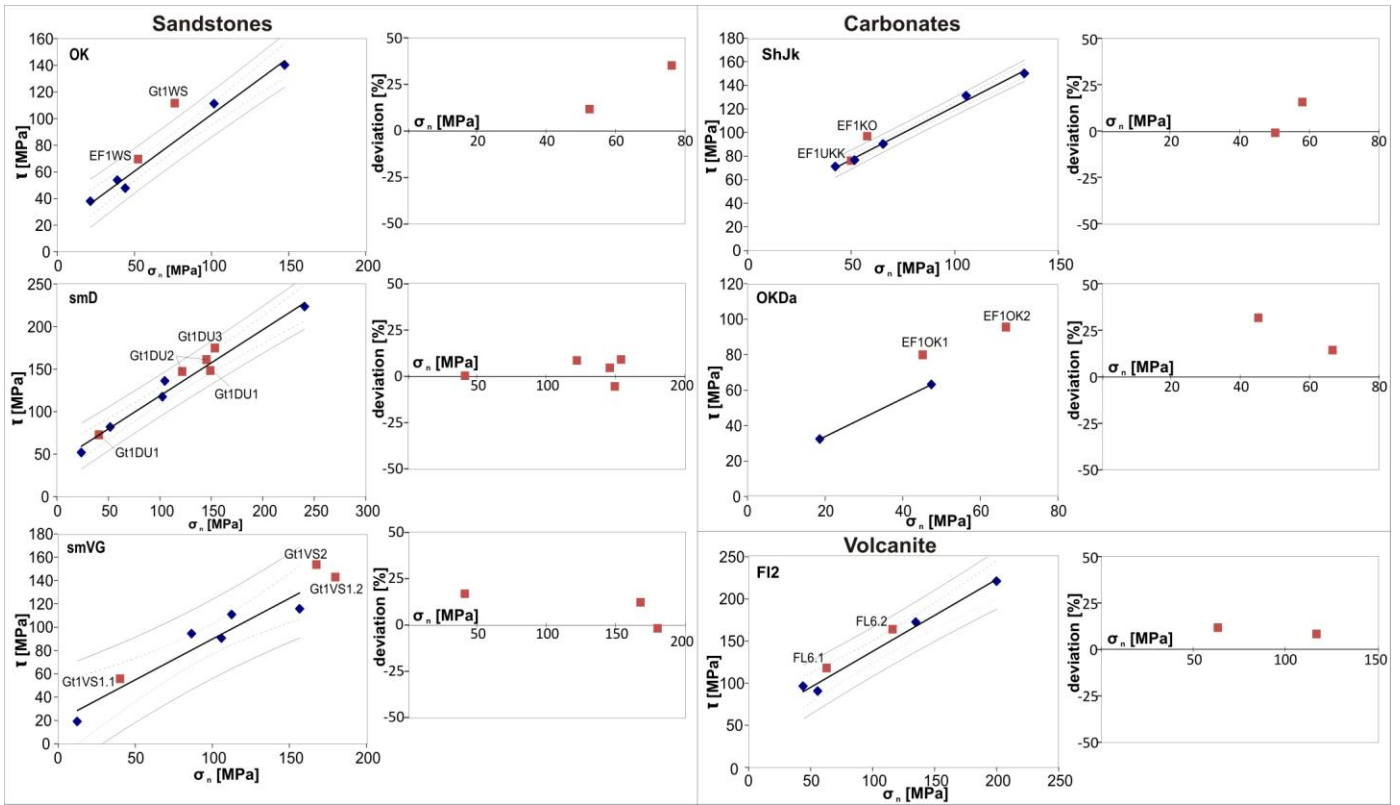| Sample ID	MC failure criterion: normal/shear stresses
OK	$\tau = 0.85 \cdot \sigma_n + 17.8$ MPa
OKDa	$\tau = 1.07 \cdot \sigma_n + 12.3$ MPa
ShJk	$\tau = 0.90 \cdot \sigma_n + 31.8$ MPa
AlWo	$\tau = 0.61 \cdot \sigma_n + 25.8$ MPa
koQ	$\tau = 0.78 \cdot \sigma_n + 37.1$ MPa
koVe	$\tau = 0.92 \cdot \sigma_n + 34.1$ MPa
EM	$\tau = 0.46 \cdot \sigma_n + 34.3$ MPa
EL1	$\tau = 0.52 \cdot \sigma_n + 51.2$ MPa
EL2	$\tau = 0.69 \cdot \sigma_n + 51.4$ MPa
smD	$\tau = 0.78 \cdot \sigma_n + 40.6$ MPa
smVG	$\tau = 0.70 \cdot \sigma_n + 19.6$ MPa
suHe	$\tau = 0.83 \cdot \sigma_n + 23.2$ MPa
BiSu	$\tau = 0.63 \cdot \sigma_n + 19.9$ MPa
BeRo	$\tau = 0.76 \cdot \sigma_n + 29.9$ MPa
DöRo	$\tau = 0.85 \cdot \sigma_n + 70.2$ MPa
FL2	$\tau = 0.86 \cdot \sigma_n + 51.8$ MPa

Fig. 6.8. Shear and normal stresses of all samples from depth (red squares) and equivalent outcrop samples (blue diamonds). Mohr-Coulomb failure criteria calculated from equivalent outcrop sample results, 90% confidence (pointed lines) and prediction bands (grey lines), and porosities φ are included. For core samples, residuals in percent of outcrop sample failure criteria application are calculated (see text).

Table 6.3. Mohr-Coulomb friction criteria of outcrop samples.

Sample ID	MC friction criterion
OK	$\tau_{res} = 0.71 \cdot \sigma_{n,res} + 8.6$ MPa
OKDa	$\tau_{res} = 1.11 \cdot \sigma_{n,res} + 1.9$ MPa
ShJk	$\tau_{res} = 0.89 \cdot \sigma_{n,res} + 16.2$ MPa
AlWo	$\tau_{res} = 0.72 \cdot \sigma_{n,res} + 8.8$ MPa
koQ	$\tau_{res} = 0.91 \cdot \sigma_{n,res} + 3.6$ MPa
koVe	$\tau_{res} = 0.79 \cdot \sigma_{n,res} + 9.6$ MPa
EM	$\tau_{res} = 0.62 \cdot \sigma_{n,res} + 17.7$ MPa
EL1	$\tau_{res} = 0.47 \cdot \sigma_{n,res} + 33.0$ MPa
EL2	$\tau_{res} = 0.97 \cdot \sigma_{n,res} + 7.8$ MPa
smD	$\tau_{res} = 0.82 \cdot \sigma_{n,res} + 11.3$ MPa
smVG	$\tau_{res} = 0.81 \cdot \sigma_{n,res} + 1.7$ MPa
suHe	$\tau_{res} = 0.82 \cdot \sigma_{n,res} + 16.1$ MPa
BiSu	$\tau_{res} = 0.70 \cdot \sigma_{n,res} + 5.9$ MPa
BeRo	$\tau_{res} = 0.95 \cdot \sigma_{n,res} + 3.6$ MPa
DöRo	$\tau_{res} = 0.71 \cdot \sigma_{n,res} + 18.8$ MPa
FL2	$\tau_{res} = 0.73 \cdot \sigma_{n,res} + 12.5$ MPa

In the triaxial tests, not every specimen developed a discrete fault plane. However, to calculate shear stresses, angle β of the induced fault is needed. Therefore, for specimens without a discrete fault plane, it was impossible to calculate τ and τ_{res}, respectively. This occurred in the high-porosity sample *OKDa*. Strain

was accumulated in sub-horizontal compaction bands and destruction of pore space. That is why both criteria of *OKDa* base on results of two specimens only (Tables 6.2, 6.3).

The triaxial testing procedure includes recording of the residual stress after failure. With residual stress values friction criteria are calculated (Table 6.3; Fig. 6.9). Widths of confidence and prediction bands of outcrop sample friction criteria are comparably small. That is, there is a strong linear relationship for all samples. Measured residual stresses of core samples *Gt1VS1* and *Gt1VS2* are considerably higher than of equivalent outcrop sample *smVG*. This results in shear and normal stresses which plot in the extrapolation of the function of friction criterion. That is, the ratio between residual shear and normal stresses remains more or less the same despite the fact that residual stresses of core samples are higher than of outcrop samples. Every core sample plots within the confidence bands of its equivalent outcrop sample. Calculated deviations stay within and mostly even far below the 25% deviation lines. We conclude a strong applicability of outcrop sample friction criteria on samples from depth.
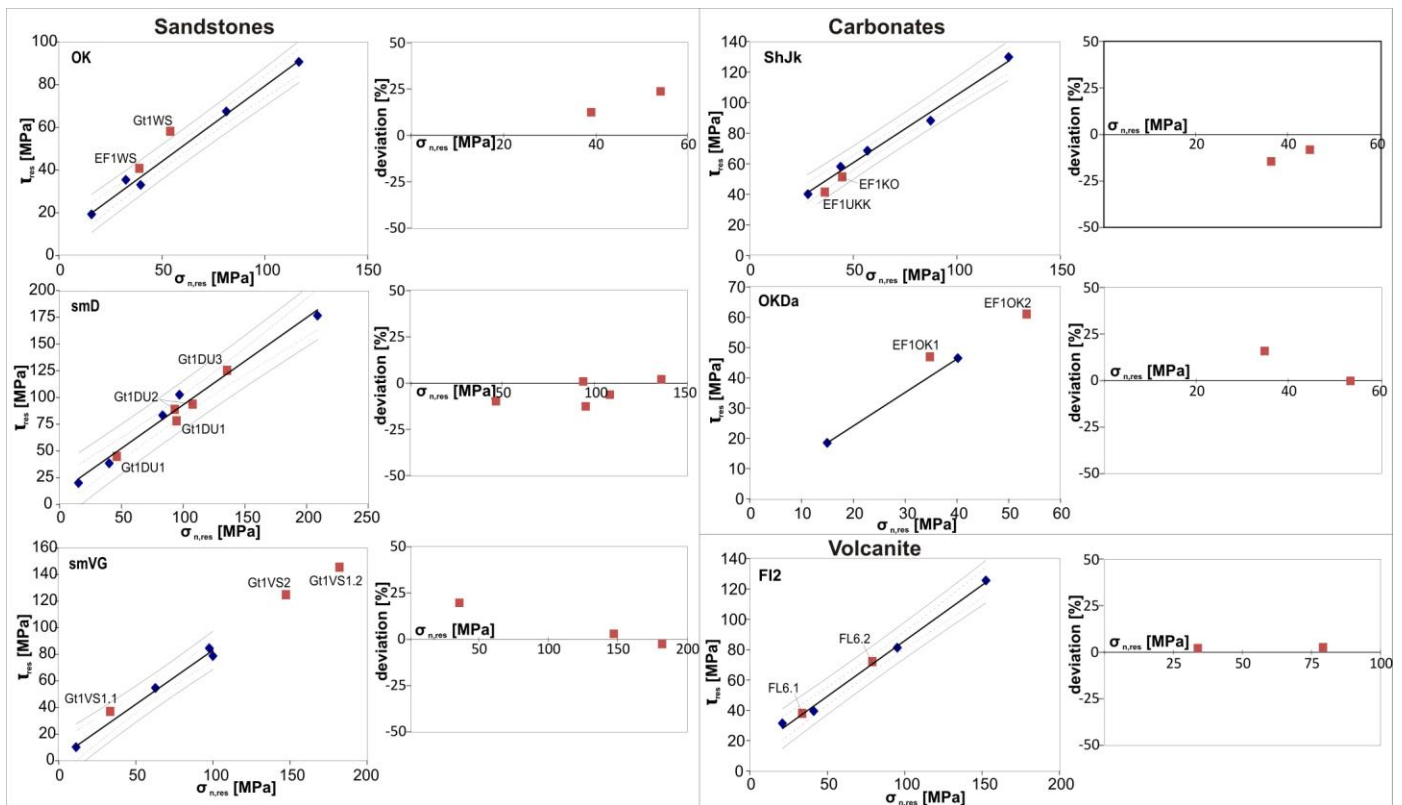
Fig. 6.9. Residual shear and normal stresses of all samples from depth (squares) and equivalent outcrop samples (blue diamonds). Mohr-Coulomb friction criteria calculated from equivalent outcrop sample results, 90% confidence (pointed lines) and prediction bands (grey lines), and porosities ɸ are included. For core samples residuals of outcrop sample friction criteria application are calculated (see text).

7. Discussion

7.1. Outcrop samples for core property prediction

The subsurface of the North German Basin (NGB) is well explored with numerous hydrocarbon wells [11]. That is, there already is broad knowledge about the sedimentary alternation and facies distribution. This large database can be used to better plan future drilling projects. However, the direct link with mechanical properties to improve wellbore stability analyses is not yet viable because, in most cases, core material is limited or even lacking. Our approach to use outcrop samples for core property prediction gives the opportunity to obtain the required information with comparably small investments in time and expenditure by predicting the facies of the rocks that have to be drilled through. It will then be easy to find appropriate outcrop samples for core property prediction because the stratigraphic units that are located at greater depths in the center of the NGB crop out at the southern margins of the NGB.

Comparing rock properties of core samples with those of equivalents taken in outcrop analogues is a problematic issue because already small textural differences may affect rock mechanical properties (e.g., [27]). Mineral composition, textural aspects, such as grain size and grain interlocking, cementation and

differing porosities have great effects on rock strength [28,29]. In accordance with previous studies [30-32], our data suggest that porosities and friction angles µ of sandstone samples are related (cf. Fig. 6.8). High porosity sandstones (e.g., *smVG*, *AlWo*) tend to have lower values of µ than sandstones with lower porosities (*smD*, *OK*, *koVe*). There is a stabilizing effect of an enhanced confining pressure on rock strength [20,33]. However, it is less effective in terms of preventing pore space destruction. That is, the rise of strength with increasing confining pressure is smaller for high porosity sandstones. Similarly, for carbonates the fracture initiation stress is inversely related to both porosity and mean grain size (e.g., [34]).

Thin section analyses show that *Gt1VS2* contains considerably more feldspar and lithoclasts than the other two Volpriehausen sandstones (*Gt1VS1, smVG*; cf. Figure 6.2). Its mechanical behaviour, however, suits the failure and friction criteria of outcrop sample *smVG* fairly well (Figs. 6.8, 6.9). The result of the *Gt1VS2* plots only slightly above the *smVG* failure lines and predicted values are consequently somewhat lower than the true values. This may be the result of similar degrees of grain interlocking and sorting in combination with equal grain size distribution and cementation type. Similarly, the compositional differences of core sample *Gt1DU1* and the equivalent outcrop sample *smD* have no obvious

influence on the predictability of the properties of the core sample because *Gt1DU1* shows the similar failure behaviour as samples *Gt1DU2-3* (Figs. 6.8, 6.9) which have the same composition as *smD* (Fig. 6.2). The chosen outcrop samples of both Detfurth and Volpriehausen sandstones (*smD, smVG*), however, are both more porous than the core samples. This appears to be than main reason for the deviation between predicted and measured core properties. Based on the data, it is assumed that the mineral composition of sandstones is comparatively less important. That is, when searching equivalent outcrop samples one has to focus on textural aspects and porosity, and less on mineral composition's comparability.

A considerable difference between core and outcrop samples with respect to the degree of weathering is to be expected. It is reasonable that changes of rock properties in consequence of weathering can be neglected for core samples. In contrast, although we were careful to choose outcrop samples as freshly exposed as possible, these samples suffered effects of climate and infiltrating surface waters for a certain time. In sandstones and volcanic rocks such exposure leads to the transformation of some feldspar to clay minerals. In all samples, there are dissolution processes leading to reduction of v_p and strengths, respectively. v_p therefore can give great insight on a rock's weathering state and, respectively, on quality of chosen outcrop and core samples.
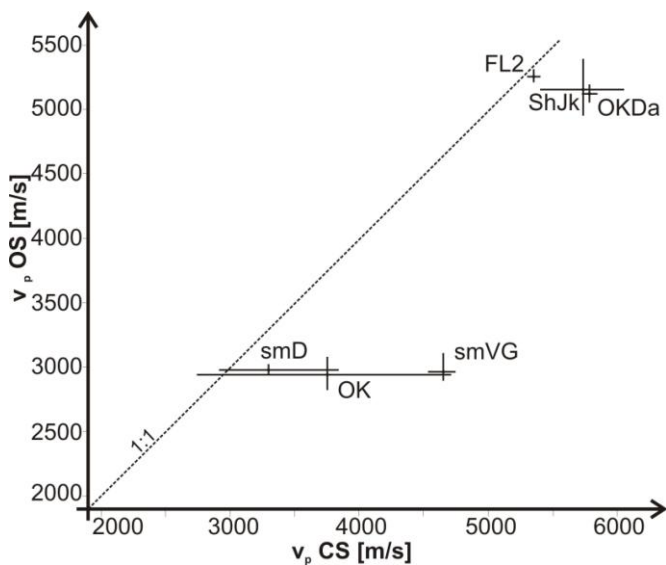
because v_p reduction is not pronounced, and core and outcrop equivalents all plot near the line of equal v_p. Sample *smVG*, however, has a small v_p value and high porosity and is obviously influenced by surface conditions and unloading, whereas core equivalents are of good quality. Nevertheless, the applicability of *smVG* failure criterion on core samples is fairly well because all core samples plot within calculated prediction. The main difference is that at the same confining pressures core sample failure happens at higher shear and normal stress values than failure of its equivalent outcrop sample (cf. Fig. 6.8). That is, although the strengths are higher than of their outcrop equivalents, the ratios between normal and shear stresses appear to remain similar. This indicates that, although the porosity is an important parameter, it has minor effect on the ratio between acting normal and shear stresses than the texture which is similar for both types of samples.

For most outcrop-core sample couples we observed that core samples tend to plot slightly above the calculated failure lines of outcrop samples, yet within calculated prediction bands (cf., Fig. 6.8). This may indicate a systematic positive deviation of predicted values. We have to consider adding a positive deviation of several percent to calculated values when using failure criteria of equivalent outcrop samples for core property prediction. For a statistical investigation of the deviation, however, the presented database is not sufficient and should be enlarged. Nevertheless, based on presented data it seems reasonable to use such samples from outcrop analogues.
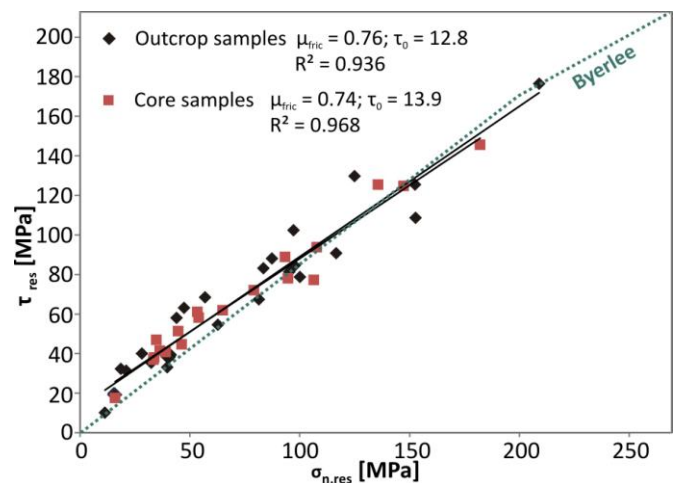

Fig. 6.10. P-wave velocities (v_p) of outcrop (OS) and core samples (CS) of all outcrop-core sample couples. Lengths of bars represent range of measured values; intersection of bars indicates mean values of v_p.

In Figure 6.10, P-wave velocities v_p of all core-outcrop couples are cross plotted. All outcrop-core sample couples plot either on the line of equal v_p (*GVa, FL2*) or in the field of higher v_p of core samples. That is, the degree of weathering of outcrop samples, except for outcrop sample *smVG*, seems to be comparatively small

Fig. 6.11. Residual shear and normal stresses of all samples (see key) with linear regression lines and calculated values of friction coefficient and friction cohesion for outcrop and core samples separately. Byerlee friction [38] is added (dotted green line).

Additionally, all test results together are re-plotted in one cross plot to assess variations of friction criteria of the different samples (Fig. 6.11). The friction coefficient is usually between 0.6 and 0.85 and decreases with

increasing confining pressure [35]. When discussing all data together, no significant difference of frictional strength between core and outcrop samples is detectable. Coefficients of friction and friction cohesions of outcrop and core samples are very similar. The great fit of core samples in outcrop friction criteria (cf. Fig. 6.9) is reflected in the narrow range of all values (Fig. 6.11). We conclude that both outcrop and core samples provide applicable values of friction coefficients.

7.2. Alternative methods of parameter determination

There is already a method to determine failure criteria which deals with the issue of limited core material. The `multiple failure state test´ simulates different stress states with the same specimen [36,37]. The main problem of this procedure, however, is that at every stress state, before confining pressure is increased, minor failure and associated strain occurs. Mean orientations of induced microfractures depend on the stress state: dip angles β of induced microfractures decrease with increasing confining pressure [20]. The weakening effect of these microfractures causes the determination of both a lower friction angle μ but a higher unconfined compressive strength C_0. For the here discussed question of wellbore stability it is preferred to perform a set of different measurements to obtain more conservative failure criteria. This encourages the approach to rather perform complete sets of triaxial measurements with carefully chosen outcrop samples when only limited core material is available.
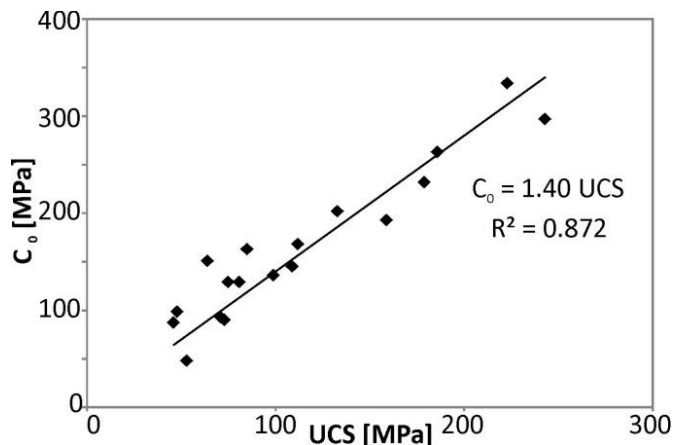

Fig. 6.12. Ratio of unconfined compressive strengths of all samples determined with uniaxial compressive strength test (UCS; Reyer and Philipp [41]) and with triaxial testing (C_0).

The unconfined compressive strength is a parameter with importance regarding wellbore stability prediction with geomechanical models [6,31,38,39]. There are two ways to determine the unconfined compressive strength: 1. derivation from a series of triaxial measurements (C_0; cf. Section 5) and 2. direct measurement with uniaxial compressive strength test (UCS; [40]). A comparison of C_0, determined in this study, with UCS values of the same samples, compiled by Reyer and Philipp [41], shows that there is a good positive correlation between these two parameters, and C_0 values tend to be 1.4 times higher than UCS values (Fig. 6.12). Deriving C_0 from a triaxial testing series neglects the curved increase of strength for very small confining pressures [20] leading to higher values of C_0 compared with UCS. For conservative estimations of wellbore stability, it is preferred to use conventional UCS and not C_0 values. Using the C_0-UCS relationship, however, gives the opportunity to derive C_0 values for upper boundaries of wellbore failure analysis from conventionally measured UCS for NGB rocks.

8. Conclusions

From conventional triaxial tests and thin section analyses of cores and well-chosen equivalent outcrop samples, we obtained the following conclusions regarding the applicability of Mohr-Coulomb failure and friction criteria on predictions of core properties and, respectively, of rocks at greater depths:

1. If failure criteria, obtained from triaxial test sequences of outcrop samples, are applied on core samples there are minor deviations between predicted and calculated values of normal and shear stresses when equivalence regarding texture and porosity is given. If the outcrop sample has a higher porosity than the core sample and only the texture is equivalent, it is observed that the core sample still plots within calculated prediction bands in most cases, yet at higher stress values. The study shows that predicting failure properties of core samples from equivalent outcrop samples is still a problematic issue. Presented data, however, indicate that - under certain conditions - it is indeed possible to use outcrop samples. One has to be extra careful when selecting representative samples from outcrops. It is recommended to re-check the conclusions drawn from this study with further comparative analyses of core samples with equivalent outcrop samples.

2. Outcrop friction criteria can be applied on core samples for all tested rock types. No considerable differences of friction between core and outcrop samples were detected. That is, friction stress values react less sensitively on textural variations than normal and shear stresses at failure.

3. It is possible to use failure and friction criteria for predictions of rock strength at larger depths if equivalent outcrop samples are chosen with care. Presented data showed that the most important points are a comparable texture and porosity similarity. The mineralogical composition is of minor importance in all cases.

Acknowledgements

References

[1] Zeynali ME. Mechanical and physico-chemical aspects of wellbore stability during drilling operations. J Pet Sci Eng 2012; 82-83:120-124.

[2] Proehl TS. Geomechanical uncertainties and exploratory drilling costs. SPE/ISRM Rock Mechanics Conference, Irving, USA, 2002.

[3] York P, Pritchard D, Dodson JK, Rosenberg S, Gala S, Utama B. Eliminating non-productive time associated with drilling trouble zones. Offshore Technology Conference, Houston, USA, 2009.

[4] Li S, George J, Purdy C. Pore-pressure and wellbore-stability prediction to increase drilling efficiency. J PetTechnol 2012;64:99-101.

[5] McLean MR, Addis MA. Wellbore stability: The effect of strength criteria on mud weight recommendations. SPE 20405-MS, SPE Annual Technical Conference, New Orleans, USA, 1990.

[6] Moos D, Peska P, Finkbeiner T, Zoback M. Comprehensive wellbore stability analysis utilizing quantitative risk assessment. J Pet Sci Eng 2003; 38:97-109.

[7] Abdideh M, Fathabadi MR. Analysis of stress field and determination of safe mud window in borehole drilling (case study: SW Iran). J Petrol Explor Prod Technol 2013; 3:105-110.

[8] Zoback MD, Barton CA, Brudy M, Castillo DA, Finkbeiner T, Grollimund BR, Moos DB, Peska P, Ward CD, Wiprut DJ. Determination of stress orientation and magnitude in deep wells. Int J Rock Mech Min Sci 2003; 40:1049-1076.

[9] Lockner DA. Rock failure. In: Ahrens T, editor. Rock Physics and Phase Relations: A Handbook of Physical Constants. Washington: AGU Reference Shelf 3; 1995, p. 127-147.

[10] Paschen H, Oertel D, Grünwald R. Möglichkeiten geothermischer Stromerzeugung in Deutschland. TAB Arbeitsbericht 84, 2003.

[11] NIBIS Kartenserver. Bohrungen und Profilbohrungen. LBEG, Hannover, 2012.

[12] Hesshaus A, Eichhorn P, Gerling JP, Hauswirth H, Hübner W, Jatho R, Kosinowski M, Krug S, Orilski J, Pletsch T, Tischner T, Wonik T. Das GeneSys-Projekt - Geothermiebohrung erfolgreich abgeteuft. Geotherm Energ 2010; 19:28-30.

[13] Schäfer F, Hesshaus A, Hunze S, Jatho R, Luppold FW, Orilski J, Pletsch T, Röhling HG, Tischner T, Wonik T. Summarized report of geothermal well Gt1. Erdöl Erdgas Kohle 2012; 128:20-26.

[14] Erbacher J, Luppold FW, Heunisch C, Heldt M, Caesar S. Chemo- and biostratigraphy of the Late Jurassic from the Lower Saxony Basin, North Germany. EGU2013-2972, Geophys Res Abstr 15, 2013.

[15] Walter R. Geologie von Mitteleuropa. 7th ed. Stuttgart: Schweizerbarth; 2007.

[16] Betz D, Führer F, Greiner G, Plein E. Evolution of the Lower Saxony Basin. Tectonophys 1987; 137:127-170.

[17] Ziegler P. Geological Atlas of Western and Central Europe. Geological Society Publishing House/Shell International Petroleum Maatschappij BV; 1990.

[18] Baldschuhn R, Frisch U, Kockel F. Geotektonischer Atlas von Nordwest-Deutschland, 1:300.000. BGR, Hannover, 1996.

[19] Reyer D, Bauer JF, Philipp SL. Fracture systems in normal fault zones crosscutting sedimentary rocks, Northwest German Basin. J Struct Geol 2012; 45:38-51.

[20] Jaeger JC, Cook NGW, Zimmerman RW. Fundamentals of Rock Mechanics. 4th ed. Malden: Blackwell Publishing; 2007.

[21] Wooldridge JM. Introductory Econometrics: A Modern Approach. 4th ed. Mason: South-Western, Cengage Learning; 2009.

[22] Brink D. Essentials of Statistics. 2nd ed. David Brink & Ventus Publishing, bookboon.com, ISBN: 978-87-7681-408-3; 2010.

[23] McBride EF. A classification of common sandstones. J Sediment Petrol 1963; 33:664-669.

[24] Lama RD, Vutukuri VS. Handbook on Mechanical Properties of Rocks – Testing Techniques and Results, Vol. II. Clausthal: Trans Tech Publications; 1978.

[25] Palchik V. Influence of porosity and elastic modulus on uniaxial compressive strength in soft brittle porous sandstones. Rock Mech Rock Eng 1999; 32:303-309.

[26] Dunham RJ. Classification of carbonate rocks according to depositional texture. In: Ham WE, editor. Classification of Carbonate Rocks. AAPG Memoir; 1962, p. 108-121.

[27] Sun S, Ji SC, Wang Q, Salisbury MH, Kern H. P-wave velocity differences between surface-derived and core samples from the Sulu ultrahigh-pressure terrane: Implications for in situ velocities at great depths. Geol 2012; 40:651-654.

[28] Dyke CG, Dobereiner L. Evaluating the strength and deformability of sandstones. Q J Eng Geol 1991; 24:123-134.

[29] Plumb RA. Influence of composition and texture on the failure properties of clastic rocks. Eurock 94, Rock Mechanics in Petroleum Engineering conference, Delft; 1994, p. 13-20.

[30] Vernik L, Bruno M, Bovberg C. Empirical relations between compressive strength and porosity of siliciclastic rocks. Int J Rock Mech Min Sci 1993; 30:677-80.

[31] Chang C, Zoback MD, Khaksar A. Empirical relations between rock strength and physical properties in sedimentary rocks. J Pet Sci Eng 2006; 51:223-237.

[32] Schöpfer MPJ, Abe S, Childs C, Walsh JJ. The impact of porosity and crack density on the elasticity, strength and friction of cohesive granular materials : insights from DEM modelling. Int J Rock Mech Min Sci 2009; 46:250-261.

[33] Zoback MD. Reservoir Geomechanics. First ed. New York: Cambridge University Press; 2007.

[34] Hatzor YH, Palchik V. The influence of grain size and porosity on crack initiation stress and critical flaw length in dolomites. Int. J Rock Mech Min Sci 1997; 34:805-816.

[35] Byerlee JD. Friction of rocks. PAGEOPH 1978; 116:615-626.

[36] Kovari K, Tisa A. Multiple failure state and strain controlled triaxial tests. Rock Mech 1975; 7:17-33.

[37] Kovari K, Tisa A, Einstein HH, Franklin JA. Suggested methods for determining the strength of rock materials in triaxial compression: Revised version. Int J Rock Mech Min Sci Geomech Abstr 1983; 20:283-290.

[38] Nabaei M, Shahbazi K. A new approach for predrilling the unconfined rock compressive strength prediction. Pet Sci Technol 2012; 30/4:350-359.

[39] Vogt E, Reyer D, Schulze KC, Bartetzko A, Wonik T. Modeling of geomechanical parameters required for safe drilling of geothermal wells in the North German Basin. Celle Drilling, Germany, 2012.

[40] ISRM. The Complete ISRM Suggested Methods for Rock Characterization, Testing and Monitoring: 1974-2006. In: Ulusay R, Hudson JA, editors. Suggested Methods Prepared by the Commission on Testing Methods, International Society for Rock Mechanics. Compilation arranged by the ISRM Turkish National Group, Ankara, Turkey, 2007.

[41] Reyer D, Philipp SL. Empirical relations of rock properties of outcrop and core samples from the Northwest German Basin for geothermal drilling. Geotherm Energ Sci 2014; 2:21-37.

7 Understanding and predicting coupled hydromechanical fracture propagation

Ernesto Meneses Rioseco[1], Dorothea Reyer[2], Rüdiger Schellschmidt[1]

[1] Leibniz Institute for Applied Geophysics, Stilleweg 2, 30655 Hannover, Germany

[2] University of Göttingen, Geoscience Centre, Goldschmidtstraße 3, 37077 Göttingen, Germany

Abstract

Hydromechanical processes involved in geothermal reservoir engineering are highly complex. Apart from additional thermal and chemical effects, their dynamic interaction has been the focus of attention of many geoscientists addressing hydraulic fracturing in natural and engineered geosystems. In particular, hydraulic fracturing represents a key component in enhanced geothermal systems (EGS). Especially the fracture path and geometry in a layered reservoir is influenced by a variety of factors such as different mechanical and hydraulic material properties, different stress regimes in the respective layers, material heterogeneities, interaction with pre-existing fractures, and others.

The North German Basin with its typical low-permeable sedimentary alternation has been the subject of recent intensive geothermal studies to evaluate the potentiality of cost-effective extraction of geothermal energy. Among the prominent projects currently in progress, the project "Hydromechanical response of geothermal reservoirs in the stress field generated by complex geological structures is a subproject of the interdisciplinary research association "Geothermal energy and high-performance drilling techniques" (Geothermie und Hochleistungsbohrtechnik "gebo") in Lower Saxony, Germany. The goal of this subproject is to advance and refine the understanding of the hydromechanical behavior of geothermal reservoirs typical of the North German Basin.

Using FRACOD as two-dimensional boundary element code, a series of numerical models involving relevant scenarios were tested. Different numerical simulations with dissimilar layer sequences characteristic of the North German Basin at targeted depths were performed. By means of this a broad range of possible scenarios was examined. Loading conditions provided by previous modelling and data on the stress field in the region under investigation as well as material properties from laboratory data were varied over a wide parameter space. Specifically, the drilling demonstration project GeneSys-Borehole Groß Buchholz Gt1 in Hanover Groß-Buchholz together with vast data obtained from laboratory measurements on specimens typical of the study area have provided valuable constraints on the hydraulic and mechanical properties of the modelled geothermal reservoirs. A multiple fracture scenario is also included to study fracture interaction, an applicable scenario in deeper targets such as fault zones and volcanic rocks. First, preliminary modelling results show that the difference in elastic properties such as Young's modulus and Poisson's ratio between the sedimentary layers has little influence on the fracture trajectory. The difference in these elastic properties does not lead to fracture containment or arrest at material interfaces, but rather has an influence on fracture aperture. This corroborates previous field observations but disagrees with recent numerical modelling. Difference in mechanical properties like fracture toughness in mode I and II and their ratio around sediment interfaces proofed to have a significant impact on the fracture path and mode of deformation. Model results demonstrate that with specific but in laboratory measured values of this parameter in both modes of deformation, fracture paths through interfaces may be clinked or splayed and switch to a mixed mode of deformation.

Model results of multiple fracture scenarios reveal the complex interaction of pre-existing fractures with a hydraulically induced fracture. Pre-existing fractures experience displacement and hydraulic changes before they are hit by the hydraulically induced fracture. Moreover, when this latter hits the natural fractures it does not continue its previous path but rather the pre-existing fractures propagate in the direction of maximum shear stress.

1. Introduction

Geothermal energy has gained significant importance worldwide in the last two decades since it represents an alternative green energy to conventional carbon-based energy. High-temperature fields have a great potential for the long-term extraction of clean energy since they constitute an unlimited and self-sustaining resource of non-pollutant, eco-friendly geothermal energy. Specially hotspots across the world where thermal, hydraulic and tectonic conditions make possible the extraction of huge quantities of energy from the underground has drawn special attention from public, academic and commercial institutions. Prominent examples of such attractive sites in the world are Iceland, New Zeeland and southern Italy where volcanic activity is intensive (Arias et al. 2010, Bignall 2010, Bignall et al. 2010, Harvey et al. 2010). Generally speaking, places where tectonic activity is taking place such as plate boundaries seem to be particularly suitable to recovering considerable amounts of geothermal energy.

Favourable conditions for cost-effective and profitable extraction of geothermal energy include at least high

underground temperatures and high hydraulic conductivity of the geothermal reservoir (e.g., Huenges 2010, and references therein). When the latter aspect is not fulfilled the geothermal reservoir has to be engineered to create paths within the rock mass to allow for sufficient heat exchange and fluid production at acceptable extraction rates. This falls under the category of the so-called enhanced geothermal systems (EGS). Basically, they involved hydraulic fracturing the geothermal reservoirs to either connect the hydraulically induced fracture with the natural pre-existing fractures or simply create a possibly large and highly conductive hydraulic fracturing penetrating in the geothermal reservoir as much as possible.

EGS has become very popular in the last decades as it has proofed to substantially improve the thermal output of geothermal reservoirs (e.g., Ziagos et al. 2013). Previously, it has been broadly implemented in the hydrocarbon industry to facilitate the extraction of hydrocarbon resources (e.g., Economides and Nolte 2000, Fisher 2010, Reinicke 2012). Vast and valuable experiences concerning hydraulic fracturing have also been accumulated in a particular form of EGS, the so-called Hot Dry Rock (HDR) systems in the last years (Tischner et al. 2007). A pioneering work intended to study different exploitation concepts of heat from low-permeable crystalline rock mass has been successfully carried out in the early seventies by a team of scientists in Los Alamos National Laboratory, New Mexico, USA (Brown 1012, Tester et al. 2006, and references therein). Since then a great deal of follow-up projects have been initiated across the world to perfect and further elaborate heat extraction concepts from tight sedimentary or crystalline rock. Another outstanding geothermal project launched in Europe to put to the test the workability and usefulness of such HDR heat exploitation concepts constitutes Soultz (e.g., Baumgärtner et al. 2004, Jung & Weidler 2000, and references therein).

Among numerous projects dealing with EGS across the World, the project "Hydromechanical response of geothermal reservoirs in the stress field generated by complex geological structures is a subproject of the interdisciplinary research association "Geothermal energy and high-performance drilling techniques" (Geothermie und Hochleistungsbohrtechnik "gebo") in Lower Saxony, Germany (Reinicke et al. 2010). This subproject is generally aimed at advancing and refining the knowledge and understanding of the hydro-mechanical behavior of geothermal reservoirs typical of the North German Basin (NGB). Particularly this part of Germany has been the recent target of extensive

studies dealing with the feasibility and practicability at affordable costs of geothermal energy extraction.

The NGB is specifically characterised by relatively highly conductive units deep underground, but exhibits extremely low-permeability and low-porosity sedimentary rocks. Economical and profitable geothermal resource exploitation under the circumstances mentioned before requires the creation of relatively large and highly conductive artificial fractures to improve the heat exchange and production rate, i.e. the performance of the geothermal reservoir. Among the recent EGS research and demonstration sites situated in the NGB, Groß Schönebeck (north of Berlin) (e.g., Blöcher et al. 2010, Legarth et al. 2005, Moeck et al. 2009, Zimmermann et al. 2007), Horstberg Z1 (north of Celle) (e.g., Sulzbacher & Jung 2010, Wessling et al. 2008), and Groß Buchholz Gt1 (in Hannover) (e.g., Jung et al. 2005; Kehrer et al. 2007; Orzol et al. 2004, 2005; Tischner et al. 2010, 2013, and references therein) constitute classic examples of remarkable efforts made to put to the test different drilling and geothermal concepts intended to evaluate the potentiality and practicability of small-scale deep geothermal energy extraction under such harsh hydraulic conditions.
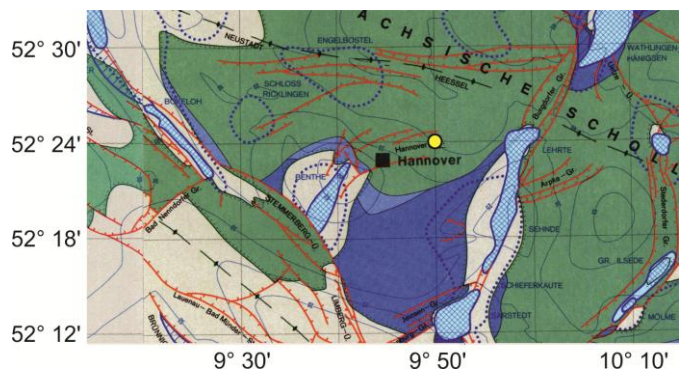

Fig. 7.1. Map showing a representative part of the North German Basin (NGB) in the region of Lower Saxony, Germany. The location of the drilling demonstration site GeneSys Groß-Buchholz is depicted with a yellow circle. Light blue shaded areas display salt diapirs. This map has been drawn with the help of the geotectonic atlas of NW Germany (Baldschuhn et al. 2001).

Specifically the GeneSys project (GeneSys: Generated geothermal energy systems), situated in Hannover Groß-Buchholz (Fig. 7.1), is aimed at supplying geothermal heat to the GEOZENTRUM Hanover with a thermal output of 2 MW. To achieve this, the planning and designing of adequate utilisation concepts has been pivotal for the encountered tight (low-permeable) sediments of low porosity. The GeneSys project of the Federal Institute for Geosciences and Natural Resources (BGR) essentially involves the arrangement of single-well concepts as well as the employment of water-frac techniques to sedimentary rocks, see Fig. 7.2. An extensive and in-depth description of target, goals as well as milestones reports of this demonstration site can be found in http://www.genesys-hannover.de. The data

collected in this project has provided valuable constraints. Therefore, similar geological scenarios to the encountered sediment layers at the targeted depth were assumed in the present study to possibly answer key questions raised within the framework of the GeneSys project.
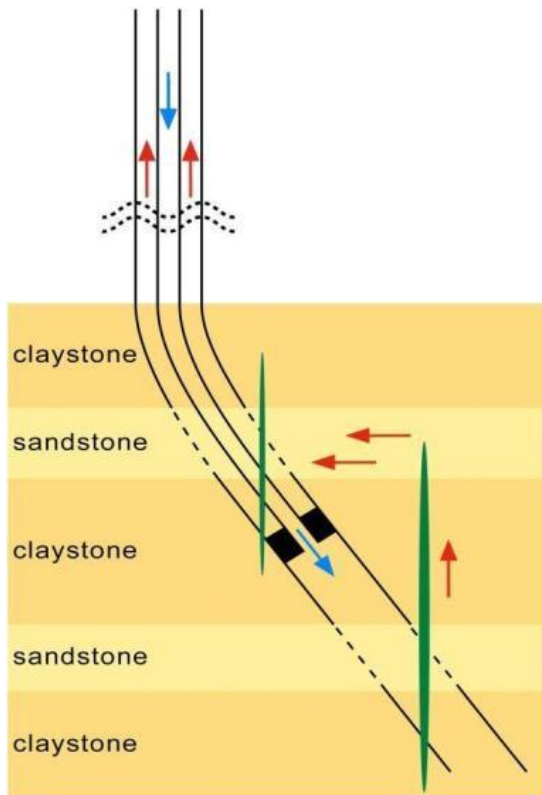

Fig. 7.2. Schematic representation of the drilling, injection as well as extraction concept drawn and implemented in the framework of the GeneSys Groß-Buchholz Gt1 geothermal drilling project. Note the large vertical hydrofractures (vertical green elliptical features) planned as part of the production concept.

Studying fluid-driven fracture path and geometry is at the heart of every geothermal project dealing with EGS in low-permeable rock formations. Key questions also raised within the GeneSys project concern the fracture trajectory, the fracture dimensions, and factors controlling them. Apart from the complex hydro-mechanical dynamic interaction that extensively dominates fracture initiation and further propagation, a variety of factors directly affects the fracture passage and geometry (e.g., Naceur et al. 1990, and references therein). Among these factors counts the elastic properties of the involved sedimentary alternation, the mechanical intrinsic properties (e.g., fracture toughness), the hydraulic properties of the rock matrix, the mechanical and hydraulic properties of the interfaces between different materials involved, the in-situ stress distribution, and pre-existing fracture network, fracture density, fracture percolation etc. (e.g., Gudmundsson 2011, McClure 2012, McClure & Horn 2013, Rossmanith 1998, and references therein).

Although remarkable progress in understanding fracture formation and growth has been achieved in the last decades, the science and engineering of fluid-driven fracturing, and in particular the hydromechanical processes involved, are not completely understood and are therefore the subject of a great deal of recent and current investigations. Especially, understanding the hydromechanical coupling and feedback have been the focus of numerous scientific and engineering works (e.g., Adachi et al. 2007, Economides and Nolte 2000). Theoretical (e.g., Detournay 2004, Anderson 2005, Gudmundsson 2011, and references therein) and numerical efforts (e.g., Adachi et al. 2007, McClure 2012, McClure & Horn 2013, Mutlu and Pollard 2008, and references therein) have been devoted to refining and improving the knowledge of the mechanisms involved.

Whereas field observations (Cooke et al. 2000, De Joussineau et al. 2007, Granier 1985, Leroy and Sassy 2000, Segall and Pollard 1983, Willemse et al. 1996, and references therein), *in-situ* and laboratory experiments (e.g., Fisher and Warpinski 2012, Teufel and Clark 1984, Warpinski et al. 1982), as well as theoretical considerations derived from the preceding studies have substantially helped shape a more complete picture of the behaviour of fluid-driven fractures; their complex dynamic hydromechanical behaviour, their geometry and interaction with the rock matrix and natural pre-existing fractures can only be studied at large spatial- and time-scale on computers. Fully coupled hydro-mechanical numerical models that consider fracture initiation and fracture propagation in at least two modes of deformation as well as fracture interaction are extremely rare. FRACOD is a promising code still in progress that includes these model capabilities (Shen et al. 2013).

Using FRACOD, as two-dimensional boundary element code, the present study addresses the hydromechanical behaviour of fluid-driven fractures in layered reservoirs with similar loading conditions and material properties to the ones encountered at targeted depths in GeneSys Groß Buchholz Gt1 and in general typical of the NGB region. In addition, fracture interaction between hydraulically induced and natural fractures is included to come closer to more realistic conditions at deeper targets such as fault zones and volcanic rocks. This work focuses on fracture path and fracture geometry controlling factors such as differently stratigraphically layered reservoirs with differing elastic properties and fracture toughness, as well as the influence of the interaction between pre-existing fractures with the newly generated hydraulic fracture on the fracture trajectory and dimensions.

2. Model setup and physics behind

Because of the data wealth collected within the framework of the GeneSys project, similar reservoir layering and material properties to the ones encountered at targeted depths were adopted. This makes possible to answer crucial questions raised within the GeneSys project related to fracture path and fracture geometry under similar loading and hydraulic conditions. Additional important data on fracture systems, associated with normal faults, and the mechanical properties of rocks typical of this region has been provided by Reyer et al. (2012), Reyer and Phillipp (2014) and Backers and Stephansson (2012). The considered layered reservoir scenarios are displayed in Figs. 7.3-7.5.
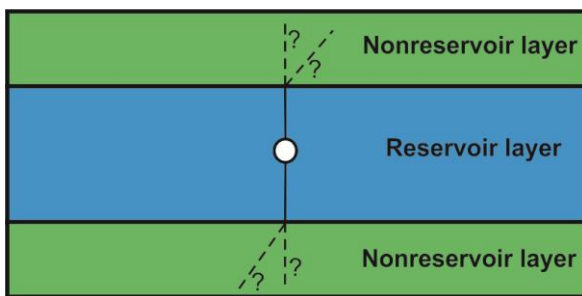

Fig. 7.3. 2-D model setup of layered reservoir with vertically symmetric layering. A specific case typical of the NGB represents a sandstone layer (reservoir layer) with overlying and underlying claystone layers. The white circle in the middle depicts the injection hole from which the hydraulically induced fracture (black lines) propagates. Black dashed lines denote possible paths of the through-going fractures.
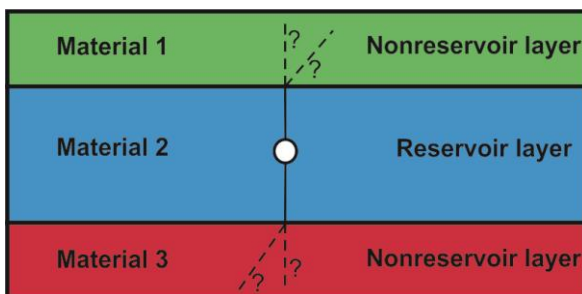

Fig. 7.4. Analogous to Fig. 7.3, this case concerns a three-layered scenario of vertically asymmetric distribution of sediments. A combination of three possible sedimentary layers encountered at targeted depths in the NGB may be halite, sandstone and claystone or siltstone alternated with two of the other preceding sedimentary rocks. White circle and white solid as well as dashed lines are described in Fig. 7.3 caption.
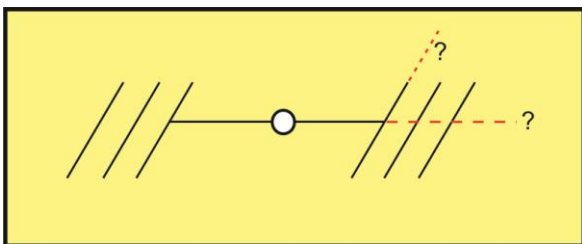

Fig. 7.5. Model setup considering a multiple fracture scenario relevant to deeper geothermal reservoirs in the NGB such as fault zones and volcanic rocks. Black inclined solid lines represent pre-existing fractures. Red dashed lines denote possible fracture propagations after the hydraulically induced fracture hits the pre-existing fractures. See also Fig. 7.3 and 7.4 captions for further picture details.

The in-situ or far-field stresses in the reservoir region have been assumed according to previous geo-mechanical modelling (Meneses Rioseco et al. 2013) and the results of a minifrac test performed in the context of the GeneSys project. In addition, data on the regional/local stress field recently published by Röckel and Lempp (2003) was also taken into account. Finally, the loading conditions as well as the material properties were varied over a wide range. Fluid pressure was held constant during the whole simulation time for all the models considered in the present study.

2.1. Modelling technique and underlying physics

To address the hydromechanical coupling mechanism in the geothermal reservoir, the code FRACOD was selected (Shen et al. 2013). This fracture initiation and propagation code is a two-dimensional boundary-element numerical tool especially designed to capture the fundamental features of the fully coupled hydro-mechanical behaviour of a rock matrix exposed to mechanical and hydraulic loading (see Fig. 7.6 and 7.7). It employs more specifically the Displacement Discontinuity Method (DDM). FRACOD is particularly appropriate for modelling fracture initiation and fracture growth in elastic and isotropic media (e.g., Shen and Stephansson 1992, 1993a, 1993b, Shen 1994, 1995, Shen et al. 1995, 2002, 2004, 2013).
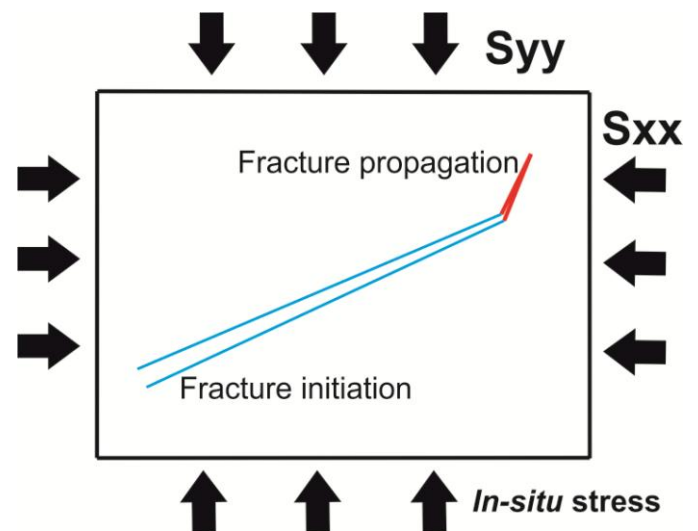
Fig. 7.6. Cartoon representing fracture initiation and further propagation within far-field or in-situ stresses as considered in FRACOD.

Fracture initiation is modelled utilizing the well-known Mohr-Coulomb failure criterion. Fracture propagation or the possible crack growth behaviour is simulated using a modified G-criterion (G: strain energy release rate) suggested by Shen and Stephansson (1993a, b). A more detailed description can be found in the user manual of FRACOD.

In tight sedimentary rocks or fractured hard rock, e.g. granite, fluid flow takes places fundamentally through fractures. Porous flow, though negligible under such

exceedingly low-permeable conditions, is modelled using Darcy's law. Especially fluid withdrawal from fracture regions to the rock mass or vice versa is incorporated in FRACOD by Darcy's law. The fluid flow in fractured domains is implemented in FRACOD using the channel flow, more explicitly given by the cubic law, whereby the fluid flow is proportional to the fracture aperture to the power of three.
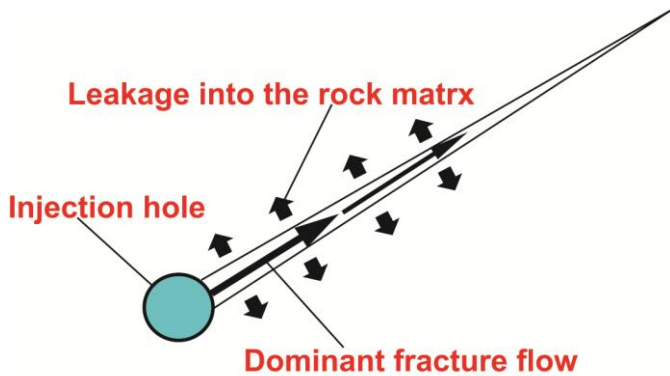

Fig. 7.7. Schematic representation of the fluid flow mechanism considered in FRACOD. Note the predominant fracture fluid flow and minor drainage into the rock mass.

Finally, fluid pressure contained in fractures may lead to fracture walls displacement, further opening fracture width, or eventually fracture growth. These effects basically summarized in fracture mechanical deformation and propagation directly influence in turn the fracture hydraulic conductivity and possibly generate new fluid conduits. This dynamic interaction between fracture mechanical reactions to fluid flow alterations and feedbacks is a crucial component in coupled hydromechanical processes and it is appropriately handled in FRACOD.

3. Model Results

A variety of models was tested with different vertical lithological stratification typical of the targeted depths envisaged in GeneSys project or in general of the NGB reservoir-relevant encountered layering. On the basis of laboratory values as well as core and log measurements of elastic parameters and mechanical (e.g., fracture toughness in mode I and II) and hydraulic parameters (e.g., hydraulic conductivity of the rock matrix and porosity) the possible fracture path and geometry were examined. Factors controlling fracture trajectory through interfaces between different sedimentary sequences were studied. A special case of multiple fracture interaction is included to simulate the case of deeper reservoirs such as fault zones and volcanic rocks, where in both cases multiple pre-existing fractures are expected.

Several scenarios of sandstone layers sandwiched with claystone layers as well as different combinations of three-layered reservoirs with halite, sandstone,

claystone and siltstone were considered. The elastic parameters of these materials were additionally varied over a wide range to assess the impact of the variation of such parameters on fracture arrest and fracture deformation in general.
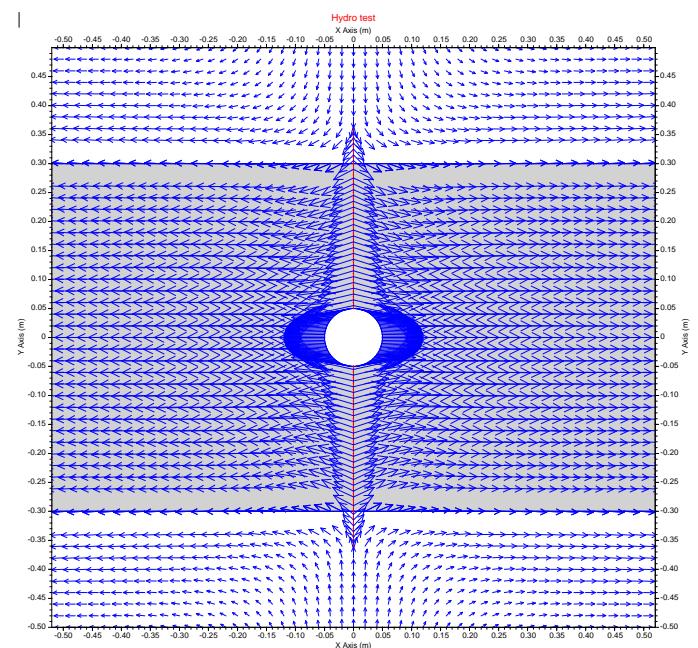

Fig. 7.8. Schematic representation of the fluid flow mechanism considered in FRACOD. Note the predominant fracture fluid flow and minor drainage into the rock mass. Different background colours (white and gray) refer to different material properties. Red solid line depicts the hydrofracture. White circle displays the injection hole. Blue arrows exhibit the displacement field.

Model results show that varying the Young's modulus and the Poisson's ratio over a wide range of values do not lead to fracture arrest but rather fracture containment, whereby fractures going through material interfaces experience damping. This has already been observed in experimental and *in-situ* experiments (e.g.. Fisher and Warpinski 2012, Teufel and Clark 1984, Warpinski et al. 1982). These model results, however, contradict previous numerical modelling concerning hydraulic fractures intersecting geological formations of similar type (Jung and Sperber 2009). Moreover, these results strengthen the point that the concepts envisaged in the GeneSys project of generating hydraulically-induced fractures crossing material interfaces and connecting hydraulically different sediment layers are feasible. At least the contrast in elastic properties of the different materials does not seem to arrest or deflect the fracture at the material interfaces (see Fig. 7.8 and 7.9). However, this needs to be taken carefully since some simplifications are made in this modelling. For instance, it is known from field and laboratory observations that the interfaces themselves play a considerable role in fracture path. Under certain conditions, most likely at shallow depths, the boundedness of the interfaces may be not strong enough and the vertical hydrofractures, when hitting

the material contacts, may continue along the material contacts, in the literature known as T-shaped fracture (see for instance Gudmundsson 2011, and references therein). At considerable depths, as is the case of the targeted depths in the GeneSys project such effect can hardly be expected.

Another important aspect relates to the fracture aperture. Model results demonstrate that depending on the contrast in the elastic properties of the different material layers the fracture aperture may exhibit different values. In stiffer materials the fracture seems to suffer more squeezing, or in other words, the fracture conductivity seems to be slightly reduced. This may have significant implications for the spatiotemporal evolution of the hydraulic behaviour of hydrofractures and the different flow regimes (e.g., linear, bilinear and radial) in the injection and shut-in phases of hydraulic stimulation (Wessling et al. 2008).
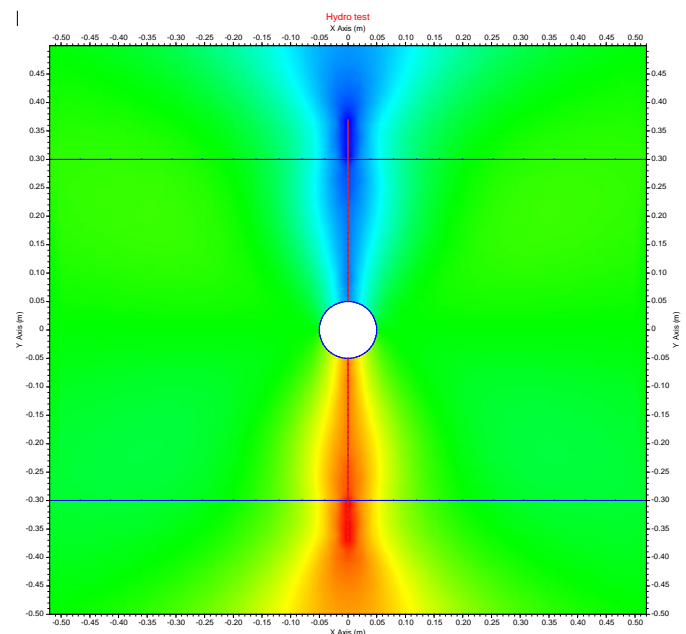

Fig. 7.9. Deformation distribution related to fracture propagation. The corresponding colour bar is preferentially omitted and here explained. Maximum negative displacement (on the order of 6.0×10^{-5}m) is depicted with dark blue. As the displacement dies out the blue colour get lighter and lighter. Green colour denotes almost no deformation. The dark red colour corresponds to maximum positive displacement (order of 6.0×10^{-5}m). As deformation lessens the red colour gets lighter and lighter and goes into yellow. Other picture features are explained in figure caption 7.8.

Mechanical material properties such as fracture toughness (mode I and mode II of deformation) corresponding to the differently stratified sequences of sedimentary material seem to influence fracture path through material contacts and its hydraulic properties in the newly entered material domain. Fracture toughnesses in mode I and II of deformation were first derived from laboratory data on samples typical of the study area and later varied over a relatively broad range. Although some laboratory values are available, in

general data on fracture toughness in mode II of deformation is very scarce.

Especially for a range of values of these two parameters close to one another the fracture path deviates from its initial orientation when crossing material interfaces (see Fig. 7.10 and 7.12). Besides, the fracture mode switches from a fluid-filled extensional fracture to a shear-dominated fracture. This has direct implications for the hydraulic properties of the through-going fracture. The hydraulic conductivity of the section of the fracture that has traversed through the material contacts has been drastically reduced (see Fig. 7.11).
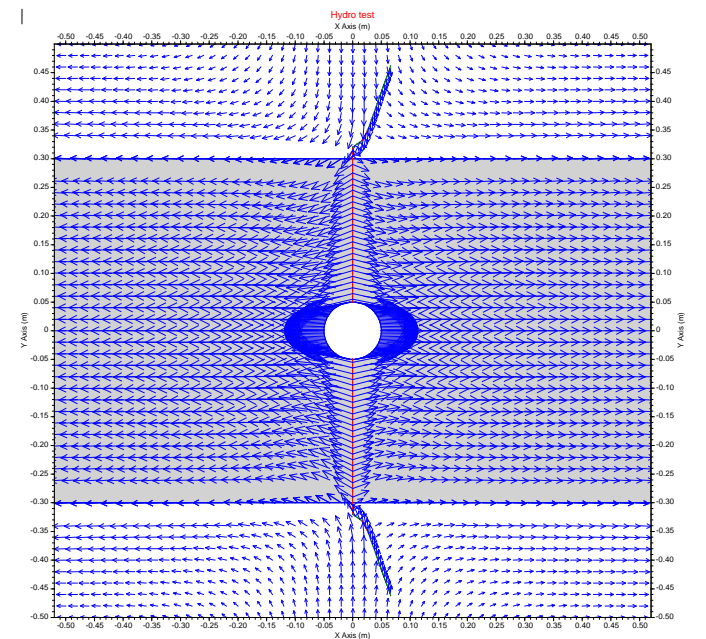
Fig. 7.10. Similar to Fig. 7.8, the fracture-induced displacement field around an injection hole and hydraulically generated fractures is displayed. Red lines depict open, fluid-filled, hydraulically induced fractures. Green lines denote slipping fractures. Note the fracture deflection after crossing the material contacts and the switch to model of deformation II.

Since dissimilar kinds of fractures originate in different orientations with respect to the in-situ or far-field stresses that apparently persist at the time of fracturing (e.g., Mutlu and Pollard 2008, and references therein), several scenarios were setup to model the hydromechanical interaction between multiple pre-existing fractures and a fluid-driven fracture. As mentioned earlier, these scenarios are relevant for deeper sections of the upper crust (e.g., volcanic rocks), also envisioned for future geothermal projects in the study area that equally requires hydro-fracturing. Properly classifying fracture types and fracture mechanical and hydraulic properties is a crucial component for assessing the orientation of fracture populations as an entire entity and hence for envisaging ideal drilling trajectories and designing reservoir models.

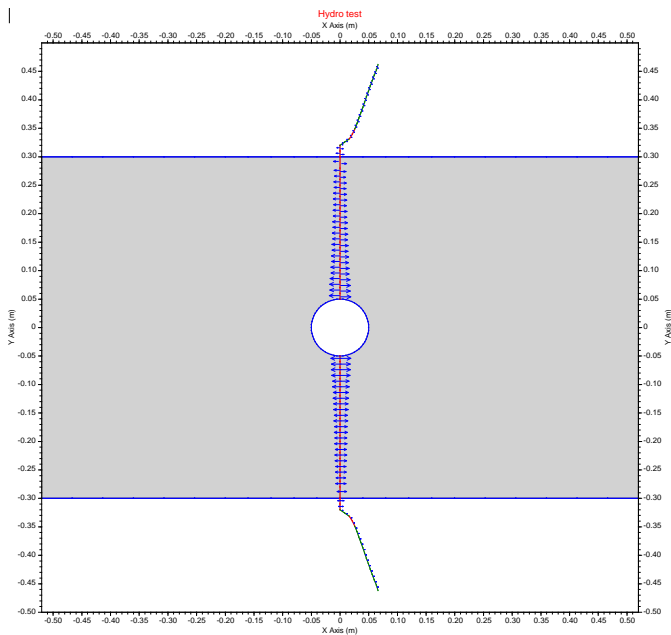**Fig. 7.11.** Fracture aperture or fracture-perpendicular displacement corresponding to the case displayed in Fig. 7.10. Blue arrows show the displacement field. Other features of this picture can be read in the figure captions 7.8, 7.9, and 7.10.
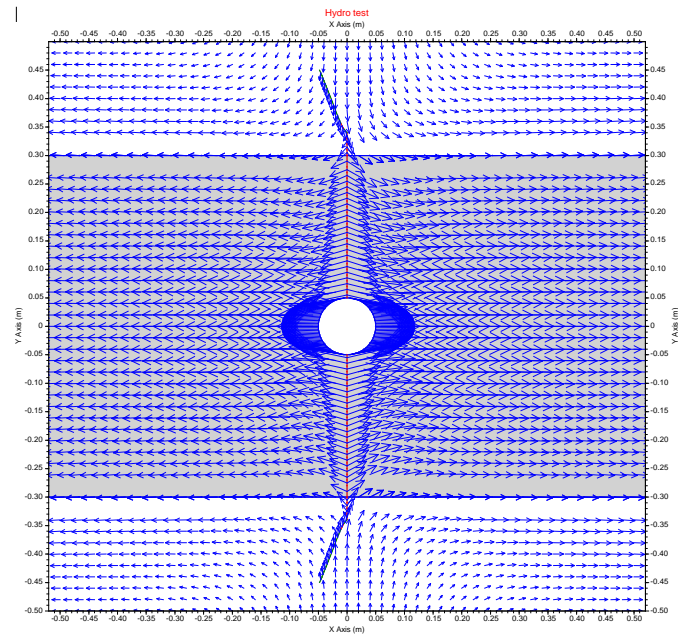

Fig. 7.12. Displacement field and fracture path caused by a hydraulically generated fracture and its advancing through different sedimentary material. See previous figure captions of this section for other features of this picture.

As Fig. 7.13 shows, four natural fractures (blue solid inclined lines) are placed within the reservoir with a randomly selected orientation with respect to the *in-situ* stress field. As the hydraulically induced fractures advance, the pre-existing fractures walls already slide past each other as a result of the "pressure wave". Some sections of the pre-existing fractures, close to the advancing hydrofractures tips, even experience fluid-filled extension deformation (see Fig. 13). Already at this stage of the advancing hydraulically induced fracture, it is clear that different cracks, fractures or joints are characterised by different hydraulic properties (see Fig. 7.15). Although at the present stage of this work

only one model material has been selected where fractures are embedded, it is expected that special kinds of fractures generate solely in specific rock types or in particular geologic settings.
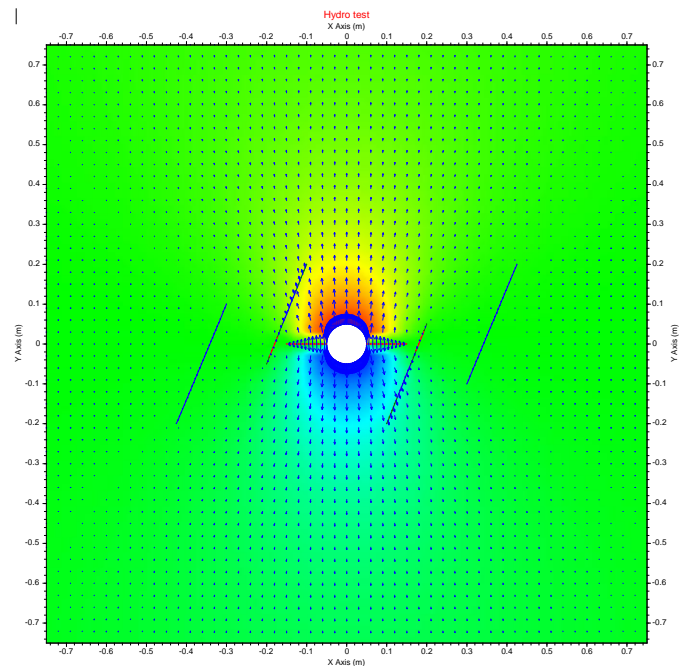
Fig. 7.13. Initial displacement field concerning the scenario of multiple pre-existing fractures and their interaction with a newly hydraulically generated fracture. Blue inclined lines depict natural pre-existing fractures closed (both walls of the fractures are in contact, no fluid content). Red lines as well as explanations for the colour bar can be read in previous figure captions in this section.
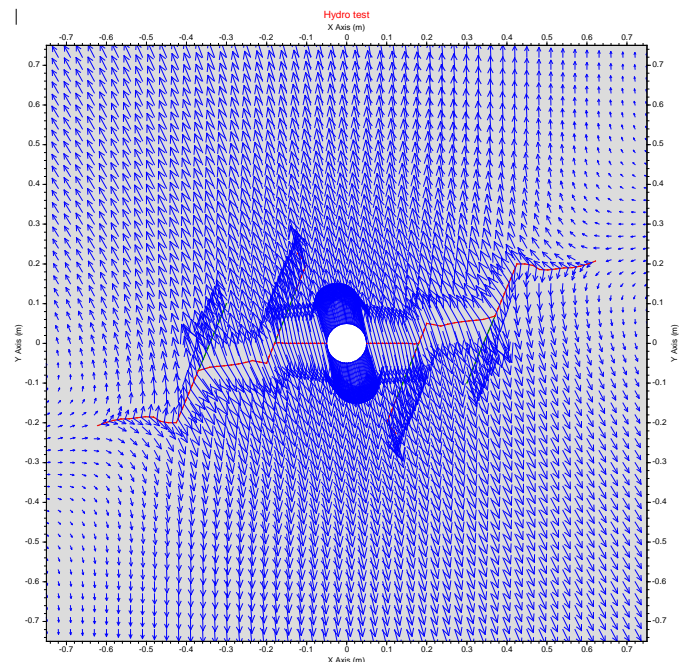
Fig. 7.14. Displacement field at an advanced stage of modelling corresponding to an initial scenario illustrated in Fig. 7.13. Note how the newly hydraulically generated fracture coalescence with the pre-existing fractures. See text and other preceding figure captions of this section for further details.

Fig. 7.14 displays the fracture interaction between four pre-existing fractures and a newly hydraulically induced fracture (see Fig. 7.13) in an advanced stage of the

modelling. As shown in Fig. 7.13, at the beginning of pressurisation the hydrofracture propagates in the direction of one of the exerted boundary stresses. When running into the pre-existing fractures the fluid pressure creates a fracture at the tips and the newly generated fracture tends to coalesce with the neighbouring pre-existing fracture (see Fig. 7.14). Furthermore, the new fracture created at the tip of the pre-existing fractures, propagates in the direction of maximum shear applied to the entire host rock. Hence, the pre-existing joints or fractures exhibit a controlling character on the hydromechanical properties of the rock matrix. This is line with similar modelling previously performed by Shen et al. (2013).

Hydraulic properties, and in particular the fracture conductivity spatiotemporal evolution can be better seen in Figs. 7.15 and 7.16. Initially, the hydraulically induced fracture has much greater hydraulic conductivity than the pre-existing fractures. As the hydraulically generated fracture advances and hits the pre-existing fractures, different sections of the latter are hydraulically activated and show significant hydraulically conductivity (see Fig. 7.16). Especially the newly originated fractures stemming from the pre-existing fractures tips take up a considerable part of the hydraulic conductivity of the fracture system, playing a hydraulically prominent role.
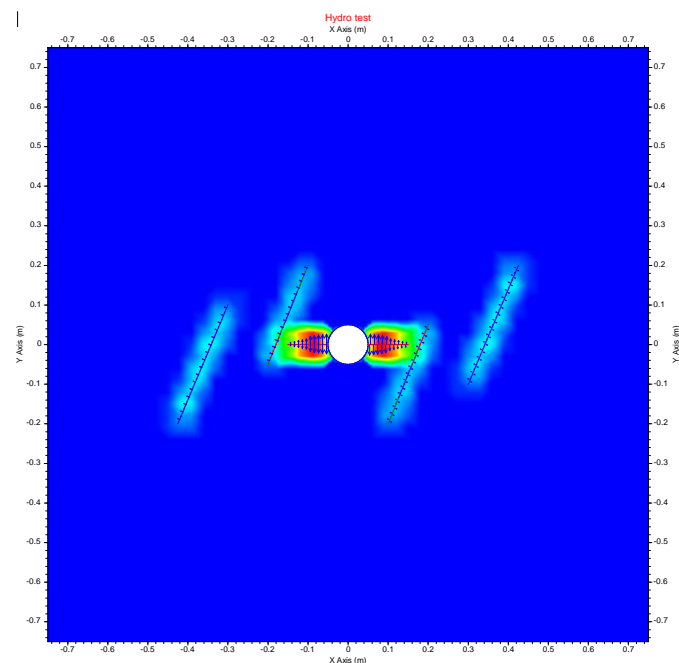

Fig. 7.15. Hydraulic conductivity of fractures and porous rock matrix corresponding to the initial case displayed in Fig. 7.13. The colour bar has been preferentially omitted. Dark blue (background colour of rock matrix) corresponds to minimum permeability (1×10^{-9} m^2). Rock matrix permeability has been set to 1×10^{-19} m^2. As domains gets more conductive the blue colour gets lighter (6.3×10^{-9} m^2). Highly conductive fracture domains (green to yellow colours) exhibit permeabilities on the order of 1×10^{-7} m^2 – 2.5×10^{-6} m^2. Maximum values are depicted with red colour, in the order of 1.6×10^{-5} m^2. See text for details.

Obviously, there are other mechanisms such as so-called stress barriers that may significantly contribute to fracture arrest. Extensive literature can be found about this issue (e.g., Naceur et al. 1990, Gudmundsson 2011, and references therein). Fracture arrest and confinement due to considerable stress differences between material layers is considered to be the most effective mechanism. However, this does not constitute the focus of this study.
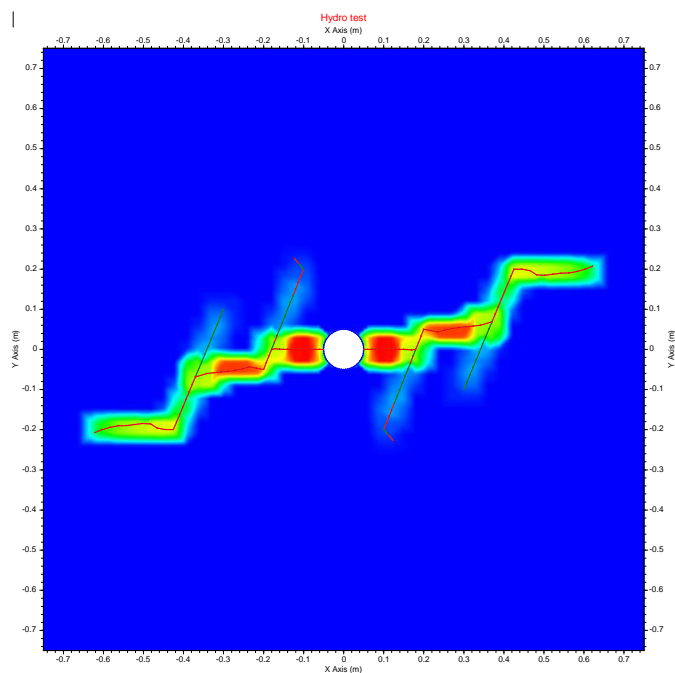
Fig. 7.16. Hydraulic conductivity of fractures and porous rock matrix corresponding to an advanced stage of modelling case displayed in Fig. 7.14. Further details can be read in the preceding figure caption and other figure captions of this section.

4. Summary and concluding remarks

Using FRACOD as boundary-element two-dimensional numerical tool, a variety of models was tested aimed at studying factors controlling hydrofracture path and geometry in different geological settings. Especially the hydromechanical response of fluid-driven fractures under region-specific mechanical and hydraulic loading conditions was investigated. Possible fracture trajectory and geometry controlling model parameters such as Young's modulus and Poisson's ratio as well as fracture toughness in mode I and II were varied over a broad range of region-specific values from laboratory experiments. Particular focus was given to scenarios involving lithologically layered sediment sequences typical of the North German Basin. Typical sediment layering (Middle Bunter) as encountered at targeted depths in the borehole Gt1 geothermal demonstration site was adopted for the numerical simulation since the GeneSys project provided valuable constraining data for the modelling. In addition, scenarios involving the hydromechanical interaction between multiple pre-existing fractures and a newly hydraulically generated

fracture were considered, as this would be the case of deeper laying volcanic rocks and fault zones that may be the future targets of hydraulic stimulation.

First, preliminary model results reveal important features of the fractures growth pattern over a broad parameter range and loading conditions. Simulation results show that in scenarios considering sandstone sequences sandwiched between overriding and underlying sequences of claystone, halite or siltstone layers, elastic properties such as Young's modulus or Poisson's ratio do not seem to arrest hydrofracture growth at layer contacts. This means that as far as elastic properties are concerned, hydrofractures connecting different sediment layers as envisaged in the GeneSys project are realizable. However, the hydrofracture aperture may decrease while crossing material interfaces. This corroborates previous laboratory and field observations. Another fracture path and geometry controlling factor is the fracture toughness in mode I and II and their ratio. Model results demonstrate that considerable differences in this material property between adjacent material layers may lead to significant deflections of the fracture trajectory when crossing material contacts. Besides, the fracture deformation mode may switch from opening to shearing. This is in accordance with the obtained reduction in fracture aperture in lithologically layered reservoir. This has considerable implications for the dynamic hydromechanical behaviour analysis of hydrofractures.

Numerical simulations of the hydromechanical interaction of multiple pre-existing fractures with a newly, hydraulically created fracture clearly demonstrate that some shear displacement is accompanied by the opening mode of deformation in naturally pre-existing fractures, ahead of meeting the advancing, hydraulically generated fracture. This is in line with previous modelling and theoretical considerations claiming that as pressure in the rock matrix grows, the effective principal stresses exerting on the natural fractures are reduced, facilitating shear movement along natural fracture walls. Moreover, model results show that when the newly, fluid-driven fracture encounters the pre-existing fractures, it does not continue its previous path trend. Pre-existing fractures experience dramatic hydraulic and mechanical alterations, and they tend to propagate at their tips in the direction of the maximum shear stress. While initially propagating in the direction of the minimum stress component, the growth of the newly, hydraulically induced fracture is severely affected by the pre-existing fracture network. The fracture system experiences major hydraulic alterations. While the initial

hydrofracture shows comparatively high values of hydraulic conductivity over the entire simulation time, only some sections of the pre-existing fractures significantly open and serve as valuable hydraulic paths, exhibiting considerable fracture aperture. Some others, however, show only shear mode of deformation.

Acknowledgements

References

Adachi J, Siebrits E, Peirce A, Desroches J: Computer simulation of hydraulic fractures, *Int J Rock Mech Min Sci*, 44, 739-757, (2007).

Anderson, T L: Fracture mechanics: Fundamentals and Applications, *Taylor & Francis*, 3rd ed., Boca Raton, USA, (2005).

Arias A, Dini I, Casini M, Fiordelisi A, Perticone I, Dell'Aiuto P: Geoscientific Feature Update of the Larderello-Travale Geothermal System (Italy) for a Regional Numerical Modeling, *Proceedings World Geothermal Congress 2010*, Bali, Indonesia, 0614, (2010).

Baldschuhn R, Binot F, Fleig S, Kockel F: Geotektonischer Atlas von Nordwestdeutschland und dem deutschen Nordsee-Sektor. *Geologisches Jahrbuch* A 153, *Schweizerbart*, Stuttgart, (2001).

Backers T, Stephansson O: ISRM suggested method for the determination of mode II fracture toughness, *Rock Mech Rock Eng* 45: 1011-1012, (2012).

Baumgärtner J, Jung R, Hettkamp T, Teza D: The status of the Hot Dry Rock scientific power plant Soultz-sous-Forêts, *Z Angew Geol* 50:12-16, (2004).

Bignall G: Hotter and Deeper: New Zealand's Research Programme to Harness its Deep Geothermal Resources, *Proceedings World Geothermal Congress 2010*, Bali, Indonesia, 1143, (2010).

Bignall G, Rae A, Rosenberg M: Rationale for Targeting Fault Versus Formation-Hosted Permeability in High-Temperature Geothermal Systems of the Taupo Volcanic Zone, New Zealand, *Proceedings World Geothermal Congress 2010*, Bali, Indonesia, 1148, (2010).

Blöcher MG, Zimmermann G, Moeck I, Brandt W, Hassanzadegan A, Magri F: 3D numerical modelling of hydrothermal processes during the lifetime of a deep geothermal reservoir, *Geofluids* 10:406-421, (2010).

Brown DW, Duchane DV, Heiken G, Hriscu VT: Mining the Earth's Heat: Hot Dry Rock Geothermal Energy. *Springer*, Berlin, (2012).

Cooke M, Mollema P, Pollard DD, Aydin A: Interlayer slip and fracture clusters within East Kaibab monocline: Numerical analysis and field investigations, In: Cosgrove J, Ameen M (eds.): Drape Folds and Associated Fractures, *Geol Soc London Spec Publ* 169:23-49, (2000).

De Joussineau G, Mutlu O, Aydin A, Pollard DD: Characterization of strike-slip fault-splay relationships in sandstone, *J Struct Geol* 29:1831-1842, (2007).

Detournay E: Propagation regimes of fluid-driven fractures in impermeable rocks, *Int J Geomech*, (2004), doi: 10.1061/(ASCE)1532-3641(2004)4:1(35).

Economides MJ, Nolte KG: Reservoir Stimulation, 3nd ed., *Wiley*, Chichester, England, (2000).

Fisher K, Warpinski N: Hydraulic-fracture-height growth: Real data, *SPE Annual Technical Conference*, Stanford, USA, SPE 145949, (2012).

Fisher K: Data Confirm Safety of Well Fracturing, *The American Oil & Gas Reporter*, July, (2010).

Granier T: Origin, damping and pattern of development of faults in granite, *Tectonics* 4:721-737, (1985).

Gudmundsson A: Rock Fractures in Geological Processes, *Cambridge University Press*, Cambridge, (2011).

Harvey CC, Harvey MC: The Prospectivity of Hotspot Volcanic Islands for Geothermal Exploration, *Proceedings World Geothermal Congress 2010*, Bali, Indonesia, 1182, (2010).

Huenges E (Ed.): Geothermal Energy Systems: Exploration, development, and utilization, *Wiley*, Weinheim, (2010).

Jung R, Weidler R: A conceptual model for the stimulation process of the HDR-system at Soultz, *Geoth Resour Council Transact* 24:143-147, (2000).

Jung R, Orzol J, Jatho R, Kehrer P, Tischner T: The GeneSys-Project: Extraction of geothermal heat from tight sediments, 30th *Workshop on Geothermal Reservoir Engineering 2005*, Stanford University, USA, SGP-TR-176, (2005).

Jung R, Sperber A: Erschließung der Vulkanite des Norddeutschen Beckens mit Multiriss-Systemen, *Geothermiekongress 2009*, Bochum, (2009).

Kehrer P, Orzol J, Jung R, Jatho R, Junker R: The GeneSys project – a contribution of the GEOZENTRUM Hanover to the development of Enhanced Geothermal Systems (EGS), *ZDGG* 158/1:119-132, (2007).

Legarth B, Huenges E, Zimmermann G: Hydraulic fracturing in a sedimentary geothermal reservoir: results and implications, *Int J Rock Mech Min Sci* 42:1028-1041, (2005).

Leroy YM, Sassi W: A plasticity model for discontinua, In: Lehner FK, Urai JL (eds.): Aspect of Tectonic Faulting. *Springer*, 77-108, (2000).

McClure M: Modelling and characterization of hydraulic stimulation and induced seismicity in geothermal and shale gas reservoirs. *PhD thesis*, Stanford University, USA, (2012).

McClure M, Horne R: Is pure shear stimulation the mechanism of stimulation in EGS?, 38th *Workshop on Geothermal Reservoir Engineering 2013*, Stanford University, USA, SGP-TR-198, (2013).

Meneses Rioseco E, Löhken J, Schellschmidt R, Tischner T: 3-D geomechanical modelling of the stress field in the North German Basin: Case study GeneSys-Borehole Gt1 in Hanover Groß-Buchholz, 38th *Workshop on Geothermal Reservoir Engineering 2013*, Stanford University, USA, SGP-TR-198, (2013).

Moeck I, Kwiatek G, Zimmermann G: Slip tendency analysis, fault reactivation potential and induced seismicity in a deep geothermal reservoir, *J Struct Geol* 31:1174-1182, (2009).

Mutlu O, Pollard DD: On the patterns of wing cracks along an outcrop scale flaw: A numerical modelling approach using complementarity, *J Geophys Res* 113, B06403, (2008).

Naceur KB, SPE, Touboul E, Schlumberger D: Mechanisms controlling fracture-height growth in layered media, *SPE Production Engineering*, *Society of Petroleum Engineers*, May, (1990).

Orzol J, Jatho R, Jung R, Kehrer P, Tischner T: The GeneSys Project – Development of concepts for extraction of heat from tight sedimentary rocks, *Z Angew Geol* 2:17-23, (2004).

Orzol J, Jung R, Jatho R, Tischner T, Kehrer P: The GeneSys-Project: Extraction of geothermal heat from tight sediments, *Proceedings World Geothermal Congress 2005*, Antalya, Turkey, 001, 1-6, (2005).

Reinicke KM, Oppelt J, Ostermeyer GP, Overmeyer L, Teodoriu C, Thomas R: Enhanced Technology Transfer for Geothermal Exploitation through a New Research Concept: The Geothermal Energy and High-Performance Drilling Research Program: gebo, In: *SPE Annual Technical Conference and Exhibition*, Florence, Italy, (2010).

Reinicke KM: Fracken in Deutschland, *Erdöl Erdgas Kohle*, 128/1:2-6, (2012).

Rossmanith HP (ed.): Mechanics of Jointed and Faulted Rock. *Balkema,* Rotterdam, (1998).

Reyer D, Bauer JF, Philipp SL: Fracture systems in normal fault zones crosscutting sedimentary rocks, Northwest German Basin, *J Struct Geol* 45:38-51, (2012).

Reyer D, Philipp SL: Empirical relations of rock properties of outcrop and core samples from the Northwest German Basin for geothermal drilling, *Geotherm Energ Sci* 2:21-37 (2014).

Röckel T, Lempp C: Der Spannungszustand im Norddeutschen Becken, *Erdöl Erdgas Kohle* 119:73-80, (2003).

Segall P, Pollard DD: Nucleation and growth of strike-slip faults in granite, J *Geophys Res* 88:555-568, (1983).

Shen B, Stephansson O: Deformation and propagation of finite joints in rock masses, In: Myer et al. (eds), Fractured and Jointed Rock Masses. 303-309, (1992).

Shen B, Stephansson O: Modification of the G-criterion of crack propagation in compression. *Int J Eng Frac Mech* 47:177-189, (1993).

Shen B, Stephansson O: Numerical analysis of Mode I and Mode II propagation of rock fractures, *Int J Rock Mech Min Sci Geomech* 30(7):861-867, (1993).

Shen B: Mechanics of fractures and intervening bridges in hard rock, *Bergmekanikdag*, 213-231, (1994).

Shen B, Stephansson O, Einstein HH, Ghahreman B: Coalescence of fractures under shear stresses in experiments, *J Geophys Res* 100(B4):5975-5990, (1995).

Shen B: The mechanism of fracture coalescence in compression - experimental study and numerical simulation, *Int J Eng Frac Mech*, 51(1):73-85, (1995).

Shen B, Stephansson O, Rinne M: Simulation of borehole breakouts using FRACOD2D, In: Oil & Gas Science and Technology - Revue de l'IFP, *International Workshop of Geomechanics in Reservoir Simulation*, IFP. Rueil-Malmaison, France, 57(5):579-590, (2002).

Shen B, Stephansson O, Rinne M, Lee HS, Jing L, Roshoff K: A fracture propagation code and its applications to nuclear waste disposal, *Int J Rock Mech Min Sci* 41/3:448–449, 2B 02, (2004).

Shen B, Stephansson O, Rinne M: Modelling fractured rocks. A fracture mechanics approach using FRACOD.*Springer*, Heidelberg (2013).

Sulzbacher H, Jung R: Numerical simulation of geothermal energy production from hydraulic fractures in tight sedimentary rock formation by cyclic-injection-production-schemes, *ZDGG*, 161/1:99-109, (2010).

Teufel LW, Clark JA: Hydraulic fracture propagation in layered rock: Experiment studies of fracture containment, *Soc Petr Eng J*, (1984).

Tischner T, Schindler M, Jung R, Nami P: HDR Project Soultz: Hydraulic and seismic observations during stimulation of the 3 deep wells by massive water injections, *32nd Workshop on Geothermal Reservoir Engineering*, Stanford University, USA, (2007).

Tischner T, Hermann E, Hauswirth H, Jatho R, Kosinowski M, Sulzbacher H: New concepts for extracting geothermal energy from one well: The GeneSys-Project, *Proceedings of the World Geothermal Congress 2010*, Bali, Indonesia, (2010).

Tischner T, Krug S, Pechan E, Hesshaus A, Jatho R, Bischoff M, Wonik T: Massive hydraulic fracturing in low permeable sedimentary rock in the GeneSys project, *Proceedings 38th Workshop on Geothermal Reservoir Engineering*, Stanford University, USA, SGP-TR-198, (2013).

Warpinski NR, Schmidt RA, Northrop DA: In-Situ Stresses: The predominant influence on hydraulic fracture containment, *J Petr Tech*, (1982).

Wessling S, Junker R, Rutqvist J, Silin D, Sulzbacher H, Tischner T, Tsang C: Pressure analysis of the hydromechanical fracture behaviour in stimulated tight sedimentary geothermal reservoirs, *Geothermics*, (2008), doi:10.1016/j.geothermics.2008.10.003.

Willemse EM, Pollard DD, Aydin A: Three-dimensional analyses of slip distribution on normal fault arrays with consequences for fault scaling, J *Struct Geol*, 18, 295-309, (1996).

Ziagos J, Phillips BR, Boyd L, Jelacic A, Stillman G, Hass E: A Technical Roadmap for Strategic Development of Enhanced Geothermal Systems, *38th Workshop on Geothermal Reservoir Engineering*, Stanford University, USA, (2013).

Zimmermann G, Reinicke A, Blöcher G, Milsch H, Gehrke D, Holl HG, Moeck I, Brandt W, Saadat A, Huenges E: Well path design and stimulation treatments at the geothermal research well GTGRSK4/05 in Groß Schönebeck, 38th *Workshop on Geothermal Reservoir Engineering*, SGP-TR-183, Stanford University, USA, (2007).

8 Continuative results of laboratory analyses

In the following chapter continuative results of laboratory analyses are presented. First, these results are of interest in terms of characterising the geomechanical behaviour of the taken samples. Textural aspects of sandstones are analysed regarding possible correlations with UCS. Secondly, for each given sample the shape and scale effect on UCS values is shortly investigated as well as the change of Young's modulus with increasing confining pressure.

8.1 Textural aspects and composition of sandstone samples

In Chapter 6, solely thin section results of samples used for failure and friction analyses were presented. However, thin sections of sandstone samples, which did not serve as triaxial test samples, were analysed, too. To supplement the QFL-data (Quartz, feldspar, lithoclasts), presented in Chapter 6, mean and maximum grain sizes, sorting, and rounding are listed for all sandstone samples (Table 8.1). The QFL-data and the amounts of cement and clay minerals are determined by point-counting of 500 grains per thin section (cf. Chapter 3.2.1). QFL-data are shown in normed percent taking only QFL-components into account; the amounts of cement and clay minerals refer to volume-percent of the whole thin section.

Table 8.1: QFL-data (Quartz, feldspar, lithoclasts), amount of cement and clay minerals, mean and maximum grain sizes, rounding, and sorting for the 23 sandstone samples.

Sample	d_{mean} [mm]	d_{max} [mm]	Sorting	Rounding	Q [%]	F [%]	L [%]	Cement [Vol.-%]	Clay minerals [Vol.-%]
GoSa	0.32	2	2	1.5	52.3	0	47.7	31.1	3.0
OLH	0.24	0.48	2.5	3.5	92.9	5.1	2	12.2	2.2
GiUK	0.25	0.4	2	2.5	94.9	2.4	2.7	16.8	1.3
FrUK	0.1	0.4	3.5	3.5	96.1	2.1	1.8	17	4.3
OK	0.2	0.26	2	3	94.2	4	1.8	17.4	2.8
AlWo	0.35	0.5	2	2.5	96.6	1.7	1.7	4.4	0.2
koQ	0.2	0.22	1	3	78.6	4.7	16.7	31	0
koVe	0.1	0.15	1	3	83.2	3.8	13	40	0
smHN	0.4	1	3	2	76.4	11.2	12.4	11.3	0
smD	0.22	0.54	2	4	92.3	3.7	4	18.5	0
smVG	0.21	0.65	3.5	3	80.1	15.8	4.1	23.8	0.8
smVG2	0.4	1.5	3.5	2	93.8	3.4	2.8	19.3	0.8
BiSu	0.21	0.7	2	3	72.2	17.1	10.7	12.3	0.9
BeRoK	0.5	5.5	5	2.5	73.1	2.8	24.1	11.8	3.4
BeRo	0.4	1.1	4	2.5	59.1	4.2	36.7	17.6	3.3
Gt1WS1	0.6	1.5	2.5	2.5	92.5	5.1	2.4	11.7	4.3
Gt1DU2	0.65	0.9	2	1.5	84.4	6	9.6	13.4	3.2
Gt1DU1	0.35	1.1	3.5	2	98.2	1.8	0	24	3.2
Gt1DU3	0.3	0.85	2.5	3	93.3	6.5	0.2	7.4	2.6
Gt1VS1	0.3	1.1	3.5	2.5	59.1	23.7	17.2	15.8	4.0
Gt1VS2.1	0.6	1	2.5	2.5	73.4	12.3	14.3	18.8	0
Gt1VS2.2	0.3	1.2	2.5	1.5	94.4	4.9	0.7	14.2	0

d_{mean} mean grain size; d_{max} maximum grain size; 1: very good; 2: good; 3: intermediate; 4: poor; 5: very poor

Most sandstone samples are fine and middle grained sandstones with good or intermediate sorting and rounding of the grains, varying amounts of cement between 4.4 and 40 Vol.-% and minor amounts of clay minerals (<5 Vol.-%). Exceptions are the two Rhaetian sandstones (koQ, koVe; cf. Table 2.2) with very good sorting and highest amounts of cement, and the two Permian (Rotliegend) sandstones (BeRo, BeRoK) with poor sorting.

Data on QFL-compositions of all sandstone samples from quarries are shown in Figure 8.1. Most sandstones plot in the quartz-rich corner of the QFL-triangle. There are few exceptions. Sample GoSa (Upper Creataceous age) which comes from north of the Harz Mountains has a different provenience with short sediment transport leading to higher amounts of lithoclasts. Sample BeRo (Permian –

Rotliegend) has a QFL-composition similar to GoSa. The Early Permian fluvial sediments had rather short transport resulting in poor sorting, bigger grain sizes and higher amounts of lithoclasts (Gast 1988; Table 8.1).
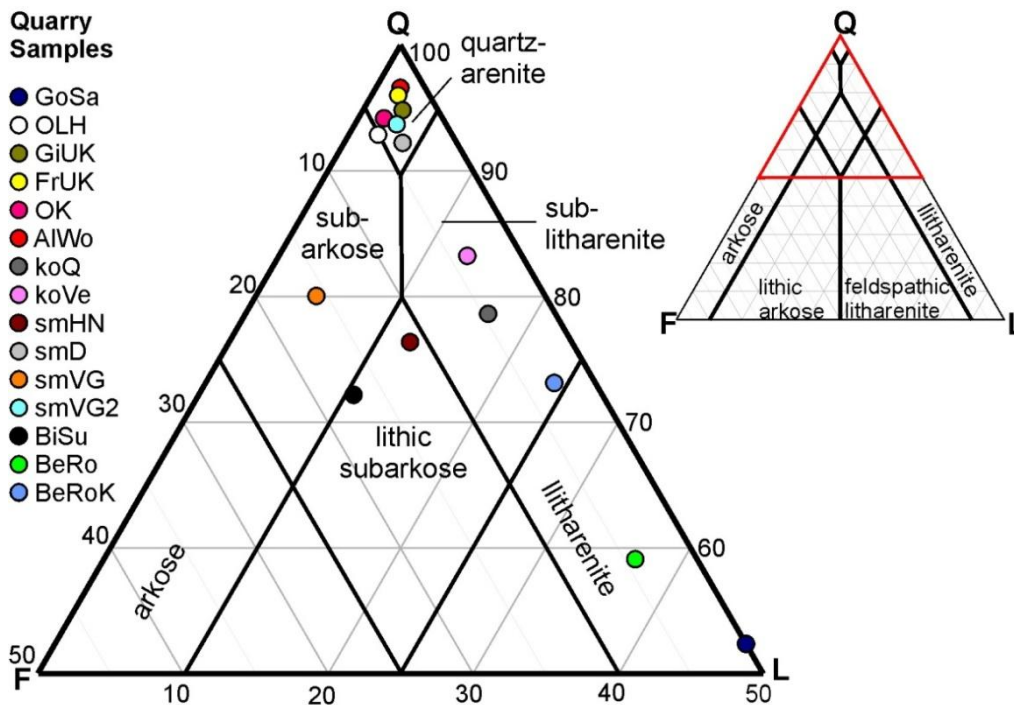

Figure 8.1: Classification of all sandstone samples from quarries (see key) according to McBride (1963) determined with point-counting with 500 counts (n=15).

It is conspicuous that sandstone samples, though they have similar normed QFL-compositions and amounts of clay minerals, are characterised by varying amounts of cement and degrees of rounding and sorting (Table 8.1). Correlations between sedimentary properties sorting, rounding and composition with UCS may therefore show possible interdependencies. In Figure 8.2, these parameters are plotted against UCS.
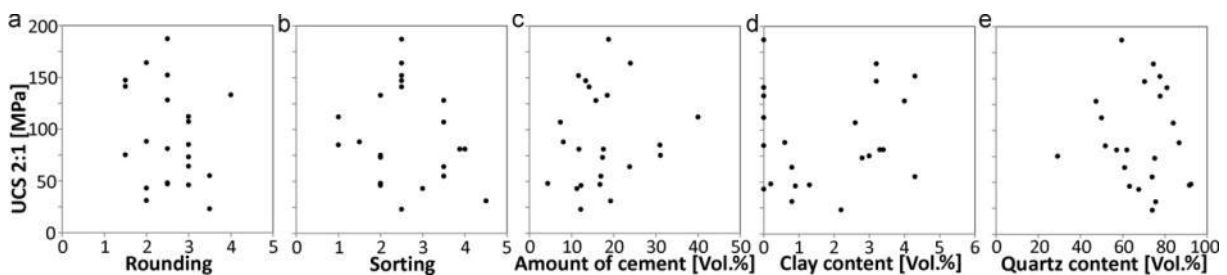
Figure 8.2: UCS2:1 versus a) rounding, b) sorting, c) amount of cement, d) clay mineral content and e) quartz content for sandstone samples (n=23).

It is obvious that there are no strong direct correlations between any of the sedimentary properties with UCS. For grains' rounding and sorting, as well as clay and quartz content, there are no relationships with UCS if analysed separately. The sandstone samples plot randomly (Figures 8.1a, b, d, e). In contrast, regarding the amount of cement there is a certain trend to higher UCS values with increasing cementation (Figure 8.1c). This trend, however, is only poor and cannot be the only explanation of the variations in sandstone UCS values. It is known that texture strongly affects mechanical properties of rocks (e.g., Öztürk et al. 2004). The determined variations of the sedimentary properties grain sorting, rounding and the amount of cement, clay minerals and quartz are at least indicators that strength differences of sandstone samples are based on such texture variations.

8.2 Comparison of 1:1 and 2:1 UCS values

It is well known that there are shape and scale effects on UCS values (Bieniawski 1968; Hoek and Brown 1980; ISRM 1999; ISRM 2007; Hawkins 1998; Thuro et al. 2001; Tuncay and Hasancebi 2009). In particular, cylindrical rock specimens with small L/D-ratios are expected to have higher UCS values than those with higher L/D-ratios. Maximum rock strengths are interesting parameters when discussing the issue of drilling efficiency, which is the drilling progress achieved for a given amount of energy input. There are correlations of this specific energy with maximum rock strengths which are used for drilling dimensioning (Teale 1965). To determine the maximum compressive strength of the rock samples additional specimens with L/D-ratios of ~1:1 are measured.

Against these expectations, Fig. 8.3a does not show any significant difference between UCS values determined with L/D-ratios of 1:1 and 2:1. UCS values of samples taken parallel to layering are similar to the trend of equal strength values and tend to have slightly higher UCS1:1 (Figure 8.3b). The coefficients of determination are stated separately for samples taken parallel and perpendicular to layering (Figures 8.3b, c). Both plots show strong correlations. The coefficient of determination of 0.901 for samples taken parallel to layering is excellent. Nevertheless, it is conspicuous that, for some samples taken perpendicular to layering (Figure 8.3c), determined UCS2:1 values are even higher. The calculated regression line slope is 1.17, meaning that UCS2:1 are higher than UCS1:1 values:

$$1)\ \text{UCS2:1} = 0.96 \cdot \text{UCS1:1};\ R^2 = 0.901 \qquad 2)\ \text{UCS2:1} = 1.17 \cdot \text{UCS1:1};\ R^2 = 0.768$$
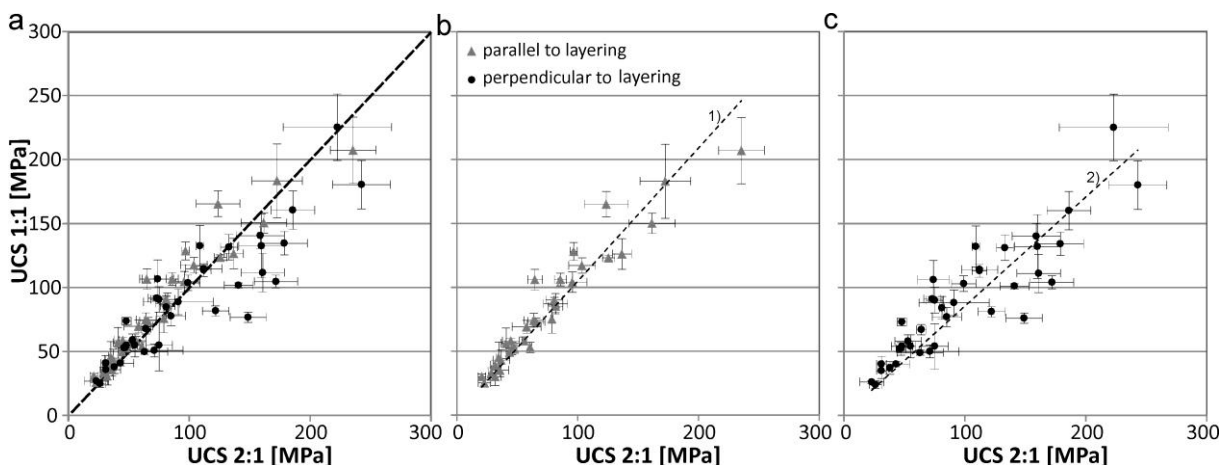
Figure 8.3: Comparison of UCS values measured with two different length-diameter ratios: 1:1 and 2:1 for a) specimens taken both parallel (n=33) and perpendicular to layering (n=49; see key). The pointed line in a) represents equal strength values (1:1). Regression curve (dashed line) for b) samples taken parallel to layering and c) samples taken perpendicular to layering; for regression functions see text. Error bars stand for standard deviations of all measurements of every sample.

The reason for this unexpected behaviour may be that there is a combined effect of both different shapes and different sizes of specimens used for parameter determination. Specimens used for 2:1 UCS have diameters of 40 mm, 1:1 specimens, in contrast, 50 mm. Small specimens tend to have higher strengths than larger ones (e.g., Thuro et al. 2001). That means the diminishing effect of the larger L/D may be compensated by the smaller diameter of 2:1 specimens compared with 1:1 specimens resulting in similar UCS values as observed in Figure 8.3.

8.3 Depths dependency of Young's modulus

The static Young's modulus E_s is an important parameter regarding hydromechanical fracture propagation and its simulation (cf. Chapter 7 and references therein). Presented values of Young's moduli (Chapter 5) were determined from uniaxial compressive strength test at surface conditions. At depths with increasing confining pressures, however, values may change considerably. From triaxial tests, Young's modulus was derived from recorded stress and strain values at different confining pressures.

In Figure 8.4, the effect of increasing confining pressure on Young's modulus is shown for eight exemplified sandstone and carbonate samples. A distinct linear increase of E_s values with very good data fit for both sandstone and carbonate rocks is observed in triaxial tests (blue diamonds). For comparison uniaxial E_s values are included (red circles). The exemplified sandstone samples comprise two well-cemented samples with strong grain interlocking (koVe, smD; cf. Table 2.2) and two with weaker grain interlocking and intermediate porosities (OK, smVG). Examples for carbonates are two high-porosity (GVa, OKDa) and two low-porosity limestones (ShJk, suHe; cf. Chapter 5).
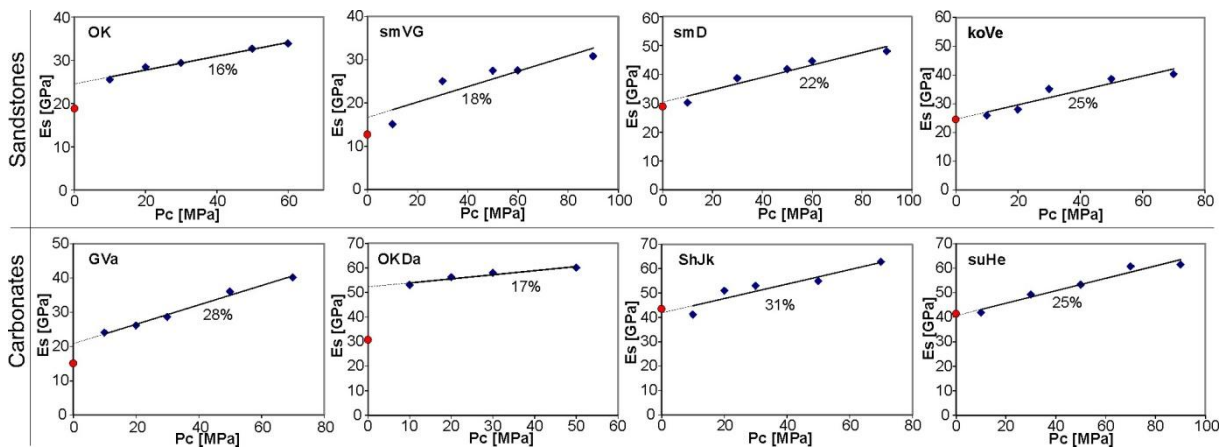

Figure 8.4: Effect of increasing confining pressure p_c on Young's modulus E_s for exemplified sandstone and carbonate samples (cf. Chapter 6). E_s values determined from uniaxial compressive strength test (red circles; cf. Chapter 5) and the percentage increase of E_s with confining pressure are included.

It is noticeable that Young's modulus, derived from triaxial test results, is the same as the uniaxial Young's modulus for samples smD, koVe. The uniaxial E_s values of the samples smVG and OK plot below the elongated triaxial test results. Sample koVe has a much stronger cementation and grain interlocking than sample OK though porosities are similar. There is a different behaviour of carbonate samples, too. Whereas for samples ShJk and suHe – both well-cemented with low porosities – we get comparable results of uniaxial Young's modulus and E_s derived from triaxial tests, uniaxial Young's modulus is much lower for high-porosity samples GVa and OKDa (Figure 8.4). That means there have to be mechanisms which control how strong an absent confinement affects the elastic behaviour.

Microfracture catalogue has strong effect on the strain at low axial loads (e.g., Jaeger et al. 2007). As discussed in Chapter 6 (Section 6.2) applying certain confining pressure on the specimen already closes most of the respective microfractures. This leads to steeper stress-strain curves. Consequently, in rock samples where high amounts of microfractures are present, measured uniaxial Young's moduli are expected to give lower values than deduced ones from triaxial test series. Investigation of mechanisms controlling uniaxial Young's moduli in comparison with derived ones from triaxial tests require systematic testing of rocks with changing facies/properties (e.g., fabric, texture, grain size, porosity, grain interlocking, etc.) held for different lithologies.

8.4 Failure criteria expressed in principal stresses

There are two common ways to express Mohr-Coulomb failure criteria: 1) expressed in normal and shear stresses, as presented in Chapter 6, and 2) expressed in principal stresses (cf., Zoback 2007). In the latter case, failure criteria are determined with Eq. 1 using the differential peak stresses and confining pressures of the respective triaxial testing sequence for each outcrop sample. In Table 8.2, the calculated Mohr-Coulomb failure criteria are listed.

Table 8.2: Mohr-Coulomb failure criteria, expressed in principal stresses, for outcrop samples

Sample ID	MC failure criterion: principal stresses
OK	$\Delta\sigma_{max} = 3.7 \cdot p_c + 90$ MPa
GVa	$\Delta\sigma_{max} = 1.7 \cdot p_c + 48$ MPa
OKDa	$\Delta\sigma_{max} = 4.3 \cdot p_c + 86$ MPa
ShJk	$\Delta\sigma_{max} = 4.0 \cdot p_c + 145$ MPa
AlWo	$\Delta\sigma_{max} = 2.1 \cdot p_c + 99$ MPa
koQ	$\Delta\sigma_{max} = 3.2 \cdot p_c + 163$ MPa
koVe	$\Delta\sigma_{max} = 3.9 \cdot p_c + 168$ MPa
EM	$\Delta\sigma_{max} = 1.0 \cdot p_c + 129$ MPa
EL1	$\Delta\sigma_{max} = 2.3 \cdot p_c + 193$ MPa
EL2	$\Delta\sigma_{max} = 2.1 \cdot p_c + 232$ MPa
smHN	$\Delta\sigma_{max} = 1.9 \cdot p_c + 82$ MPa
smD	$\Delta\sigma_{max} = 3.2 \cdot p_c + 202$ MPa
smVG	$\Delta\sigma_{max} = 1.4 \cdot p_c + 151$ MPa
suHe	$\Delta\sigma_{max} = 2.2 \cdot p_c + 136$ MPa
BiSu	$\Delta\sigma_{max} = 1.9 \cdot p_c + 88$ MPa
BeRo	$\Delta\sigma_{max} = 2.7 \cdot p_c + 129$ MPa
DöRo	$\Delta\sigma_{max} = 3.2 \cdot p_c + 334$ MPa
FL2	$\Delta\sigma_{max} = 3.3 \cdot p_c + 263$ MPa

In Figure 8.5, differential peak stresses $\Delta\sigma_{max}$ are plotted as a function of confining pressures separately for all outcrop-core sample couples. With linear regression analyses, failure criteria of equivalent outcrop samples are calculated, 90% confidence bands are added. In accordance to the procedure, presented in Chapter 6, failure criteria are then applied on equivalent core samples to calculate deviations between predicted and measured failure values.

For sandstone samples *smD*, *smVG* and *OK*, failure criteria are less precise than those of carbonate and volcanic rock samples which is reflected in wider confidence bands. Core sample values tend to plot slightly above the Mohr-Coulomb failure line for sandstones. That is, at the same confining pressures, core samples can stand slightly higher axial stresses before failure. However, core samples plot within confidence bands in most cases. Exceptions are sample *Gt1WS* (equivalent: *OK*) and *Gt1VS2* (equivalent: *smVG*). These two samples were already described in Chapter 6 (Section 4.1) as samples with suboptimal comparability to their outcrop equivalents. Volcanic rock sample *FL6* from depth plots perfectly well within confidence bands of *FL2*. Carbonate core samples, however, diverge from failure criteria of equivalent outcrop samples. They, in most cases, plot far above confidence bands, and calculated residuals are rather high.
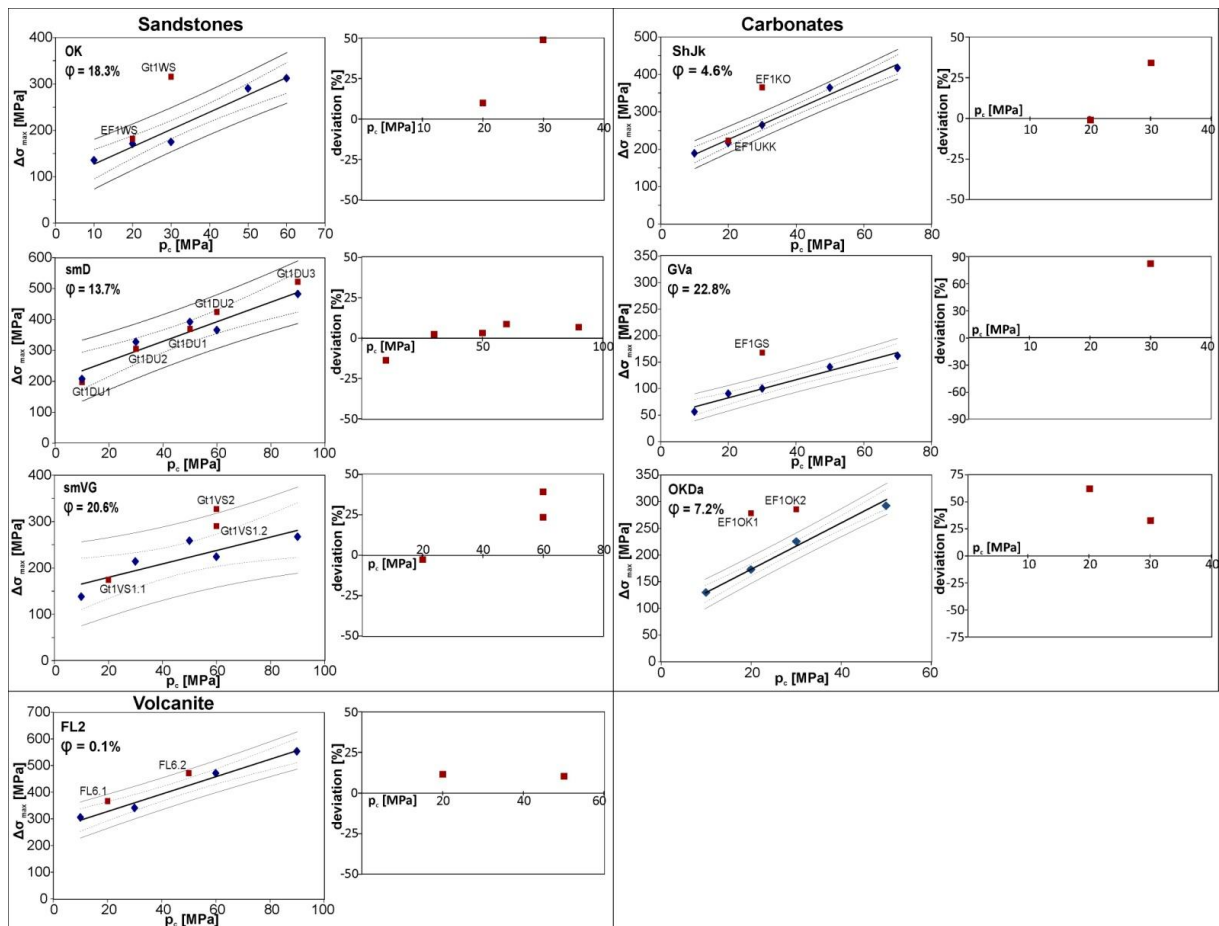
Figure 8.5: Maximum stress differences and confining pressures of all samples from depth (red squares) and equivalent outcrop samples (blue diamonds). Mohr-Coulomb failure criteria calculated from equivalent outcrop sample results, 90% confidence (pointed lines) and prediction bands (grey lines), and porosities φ are included. For core samples, residuals of outcrop sample failure criteria application are calculated (see text).

The main difference between these two ways to express failure criteria is that in the normal-/shear stress expression fault angles are taken into account. For the expression in principal stresses (confining pressure and axial stress) no such angle is necessary.

It is observed that core samples tend to develop steeper fault angles compared with their outcrop equivalents. These different fault angles lead to variations regarding the predictions of stress values (cf. Figs. 6.8, 8.5). Using the principal stresses larger deviations between predicted and measured values are observed than if taking the fault angles into account. That is, when considering predictions of core properties using failure criteria the ones expressed in shear and normal stresses are appropriate.

9   Discussion

Results of this thesis, presented in previous chapters, reveal that both normal fault structures and mechanical conditions are affected by rock heterogeneities and have to be considered in terms of geothermal exploration and exploitation in the NWGB. Both normal fault-related deformation patterns and rock mechanical properties, however, are affected by variations of stress and temperature conditions. That is, we face the problem of applying the results, which base on surface data, to geothermal reservoirs at depths. In the following, these aspects regarding normal fault zones, rock mechanical properties, triaxial test results, and stimulation modelling are discussed in more detail.

9.1 Normal fault zones

In Chapter 4, the lithological dependency of normal fault structures and associated fracture systems, and the effects of heterogeneities are extensively discussed (Section 6.2). Here, main findings are shortly presented and followed by further interpretations:

Investigations of structural indices (Caine et al. 1996) reveal that there is a wide range of structural indices for clastic rocks from very low to relatively high resulting from the heterogeneities of studied clastic rocks regarding different grain sizes, clay contents, or porosities (cf. Figure 4.11a). Similarly, for carbonate rocks the structural index correlates negatively with the amount of soft marl layers (Figure 4.11b) because it was found that fault cores tend to grow wider with increasing amounts of marl layers. The more soft layers there are in a sedimentary succession, the lower is the structural index of a cutting normal fault zone. Aside from this, data show that the existence of layer-parallel heterogeneities (mechanical layering) in the rock mass directly controls the amount of stratabound fractures (Odling et al. 1999) because many fractures become arrested at layer contacts. Summing up all results, it is concluded that normal fault zones in carbonate rocks are more damage-zone dominated than those in clastic rocks. They are therefore assumed to have a stronger positive effect on the fault-related permeability increase.

This, however, does not imply that fault damage zones in clastic rocks generally feature low permeabilities. The geothermal well Brühl GT1, for example, which targeted a fault damage zone in sandstones (Middle Bunter) found exceedingly high natural permeabilities (http://www.geothermie-bruehl.de). In accordance, presented normal fault data showed that, depending on porosity and cementation, clastic rock deformation may be characterised either by brittle failure or by compaction of pores and deformation band development (cf. Chapter 4, Section 6.2; e.g., Aydin 1978; Antonellini et al. 1994). In low-porosity sandstones, fault deformation rather leads to brittle failure and development of fractures than in sandstones with high porosities. That is, fracture-dominated damage zones with high natural permeabilities may also occur in clastic rocks, preferably in well cemented low-porous sandstones.

Independent of lithology this positive effect, however, is restricted to the comparatively narrow damage zones. In fault cores, in contrast, permeabilities are known to be very low (e.g., Lockner et al. 2000; Gudmundsson et al. 2001). The exploration of fault-related geothermal reservoirs regarding the target point selection has to be performed with care to encounter a fault's high-permeability damage zone. Analyses of the normal fault damage zones show that damage zones are significantly thicker in the hanging walls compared with footwalls (cf. Figure 4.10). From presented data one can draw the conclusion that the hanging walls of normal faults are most promising and should be targeted. There are, however, different approaches to interpret such asymmetric deformation patterns across normal fault zones. Some authors distinguish between extensional fields and contractional fields (Figure 9.1): at the upper fault termination the extensional field leads to wider hanging wall damage zones, at the lower termination to wider footwall damage zones (e.g., Muraoka and Kamata 1983; Knott et al. 1996). Other authors describe generally wider hanging wall deformation (White et al. 1986; Koestler and Ehrman 1991; Aarland and Skjerven 1998; Berg and

Skar 2005), mainly for listric and small-scale normal fault zones. Our data are more in accordance to latter studies. One reason may be that the focus was on analysing comparably small outcrop-scale faults like Koestler and Ehrmann (1991), not major normal fault zones. It is concluded that the most important cause of the asymmetric deformation pattern is related to the asymmetric stress field that develops during fault propagation within the hanging wall (cf. Aarland and Skjerven 1998; Berg and Skar 2005).
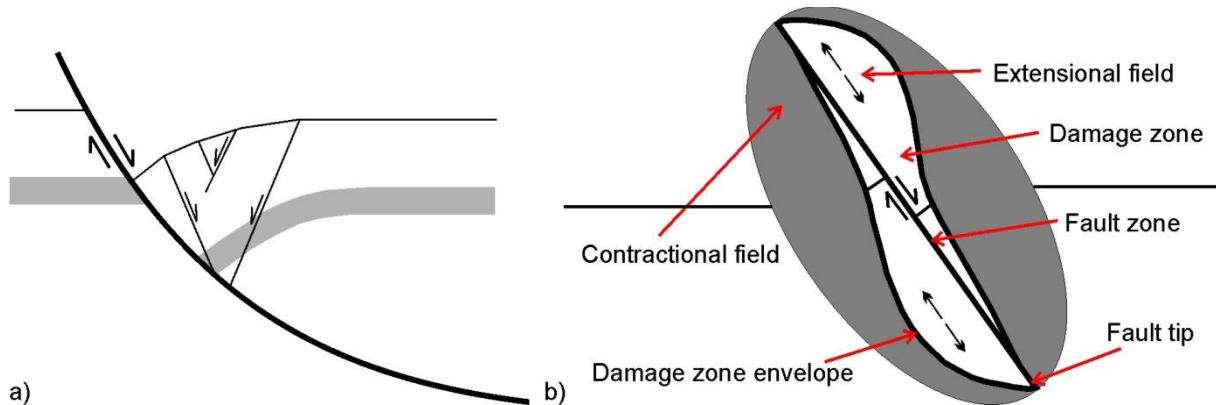

Figure 9.1: a) Sketch of asymmetric deformation pattern in the hanging wall of a listric normal fault zone (mod. from Twiss and Moores 1992); b) Cross sectional damage zone geometry according to Knott et al. 1996. Maximum damage zone widths occur in extensional fields, minimum widths at contractional fields.

In geothermal reservoirs, however, larger normal fault systems may be of even greater importance. Torabi and Berg (2011) extensively reviewed the scaling problem as to how results based on data from small-scale fault zones can be transferred to larger fault zones. They showed that the correlation of fault core thickness and fault displacement may not be scalable directly because there are breaks in this correlation between faults at different scales. Regarding the other aspects, especially damage zone widths of normal fault structures, the possibility of extrapolation of the achieved results is concluded (Torabi and Berg 2011). This is in agreement with many other studies (e.g., King 1983; Turcotte 1989; Gudmundsson 1992; Davy et al. 2010), concluding that fault zones can be regarded as self-similar. That means that small faults in principal look like larger ones and have similar internal structures. For most parameters presented in Chapter 4, except for the correlation of fault core thickness and displacement (cf. Torabi and Berg 2011), it should therefore be possible to apply achieved findings to larger normal fault zones.

We generally face the problem of extrapolating the results, which base on surface data, to geothermal reservoirs at depths. Both fractures and rock mechanical properties are affected by the different stress and temperature conditions. The fracture apertures and densities are known to decrease significantly with increasing depths (Zoback 2007). Apertures may change from one tenth to one hundredth of the values measured in the outcrops (Lee and Farmer 1993). Outcrop analogue studies, however, provide unique opportunities to study fracture systems in fault zones. Analyses presented in Chapter 4 reveal that in normal fault damage zones in sedimentary rocks of the NWGB the percentage of fractures with large apertures is much higher than in the host rocks. Fracture apertures additionally depend on the fracture orientation relative to fault-zone orientation. Oblique fractures feature lower mean apertures and lengths than parallel ones. Deduced from the previously discussed self-similarity hypothesis (Torabi and Berg 2011), distribution of fracture apertures and lengths in damage zones is supposed to be equal, too, even at greater depths. In principle, the results on different fracture system parameters in damage zones and host rocks are likely to be similar in deep normal fault zones even though a general reduction of fracture densities and apertures is to be considered.

Similarly, at higher confining pressures a significant increase of both compressive strength and Young's modulus is expected (cf. Chapters 6, 8.3). This has an impact on the calculation of the effective stiffness (E_e) distribution in normal faults. As discussed in Chapter 4 (Section 6.1), the E_e-

distribution strongly depends on the input data. The fracture density was recognized as the most important parameter in the calculations of the E_e-distributions within normal fault zone. Weakening of the rock mass due to normal faulting is concluded to be more pronounced in carbonate rocks than in clastic rocks. UCS values used to calculate effective Young's moduli E_e refer to surface conditions (Chapter 4). The compressive strength of rock samples, however, is shown to increase with confining pressure (Chapter 6). Furthermore, the assumed discontinuity stiffness (k_n) of 20% UCS is an approximation for macrofractures at near-surface conditions (Priest 1993). Consequently, effective stiffnesses at depths should be higher than the calculated E_e values, too. Presented E_e calculations revealed a reduction of initial Young's modulus (E_i) in damage zones of at least 75% (Chapter 4, Section 5). Griffith et al. (2009) used a numerical approach with discrete mesoscopic fractures to model respective effective stiffnesses in damage zones. This analysis showed that an overall stiffness reduction of more than 75% compared with the unaffected host rock is realistic, even at seismogenic depths. This is in comparatively good accordance with the presented E_e calculations in Chapter 4 although they were performed with simplified assumptions based on surface conditions.

9.2 Rock mechanical property determination

As described in Chapter 5, in heterogeneous sedimentary successions it is important to have good estimates about the geomechanical conditions in both reservoir and overlying strata to better adapt the drilling strategy and prevent problems with wellbore stability. For this purpose numerous parameters with importance in different stages of geothermal project development were measured for 35 outcrop and 14 core samples of various rock types present in the NWGB. With regression analyses empirical relations between UCS and the other parameters were determined for all samples together as well as lithologically separated. The approach to analyse applicability of these correlations for prediction of in situ rock properties is to compare relationships, developed from outcrop samples, with core sample properties. It is found that the developed empirical relations with or without core samples are quite similar for all analysed parameters (cf. Table 5.5). Merely, core samples have similar or only slightly higher values than outcrop samples. That is, these parameters are affected by unloading in a similar manner so that the ratio of UCS with the parameter considered does not change considerably (cf. Chapter 5, Section 6).

Another, more immediate approach is, to directly use the measured parameter values as input data for specific rock units for numerical modelling and wellbore stability analyses. For many different rock types which occur in the NWGB various properties were compiled in several tables (cf. Tables 5.2-5.4). The advantage is that they give, if not absolute values – because depths dependency is not considered –, at least relative parameter values, respectively mechanical contrasts, for these rocks. This is often sufficient for numerical approaches. Better data would be provided, however, if they were converted, considering the depths dependencies of compressive strength and Young's modulus, which are presented in Chapters 6 and 8.3. Furthermore, applicability of failure criteria and empirical relations on core samples was concluded in Chapters 5 and 6. It therefore appears reasonable that geomechanical and physical properties of the different stratigraphic rock units can also be used without much restriction. If core material is unavailable, these outcrop data are a good approximation to the 'true' properties of a specific stratigraphic rock unit. Anyhow, when investigating empirical relations which rely on parameters that were determined from unconfined measurements, difficulties arise from pressure and temperature variations between in situ and laboratory conditions which affect rock properties (Jaeger et al. 2007). Consequently, the same applies to directly measured properties. For this it is important to have a look at the different ways to measure the respective parameters and how they change with increasing confining pressure (cf. Chapter 5, Section 6).

For example, there are several ways to measure Young's modulus. Most common techniques include laboratory static measurements in uniaxial and triaxial compression (E_s; Chapters 5, 8.3) and borehole dynamic measurements with acoustic logs (e.g., Rider and Kennedy 2011). According to

McCann and Entwisle (1992), the dynamic values of Young's modulus appear to agree approximately with the triaxial static ones from laboratory. If no triaxial tests can be performed – either because funds are limited or triaxial test apparatus is lacking – it will be very helpful to use uniaxial E_s values instead. At triaxial tests, however, a distinct linear increase of E_s values with increasing confining pressure for both sandstone and carbonate rocks is observed (cf. Chapter 8.3). E_s values, determined with uniaxial compressive strength test (cf. Chapter 3.2.4), are in accordance with unconfined E_s deduced from triaxial tests of low-porosity carbonate and well-cemented sandstone samples (cf. Figure 8.4). That is, if the linear increase of E_s with confining pressure is known we can deduce the respective E_s value from uniaxial measurements but with less precise values.

9.3 Triaxial test interpretation

As described in Chapters 6 and 8.4, triaxial tests provide information about rock strength change with increasing confining pressure. In the linearized Mohr-Coulomb failure criterion, expressed in principal stresses, this dependency is reflected in both failure line slopes μ and unconfined compressive strength C_0 (cf. Figure 8.5). Presented data suggest that porosities and failure line slopes μ of sandstone samples are related: high-porosity sandstones tend to have lower values of μ than low-porosity sandstones. Although an enhanced confining pressure has a stabilizing effect on rock strength (Jaeger et al. 2007; Zoback 2007), this effect, however, is less effective in terms of preventing pore space destruction. Similarly, the fracture initiation stress for carbonates is inversely related to both porosity and mean grain size (Hatzor and Palchik 1997). That is, heterogeneities in terms of varying porosities and grain sizes are directly expressed in different failure line slopes μ. Comparing C_0 with UCS values (Chapter 5) gives a good positive correlation between these two parameters. Deriving C_0 from a triaxial testing series, however, neglects the curved increase of strength for very small confining pressures leading to 1.4 times higher values of C_0 compared with UCS (cf. Figure 6.12). For conservative estimations of wellbore stability, it is preferred to use conventional UCS, not C_0 values (e.g., Vogt et al. 2012).

In Section 8.4, it is shown that failure criteria based on principal stresses and those based on shear and normal stresses lead to differing results. If only principal stresses are analysed, core samples tend to have higher values of σ_1 compared with outcrop samples (cf. Fig. 8.5), especially for carbonate samples. If fault angle β is considered, however, the residuals between outcrop and core samples are reduced. In general, in carbonate core samples a larger angle β is induced at slightly higher values of σ_1 compared with the equivalent outcrop sample measured at the same confining pressure. That is, cores tend to develop steeper fault planes. The effect of such a larger angle β on resulting shear and normal stresses is illustrated in Mohr Circle plot (Fig. 9.2; Jaeger et al. 2007).
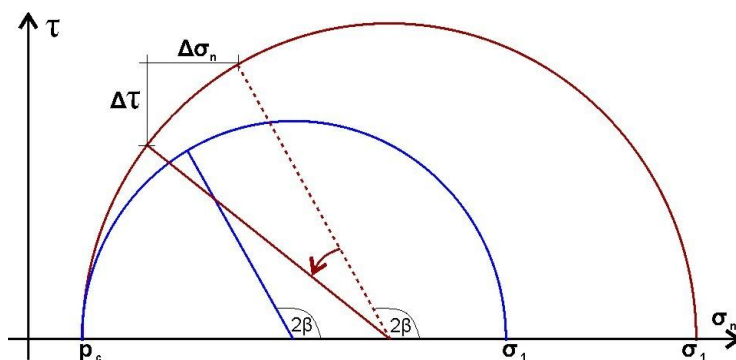
Fig. 9.2: Schematic Mohr circles and fault angles β of core (red circle) and equivalent outcrop sample (blue circle) measured with the same confining pressure p_c.

For the same confining pressures p_c, plotted in red, the higher values of σ_1 of cores are displayed in a greater diameter of the Mohr circle. A larger fault angle β, however, leads to a reduction of both effective shear and normal stresses. Consequently, deviations between shear and normal stress values of cores and outcrop samples are reduced, and cores are approaching failure lines of outcrop samples.

The observed larger angles of β in core samples cannot be explained only by textural differences between core and outcrop samples. That is, there has to be another and more significant reason for this diverging failure behaviour. One possible explanation is that in core and outcrop samples, there are different microfracture catalogues present. Core samples and outcrop samples have differing histories of unloading at which microfractures are induced. Outcrop samples received a comparative slow natural unloading. In undisturbed rocks randomly oriented background microfractures are expected. Microfractures with orientations depending on in situ stress states are induced by unloading (e.g., Carter et al. 1981). In contrast, core samples are influenced by fast unloading and penetrated while drilling. Core disking, i.e. layer parallel fracturing, is a common phenomenon (Haimson 1997; Li and Schmitt 1997). Even if core disking is absent, numerous layer parallel microfractures have to be expected. Microfractures with other orientation are comparatively rare. That is, cores contain less pre-existing weak planes sub-parallel to the newly induced fault planes which preprint the failure zone and reduce rock strength than outcrop samples.

Differing microfracture catalogues not only affect rock strengths and fault angles but also P-wave velocities. During triaxial testing, enclosed microfractures are partly or even completely closed by confining pressure. Consequently, the influence of microfractures on rock strength is smaller than on v_p which are measured at atmospheric pressures. Layering parallel microfractures have little effects on rock strength but large effects on v_p (e.g., Jaeger et al. 2007). Core samples perpendicular to layering have slower v_p but higher strengths compared with outcrop samples with randomly oriented microfractures. If sampled cores show slower v_p than the outcrop equivalents, we can conclude that they are strongly influenced by core disking. To evaluate if weathering rather than core disking is more affecting rock strength, P-wave velocities of all core-outcrop couples were cross plotted (cf. Figure 6.10). It is concluded that both cores and outcrop samples are of good quality. Another reason for steeper fault angles in carbonate core samples than in equivalent outcrop samples may be that carbonate rocks are characterised by complicated interdepending deposition conditions (e.g., Flügel 2010). Equivalence of outcrop/core samples is therefore more difficult to ensure than for clastic rocks.
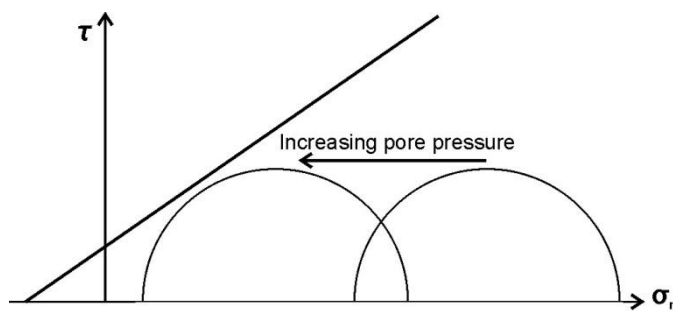

Figure 9.3: The effect of increasing pore pressure on rock failure illustrated in Mohr circle plot (mod. from Jaeger et al. 2007) with linearized Mohr-Coulomb failure criterion (cf. Chapter 6).

Evaluation of in situ rock mechanical behaviour requires different information; knowledge of elastic moduli and strength of rocks, as discussed in Chapter 9.2, is only one aspect. Important input data are also estimates of pore pressures (e.g., Duda and Renner 2012) and stress state (e.g., Zoback 2007). Triaxial tests can simulate in situ pressure conditions. For all samples confining pressures, selected for the set of triaxial tests, were adapted to realistic depths in which the respective rock units occur in the NWGB (cf. Chapter 3.2.6). In this way, the obtained failure criteria and changes of Young's modulus cover the complete stress conditions the specific rock unit can face in the NWGB. Effects of fluids, however, have not yet been taken into account. Presence of fluid in the pores, however, has strong influence on the acting stresses (e.g., Zoback 2007; Duda and Renner 2012). Thus, when determining the 'right' stress conditions, effective stresses have to be considered. Effective stresses represent the forces transmitted through the rock skeleton, which in turn causes the deformation of the material (Jaeger et al. 2007). The remaining parts of the total stresses are carried by the pore fluid which is equal in all directions. Consequently, an increase of pore pressure affects solely normal stresses not shear stresses (Figure 9.3). That is, at high pore pressures already

small differential stresses may lead to rock failure. The in situ stress state is almost never known. However, according to Peška and Zoback (1995) observations of compressive and tensile failures in inclined wellbores can be used to determine in situ stress states if there are data on the magnitude of the minimum principal stress σ_3 and on pore pressure conditions.

Apart from that, failure criteria determination is a key task in the analysis of wellbore stability (Fjaer et al. 2008). The approach to use core samples to validate the applicability of results from outcrop samples is to my knowledge new. Until now, rock property determination is more or less exclusively performed on core samples (Zoback 2007). To be of any use regarding the evaluation of in situ rock mechanical behaviour, cores, however, have to be representative for the formation of interest and of good quality. It has to be kept in mind that core samples are most likely altered when taken from in situ to laboratory conditions. Stress release, temperature release, and fluid exposure may lead to a reduction of UCS, Young's modulus and P-wave velocities (Fjaer et al. 2008).

As discussed above, core material is rare and this study therefore aims at predicting in situ rock properties from equivalent outcrop samples. There are other methods to determine failure criteria dealing differently with the shortage of core material. A comparatively common procedure is the so-called multiple failure state test (Kovari and Tisa 1975; Kovari et al. 1983). The principle is that the complete failure conditions are determined from one core specimen only. The test starts at a relatively small confining pressure. Every time when failure is almost reached – reflected in an abrupt change of the stress strain-curve – the confining pressure is increased (Figure 9.3). In this way it is possible to simulate different stress states with the same specimen (Kovari and Tisa 1975; Kovari et al. 1983).
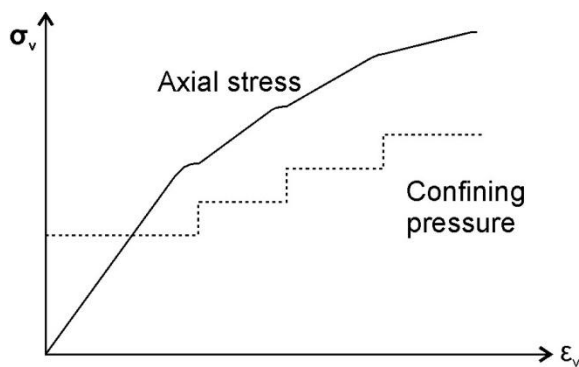
Figure 9.3: Sketch of the vertical stress σ_v and confining pressure path followed in a multiple failure state test with vertical strain ε_v (mod. from Fjaer et al. 2008).

The main problem of this procedure is that at every stress state, before confining pressure is increased, minor failure and associated strain occurs. Mean orientations of induced microfractures depend on the stress state: dip angles β of induced microfractures decrease with increasing confining pressure (Jaeger et al. 2007; cf. Chapter 3). These microfractures are expected to weaken the material. That is, the peak stresses, measured at higher stress levels, will be lower than if measured with a single triaxial test at the same constant confining pressure. This behaviour causes the determination of both a lower value for failure line slope μ_i but a higher unconfined compressive strength C_0 (cf. Chapter 6, Eq. 1). For the here discussed question of stability analysis it is preferred to perform a set of different measurements to obtain good and trust-worthy failure criteria. This encourages the approach to perform complete sets of triaxial measurements with equivalent outcrop samples when core material is limited.

In this thesis a linearized Mohr-Coulomb criterion is used for failure description of samples. This failure criterion assumes that the intermediate principal stress has no influence on failure. However, other criteria such as *Lade criterion* (Lade 1977) and *Wiebols and Cook criterion* (Wiebols and Cook 1968) depend on all three principal stresses. Wiebols and Cook (1968) developed an energy-based theoretical strength criterion saying that under true triaxial stress conditions the intermediate principal stress σ_2 has a great effect on rock's strength. Lade (1977) postulated a strengthening effect with increasing σ_2 followed by a small strength reduction when σ_2 is close to σ_1. In accordance, Fjaer

and Ruistuen (2002) showed that not only stress magnitude but also stress symmetry has an impact on rock strength. The strength is found to be highest for values of σ_2 close to $0.5(\sigma_1+\sigma_3)$, and lowest for $\sigma_2=\sigma_1$ and $\sigma_2=\sigma_3$. Furthermore, Haimson and Chang (2005) showed that σ_2 has a perceived strengthening effect on rocks regarding wellbore stability. Ewy (1998) therefore assumes that Mohr-Coulomb failure criterion leads to over-conservative predictions of critical mud weights. Coefficients of internal friction μ_i depict the growth in strength with increasing confining pressures and permit estimations on rock strengths and wellbore stability. Correlations between wellbore log results and μ_i are used to better predict wellbore instabilities based on well logs and geomechanical models (Chang et al. 2006; Zoback 2007). There is a general decrease of μ_i with increasing confining pressure reflecting curvature of Mohr envelope. However, the simplification of a linearized Mohr-Coulomb failure criterion is best for the presented approach. The database for each sample of five measurements does not allow a confidential estimation of the Mohr envelope. Consequently, determined coefficients of internal friction μ_i are conservative estimations for wellbore stability analyses. From all these points it is concluded, that presented failure and friction criteria yield conservative estimations of wellbore stability and leave a wide margin of safety.

9.4 Stimulation of geothermal reservoirs

If the encountered reservoir permeability is too low for economic use, we have to give consideration to engineering techniques in order to enhance the flow rate. In general, hydraulic reservoir stimulation comprises high-pressure injection of water into the prospective geothermal reservoir (e.g., Huenges 2010). The stimulation aims at either widening, respectively connecting pre-existing fractures or at simply generating a new fracture that penetrates the reservoir and increases the permeability (cf. Chapter 1). Stimulation treatment may be necessary in both types of geothermal reservoirs: 1) dense rock units which require massive hydraulic enhancement and 2) fault-related reservoirs, if the natural permeability is too low. For both cases, with trust-worthy simulation results required fluid pressures for hydrofracture creation in the specific rock unit can be calculated beforehand.

For stimulation of dense heterogeneous rocks, such as an alternation of sandstones and claystones (e.g., Middle Bunter; cf. Chapter 7), it is important to predict fracture path and termination (Jung et al. 2005). One parameter with special importance regarding stress distribution and fracture propagation is the static Young's modulus E_s. This was varied over a wide range in presented hydromechanical models (cf. Chapter 7) taking the observed linear increase of E_s values (Chapter 8.3) into account. That is, when allocating material properties the used values of Young's modulus were adapted to the applied stress conditions. Model results demonstrate that depending on the contrast in the elastic properties of the different layers the fracture aperture may obtain different values. In stiffer layers (high Young's modulus) the hydrofracture aperture seems to be diminished, or, in other words, the hydraulic conductivity of the fracture seems to be slightly reduced compared with less stiff layers.

Fracture termination at contacts between layers with different rock mechanical behaviour has been widely observed (e.g., Naceur et al. 1990; Odling et al. 1999; Brenner 2003; Larsen et al. 2010; Singhal and Gupta 2010). Stress distribution in mechanically layered successions is strongly affected by heterogeneous mechanical and elastic properties of the alternating rocks. Consequently, there is an increased risk of creating a hydrofracture with too small fracture area and, therefore, too small heat exchange area. To simulate the stimulation treatment, property variations of alternating rock types were considered. Modelling results show that varying Young's modulus and Poisson's ratio over a wide range of values does not lead to fracture arrest but rather to fracture containment. That is, with increasing property contrast fractures tend to stop within the layer without even reaching the layer interface. Fractures propagating through material interfaces experience a considerable aperture reduction in stiffer layers (Chapter 7). The bonding of the interfaces may be not strong enough under certain conditions so that the hydrofracture may propagate along layer contacts

(Atkins and Mai 1985; Gulrajani and Nolte 2000). Hereby, trajectories of maximum principal stress reflect the propagation path of the induced hydrofracture (e.g., Gudmundsson 2011).

In normal fault zones, conditions for stimulation are completely different. Presented studies on normal fault zones showed that fracture densities in damage zones are increased and most of the fault-related fractures have an orientation similar to the fault strike (cf. Chapter 4). This increased fracture density leads to a decrease of both UCS (Lockner et al. 2000) and Young's modulus (Fjaer et al. 2008) of damage zone rocks. To simulate a stimulation treatment within normal fault zones, a hydromechanical approach has to be used which respects the effects of pre-existing fractures on rock properties (cf. Chapter 7).

The discrete modelling of pre-existing fractures shows that the newly generated fracture tends to coalesce with the neighbouring pre-existing fracture (cf. Figure 7.14). At the tips of the pre-existing fractures new fractures are created, which, at the assumed loading conditions, propagate in the direction of maximum shear stress applied to the entire host rock. Hence, pre-existing fractures exhibit a controlling character on the hydromechanical properties of the rock matrix.
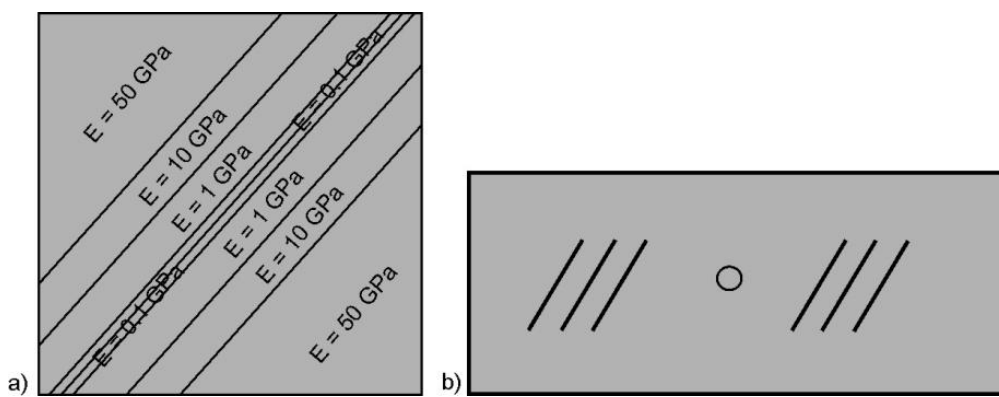

Figure 9.4: Different approaches to simulate fractured damage zones of normal fault zones. a) Effective Young's moduli *E* in different parts of the damage zones with respect to changing fracture densities (Gudmundsson et al. 2010); b) Discrete fracture modelling according to Meneses Rioseco et al. 2013 (Chapter 7), black inclined solid lines represent pre-existing fractures.

There are two different approaches to simulate fractures in normal fault zones. Similar to presented modelling approach in Chapter 7 (Figure 9.4b) some authors define discrete pre-existing fractures to represent damage zones (e.g., Griffith et al. 2009). Others simulate a fractured rock mass by applying effective Young's moduli (cf. Chapter 4) for different previously defined zones representing the typical fracture density distribution (e.g., Gudmundsson et al. 2010; Figure 9.4a). Depending on the respective problem which shall be solved, the one or the other approach is preferably used. In Chapter 7 we aim at analysing the problem of interaction between pre-existing fractures and induced hydrofracture regarding the propagation path. This is a problem on a comparatively small scale regarding discrete fractures. If the interest is more on the effects of fault zones on large scale variations of stress distributions, it is preferred to use effective Young's moduli for different zones (as in Chapter 4). In any case, having knowledge or at least good estimations about the distribution of effective Young's moduli will be of great use in modelling the hydromechanical behaviour of both normal fault zones and induced hydrofractures in fractured rock units in sedimentary successions.

10   Summarizing Conclusions

Rock heterogeneities in terms of layering and normal fault structure are common phenomena in typical sedimentary and volcanic rocks of the NWGB. Heterogeneous rock properties affect many issues and problems at different stages of geothermal project development. This study contributes to current geothermal exploration and exploitation concepts for the NWGB with emphasis on fault zone utilization, and prediction of geomechanical conditions for drilling and stimulation modelling from data collected in outcrop analogues. Structural geological field studies in 40 different outcrops (sedimentary and volcanic) and rock analyses of 35 outcrop and 14 core samples from two wellbores reveal following main conclusions regarding the specified main aims of this thesis (cf. Chapter 2):

1. Understanding of normal fault structure and associated fracture systems in typical sedimentary rocks of the NWGB

Normal fault zones in carbonate rocks are found to be more damage-zone dominated than those in clastic rocks, meaning that in general faults in carbonates feature both wider total fault zone widths and higher structural indices than those in clastic rocks. Independent of lithology, most of the fault-related fractures have an orientation similar to the fault strike and enlarged fracture aperture, -length, and -connectivity. Aside from this, data show that the existence of layer-parallel heterogeneities (mechanical layering) in the rock mass directly controls the amount of stratabound fractures and therefore the fracture connectivity. For damage zones in carbonate rocks, there is a distinct fracture density increase towards the fault planes. In clastic rocks, fracture dominated damage zones are more common in low-porosity sandstones with strong cementation than in less compacted sandstones. Presented data lead to the conclusion that there is a higher positive effect of normal fault zones on permeability increase in carbonate rocks compared with that in clastic rocks.

Therefore, normal fault zones crosscutting carbonate rocks are identified as promising geothermal reservoirs. The geothermal potential of normal fault zones in clastic rocks, however, may also be high, strongly depending on cementation and porosity. In both cases, natural permeabilities parallel to fault planes within damage zones are expected to be enhanced and damage zones are the recommended target point of geothermal wells. Calculated effective Young's moduli (stiffnesses) give insights on today's distribution of elastic properties in normal fault zones. Due to higher fracture densities the computed effective Young's moduli of damage zones in carbonate rocks are much lower than in clastic rocks. For numerical modelling of stimulation treatments in normal fault-related geothermal reservoirs this has to be taken into account.

Applicability of the achieved information and data to geothermal relevant depths is a critical point. Regarding normal fault-associated fracture system data it is concluded that it should be possible to apply presented results to hydromechanical models of larger normal fault zones due to normal fault's self-similarity.

2. Improving knowledge about geomechanical and physical properties of typical rocks of the NWGB

Geomechanical and physical rock properties of typical rocks from the NWGB were determined. The selected rock samples represent the wide range of probable physical and geomechanical properties to achieve large scale coverage from very low to high property values. Values of UCS, indirect tensile strength, Young's modulus, destruction work, porosity, and density are compiled in Chapters 5 and 6. These values are now usable as input parameters for any kind of numerical modelling which requires rock mechanical information as long as the depth dependency of the parameters is considered. Ascertained information on depth/confining-pressure dependency of compressive strength (failure criteria) and Young's modulus is provided by triaxial test evaluation (Chapters 6 and 8.3). The changes of the parameters porosity, tensile strength, and destruction work with increasing confining pressures could not be determined due to lacking adequate measuring techniques. However, they give, if not absolute values, at least relative parameter values, respectively mechanical contrasts, for these rocks. This is often good enough for numerical approaches.

Special emphasis was placed on strength measurements because rock strengths are crucial for planning and dimensioning of drilling operations and stimulation treatments. Predictions of rock strength, especially UCS, are the key to keep a wellbore stable by adapting the drilling mud weight to the respective conditions (cf. Chapter 1). Linear and non-linear regression analyses were performed separately for carbonate and clastic rocks due to varying mechanical behaviour. Calculated empirical relations for UCS with the parameters porosity, bulk density, and P-wave velocity yield comparatively low statistical significance for both clastic and carbonate rocks. In contrast, empirical relations of UCS with Young's modulus, destruction work and indirect tensile strength have high coefficients of determination. All empirical relations were specifically developed for NWGB conditions. By adjusting them with wellbore logs from adjacent boreholes, predictions of mechanical conditions at future geothermal projects may be even improved.

3. Analysing if rock properties at reservoir conditions are predictable from a database composed of outcrop samples

Until now, geomechanical input data for mud weight calculations and deep reservoir applications come either from rare core material or simply from assumptions of rock strengths. In this thesis, however, the approach was to use core samples to validate the applicability of results from samples from outcrop analogues on predictions of reservoir conditions. Selection of appropriate outcrop samples, which are supposed to be equivalent to respective core samples, was ensured by respecting stratigraphic age, lithology, and facies with special emphasis on similar grain sizes, compositions, and porosities. The comparison of core sample properties with results of outcrop samples was performed by using statistical methods such as residual analyses, 90% confidence and prediction bands of empirical relations and failure and friction criteria developed for outcrop samples.

Regression analyses for UCS with the parameters porosity, bulk density, and P-wave velocity show, although the statistical significance is low, that properties of core samples fit perfectly well within the scatter of outcrop samples. That is, developed empirical relations work well for at least estimating core sample properties with comparatively small deviation. In terms of the good correlations between UCS and Young's modulus, destruction work and indirect tensile strength for outcrop samples, core samples plot within 90% prediction bands. That is, parameter values of core samples are predictable from equations developed from an outcrop sample data set. Results let one assume that it is possible to consult outcrop samples of the rocks that have to be drilled through to provide good assumptions on rock mechanical properties at varying depths.

Triaxial tests are used to simulate in situ stress conditions for core samples and equivalent outcrop samples, as well as additional selected outcrop samples. It is concluded that Mohr-Coulomb failure criteria, expressed in principal stresses, for clastic and volcanite outcrop samples are applicable to core samples. Residual analyses show that failure conditions of carbonate core samples, however, differ considerably from the conditions, which were predicted from outcrop failure criteria due to more complicated interdepending deposition conditions of carbonate rocks leading to differing microfracture catalogues. Carbonate core samples feature both higher strengths and larger angles between fault normal and maximum principal stress σ_1 than equivalent outcrop samples. These larger angles considerably reduce the residuals between outcrop failure criteria and core test results. Therefore, the application of outcrop Mohr-Coulomb failure criteria, expressed in shear and normal stresses, for rock failure prediction is recommended. However, predictions of sandstone failure conditions are more straightforward than that of carbonate rocks.

Outcrop friction criteria can be applied on texturally similar core samples for all tested rock types. Calculated deviations are extremely low and plot within 90% prediction bands in all cases. No considerable differences of friction between core and outcrop samples were detected and data are in good accordance with Byerlee friction. That is, friction stress values react less sensitively on textural variations of samples than normal and shear stresses at failure.

Mohr-Coulomb failure and friction criteria of outcrop samples are applicable for predictions of rock strength at larger depths if equivalent outcrop samples are chosen with care. The most important points are comparable texture, similar porosity and grain interlocking, whereas the mineralogical composition is of minor importance.

Presented geomechanical data, failure criteria, and empirical relations reflect the rock properties occurring in the NWGB. Therefore these data may help predict rock mechanical conditions, and more explicitly UCS values, for NWGB rocks at greater depth.

4. Analysing the effect of heterogeneous rock properties and pre-existing fractures on hydrofracture propagation

Two different types of geothermal reservoirs may be present in the NWGB. Reservoir permeabilities may result from both high matrix-porosities and from fracture flow through existing fractures. In both cases, however, flow rates may be too small for economic geothermal power production and hydraulic stimulation is required. Coupled hydromechanical modelling of induced hydrofracture propagation was performed with FRACOD for different scenarios in the NGB. Particular focus was given to layered successions typical for the NGB and interaction with pre-existing fractures. The model geometries are adapted to the encountered sedimentary layering of Middle Bunter in the wellbore Gt1 (cf. Chapters 5, 6). For investigations of the fracture path in this heterogeneous succession, the parameters Young's modulus, Poisson's ratio, and fracture toughness (deduced from Young's modulus according to Yuan and Xi, 2011) were varied over the total range of measured values for the Middle Bunter from core and outcrop samples (Chapters 5, 6).

Simulation results show that in the assumed sedimentary succession of Middle Bunter the contrasts of Young's modulus or Poisson's ratio do not lead to a restriction of the induced hydrofracture to one layer. Regarding these elastic parameters it is concluded that hydrofractures connecting different sediment layers as encountered in wellbore Gt1 are realizable. The fracture toughness in mode I and II, however, is recognized as controlling factor of fracture path and geometry. The fluid-induced fracture initially propagates in the direction of the minimum stress component. As soon as it reaches pre-existing fractures, it is severely affected and changes its previous path depending on the applied boundary conditions (stress state). The hydrofracture shows comparatively high values of hydraulic conductivity over the entire simulation time. In contrast, although some shear displacement is accompanied by the opening mode of deformation in pre-existing fractures, they open only partly to serve as hydraulic paths.

Finally, the applicability of data obtained in outcrop analogues of deep geothermal reservoirs and overlying strata is still a critical and not completely solved problem. Every topic, presented in the different chapters, has its own complications which have to be evaluated with care when extrapolating properties to conditions at greater depths. In any case, rock heterogeneities have to be taken into account during geothermal exploration, drilling, and reservoir exploitation and stimulation. This thesis features approaches, as to how high resolution data from outcrop analogues can be used to improve predictions of fault zone structure and rock properties at reservoir conditions.

11 Perspectives

The usage of outcrop data for geothermal exploration and their applicability to reservoir conditions is still not completely solved and requires future investigations. From the results of this thesis some topics can be deduced which require further examinations and enquiries. In the following, these topics are to be outlined:

1. The interpretation and deduction of normal fault permeability (Chapter 4) relies exclusively on evaluation of fracture system parameters and is solely qualitatively. A quantitative determination is worthwhile to better assess resulting permeability distribution. This could, for instance, be done by in situ pumping tests at shallow depths targeting known fault zones. Further, it would be interesting to perform numerical modelling of fluid flow using the discrete fault structure – taken from a normal fault cropping out in a quarry – as input geometry. In this way we have the opportunity to easily control the interdependency of fault zone structure and resulting permeabilities.

2. Rock property values are the key to rock engineering design, whether it is by an empirical approach (cf. Chapter 5) or by numerical modelling (cf. Chapter 7). Therefore it is recommended to enlarge the already comprehensive database presented. It is suggested to take more core samples with different lithologies from other wellbores located in the NWGB. Laboratory testing of these core samples – together with their outcrop equivalents – will broaden the knowledge on crucial aspects of rock texture and fabric affecting predictability of geomechanical properties based on outcrop samples.

3. Presented results of texture of sandstone samples (Chapter 8.1) provide grounds for assuming that there are interdependencies with geomechanical properties of rocks, and especially UCS. For carbonate rocks, similar studies should comprise assessment of cementation, porosity, components, etc. with rock strength. Application of multivariate statistical analyses should be performed to better assess such interdependencies between different aspects of texture and fabric with geomechanical behaviour. Similarly, gaining insights on the drillability of rocks from texture analyses of equivalent outcrop samples would be desirable. There are already some approaches to deduce the drillability from texture. For instance, Howarth and Rowlands (1987) use a texture coefficient for sandstones and magmatic rocks as a predictive tool for the assessment of drillability and rock strength properties. To better characterise the sampled sandstone units in the NWGB regarding rock strength and drillability, further studies therefore should include texture analyses.

4. Young's modulus is recognized as important parameter regarding both fracture propagation and as predictive logging parameter. Investigation of mechanisms controlling uniaxial Young's moduli in comparison with derived ones from triaxial tests require systematic testing of rocks with changing facies and rock properties (e.g., fabric, texture, grain size, porosity, grain interlocking, etc.) held for different lithologies.

5. In most cases, geomechanical input data for wellbore stability analyses and mud weight calculations either come from rare core material or simply from rock strength assumptions. This thesis shows that it is also possible to utilise samples from outcrop analogues of rocks of the overlying strata for wellbore stability analyses. Referring to the geothermal exploration of the NWGB, it is recommended to use the newly generated geomechanical data for future predictive calculations of in situ rock strengths. An evaluation of these previously predicted rock strengths with measured values (well-logs) after drilling will help to further improve developed relations.

6. Conventional triaxial tests were performed to develop linearized Mohr-Coulomb failure and friction criteria of the different rock samples. This failure criterion assumes that the intermediate principal stress σ_2 has no influence on failure. Haimson and Chang (2005), however, showed that σ_2 has a perceived strengthening effect on rocks regarding wellbore stability. As discussed in Chapter 6, Mohr-Coulomb failure criterion leads to over-conservative predictions of critical mud weights. With true triaxial tests (Figure 11.1) using *Lade* (Lade 1977) or *Wiebols and Cook criterion* (Wiebols and Cook 1968) more concrete predictions may be possible. These tests are,

however, only of use if the true stress state with dimension of all three principal stresses is known which is very difficult beforehand.
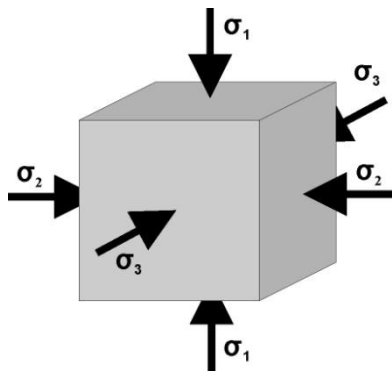
Figure 11.1: Test specimen under true triaxial loading (e.g., Zoback 2007).

7. One main conclusion drawn from this thesis is that samples from quarries are usable for prediction of rock strength and failure behaviour under reservoir conditions. Regarding this applicability of outcrop samples for prediction of further core sample properties continuative tests might be of interest. The performed conventional triaxial tests simulate in situ stress conditions but not temperature conditions. It is known that there is an effect of an increased temperature on rock strength and failure condition (e.g., Christensen 1985). This could be studied in more detail with a heatable triaxial test apparatus. Furthermore, the effects of fluids on rock strength have not yet been taken into account (cf. Chapter 9). It would be interesting to repeat triaxial measurements at different pore pressures.

8. There are other rock properties with importance in terms of geothermal heat extraction. The thermal conductivity and the matrix permeability of the reservoir rocks are two parameters not considered in this thesis. Sass and Götz (2012) developed a thermofacies concept to determine the geothermal potential of a specific rock unit as a function of the facies. The geothermal potential is valuated based on facies-typical thermal conductivities and matrix permeabilities of the prospective reservoir rocks (Figure 11.2).
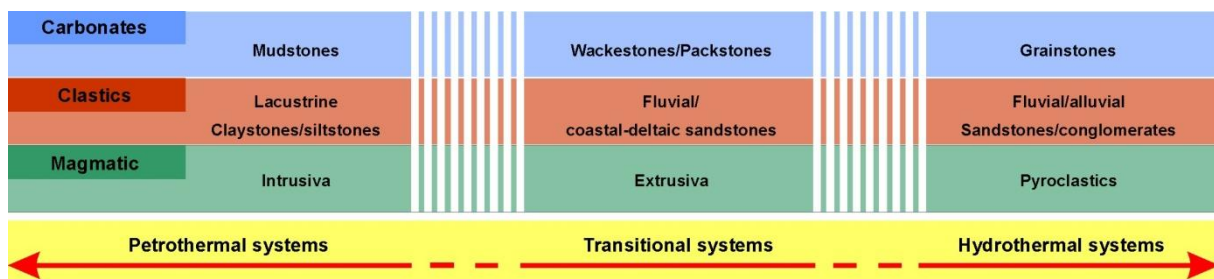

Figure 11.2: Conceptual thermofacies approach according to Sass and Götz (2012): carbonate, clastic and magmatic rocks in relation to hydrothermal, transitional and petrothermal systems.

Their database is, just as this study on rock mechanics, made up of samples taken in outcrop analogues. Combination of mechanical data with the thermofacies concept of Sass and Götz (2012) for reservoir characterisation may be an interesting way to generate a more complete and well-founded picture of both rock properties and geothermal potential of the respective rock units. Respective measurements of matrix permeability and thermal conductivity for presented rock samples are required.

References

Please note that this list refers to Chapters 1-3 and 8-11. References which are solely cited in the articles (Chapters 4-7) are displayed at the end of the respective chapter.

Aarland RK, Skjerven J (1998) Fault and fracture characteristics of major fault zone in the northern North Sea: analyses of 3D seismic and oriented cores in the Brage Field (Block 31/4). In: Coward MP, Daltaban TS, Johnson H (eds) Structural Geology in Reservoir Characterization 127, pp 209-229

Abdideh M, Fathabadi MR (2013) Analysis of stress field and determination of safe mud window in borehole drilling (case study: SW Iran). J Petrol Explor Prod Technol, doi: 10.1007/s13202-013-0053-2

Antonellini M, Aydin A, Pollard DD (1994) Microstructure of deformation bands in porous sandstones at Arches National Park, Utah. J Struct Geol 16:941-959

Atkins AG, Mai YW (1985) Elastic and Plastic Fracture. Horwood, Chichester

Aydin A (1978) Small faults formed as deformation bands in sandstone. Pure Appl Geophys 116:913-930

Baumgärtner J, Jung R, Hettkamp T, Teza D (2004) The status of the Hot Dry Rock scientific power plant Soultz-sous-Forêts. Z Angew Geol 50:12-16

Berg SS, Skar T (2005) Controls on damage zone asymmetry of a normal fault zone: outcrop analyses of a segment of the Moab fault, SE Utah. J Struct Geol 27:1803-1822

Bieniawski ZT (1968) The effect of specimen size on compressive strength of coal. Int J Rock Mech Min Sci 5:325–335

Bozau E, van Berk W (2012) Die Modellierung hydrogeochemischer Prozesse bei der geothermischen Nutzung von Formationswasser. Schriftenreihe DGG 80, 195

Brebbia CA, Dominguez J (1992) Boundary Elements: An Introductory Course. Computational Mechanics, Boston

Brenner SL (2003) Field Studies and Models of Hydrofractures in Heterogeneous Reservoirs. Dissertation, University of Bergen, Norway

Brink D (2010) Essentials of Statistics. David Brink & Ventus Publishing ApS

Caine JS, Evans JP, Forster CB (1996) Fault zone architecture and permeability structure. Geol 24:1025-1028

Carter NL, Friedman M, Logan JM, Stearns DW (eds) (1981) Mechanical Behavior of Crustal Rocks. AGU, Washington, D. C., Geophys Monogr Ser 24.

Christensen NI (1985) Measurement of dynamic properties of rock at elevated temperatures and pressures. In: Annual Book of Standards for Testing and Materials. ASTM International, STP 869, 93-107

Davy P, Le Goc R, Darcel C, Bour O, de Dreuzy JR, Munier R (2010) A likely universal model of fracture scaling and its consequence for crustal hydromechanics. J Geophys Res 115, B10411, doi:10.1029/2009JB007043

Dickson MH, Fanelli M (2003) Geothermal Energy – Utilization and Technology. Earthscan, London

DiPippo R (2005) Geothermal Power Plants: Principles, Applications & Case Studies. Elsevier, Oxford

Duda M, Renner J (2012) The weakening effect of water on the brittle failure strength of sandstone. Geophys J Int 192:1091-1108

Ewy RT (1998) Wellbore stability predictions using a modified Lade criterion. Rock Mech Pet Eng 1:247-254

Faulkner DR, Jackson CAL, Lun RJ, Schlische RW, Shipton ZK, Wibberley CAJ, Withjack MO (2010) A review of recent developments concerning the structure, mechanics and fluid flow properties of fault zones. J Struct Geol 32:1557-1575

Faulkner DR, Mitchell TM, Jensen E, Cembrano J (2011) Scaling of fault damage zones with displacement and the implications for fault growth processes. J Geophys Res 116:B05403, doi:10.1029/2010JB007788

Fjaer E, Ruistuen H (2002) Impact of the intermediate principal stress on the strength of heterogeneous rock. J Geophys Res 107, B2, 2032. doi: 10.1029/2001JB000277

Fjaer E, Holt RM, Horsrud P, Raaen AM, Risnes R (2008) Petroleum Related Rock Mechanics. Elsevier, Developments in Petroleum Science 53, Amsterdam

Flügel E (2010) Microfacies of Carbonate Rocks: Analysis, Interpretation and Application. Springer, Heidelberg

Gast RE (1988) Rifting im Rotliegenden Niedersachsens. Geowiss 6:103-136

Griffith WA, Sanz PF, Pollard DD (2009) Influence of outcrop scale fractures on the effective stiffness of fault damage zone rocks. Pure Appl Geophys 166:1595-1627

Gudmundsson A (1992) Formation and growth of normal faults at the divergent plate boundary in Iceland. Terra Nova 4:464-471

Gudmundsson A (2011) Rock Fractures in Geological Processes. Cambridge University Press, New York

Gudmundsson A, Berg SS, Lyslo KB, Skurveit E (2001) Fracture networks and fluid transport in active fault zones. J Struct Geol 23:343-353

Gudmundsson A, Simmenes TH, Larsen B, Philipp SL (2010) Effects of internal structure and local stresses on fracture propagation, deflection, and arrest in fault zones. J Struct Geol 32:1643-1655

Gulrajani SN, Nolte KG (2000) Fracture evaluation using pressure diagnostics. In: Economides MJ, Nolte KG (eds) Reservoir Stimulation. Wiley, New York, 9:1-63

Haimson B (1997) Borehole breakouts and core discing as tools for estimating in situ stress in deep boreholes. In: Sugawara K, Obara Y (eds.) Rock stress. Rotterdam: Balkema, 35-42.

Haimson B, Chang C (2005) Brittle fracture in two crystalline rocks under true triaxial compressive stress. In: Harvey PK, Brewer TS, Pezard PA, Petrov VA (eds) Petrophysical Properties of Crystalline Rocks. Geological Society, London, Special Publications 240, pp 47-59

Hatzor YH, Palchik V (1997) The influence of grain size and porosity on crack initiation stress and critical flaw length in dolomites. Int J Rock Mech Min Sci 34:805-816

Hawkins AB (1998) Aspects of rock strength. Bull Eng Geol Environ 57:17-30

Hesshaus A, Houben G, Kringel R (2013) Halite clogging in a deep geothermal well – Geochemical and isotopic characterisation of salt origin. J Phys Chem Earth, in press. http://dx.doi.org/10.1016/j.pce.2013.06.002

Hoek E, Brown ET (1980) Underground excavations in rock. Instn Min Metall, London

Howarth DF, Rowlands JC (1987) Quantitative assessment of rock texture and correlation with drillability and strength properties. Rock Mech Rock Eng 20:57–85

Huenges E (2010) Geothermal Energy Systems: Exploration, Development, and Utilization. Wiley, Weinheim

Hübner W, Hunze S, Baumgarten H, Orilski J. Wonik T (2012) Petrophysical and sedimentary petrographic characterisation of the Bückeburg Formation (German Wealden) in the geothermal well Groß Buchholz Gt-1 (Hanover, Germany). ZDGG 163:483-492

ISRM Commission on Testing Methods (1999) Draft ISRM suggested method for the complete stress-strain curve for intact rock in uniaxial compression. Intl J Rock Mech Min Sci 36:279-289

ISRM (2007) The Complete ISRM Suggested Methods for Rock Characterization, Testing and Monitoring: 1974-2006. In: Ulusay R, Hudson JA (eds) Suggested Methods Prepared by the Commission on Testing Methods, International Society for Rock Mechanics. Compilation ISRM Turkish National Group, Ankara, Turkey

Jaeger JC, Cook NGW, Zimmerman RW (2007) Fundamentals of Rock Mechanics. Blackwell Publishing, Malden

Jung R, Orzol J, Jatho R, Kehrer P, Tischner T (2005) The GeneSys-Project: Extraction of geothermal heat from tight sediments. Proc 30. Workshop on Geothermal Reservoir Engineering, SGP-TR-176

King G (1983) The accommodation of large strains in the upper lithosphere of the earth and other solids by self-similar fault systems - the geometrical origin of b-Value. Pure Appl Geophys 121:761-815

Knott SD, Beach A, Brockbank PJ, Lawson Brown J, McCallum JE, Welbon AI (1996) Spatial and mechanical controls on normal fault populations. J Struct Geol 18:359-372

Koestler AG, Ehrmann WU (1991) Description of brittle extensional features in chalk on the crest of a salt ridge (NW Germany). In: Roberts AM, Yielding G, Freeman B (eds) The Geometry of Normal Faults. Geological Society, London, Special Publications 56, pp 113-123

Kovari K, Tisa A (1975) Multiple failure state and strain controlled triaxial tests. Rock Mech 7:17-33

Kovari K, Tisa A, Einstein HH, Franklin JA (1983) Suggested methods for determining the strength of rock materials in triaxial compression: Revised version. Int J Rock Mech Min Sci Geomech Abstr 20:283-290

Lade P (1977) Elasto-plasto stress-strain theory for cohesionless soil with curved yield surfaces. J Solid Struct 13:1019-1035

Larsen B, Gudmundsson A, Grunnaleite I, Sælen G, Talbot MR, Buckley SJ (2010) Effects of sedimentary interfaces on fracture pattern, linkage, and cluster formation in peritidal carbonate rocks. Mar Petr Geol 27:1531-1550

Lee CH, Farmer IW (1993) Fluid Flow in Discontinuous Rocks. Chapman and Hall, London, New York

Li S, George J, Purdy C (2012) Pore-pressure and wellbore-stability prediction to increase drilling efficiency. J Pet Technol 64:99-101

Li Y, Schmitt DR (1997) Well-bore bottom stress concentration and induced core fractures. AAPG Bull 81:1909-1925

Lindsay NG, Murphy FC, Walsh JJ, Watterson J (1993) Outcrop studies of shale smears on fault surfaces. In: Flint S, Bryant I (eds) The Geological Modelling of Hydrocarbon Reservoirs and Outcrop Analogues. In: International Association Sedimentologists, Special Publication 15, pp 113-123

Lockner D, Tanaka H, Ito H, Ikeda R (2000) Permeability and strength of core samples from the Nojima fault of the 1995 Kobe earthquake. Proc Internat Workshop on Nojima Fault Core and Borehole Analysis, 00-129

McBride EF (1963) A classification of common sandstones. J Sediment Petrol 33:664-669

McCann DM, Entwisle DC (1992) Determination of Young's modulus of the rock mass from geophysical logs. Geological Society, London, Special Publications 65, pp 317-325. doi: 10.1144/GSL.SP.1992.065.01.24

Meneses Rioseco E, Reyer D, Schellschmidt R (2013) Understanding and predicting coupled hydromechanical fracture propagation. Proc European Geothermal Congress, Pisa, PS2-08

Menzel H, Seibt P, Kellner T (2000) Five years of experience in the operation of the Neustadt-Glewe geothermal project. Proc World Geothermal Congress, Kyushu-Tohoku, Japan

Muraoka H, Kamata H (1983) Displacement distribution along minor fault traces. J Struct Geol 5:483-495

Naceur KB, SPE, Touboul E, Schlumberger D (1990) Mechanisms controlling fracture-height growth in layered media. SPE Production Engineering, Society of Petroleum Engineers

Nelson RA (1985) Geologic analysis of naturally fractured reservoirs. Gulf Publishing, Houston, Texas

NIBIS Kartenserver (2012): 3D-Modell Geotektonischer Atlas. LBEG, Hannover

Odling NE, Gillespie P, Bourgine B, Castaing C, Chiles JP, Christensen NP, Fillion E, Genter A, Olsen C, Thrane L, Trice R, Aarseth E, Walsh JJ, Watterson J (1999) Variations in fracture system geometry and their implications for fluid flow in fractured hydrocarbon reservoirs. Petrol Geosc 5:373-384

Öztürk CA, Nasuf E, Bilgin N (2004) The assessment of rock cutability, and physical and mechanical rock properties from a texture coefficient. J S Afr Inst Min Metall 104:397-402

Paschen H, Oertel D, Grünwald R (2003) Möglichkeiten geothermischer Stromerzeugung in Deutschland. TAB Arbeitsbericht 84

Peška P, Zoback MD (1995) Compressive and tensile failure of inclined well bores and determination of in situ stress and rock strength. J Geophy Res 100 (B7):12,791-12,811

Philipp SL, Hoffmann S, Müller C, Gudmundsson A (2005) Verringerung des Fündigkeitsrisikos für tiefen-geothermische Projekte durch strukturgeologische Geländestudien und numerische Modelle. In: Geothermie: Synergie und Effizienz. In: Proc Geothermische Jahrestagung 2005, pp 113-124

Priest SD (1993) Discontinuity Analysis for Rock Engineering. Chapman and Hall, London

Reinicke KM, Oppelt J, Ostermeyer GP, Overmeyer L, Teodoriu C, Thomas R (2010) Enhanced technology transfer for geothermal exploitation through a new research concept: the geothermal energy and high-performance drilling research program: Gebo. SPE 134436, SPE Annual Technical Conference, Italy

Rider M, Kennedy M (2011) The Geological Interpretation of Well Logs. Rider-French Consulting Ltd.

Röckel T, Lempp C (2003) Der Spannungszustand im Norddeutschen Becken. Erdöl Erdgas Kohle 119:73-80

Sass I, Götz AE (2012) Geothermal reservoir characterization: a thermofacies concept. Terra Nova 24:142-147

Schön JH (1996) Physical Properties of Rock: Fundamentals and Principles of Petrophysics. Pergamon, Oxford

Shen B (2013) Two Dimensional Fracture Propagation Code (Version 1.1): User's Manual. FRACOM Ltd., Finland; available online at www.fracom.fi

Shen B, Stephansson O (1993) Numerical analysis of Mode I and Mode II propagation of rock fractures. Int J Rock Mech Min Sci & Geomech 30:861-867

Shen B, Stephansson O, Rinne (2013) Modelling rock fracturing processes. A fracture mechanics approach using FRACOD. Springer, Heidelberg

Singhal BBS, Gupta RP (2010) Applied Hydrogeology of Fractured Rocks. Springer, Heidelberg

Teale R (1965) The concept of specific energy in rock drilling. Int J Rock Mech Min Sci 2:57-73

Thuro K (1997) Drillability prediction: geological influences in hard rock drill and blast tunneling. Geol Rundsch 86:426-438

Thuro K, Plinninger RJ, Zäh S, Schütz S (2001) Scale effects in rock strength properties. Part 1: Unconfined compressive test and Brazilian test. In: Särkka P, Eloranta P (eds) Rock mechanics – a challenge for society. Swets & Zeitlinger Lisse, 169-174

Tischner T, Evers H, Hauswirth H, Jatho R, Kosinowski M, Sulzbacher H (2010) New Concepts for Extracting Geothermal Energy from one Well: The GeneSys-Project. Proc World Geothermal Congress, Bali

Torabi A, Berg SS (2011) Scaling of fault attributes: A review. Mar Petr Geol 28:1444-1460

Tuncay E, Hasancebi N (2009) The effect of length to diameter ratio of test specimens on the uniaxial compressive strength of rock. Bull Eng Geol Environ 68:491-497

Turcotte DL (1989) Fractals in geology and geophysics. Pure Appl Geophys 131:171-196

Twiss RJ, Moores EM (1992) Structural Geology. WH Freeman and Company, New York

Vogt E, Reyer D, Schulze KC, Bartetzko A, Wonik T (2012) Modeling of geomechanical parameters required for safe drilling of geothermal wells in the North German Basin. Proc Celle Drilling, Celle

Walter R (2007) Geologie von Mitteleuropa. Schweizerbarth, Stuttgart

White NJ, Jackson JA, McKenzie DP (1986) The relationship between the geometry of normal faults and that of the sedimentary layers in their hanging walls. J Struct Geol 8:897-909

Wiebols GA, Cook NGW (1968) An energy criterion for the strength of rock in polyaxial compression. Int J Rock Mech Min Sci 5:529-549

Wooldridge JM (2009) Introductory Econometrics: A Modern Approach. South-Western, Cengage Learning, Mason, Ohio

Yuan CC, Xi XK (2011) On the correlation of Young's modulus and the fracture strength of metallic glasses. J Appl Phys 109, 033515, doi:10.1063/1.3544202

Zeynali ME (2012) Mechanical and physico-chemical aspects of wellbore stability during drilling operations. J Pet Sci Eng 82-83:120-124

Zhang L (2005) Engineering Properties of Rocks. Geoengineering Book Series 4, Elsevier, London

Ziegler P (1990) Geological Atlas of Western and Central Europe. Geological Society Publishing House/Shell International Petroleum Maatschappij B.V.

Zoback MD (2007) Reservoir Geomechanics. Cambridge University Press, New York

http://www.gebo-nds.de

http://www.geothermie-bruehl.de

CV/Lebenslauf

PERSÖNLICHE DATEN

Name	Dorothea Reyer
Geburtsdatum	13.06.1984
Geburtsort	Witzenhausen
Nationalität	deutsch

BERUFLICHER WERDEGANG

Seit 02/2014	Wissenschaftliche Mitarbeiterin und Reservoiringenieurin am Zentrum für TiefenGeothermie, Oberflächennahe Geothermie, LBEG, Celle
05/2009 – 01/2014	Wissenschaftliche Mitarbeiterin am Geowissenschaftlichen Zentrum der Universität Göttingen, Abteilung Strukturgeologie und Geodynamik
11/2008 – 05/2009	Geologin bei der Firma ENRO Geothermie Entwicklung GmbH, Ludwigsfelde

BILDUNGSWEG

24.10.2013	Erlangung des Doktorgrades "Doctor rerum naturalium"
10/2010 – 10/2013	Doktorandin am Geowissenschaftlichen Zentrum der Universität Göttingen
10/2003 – 10/2008	Studium der Geowissenschaften, Universität Göttingen
30.09.2008	Erlangung des Grades „Diplom-Geowissenschaftlerin"
	Vertiefungsrichtung: Geologie, Nebenfächer: Strukturgeologie und Geophysik
	Thema der Diplomarbeit: „Kluftsysteme im Muschelkalk des Kraichgaus, Baden-Württemberg, und Prognosen zum bruchkontrollierten Fluidtransport bei der Nutzung als tiefer geothermischer Reservoirhorizont im Oberrheingraben". Firmenkooperation mit GeoEnergy Consulting, Karlsruhe
05/2007 – 06/2008	Strukturgeologische Diplomkartierung: „Geologische Kartierung im Bereich der östlichen Grabenrandstörung des Leinetalgraben bei Sudheim"
26.10.2006	Erlangung des Grades „Bachelor of Science" für das Fach Geowissenschaften
	Thema der Bachelorarbeit: „Korngrößenverteilung und Tonmineralogie in ausgewählten Sturmflutsedimentprofilen auf der Hallig Hooge"
1990 – 06/2003	Allgemeine Hochschulreife: Gymnasium Andreanum, Hildesheim

STUDIENBEGLEITENDE TÄTIGKEITEN UND PRAKTIKA

Tutortätigkeit bei folgenden Veranstaltungen am Geowissenschaftliches Zentrum:

2005 – 2008	Sedimentologie; Angewandte Geologie; Kristallographie; Geländestudien: Bruchsysteme und Permeabilität; Strukturgeologie; Numerische Modelle in der Strukturgeologie
2005 – 2008	Studentische Hilfskraft in den Abteilungen Angewandte Geologie und Strukturgeologie, Geowissenschaftliches Zentrum der Universität Göttingen
09/2005 – 10/2005	Praktikum bei der Firma Dr. Pelzer und Partner, Hildesheim